Optimization of engine air path with hybrid boosting systems

Yang Liu

A thesis submitted for the degree of Doctor of Philosophy

University of Bath

Department of Mechanical Engineering

January 2020

Abstract

The electrification of powertrains is now the accepted roadmap for automotive vehicles. The next big step in this area will be the adoption of 48V systems, which will facilitate the use of technologies such as electric boosting and integrated starter-generators. The introduction of these technologies gives new opportunities for engine air path design as an electrical energy source may now be used in addition to the conventional mechanical and exhaust thermal power used in super- and turbo-chargers. This thesis aims to investigate the design of a mild hybrid boosting system, to determine if electrified boosting can improve overall system performance, with respect to efficiency, power and transient response. The study covers both gasoline and diesel engines, based on a series of engine air path case studies, discusses the benefits of a hybrid boost system through both an experiment and a simulation:

- The study of diesel engine with electrically driven compressor.
- The study of petrol engine with mechanically decoupled electric turbocharger.
- The study of inner-insulated turbocharger.
- The study of a T-PIECE junction in the two-stage air path.

A comprehensive literature review has been carried out for turbocharger technologies and mild hybrid system status, this details the challenges related to turbo-matching, the development of an electric boost system, and the difficulties in air path interaction in more comprehensive engine systems. The performance of the two-stage system with an electrically driven compressor (EDC) has been investigated in both experiment and simulation. A two-stage engine gas stand test rig has been constructed based on a prototype 2.2L diesel engine, with the intention to undertake steady flow and transient characterization for a complex air path system and investigate potential future system layouts and control strategies, in order to undertake the steady and transient study of two-stage electric boost system. In simulation phase, it has been demonstrated that by operating the EDC, variable geometry turbine (VGT) properly can reduce the engine output response time by 0.1s to 2s; however, these methods will reduce the system efficiency. Besides, EDC and VGT can also affect the EGR mixing, e.g., high speed EDC and lower positioned VGT could help to quantify the EGR transient flow and mixing speed (according to the O2 rate changes). The intercooler and HP EGR have

also been discussed under different air path route design. EDC operation will be affected by the hot flow from EGR if it was located downstream of the HP EGR, as it can boost the inlet flow which will affect the mixed flow rate, temperature and pressure, thus changed the EGR ratio. Intercooler mainly affects either engine inlet temperature or EDC inlet temperature as its location decides which flow will be cooled down.

The decoupled electric turbocharger (DET) engine system in both the single-stage and two-stage situation was investigated. With different size of turbocharger based on the scaling method, by the introducing of engine mean value model, the DET can generate up to 0.38kW average power in an RDE simulation which can significantly increase the engine fuel economy. In the NEDC and WLTC cycles, the e-turbo system can always generate energy and store it in a battery (0.21kW and 0.23kW average power over the whole cycle, respectively). In a transient study, the DET was mounted together with a single turbocharger. After optimizing the controlling methodologies, the E-turbine energy generated changed from 237 kJ to 244 kJ; the EDC energy consumed underwent a big difference, dropping from 954.37 kJ to 47.22 kJ, in WLTC cycle.

Further, a thermally insulated turbocharger turbine is proposed to increase the aftertreatment system inlet temperature. Steady state tests showed that the insulation could increase the T4 for the turbocharger turbine under different engine speed and load conditions. In the transient study, a small (1.5K) temperature benefit can be observed in the experiment, which is different from simulation due to the inaccuracy of the model. In engine warm up tests, the T4 enhancement was also low, but a 2kRPM turbo speed benefit was achieved at this process due to the increased turbine inner gas temperature.

Finally, the optimisation of the design of a T-piece junction in the engine intake side has been achieved by different methods. The T-piece junction between the EDC and the turbocharger compressor has been optimised for lower pressure drop and reduced swirl compared to the baseline design. The pressure drop was reduced by 0.3 kPa (15 %) and the turbocharger compressor efficiency increased by up to 2 % (compressor efficiency rises from 68 % to 70 %).

Acknowledgement

First of all, my deepest gratitude goes to my supervisor Dr Richard Burke, for everything he contributed to my PhD. It has been an honour to be his second PhD student. I learned much from him, not only the academic knowledgement but also the character and manners, without his help, this thesis would get no chance to be carried out. And also, I would like to thank Professor Sam Akehurst, Dr Colin Copeland, Professor Jamie Turner and Professor Chris Brace for their valuable advice and support for my work. I feel honourable for joining the IAAPS groups where I gain friendships as well as good advice and collaboration. Saying thanks to Dr Ramkumar Vijayakumar and Dr Misan Madamedon, for their contribution in experiments.

I am extremely grateful to my parents, for their love, caring and sacrifice for my study and living, they are the most important role exist ever in my life. I also want to say thank you to my relatives, and the encouragement from them accompanied me in the last 4 years. Besides, I am very much thankful to my undergraduate supervisor Professor Dingfang Chen, for his helping and advice.

Then, I would like to thank all my friends both in the UK and China, Zheng LIU, Haizhu Wang, Dr Zichen Liu, Minwei Sun, and my Werewolves of Miller's Hollow card game, League of Legends, Nintendo Switch game friends, for helping me, listening to my complaints and playing with me. My gratitude will also go to Wei Zeng, Hongfa Zhang, they helped me overcome the hardest time in my PhD when I was upset. I would also say thanks to Jürgen Werner from BorgWarner, who helped me a lot in turbocharger research.

This work was conducted with funding from the THOMSON project which has received funding from the European Union's Horizon 2020 Programme for research, technological development and demonstration under Agreement no. 724037.

Content

List of Figures

List of Tables

Abbreviations

1D	One dimensional
AFR	Air-Fuel Ratio
BMEP	Brake Mean Effective Pressure
BSFC	Brake Specific Fuel Consumption
BSG	Belt Starter Generator
CAC	Charge Air Cooler
CAD	Computer Aided Design
CAE	Computer Aided Engineering
CAHU	Combustion Air Handling Unit
CAN	Controller Area Network
CBPV	Compressor Back pressure Valve
CFD	Computational Fluid Dynamics
CHT	Conjugate Heat Transfer
CO	Carbon monoxide
CO2	Carbon dioxide
DEP	Divided Exhaust Period
DOC	Diesel Oxygen Catalyst
DPF	Diesel Particulate Filter
EAT	Electric Assisted Turbocharger
EATS	Exhaust Gas Aftertreatment System
EDC	Electrically Driven Compressor
EFM	Efficiency Multiplier
EGR	Exhaust Gas Recirculation
EGS	Engine Gas Stand
EHC	Electrically Heated Catalyst
e-stop	Emergency stop
FEA	Finite Element Analysis
FEM	Finite Element Method
FPGA	Field programmable Gate Array
GA	Genetic Algorithm
GS	Gas stand (Conventional)
HC	Hydro Carbon
HP-EGR	High Pressure EGR
HT	Heat Transfer
HTC	Heat Transfer Coefficient
ICE	Internal Combustion Engines
LP-EGR	Low Pressure EGR
MFM	Mass Flow Multiplier
MFP	Mass Flow Parameter
NA	Natural Aspiration
NEDC	New European Driving Cycle
NOx	Oxides of Nitrogen
PID	Proportional-Integral-Derivative Controller
PR	Pressure Ratio
RDE	Real Driving Emission
SPM	Speed Multiplier
T/H	Turbine Housing
TC	Turbocharger
TIT	Turbine Inlet Temperature
T-S	Total-to-Static
VGT	Variable Geometric Turbine
VVA	Variable Valve Actuation
WLTC	Worldwide Harmonized Light Vehicles Test Cycles

Symbols

Symbol	Description	Symbol	Description
D	Diameter	Nu	Nusselt number
F	Force	a	Coefficient in the nusselt number equation
N	Rotational Speed	Re	Reynolds number
p	Pressure	b	Exponent for Reynolds number
P	Power	Pr	in the Nusselt number equation
R	Gas constant	μ_bulk	Fluid viscosity at the bulk fluid temperature
t	Time	μ_skin	Fluid viscosity at the heat-transfer boundary surface temperature
T	Temperature	Q	Heat flux
V	Speed	σ	Stefan's constant
W	Work	ε	Emissivity
k	Multiplier factor	A	Area of the surface
μ	Efficiency	$\eta_{is\ C}$	Isentropic Compressor efficiency
τ	Torque	π_{comp}	Compressor pressure ratio
p	Pressure	κ_{Air}	Specific heat ratio of air
P	Power	$\dot{m}_T$	Mass flow rate through turbine
t	Time	$c_{p\ Exh}$	Specific heat at constant pressure of exhaust gas
T	Temperature	T_{3t}	Total turbine inlet temperature
m	mass	π_{exp}	Turbine expansion ratio
W	Work	κ_{exh}	Specific heat ratio of exhaust gas

μ	Efficiency	$\eta_{is\,T}$	Turbine isentropic efficiency
C	Specific Energy	η_T	Turbine efficiency
$\dot{m}_a$	Air mass flow rate	η_m	Mechanical efficiency of the turbocharger
γ_{3-4}	Average ratio of specific heat across turbine	$\dot{m}_C$	Flow rate through the compressor
C_{pa}	Average specific heat of air across the compressor	$c_{p\,Air}$	Specific heat at constant pressure of air
C_{pe}	Average exhaust gas specific heat across the turbine	T_{1t}	Compressor total inlet temperature
$\dot{m}_e$	Exhaust gas mass flow rate	$\dot{m}_{Tred}$	Reduced turbine mass flow rate
PR_{3-4}	Pressure ratio across the turbine	T_{02}	Total compressor outlet temperature
T_{01}	Total compressor inlet temperature	T_{03}	Total turbine inlet temperature
η_t	Turbine efficiency		

Chapter 1 – Introduction

Internal combustion engine vehicles are under extremely high emission pressure. The vehicle emission regulations have become much stricter at present, and the European Commission has announced that the target CO_2 *emission by passenger cars is 95g/km, and 145 g/km for low duty cars by 2020, which should be further reduced by 15% and 30% in 2025 and 2030 (Johnson et al., 2018). Downsizing has been proven to be one of the most efficient technologies for improving engine fuel economy, as it offers the opportunity for the engine to reduce heat loss, friction losses but not loss the power. By reducing an engine's swept volume but increasing its specific power, the engine can have a higher brake mean effective pressure. Turbochargers are widespread since they can help to downsize the natural aspiration engine just using the exhaust energy without external costs. However, due to the increasing need for higher power density, drivability and emission reduction, conventional turbocharged engines are struggling to deliver a sufficient difference. Given the rapid development and expectation of hybrid and electric vehicles, the advanced electric boost system is one of the most efficient solutions to enabling turbocharged engines to overcome these difficulties.*

This chapter introduces the background of this thesis, including the current emission regulations, engine downsizing and downspeeding technologies, and the increasing demand for a boost system. The aims and principle objectives of this thesis will be laid out, followed by the summary of each chapter in this thesis, the contribution of this thesis and what future effects this thesis may have.

1.1 Background

Road transport contributes much to air pollution, and vehicle emission regulations are much stricter at present. In Europe, European Commission announced that the target emission of passenger cars and vans should be decreased from 130 g/km CO2 to 95 g/km CO2 (Mock et al., 2014). Manufacturers found many ways to reduce the emissions in experimental testing procedure, so the emission gap between test and real-life driving becomes bigger and bigger. As a result, the Worldwide Harmonized Light Vehicles Test Procedure (WLTC) project was announced in 2007, and the first phase was proposed in 2014(Mock *et al.*, 2014). This regulation was used for type approval testing first in 2017. After 2020, new cars can only be tested in the WLTC in laboratory stage.

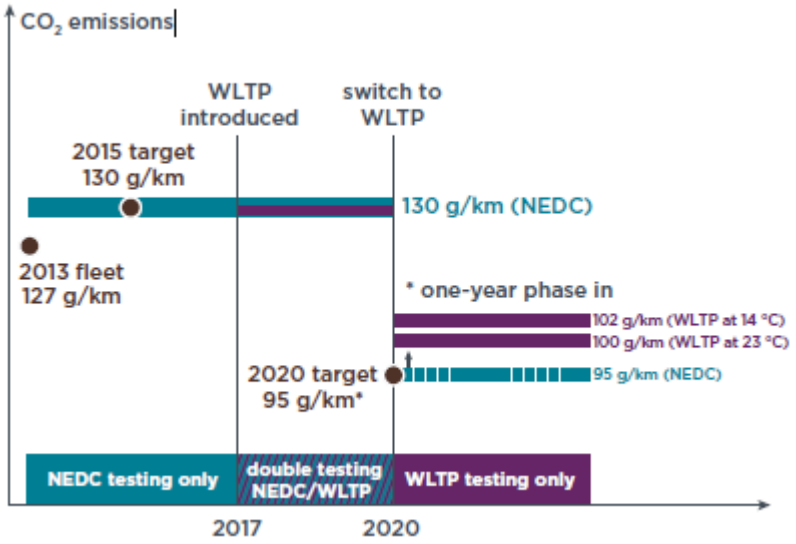

Figure 1.1Development of Emission regulations(Mock et al., 2014)

Comparing with NEDC test protocol, there are four main differences(Pavlovic *et al.*, 2018):

1. Road load determination.
2. Laboratory test methodology.
3. Post-processing of the test results.
4. Declaration of CO_2 results.

Since the WLTC cycle is more robust than NEDC, more types of driving situations were involved. This change brings an overall increase in NOx, PM and PN emission

and decrease in THC and CO emissions(Bielaczyc *et al.*, 2016), but can help reduce the emission gap between real driving and testing. However, WLTC is still a fixed test method, and manufacturers might be able to exploit the margin between real emission and laboratory tests. Another test protocol called real driving emission (RDE) test which is based on real-driving emissions. It will use vehicles with on-board portable emissions measurement systems (PEMS)(Franco *et al.*, 2015). The emission data will be measured during driving in real road condition that affected by many different real-life factors and drivers' behaviour, and the results will be compared with WLTC.

The much stricter emission legislation and the improvement of people' environmental awareness urgently lead to a requirement of increasing engine fuel economy. Over the last few decades, many different technologies are discovered for improving engine fuel economy. For example, gasoline direct injection (GDI, homogenous and stratified lean combustion)(Stone, 1988), a technique that the highly pressurised gasoline is injected directly to the combustion chamber by a common rail. Different from conventional fuel injection, as the latter injects the fuel to intake tract or cylinder port. GDI helps to control the combustion process, and high pressure liquid fuel is evaporated in the cylinder. This process draws heat out from both inlet air and cylinder, which increase the volumetric efficiency.

Exhaust gas recirculation (EGR)(Reifarth, 2010) is another way to improve fuel consumption and reduce emissions. By mixing partial exhaust with intake air, the oxygen rate is reduced, which will lower the in-cylinder temperature and reduce the emission. Variable valve train system, introduced in (Turner *et al.*, 2005), is varying the lift, duration and timing of each inlet valve to improve fuel consumption and reduce emission. All these technologies are widely used in the last few years, they improved internal combustion engine performance and reduced the emissions. Nowadays vehicle engines are designed to have higher power density, which can further increase engine efficiency and reduce fuel consumption. Engine downsizing is one of the most extensive way to improve engine brake mean specific power. By reducing the engine size and related components, the engine friction, heat loss and throttle loss (gasoline engine only) will be reduced. Current research shows that vehicle with highly downsized engine can reduce at most 35% CO2 emission and achieve 35% fuel consumption benefit(Turner *et al.*, 2014). Figure 1.2 shows the turbocharged and

naturally aspirated vehicle fuel consumption and torque under different conditions: from city driving with frequent stopping and starting, to highway driving. The 1.5L turbocharged engine has a slightly bigger torque output but lower fuel consumption as compared with the 2.4L naturally-aspirated engine(HONDA, 2019).

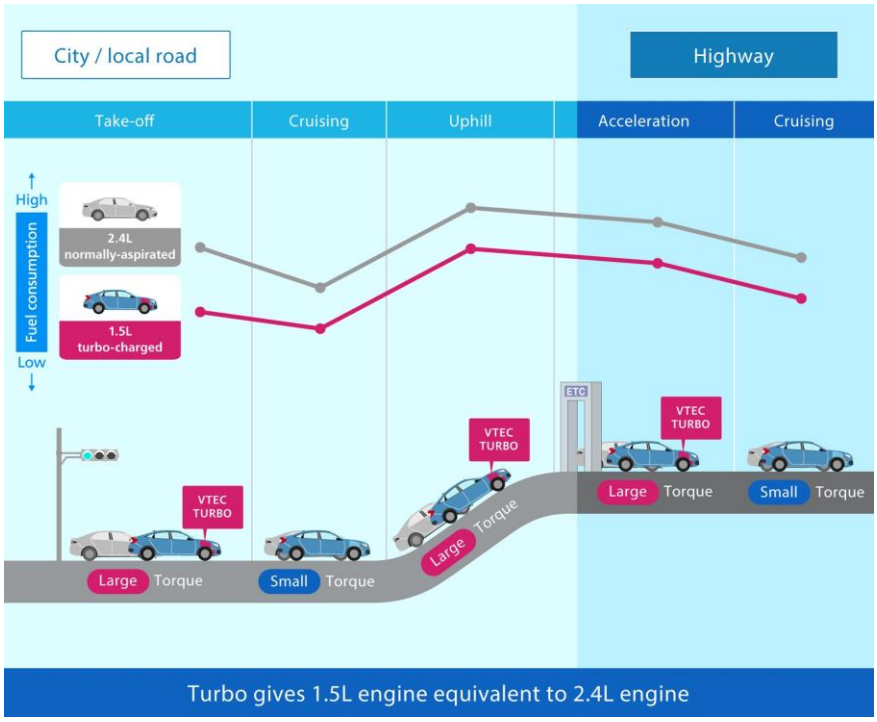

Figure 1.2 Turbocharged vehicle fuel efficient under different condition (HONDA, 2019)

However, engineers need to consider not only the fuel economy but also the engine output curve. Single stage turbocharger engine is struggling to meet both peak power and low speed torque target (Liu *et al.*, 2018; Watson *et al.*, 1982; Zhang, 2015). Highly downsized gasoline engine will have an increasing knocking risk, the transient performance is also sacrificed as the downsizing of the engine. More complicated boosting system is required to meet the design requirement in different area. Multi-stage system, EGRs, cooling system are involved, there is no straightforward design methodology for the engine air path. Figure 1.3 shows an example of controlling module for a two-stage decoupled electric boosting system, different valves, motors need to be adjusted to meet the same engine power output, considering the transient performance and power balance, challenges still exist for managing and optimising the controlling of each component.

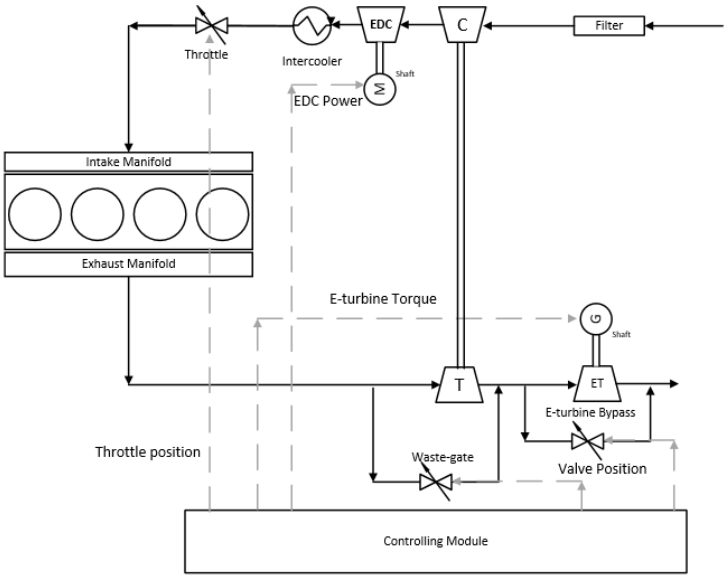

Figure 1.3 Example of engine air path diagram

1.2 Modern engine downsizing.

The power of an internal combustion engine is often limited by its engine speed and swept volume, as they decide how much air can be filled into the cylinder (Heywood, 1988). However, as the increasing demand for low carbon lifestyle, the regulation requirements of vehicle emissions are much stricter, engine downsizing is an attractive direction. This technology is achieved by combining with the reduction of engine swept volume and increasing of specific power. In this case, the engine can have higher brake mean effective pressure (BMEP), and better fuel economy (Schumann *et al.*, 2013). A downsized engine will get power and torque output loss since the engine swept volume is reduced. Attached devices will be required on downsized engine to help introduce more air into the cylinder and allows more fuel to be burnt (Thirouard *et al.*, 2009). In this way, the engine size can be reduced without losing torque or power output. Also, as the engine size is smaller, the thermal loss, friction loss and combustion performance will be improved under suitable controlling methodology.

Boosting devices are generally used for achieving this function, which can pump in more air into the cylinder, increase the engine in-cylinder pressure and BMEP. Figure 1.4 shows how the turbocharged engine differs from the same size and same power NA engine.

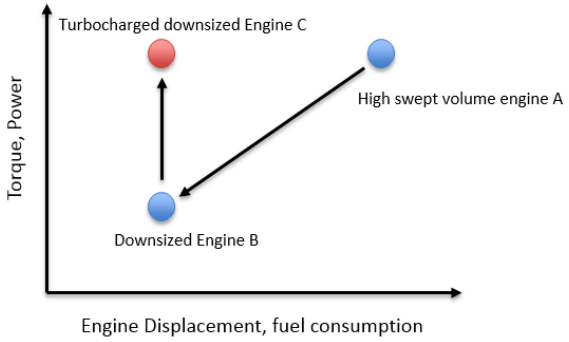

Figure 1.4 Principle of Engine Downsizing (Golloch et al., 2005)

Comparing with NA engine, downsized engine has the following advantages.

1. Engine pumping losses are reduced. In a gasoline system, downsized boosted engine has higher inlet manifold pressure comparing with the NA engine with same power output, the throttle degree can be reduced, the smaller engine can operate closer to peak efficiency point (Rose *et al.*, 2011). When using a turbocharger, the compressor can boost more air into the cylinder and force the piston down which helps to reduce pumping losses.
2. Improvement of total mechanical efficiency by reducing friction losses. Comparing with the same sized NA engine, engine with higher specific power suffered in a higher friction losses due to increased bearing sizes, spring loads et al. (Fraser *et al.*, 2009), however, when the engine is compared with the same power output but bigger NA engine, as the engine becomes smaller, some components like pistons, poppet valves and bearings will be less, engine size reduced, the friction losses are reduced.
3. Higher inlet pressure and temperature produced by turbocharger will increase the gas mixture and fuel atomisation. It will also contribute to improve in-cylinder turbulence, promote faster burning rates to achieve better combustion (Attard, 2007).
4. Reducing heat losses. The exhaust energy recuperated by the turbine and the reducing of engine surface area due to the reduction of engine size will help to decrease the heat losses.
5. Downsized engine has lower weight which contributes to vehicle dynamic applications and fuel consumption.

The great benefits of engine downsizing makes people pay more attention to boosting technology, turbocharging is the most acceptable one in passenger car application, because it can deliver enough boost without consuming extra energy. Many researches have been done in the last few decades. MAHLE Powertrain developed a 3-cylinder 1.2L gasoline engine with two-stage turbocharger, Comparing with the 2.4 L NA engine with the same power output, this engine enables lower CO2 amounts by 50% and achieved approximately 25% to 30% on-road fuel benefit comparing with the 2.4L engine. (Lumsden *et al.*, 2009). UK Technology Strategy Board sponsors another highly downsized engine project called Hyboost Project. The project developed a highly downsized 1.0L gasoline engine by using a traditional turbocharger and an electrically driven compressor. In this system, electric compressor is mainly used for mitigating turbocharger lag, typically in the order or about 1~3s to in a process before engine goes onto the conventional thermodynamic only operation, this system has a 5% CO2 reduction in NEDC and is predicted to have up to 2% improvement in fuel consumption which has not been measured in real test (King *et al.*, 2013). Another highly downsized engine is developed by JWG Turner et al. (Turner *et al.*, 2014) who demonstrated that engine capacity can be downsized by 60% and still achieve the same torque curve. In this project, they developed a 4-cylinder 2.0L gasoline engine with a turbocharger and a supercharger. Vehicle with this engine system has a potential to reduce up to 35% CO2 emissions on NEDC, which targeting to achieve 35% fuel consumption benefit for the whole vehicle and 23% in engine system alone. This system still matches the power and torque curve comparing with Jaguar Land Rover AJ133 5.0L V8 engine.

Downsized Engine with boosting technology always has higher specific power output, by modifying the overall transmission, yielding to shift engine operating points to lower speed, this is called engine downspeeding(Schumann *et al.*, 2013). Turbocharged engine delivers higher torque in low speed region comparing with similar size NA engine. When the engine is working at low speed but high torque region, the blow-down losses can also be reduced, because of the delayed opening of the exhaust valve (Terdich, 2014). Since the engine friction losses is a positive function of engine speed and engine load, in which engine speed affects more in this part(Chen *et al.*, 1965), (Johansson *et al.*, 2011), (Kopeliovich, 2017), engine down-speeding can

help to reduce friction losses and lead to a more efficient operating condition. In this way, the required power is undertaken at higher efficiency operating points. However, as single stage turbocharged and supercharged engines have limit torque in low speed region comparing with NA engines with similar peak torque and power, it will impede the development of engine downspeeding in passenger car, how to increase the low speed torque in boosting system has also been a very significant issue. Currently, there are generally two methods to achieve downspeeding: the first strategy is to reduce gear ratio value in the transmission system or the final drive, so that engine speed is decreased in all cases; however, this method leads to a reduction in vehicle peak tractive force. Another strategy is downspeed engine speed by operating transmission gear shift instead of changing gear ratio, however in this case, upshifting operation will happen earlier because the requirement of vehicle speed, downshifting operation then is avoided in some cases (Wetzel, 2013).

Engine downsizing and downspeeding are widespread in nowadays vehicle design, boosting technologies also plays a significant role in this stage (Ostrowski *et al.*, 2012), (Turner *et al.*, 2014; Wetzel, 2013). By pumping more air into the engine cylinders to improve the internal pressure, more fuel can be injected into the engine, and the BMEP is increased. Also, with boosters, the engine can be operated at high torque but low speed condition to further increase engine efficiency. Figure 1.3 (Kleeberg *et al.*, 2006) shows the comparison of brake specific fuel consumption for different NA and turbocharged engines which have similar power and torque output. Downsized engine has a lower BSFC in the same operating points. The 1.8L turbo engine has much lower BSFC but the same power output in most region.

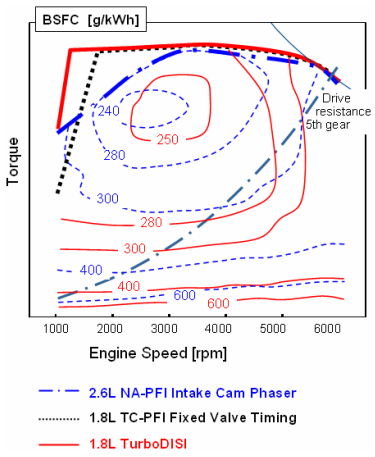

Figure 1.5 BSFC maps of different engines. (Kleeberg et al., 2006)

1.3 Challenges of turbocharged downsized engine.

Engine downsizing has been demonstrated to improve efficiency and fuel economy. Efficient downsizing is achieved with a turbocharger that recycles otherwise wasted exhaust gas energy. However, as engine downsizing becomes more aggressive, the demands on boosting system is increasing by time, higher pressure and gas temperature are more difficult to be controlled. Currently, turbocharged engine faced with the following problems:

1. Knocking problem. In a gasoline engine, there is a restrict of self-ignition limits with the air-fuel mixture (Turner *et al.*, 2005), as the in-cylinder pressure and temperature become higher for higher load that is required. The gas in the cylinder has an increasing chance of auto-ignites which is an uncontrollable process. Knock will lead to poor engine performance and mechanical damage. There are several ways to avoid knock: using fuel with more significant octane value or reducing the compression ratio can directly degrade knocking.

2. The lack of low speed torque. As the involving of the turbocharger, the smaller engine can output higher torque, but in low speed condition, the compressor cannot deliver enough boost pressure due to the energy leak on the turbine side. This low speed peak torque leak will affect pull away from rest and performance for tip-in manoeuvres (Lake *et al.*, 2004). Some assistant in low speed region can help deal with it. For example, figure 1.4 shows an example of engine torque maps for different engines, a 1L naturally aspirated engine can only deliver 70 N/m at peak point when 1.4L NA engine can deliver 115 N/m. After applying turbocharger on 1L engine, the peak torque is increased to 112 N/m which is similar to the 1.4L NA engine, however, the low speed torque is too low compared to 1.4L engine. After using another electric supercharger to deliver extra boost pressure in low speed condition, the problem is solved.

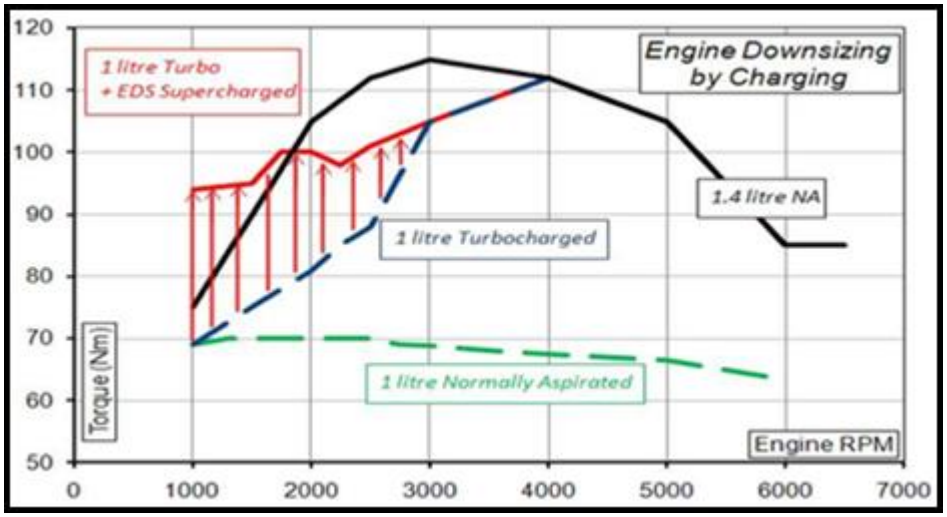

Figure 1.6 Engine downsizing torque map (DBS, 2017)

3. Poor transient response in low speed region. When a vehicle start or high load changes happen, the compressor needs time to reach the target rotating speed to accomplish specific boost pressure, due to the turbocharger inertial and power needed to accelerate it. In this period, the engine torque and the power map is not linear which will make drivers feel uncomfortable. This phenomenon has been named as turbo-lag. This problem together with the lack of low speed torque makes up a significant issue for low speed performance in turbocharged engine system.

4. Air path design. Downsized engine has a higher in-cylinder temperature, and different coolers need to be used to cool down the inlet air. Besides, due to the much stricter emission regulation, aftertreatment devices need to be installed at exhaust side, for example, EGR, DPF, and catalysts are used to reduce vehicle emissions and improve engine performance. These devices will affect the engine pre &post temperature and pressure and engine performance will be affected by them. Carefully design those devices with turbochargers certainly help to increase system performance.

4. Aftertreatment devices inlet temperature problem. Engine aftertreatment system needs to be more efficient since the emission regulation changed, as this kind of system has penalty on engine efficiency and can get significant benefit from the increase of exhaust gas temperature at device inlet

side(Burke *et al.*, 2019) , there is a compromise between turbocharger system and aftertreatment system (since turbine will drop-down the exhaust temperature.), the use of exhaust heat should be more efficient to meet the requirement for the whole engine system.

Another major challenge exists in downsized engine is the matching issue between the engine and turbocharger, even more, when the boost system has two or more stage boost devices, the matching between each boost device will also need to be concerned. The study on single stage turbocharger matching is quite straightforward and has been investigated and defined by the other researchers (Watson *et al.*, 1982; Burke *et al.*, 2019; Tancrez *et al.*, 2011) in the past. The aim of matching is to select the most suitable compressor and turbine for the targeting engine output performance(Watson *et al.*, 1982). Typically, the primary process of a single stage turbocharger is(Duda, 2017):

1. Defining the inlet air mass flow rate needed by the engine, which related to engine volumetric efficiency, scavenge flow, swept volume, boost pressure and air density.
2. Determine the target boost that engine needed under reference engine speed, select the compressor based on pressure ratio, corrected mass flow rate and speed, which should allow the engine complete operating line (speed and load range) superimposed on the compressor map, leave enough margin for surging and low efficiency area(choking).
3. Calculated the power needed for compressor, select the turbine that has enough power to drive it with overcoming the losses in the bearing system, considering the turbine thermal efficiency.

However, when related technologies are involved in the turbo-matching process, for example, two-stage boost system, more parameters and the degrees of freedom need to be considered. The difficulties now time changed from how to increase the system power density to how to achieve the target output and make the whole system efficiency, response as good as possible. For two-stage system, the core task is to solve the distribution of pressure ratios for each stage, since the pressure ratio and temperature changes in the low pressure stage is unknown at the beginning, the assumption should be undertaken for the pressure ratio for each compressor in the

system to achieve the final boost. Since the modern engine system becomes more complicated, EGRs, VGT, aftertreatment system et al. are involved at the engine exhaust air path, how to balance all these components becomes to a significant challenge, and wait for people to investigate.

In the last century, several boosting technologies have been investigated, and the turbocharger system can increase engine BMEP and reduce vehicle emissions. Comparing with supercharger and natural aspirations, it does not need extra power to achieve the boosting target, which can reduce the brake specific fuel consumption. As the WLTC and RDE test protocols have been applied, turbochargers now become the first choice for manufacturers when developing the latest internal combustion engines. However, the shortages of turbochargers also need to be carefully solved. Besides its poor performance in low speed region mentioned above, engine backpressure will be increased because of the turbine in the exhaust pipe; bigger backpressure will lead to a more significant engine pumping loss which happened during the cylinder scavenging process. Also, when an engine is running in high load and high speed, the waste-gate will be opened to bypass some of the exhaust gas, in order to make the turbine be operated at appropriate region. Some of the energy at high speed and high temperature exhaust is wasted during this stage.

Electric assisted boosting technology can be regarded as a significant method to optimise a turbocharger system(Liu *et al.*, 2018). This kind of system has many different types, but the critical factor is that the electrical devices are involved in to increase the turbocharger system's freedom or other properties. By using a motor or generator mounted the shaft, it has a great potential to reduce turbo-lag and increase the fuel economy. Panting(Panting *et al.*, 2001) breaks down the benefits of the electrically assisted system.

1. Turbine and compressor can be redesigned and optimised for better steady state efficiency.
2. Structure close to turbo compounding can utilise more energy in exhaust gas.
3. Electric part can help to generate more boost pressure in low engine speed condition which will help to increase efficiency and power.
4. The waste-gate is no longer needed here because the turbine can be controlled to achieve the target speed (Dimitriou *et al.*, 2017).

However, comparing with mechanical turbocharger, the reliability of electric boosting technology should be verifying, since electric motor need to be operated in a very high speed, packaging, reliability and cooling are the major issues need to be solved(Terdich, 2014). Matching problem is also another difficulty for multi-stage hybrid system, as electric turbocharger generally plays a role both increasing the transient performance and low speed torque, there will be a compromise between electricity costing of electric-turbo, surging of two-stage compressor and the adjusting between turbine VGT, electric turbo boost target(Liu *et al.*, 2017; Liu *et al.*, 2018). Besides, the energy from exhaust gas will be transformed several times more between turbine and compressor, which will reduce the turbocharger efficiency, so there is a compromise between energy harvesting and characteristics optimisation.

Electric-boost system nowadays has attracted the attention of researchers and engineers, as the development and expectation of hybrid tech from people. Manufacturers have chance to update 48 volts system to replace current 12V electric system on passenger vehicles, it offers the chance for vehicles to use more complicate electric system, for example, electric turbocharger, electric aftertreatment devices, dual-clutch transmission systems (Wearing *et al.*, 2018)and so on, also it can better make use of the energy harvested from vehicle braking system(De Cesare *et al.*, 2019) or turbo compounding system(Liu *et al.*, 2017). The needs of emission reduction in the recent future (2020 to 2035) not only create significant challenges but also offers the chance to researchers focusing on these kinds of hybrid system to develop higher efficiency and environmentally friendly engine system for vehicles.

1.4 Projects background.

The works in this thesis are based on two projects FETT (https://gtr.ukri.org/projects?ref=102284) and THOMSON project (http://www.thomson-project.eu/).

The FETT project is about the experimental and simulation study for optimising a new designed decoupled electric turbocharger, coupled with a 2.0L petrol engine system.

The target of this project is to map the compressor and turbine accurately, also find out the best controlling method for the electric compressor and turbine.

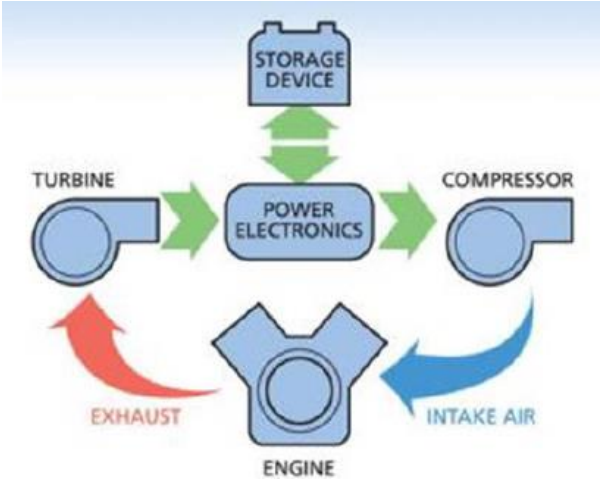

Figure 1.7 Aeristech's full electric turbocharger design(Aeristech, 2016)

The second project THOMSON aims to provide a quick transition towards high efficient, cleaner and affordable electrified powertrains focusing on 48V architectures. The key element is to increase the fuel economy, reduce environmental impact and support a quick penetration on the market. The outcomes of this project related to the thesis are the followings:

1. Engine independent boosting system performance metric.
2. Transient boosting system experimental evaluation methodology.
3. Simplified Boosting Component Models improving upon map-based approaches.
4. Methodology for two-stage transient matching.

Based on these two projects (together with other related works), the author went through the process of turbocharger system modelling and experiments, developed the knowledge and skills in multistage boosting system matching and electric boosting system optimisation.

1.5 Aim and objectives

This thesis aims to investigate the design of a mild hybrid boost system, find out if the hybrid boost system can improve system performance, considering the benefit of efficiency, power and transient response. The study covers both gasoline and diesel engine systems, based on a series of engine air path case studies, and discusses the benefits of a hybrid boost system through both an experiment and a simulation. In order to improve the performance and fuel economy of the internal combustion engine system further, a series of case studies, including engine inlet pressure drop optimisation, turbocharger heat transfer investigation, EGR transient performance and multi-stage turbocharger matching, were undertaken, all of which may contribute to the maximum improvement of the system's performance in the current stage. In order to fulfil the final aim above, a series of objectives were set:

1. To write a literature review on the multistage boosting system and its related technologies.

2. To design and build up the test facilities with the related method for evaluating the multi-stage turbocharger air path.

3. To verify the engine air path design and multi-stage turbocharger performance based on experiment results and calibration.

4. To develop the 1D diesel engine model with an electrically driven compressor, based on the experiment results, focusing on the system's steady state and transient performance.

5. To design the modelling methodology for a multi-stage turbocharger, studying the matching issues associated with a mechanically decoupled turbocharger on a gasoline engine, and considering the fuel and electricity balance.

6. To investigate the characteristics of a mechanically decoupled electric turbocharger, optimise its controlling methodology and increase the system's efficiency.

7. To study the potential benefit of an insulated turbocharger turbine, in both the simulation and experiment phases, in an attempt to achieve T4 enhancement.

8. To optimise the pipe junction geometry at the engine inlet air path, in order to increase the flow uniformity and reduce the pressure drop.

1.6 Scope of the thesis

From Chapter 2 to Chapter 8, the objectives above will be presented, respectively. The conclusion and suggestions regarding future work are summarised in Chapter 9. For each chapter, an overview is presented below:

Chapter 2 is the literature review of the current research on the engine boosting system and assesses the current studies on turbocharger technologies. The literature review details the challenges related to turbo-matching, the development of an electric boost system, and the difficulties in air path interaction in more comprehensive engine systems. This chapter helps to clarify the need for this thesis and explores the potential of a mild hybrid engine system.

Chapter 3 describes the systematic methodologies used in this thesis, illustrating the purpose of each cases study. Moreover, the test facilities and simulation models are introduced in the context of a particular research process.

Chapter 4 presents the modelling methodologies of this thesis. In this chapter, a 1D baseline multistage turbocharger model will be shown and verified based on the experiment calibration. After that, different electric boost models will be described together with their controlling methodologies, and the matching issues discussed, considering compressor scaling. Furthermore, a 1D turbocharger heat transfer model is given to study the current shortages exists in turbocharger thermal effects modelling. At the end of this chapter, the details of the 3D model case study in engine inlet air path TP junction and drive cycle simulation study will be given to help further optimise the system performance.

Chapter 5 presents the 1D modelling for the two-stage electric compressor system with the correlation of experiment results. The air path will be adapted to a 2.2L diesel engine to evaluate the steady state and transient performance, with the verification of related experiment data. This chapter explained the matching issues in multi-stage hybrid boost system with 1D simulation, comparing the differences between different types of electrically assisted turbocharger or electric compressor, showing the benefit of how they can help increase engine low speed performance and transient performance.

Chapter 6 applied the scaling method onto a 2.0L petrol engine with a decoupled electric turbocharger system. This study focused on the energy balance between EDC and E-turbine, also considering system efficiency changes. Later on, the model will be used for WLTC cycles and 0-100km acceleration process, in order to find out its benefit in both energy-saving and transient performance side.

Chapter 7 analyses the heat transfer issues exist in turbocharged diesel engine, using both heat transfer turbocharger simulation and experiment to study the benefit of insulated turbocharger, evaluate how it can increase the end exhaust temperature in different engine operation cases, without losing boost benefit on the compressor side. Since higher turbine outlet temperature can help increase the efficiency of aftertreatment system, a brief analysis of energy benefit will be given considering the cost of electric catalyst and electric compressor.

Chapter 8 presents the geometry design of the TP junction pipe between the electric compressor and turbocharger in multi-stage turbocharger engine system. By using CFD and topology analysing method, together with the genetic algorithm, this chapter evaluates how the TP junction affects the flow pressure drop and uniformity on the engine inlet side. Also, by optimising the geometry, combining with 1D simulation, the benefit of this study will be given at the end.

Chapter 9 is the conclusion of the thesis. It firstly outlined the formalisation of hybrid boost system optimisation procedures. Then the works of each chapter have been summarised. At last, the weakness and future work outlook is explained based on current research progress in this area.

Chapter 2 – Review of the electric boost system and air path design to downsize the engine

This chapter will introduce the current boosting technologies used in engine systems. The fundamentals of turbocharger and modern electric boost system will be presented in detail, illustrating how they can help to increase the engine's fuel economy and transient performance.

The challenges associated with multi-stage boosting system design will be reviewed. The issues and compromises during design are analysed, including sizing, surging, transient performance and efficiency trade-off, with examples of how they were solved by related technologies applied on the boost system.

Different electrically assisted boost systems will be compared, followed by an investigation of how electric boosting systems affect engine air path design. The current development and applications of the electric boost system will also be discussed, anticipating its potential in the near future.

At the end of this section, the difficulties of engine emission reduction will be briefly analysed, followed by a discussion of the air path interactions with the wider engine system, considering the role that the boost system and aftertreatment system plays in diesel engines, and how they contribute to engine combustion and emission reduction.

2.1 Fundamentals of boosting and turbochargers

2.1.1 Supercharging and turbocharging

Boosting technology has a history of more than 100 years (Watson *et al.*, 1982). Superchargers and turbochargers are widely used to downsize engines and reduce vehicle emissions; however, naturally, aspiration engines still play the main role in today's vehicle industry, because some deficiencies in boost devices exist and need to be solved, as before.

Superchargers are more general in high load diesel engines or highly boosted engine systems (Turner *et al.*, 2014). A supercharger has a compressor which is directly driven by the engine crankshaft via a gear train or belt and pulley system, so more fresh air is pumped into the cylinders (Bhinder, 1984). There are two types of supercharger, which are defined by how they supply boost air: positive displacement compressors and centrifugal compressors (Watson *et al.*, 1982).

Positive displacement compressors are more easily driven by the engine crankshaft due to their low speed and large size; it compresses the gas by reducing the gas volume with the displacement of a mechanical linkage. The gas will be compressed in a discrete volume and send to the exit port. This kind of compressor usually has a pipe system that can trap and discharge air in the cycle. There are many different geometry designs for positive displacement compressors; for example, Roots, Vane and Screw compressors (Watson *et al.*, 1982). These compressors are mostly used in passenger cars in the automotive area. The Eaton's twin roots type of supercharger is used in the Audi V6 3L gasoline engine (Eiser *et al.*, 2009) which reduces the fuel consumption from 10.9 L/100 km to 10.2 L/100 km. Turner et al. (Turner *et al.*, 2014) also used a root type supercharger installed serially with another turbocharger. The power and torque have been increased by 35% from a 2.0L gasoline engine and matched with a 5.0L V8 engine. The root type supercharger can deliver a high boost for downsized engines; however, it is thought to have low efficiency due to its non-internal-compression design (Stone, 1988).

The dynamic compressor compresses air by the rotating of compression impeller. It will accelerate the air to high velocity and then let the air discharged through a diffuser, and the kinetic energy is transformed into static pressure. The dynamic compressor includes the centrifugal type and axial type; the former one generally has a lower airflow range and pressure ratio; it is usually used on vehicle application.

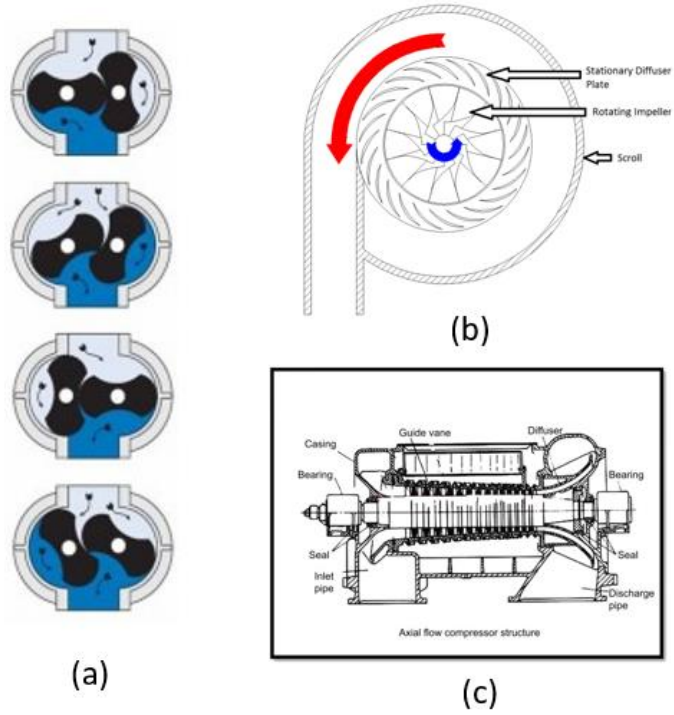

Figure 2.1 (a) Positive placement compressor (Screw type) (EnggCyclopedia, 2019) (b) Centrifugal compressor (CASCOUSA, 2019). (c) Axial compressor(Bahadori, 2014).

Centrifugal compressors or called superchargers, deliver boost pressure by accelerating the intake air to high velocity and converting it to high pressure air by diffusion. These superchargers are generally smaller but rotate faster (Watson *et al.*, 1982). The boost they supply is the square of the rotational speed, which means they can only produce a low boost at low engine speed (Rose *et al.*, 2011). Furthermore, because of its high speed requirement, a centrifugal compressor is usually driven by the crankshaft connection with step-up gears, which will produce more mechanical losses (Hu *et al.*, 2015). A centrifugal compressor is often coupled with a turbine as a form of turbocharger, using exhaust gas energy to drive the compressor.

Superchargers can deliver high boost target and an excellent transient response; however, they will cost engine power and decrease the vehicle's fuel economy. When the engine is running at high speed, the internal friction of the superchargers will be greatly increased, which leads to a negative influence on the supercharger rotation and produces a lot of noise (Uthoff *et al.*, 1987). Superchargers are rarely used in small sized engines; instead, they are more in better demand for high load engines and in the aerodynamic area.

Due to the low efficiency and high manufacturing accuracy, turbochargers almost monopolise the boosting applications in daily-use vehicle manufacturing. Turbochargers can pump more air into the cylinders by exceeding the air pressure. Unlike superchargers, turbochargers have a turbine in the exhaust manifold, which can increase the resistance in the exhaust. When the engine is working, the exhaust from the cylinders spins up the turbine. This turbine is connected to a compressor by a shaft. The compressor is installed at the inlet side of the engine, which is a type of centrifugal pump, driven by the torque from the shaft. The more exhaust goes through the turbine blade, the faster it spins, and the pressure of the intake air will be higher.

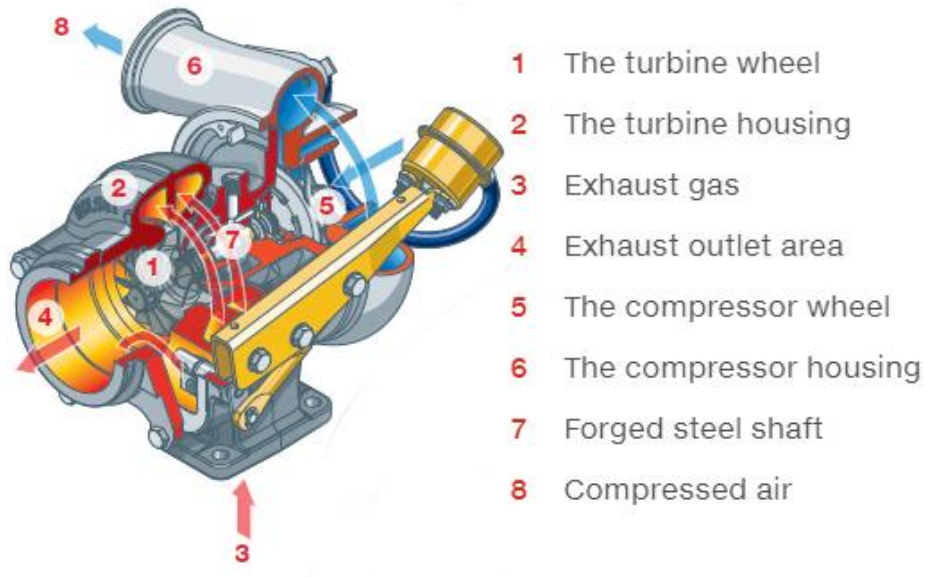

Figure 2.2 Turbocharger structure (Cummins, 2019)

As mentioned above, a turbocharger compressor is generally of the centrifugal type, which is smaller, more efficient, and faster. The air is accelerated by a compressor wheel and turns from the axial to the radial direction, which is the design of compressor

geometry. The volute of the compressor wheel will then reduce the high-speed flow, converting it into high pressure and density air. This boosted air will pass through the intercooler before entering the engine. The intercooler will reduce the air temperature and further increase the air density, which will help to increase the engine's BMEP.

Turbines on the exhaust side are designed to harvest energy from exhaust gas. With a similar appearance to a compressor, a turbine often has a volute and wheel. Some significant turbines also have nozzle rings. When the high speed and temperature exhaust gas passes through the turbine, the volute and wheel will discharge the gas from the radial to the axial direction. The gas is accelerated, but the pressure and temperature are lower. If there is a nozzle ring, this will further accelerate the gas and change the gas flow angle for being closer to the wheel (Japikse *et al.*, 1994).

Thermodynamically, turbochargers recycle the energy from the exhaust (velocity and heat) which is energy-saving, and the additional power is generally higher than for superchargers, depending on the matching of the turbocharger. It potentially has a lower BSFC compared with similar power supercharged engines and NA engines (Stone, 1999). Superchargers are driven by the engine crankshaft which makes the engine intake pressure exceed the exhaust pressure. The pumping work is a positive value, however the driving supercharger leads to more fuel being combusted. On the contrary, a turbocharger turbine will increase the engine backpressure, and the pumping loss will be greater in the engine scavenging process.

2.1.2 Single stage turbocharger related technologies.

Engine downsizing offers a proven route to improve efficiency by increasing the specific power output and provide a net reduction in friction losses of up to 25% (King *et al.*, 2013; Turner *et al.*, 2015). Efficient downsizing is achieved through the use of turbochargers that recycle otherwise wasted exhaust gas energy. As engine downsizing becomes more aggressive, the demands on the boosting system become greater such that conventional turbocharger technologies struggle to meet the flow demands and the transient performance requirements (Watson *et al.*, 1982). The design compromise for the turbocharger turbine is the balance between a small turbine that favours low

speed torque and transient response against a larger turbine that promotes peak power (Arnold, 2009). A series of technologies were developed in the last few decades, for further improving the engine performance and fuel economy.

Turbine waste-gate and compressor bypass valve

Many different methodologies are discovered by manufacturers to overcome matching and transient response problems. In order to expand the turbocharger working range, compressor bypass valve and turbine waste-gate are introduced (Figure 2.3). When an engine works in low speed, low load condition, boost pressure is no longer needed, but a low speed compressor now will resist the air absorbing into the engine. A bypass valve is introduced to allow air going through the inlet manifold without passing compressor; in this way, turbocharger stops working in that low load region but makes no negative impact on engine characteristics. A waste-gate is used to bypass part of high temperature exhaust when the engine runs at high speed and load condition (Baines, 2005). It can limit the turbocharger boost pressure and avoid over-speeding. Meanwhile, the excess exhaust energy is wasted during this stage.

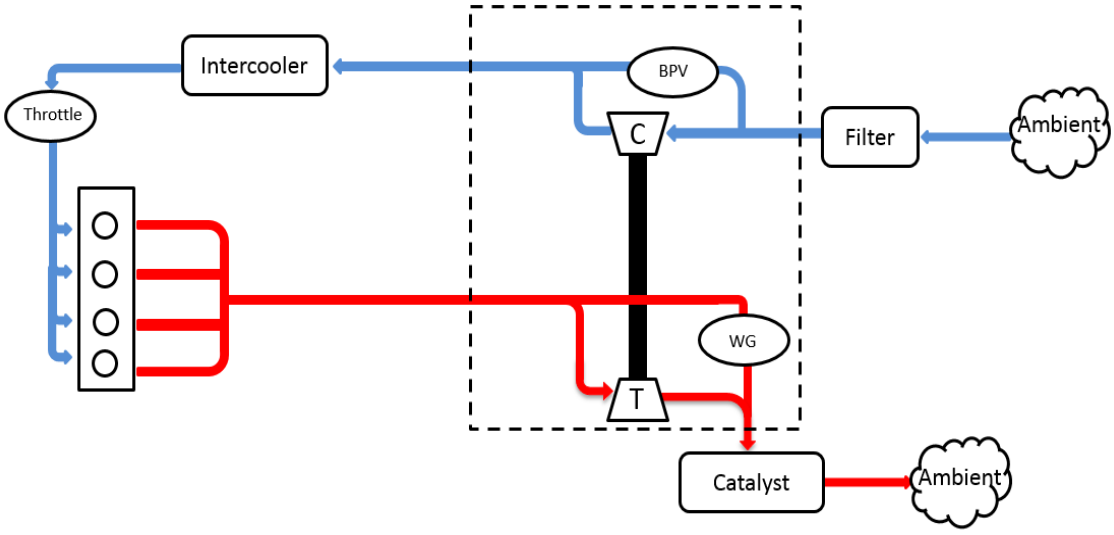

Figure 2.3 Turbocharger Structure.

Ball bearing turbocharger

Turbocharger works in high speed and temperature condition, the rotor shaft speed can exceed 200 kRPM in small turbochargers. The high exhaust temperature will also increase turbocharger temperature, so the characteristics of the bearing system

supporting the turboshaft are highly important. Most turbochargers use floating ring bearings supported by the thrust bearing in the axial direction, this bearing system is very reliable, it has low cost, and high robustness (Conley *et al.*, 2019; San Andres *et al.*, 2006). However, this system is not efficient (power dissipation 2 to 10% depends on speed and size). enough under high speed and temperature condition due to the mechanical losses and heat losses it produced Ball bearing system has been investigated in recent years, different from traditional bearing system, it used a cartridge with two angular contact ball bearing, and both axial and radial load can be supported. Ball bearing system has been demonstrated to have lower friction than that of floating ring bearings. The lower friction will help to decrease system inertial lag. Miyashita et al. (Miyashita *et al.*, 1987) developed a ball bearing turbocharger, the result shows that the mechanical efficiency of ball bearing reaches to nearly 99% at maximum, it was increased by 20% at low mass flow range and 5% at high mass flow range comparing with floating metal bearing, but this system highly relies on the lubrication properties. Keller et al. (Keller *et al.*, 1996) simulated the performance of ball bearing turbocharger in transient response analysis. It was confirmed that ball bearing has an 80% to 90% benefit on transient amplitude reduction. However, this system is much more expensive and complicated than floating ring bearings, the bearing house need to be carefully designed, its durability is generally worse, besides, ball bearings are less efficient in high speed region and produce much noisy.

Mixed flow turbocharger turbine

Nowadays, turbocharger turbines are mainly in radial structure, the exhaust flow goes through the turbine from the axial direction to the radial direction under the guidance of the zero-angle turbine cone blade. This kind of design can maintain the radial blade sections for stable centrifugal load in blades purely tensile, and it can also generate the most power in high load condition. However, for low speed but high load diesel engine, which means the exhaust gas is in low temperature but high density, the turbocharger is required to deliver enough boost, it can only be achieved by applying small general geometry designed turbocharger with high rotational speed, which has extremely low efficiency. Mixed flow turbine can help to deliver more boost in this condition, due to its higher efficiency in low velocity ratio cases (peak efficiency operating points generally laid in lower speed region (Karamanis *et al.*, 2002). However, a mixed flow turbine will reduce turbine power but increase the thrust load,

it will also be harder for applying turbo related technology on its structure, for example, variable geometry turbine design. Figure 2.4 shows the differences between the radial turbine and mixed flow turbine.

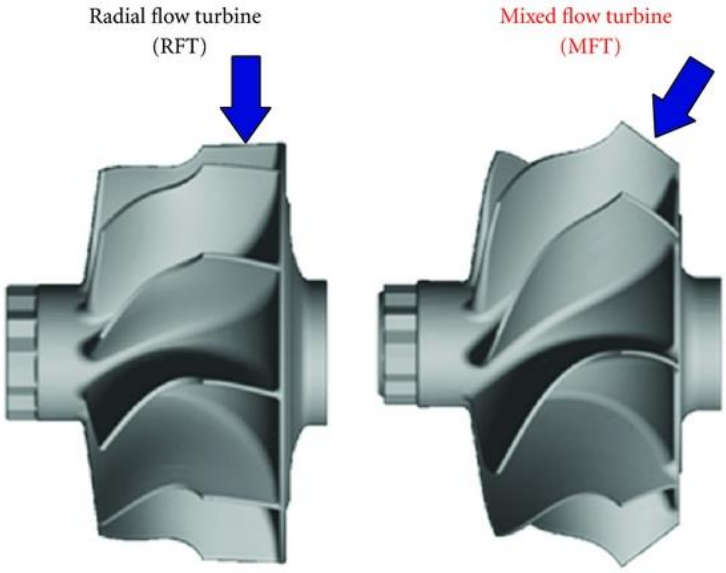

Figure 2.4 Radial turbine and mixed flow turbine (Lüddecke et al., 2012).

Variable geometry turbocharger

Variable geometry turbocharger design is another powerful way to improve turbocharger characteristics. The turbocharger aspect ratio is an essential factor that affects the boosting ability and transient response ability. VGT turbine can change the angle of variable vanes in the turbine house to adjust exhaust flow against the turbine blades. Comparing with waste-gate turbocharger, it has many advantages. By adjusting the vane angle to achieve suitable turbocharger maps, higher peak torque can be produced at low engine speed; it also improves the whole engine output performance without increasing pumping loss when the vehicle is driven in high engine speed condition (Xin, 2011). Figure 2.6 shows the expansion ratio vs mass flow rate of turbines with fixed or variable geometry; obviously, VGT turbine has a much more comprehensive application range and better performance. A series of researches shown (Baines, 2005; Kawamoto *et al.*, 2001; Matsura *et al.*, 1992) that VGT can help improving transient response at low engine speed. However, the performance of VGT mainly depends on the type of turbocharger it attached to, and transient response

cannot be solved. Complicated structure significantly increased the cost and manufacturing difficulties and reduced the reliability of this kind of system.

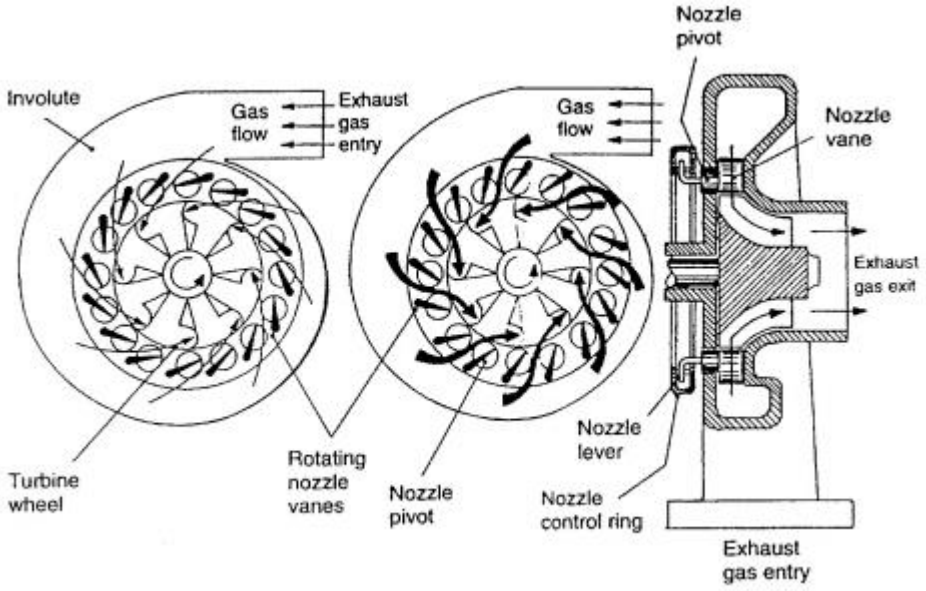

Figure 2.5 VGT (Hawley et al., 1999)

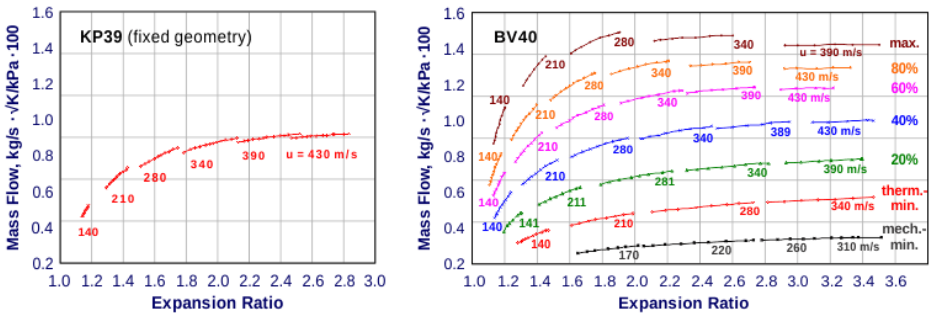

Figure 2.6 Comparison of fixed geometry (BorgWarner KP39) and variable geometry (BorgWarner BV40) mass flow vs pressure ratio (Jääskeläinen, 2016).

Turbo-compounding

Turbo-compounding is defined as a turbocharger (coupled or decoupled) that has some linkage and power transmission with the engine (Watson *et al.*, 1982). There are four different structures of turbo-compounding system, as shown in Figure 2.7.

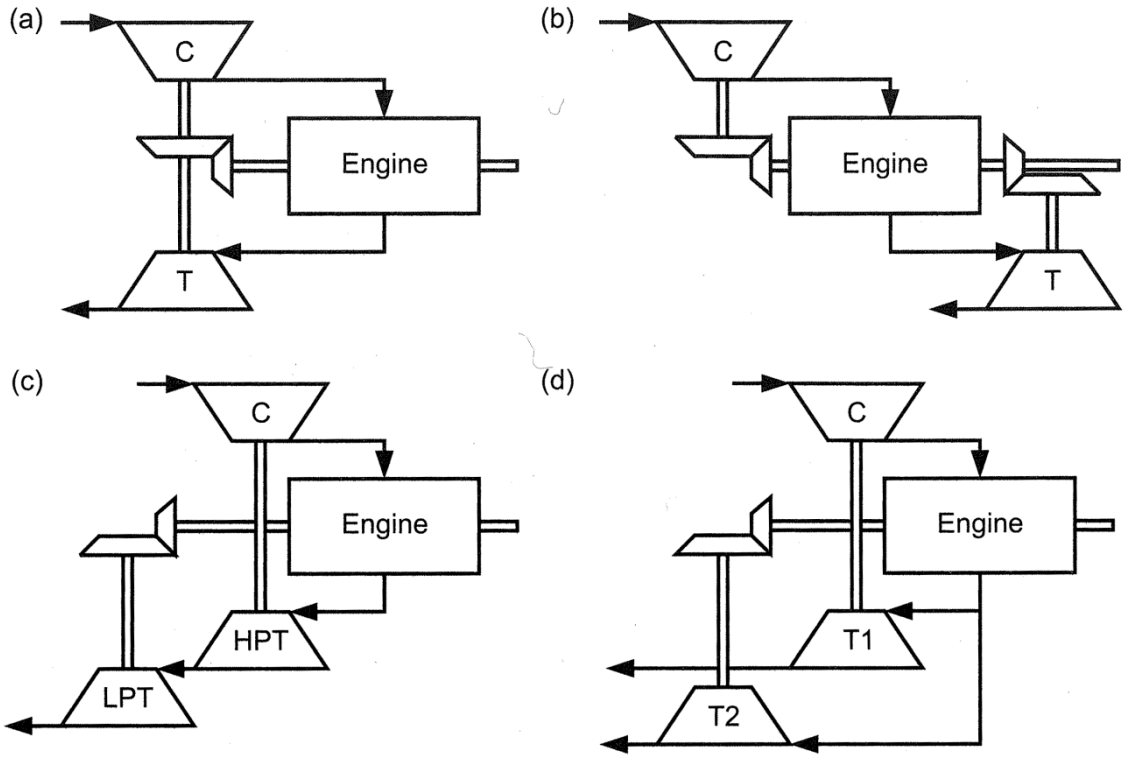

Figure 2.7 Four kinds of Turbo-compounding Layout (Baines, 2005)

In Figure 2.7(a), the engine is connected to a turbocharger by a shaft with a transmission system. It can assist the turbocharger when the boost is insufficient in the low speed and torque region, which will also improve the transient response; however, the transmission ratio matching problem is very complicated here, especially regarding the load condition (Baines, 2005; Watson *et al.*, 1982). CVT (Continuously Variable Transmission) has the potential to solve this problem, as it can enable the turbocharger to rotate independently of the engine speed (Rose, 2013). This kind of turbo-compounding system is used to downsize a 3.2L V6 gasoline engine to a 2L 4-cylinder TC engine by VanDyne et al. (VanDyne *et al.*, 2013). It was named a Super-Turbocharger, which has worse BSFC at full load but better BSFC under a part load condition. Their result shows that this system offers a 17% fuel saving benefit in the NEDC cycle compared with the original turbocharger engine.

Figure 2.7(b) shows that the compressor and turbine are connected to the engine separately. This system faces the same problem as the turbo-compounding in figure (a); however, it introduced a higher degree of freedom into the system so that the compressor and turbine can rotate at different speeds. Wallace et al. (Wallace *et al.*, 1983) conducted some iterations for this system using a two stroke and four stroke

heavy duty diesel engine. The result showed that it offers a benefit in terms of transient response and fuel economy but that this design is still in the research stage due to its complicated structure.

Figures (c) and (d) are the design of a turbocharger with the power turbine. These two kinds of systems are more useful in heavy-duty vehicles. Baines (Baines, 2005) and Wallace and Cox (Wallace *et al.*, 1998) concluded in their research that this type of turbo-compounding system can only be applied to engines that always operate with a very high level boost and BMEP, and are unsuitable for passenger cars that work with a part load generally. From the study, it was shown that the turbo-compounding engine system has better BSFC and efficiency under a full load condition but, at low loads, the engine has to drive the turbine at a loss, which reduces the turbo's efficiency.

2.1.3 Multistage boosting technologies

Low temperature combustion is regarded as an advanced technology since it has higher efficiency and less pollution (Hasegawa *et al.*, 2003; Sjöberg *et al.*, 2005; Turkcan *et al.*, 2018). In order to solve the deterioration of NOx emissions, EGR is used; however, this will lead to a soot emission problem. Increasing the boost pressure and reducing the intake temperature can help to reduce the emissions (Osada *et al.*, 2012; Wakisaka *et al.*, 2009). Single stage turbochargers with a high compression ratio can deliver a high-density intake air, but it will lead to a limited mass flow range and a high turbo speed for most of the operating area. In order to overcome this issue without losing transient performance, two-stage turbocharger systems can be used(Plianos *et al.*, 2008; Navrátil, 2006). Twin-turbos can have a better transient response, peak torque and higher efficiency compared with single stage turbochargers. It also extended the boosting system operating region, for example, Figure 2.8 shows the two-stage turbocharger system operating region, and how it extends the operating region.

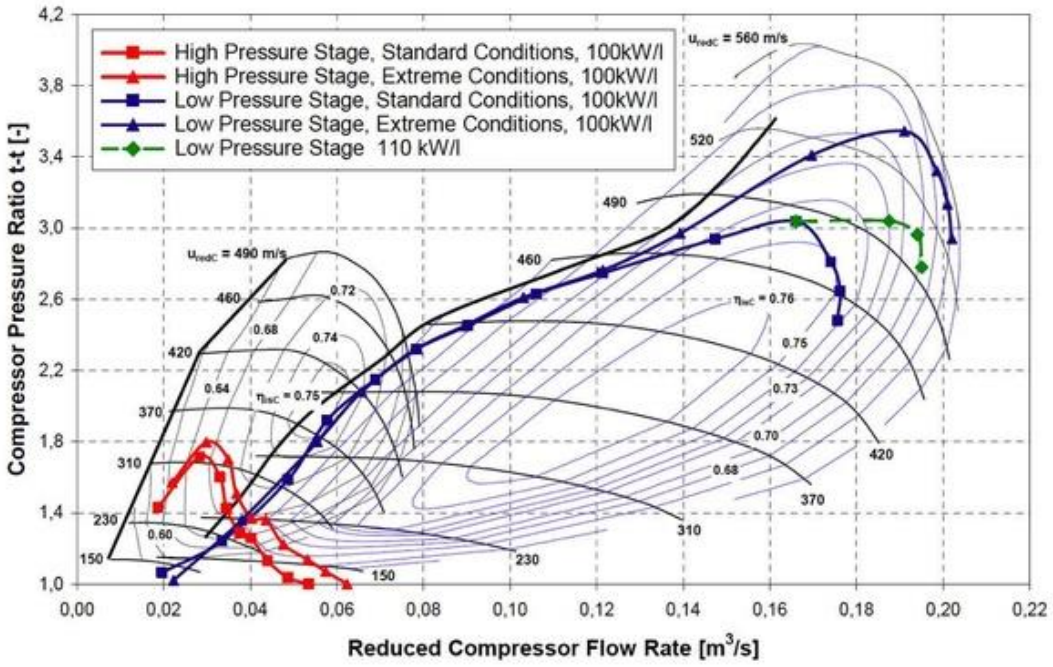

Figure 2.8 Sequential connected two-stage turbocharger operating region. (BorgWarnerTurboSytems, 2018)

Two-stage turbochargers often have two methods of connection ways: parallel and sequential connection. Each of them has different functions. Parallel twin turbo always has the same two types of turbocharger, which are used to replace large turbochargers in high displacement engines. The two turbochargers are installed in parallel. They are connected with engine exhaust manifolds and share the exhaust from the engine. The compressed air they apply will be combined in a standard intake manifold and then sent to a cylinder. Parallel twin-turbo systems use two small turbochargers to finish the same task as an individual larger turbocharger. In this way, the turbo lag can be greatly reduced (Luttermann *et al.*, 2007). It expands the pressure ratio and mass flow rate that can be applied to the boost system, but further increases the turbocharger's backpressure and decreases the turbo efficiency.

Figure 2.9 shows a typical structure of a sequential two-stage turbocharged engine system. It has a bypass valve and a waste-gate. The high pressure turbocharger is often smaller than the low pressure one. By adjusting the inlet air path between the two compressors, this kind of boosting system can be applied to a wide range of original maps to optimise them. When an engine works at low speed, the bigger turbo is

bypassed by the valve, and the boost target can be completed by the high pressure smaller turbine, which produces less turbo-lag. As the engine speed increases, high pressure turbochargers can no longer produce sufficient boost pressure so that a large turbine will be brought into action. The two turbochargers work together. The airflow path will be adjusted to control the mass flow rate passing through these two turbos, depending on the engine speed and load requirements. When the engine speed is high enough, the small turbine is bypassed and that big turbine will work alone for high boosting pressure. In this way, the sequential turbocharger can achieve good performance at both low and high engine speeds. However, there are studies on it shows that this system is not good enough, this system needs extra turbochargers and intercoolers which will significantly increase the cost and manufacturing difficulties. In most operating points, the exhaust gas energy is shared between two turbines, which will negatively affect the transient performance (Baines, 2005). Zhang (Zhang, 2015) studied a series installed twin-turbo on a 2.2L diesel engine both in simulation and experiments. The results show that the torque rising transient response speed is 50% faster than that of the novel turbocharger at 1000RPM, and it also has further emission reduction benefits, but the controlling methodology is challenging to design between the two turbochargers, which needs to be discussed in the future. Saulnier (Saulnier *et al.*, 2004) simulated the 1.5L two-stage turbocharged diesel engine transient response by using different turbocharger matching choices. However, the results show that, compared with a 2.0 L single stage turbocharged diesel engine, this one has a worse transient response in the low speed and load region, even with optimal matched turbochargers. The reason is that two-stage turbochargers cannot meet the requirements regarding either high-speed output or low-speed transient response, so the researchers advised using an electric turbocharger or compressor, which has a better transient response.

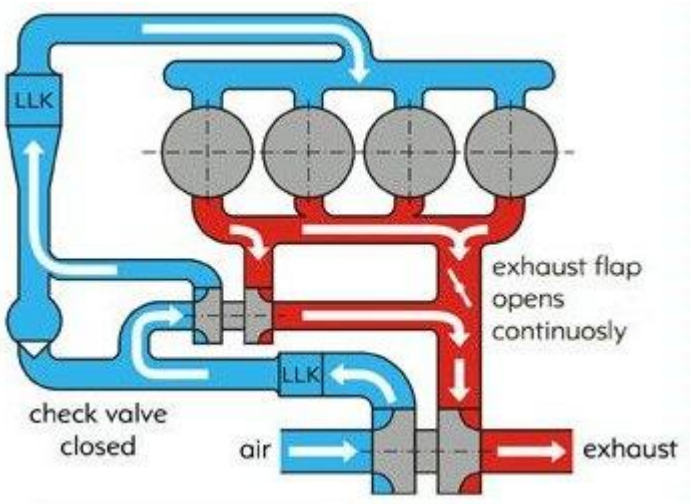

Figure 2.9 Sequential twin stage turbocharger (Wan, 2016).

Compared with traditional turbochargers, both VGT and multi-stage turbos can reduce turbo-lag, and expand the turbocharger high performance area. However, they have a complicated mechanical structure, which will reduce the reliability of the boosting system and greatly increase the manufacturing difficulties and cost. The main advantage of VGT is that it alleviates the dilemma between transient responses and rated power efficiency by changing the effective turbine area (Zhang, 2015). It 'extrapolates' the turbocharger map during operation. However, this method has a limited application. VGT turbochargers have a bigger size, they need to meet the high speed torque requirement, and have large inertia. Also, under low speed low load conditions, VGTs can reduce the transient response but not very much due to the lack of gas. VGTs are also hard to be applied on a gasoline engine because the exhaust of a gasoline engine has a higher temperature, which makes it harder for the industry to find a suitable material from which to produce the device (Hawley *et al.*, 1999). Twin turbochargers are another way to find a compromise between transient response and rate power efficiency; however, these are far more expensive than other technologies. Moreover, the matching and controlling problems are very significant in this application. Without an ideal matching and controlling scheme, twin turbos may perform worse than novel turbochargers (Saulnier *et al.*, 2004) and different control modules may fight with each other or the main ECU controller due to the unstable manner and an excessive number of many controllers used (Zhang, 2015). All of these turbocharged systems are still ultimately limited by the available exhaust gas energy due to its turbocharger-only based design, which will cause the transient response

issues to multiply in highly boosted applications (Wijetunge *et al.*, 2004). However, nowadays, the emission regulations are far stricter, which need internal combustion engines to be highly downsized to reduce the emissions. Moreover, the requirements of the customers are never reduced. Neither drivability nor safety can ever be sacrificed and even need to be improved. Electric boosting technology has been brought into this area because of the rapid development of electric motors and batteries in the last few decades, and the electrification of automotive engineering has become an inexorable trend.

2.2 Electric boost systems

Vehicle hybridisation and electrification technologies have become the most significant trend in powertrain development, and the electrification of powertrains is now the accepted roadmap for automotive vehicles (Ostrowski *et al.*, 2012). In vehicle engine systems, turbochargers and aftertreatment devices have made equally significant contributions to improving efficiency and reducing emissions (Stone, 1999; Turner *et al.*, 2015). However, turbochargers are also associated with compromises, which include poor performance at low engine speeds, high torque operating conditions, delayed transient responses (turbo-lag), and increased engine back-pressure (Watson *et al.*, 1982). To overcome these shortfalls, many different technologies related to boosting the system are being considered. The use of VGT and multistage turbochargers has been a favoured approach in the last few years, as mentioned above. They can improve the transient performance in low speed regions, and also increase the low speed torque. Due to the limitation of the mechanical design, there are still some working conditions in which they struggle because of the limited exhaust gas energy. The adoption of 48V systems offers a chance to facilitate the use of technologies, such as electric boosting and integrated starter-generators. The introduction of these technologies offers new opportunities for engine air path design, as an electrical energy source may now be used in addition to the conventional mechanical and exhaust thermal power used in super- and turbochargers (Burke *et al.*, 2019; Liu *et al.*, 2018; Xiao *et al.*, 2018; Zhao *et al.*, 2019).

Electrically-assisted boosting systems are a form of mild hybrid that makes use of electrical energy to supplement the turbine or compressor power. They have attracted

more interest in recent years as the technology required to make high speed electric motors has been developed, and the possibility of 48V vehicle systems has become more popular (Rick *et al.*, 2015; Timmann *et al.*, 2014). Currently, electrically-assisted boosting systems are being investigated both for diesel and petrol engines (Panting *et al.*, 2001):

1. The electric motor/generator supplies an extra degree of freedom, which helps to address the design compromises.
2. There is an inherent ability to recover exhaust energy if the electrical machine is linked to the turbine
3. The power used to compress the intake air becomes independent of the power available in the turbine.
4. The electrical energy can be used to address the transient response issues, meaning that the engine parameters can be designed for efficiency (valve timings, turbine and compressor sizes).

Moreover, since the turbine and compressor are independent, wastegate, throttles can be redesigned to allow the compressor and turbine to work more efficiently. The inertia of the compressor is regarded as being reduced without sacrificing its characteristics, which can help to increase the transient response considerably.

There are many different types of boosting system, which include electrically-driven compressors with turbochargers, decoupled electric turbochargers, electrically assisted turbochargers and turbo compounding systems.

2.2.1 Electrically driven compressor (EDC)

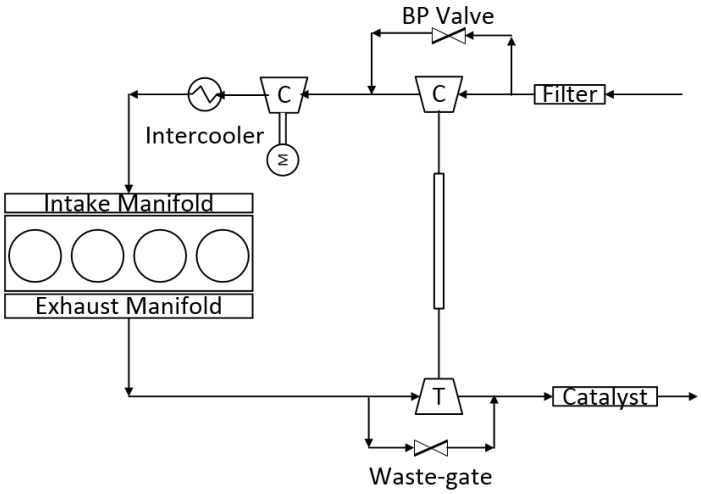

Figure 2.10 Electrically driven compressor (EDC) with a turbocharger system

Figure 2.10 shows a high-pressure, electrically-driven compressor (EDC) and a turbocharger system. The former is generally used in a multi-stage application with a turbocharger. It is used to increase the maximum boost pressure at low engine speeds and improve the transient response (Shahed, 2006; Turner *et al.*, 2015; Pallotti *et al.*, 2003; Rose, 2013). Pallotti et al. (Pallotti *et al.*, 2003) presented a simulation and experimental study where an electric compressor was used to downsize a 1.6L petrol engine to 1.4L. The smaller engine achieved a similar performance in terms of engine torque and reduced fuel consumption on an NEDC cycle by 12%. In addition, about a 1 to 1.5s transient time improvement was achieved at 60-100km/h and 80-120 km/h accelerations. The system was based on a 12V electrical supply and drew about a 200A current, which was double the expected value. This level of electrical power consumption is far better suited to a 48V system. Turner et al. (Turner *et al.*, 2015) introduced an experimental-based study of the 'Supergen' system, by mounting a compressor with an electric motor and engine crankshaft, together with another turbocharger. This system overcame the limit of the low speed torque that had been observed in a two-stage turbocharging system. An increase of about 1.3 to 4.3% system efficiency under a part load condition was achieved better transient response. Hopmann et al. (Hopmann *et al.*, 2003) built up an EDC model with the assumption of 85% electrical system efficiency for a 14.6L heavy duty diesel engine. A 2.5% to 10% fuel consumption reduction was predicted and this system also has the potential

to increase the rated power output. Wijetunge et al. (Wijetunge *et al.*, 2004) replaced a mechanical supercharger with an EDC in a two-stage turbocharging system in order to downsize a 2.0L HSDI diesel engine to 1.4L. They announced that the use of EDC makes the matching process far easier and avoids a large increase in engine backpressure, but the specific benefits in fuel consumption were not discussed. Rose (Rose, 2013) reviewed various publications: both single stage and two-stage EDC systems can provide a good transient response, because the extra compressor causes no backpressure. Therefore, the two-stage EDC can greatly help with engine downsizing but, compared with the traditional two-stage turbochargers, single stage EDC increases the electrical load whilst not recovering any exhaust energy.

The EDC generally is applied together with a turbocharger, since an EDC-only topology wastes the energy in a hot exhaust. There are two ways to consider where the energy comes from to drive the EDC. The first way is to use a battery supplying electric power. This was unrealistic before with an internal combustion engine vehicle since the battery is 12V, but the EDC needs about a 100A to 200A current to work (Pallotti *et al.*, 2003). However, the development of the 48V system offers a chance for the EDC to be applied. The whole 48V system generally can supply 5kW of power, when EDC in a two-stage passenger car engine system costs around 2kW of power (Breitbach *et al.*, 2015; Liu *et al.*, 2018). Another method to drive the electric motor is to use the crank-mounted electric system (alternator, inverter, gearbox), and some authors discussed its effects in the past (Lefebvre *et al.*, 2012; Katrašnik *et al.*, 2005; Divekar *et al.*, 2010; Terdich *et al.*, 2014). It will cost engine power instead of battery power. Burke (Burke, 2016) summarised in his review how, for small size EDC applications, the power ratio taken from the engine ranged from 0.5% to 10%., this will also drop the engine torque as EDC increases the attached load. The main difference between these two driving methods is the power sources, so it is necessary to analyse which way is more economically and environmentally friendly; however, most of the literature emphasized the fuel economy and transient response benefit introduced by EDC. Liu et al. (Liu *et al.*, 2018) examined the compromise between the EDC power consumed and engine pumping loss for these two cases, using an equivalent BSFC to evaluate the system efficiency. EDC using a battery as a power source is more efficient. However, Liu et al. assumed that electric power is ideal and there is no loss during transmission.

For the two-stage system, EDC is required to increase the system baseline peak boost pressure and improve the engine low speed output and transient response. The location of the EDC can be upstream or downstream of the turbocharger. The downstream design is supposed to have better transient performance (Lee *et al.*, 2016b), however, the authors showed no evidence for that opinion. Further investigation is still needed since the location of the EDC will affect the engine inlet temperature, the location of the EGR outlet port and intercooler; also, the EDC has the potential to increase the mixing of EGR and fresh air.

2.2.2 Electrically assisted turbocharger (EAT)

Electrically-assisted turbochargers are conventional, mechanically-coupled turbochargers with an electric motor/generator mounted on the main shaft. This system combines the mechanical efficiency of a conventional turbocharger with the ability to recuperate exhaust energy and improve the transient performance (Tavčar *et al.*, 2011; Arsie *et al.*, 2014; Dimitriou *et al.*, 2017; Katrašnik *et al.*, 2005; Panting *et al.*, 2001; Terdich, 2014).

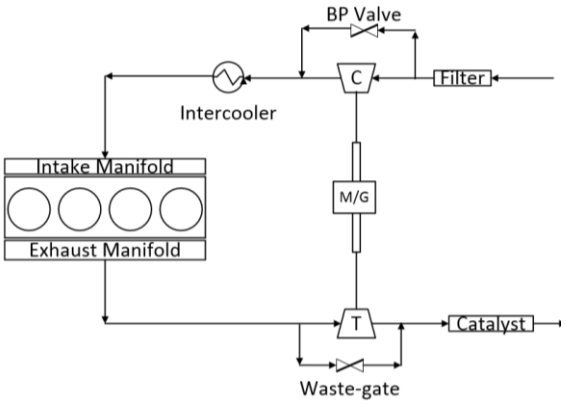

Figure 2.11 Electrically assisted turbocharger system

The system has an inherent ability to generate electrical power, meaning that it does not introduce a large burden onto the engine alternator. When the engine load and speed are increasing, the motor will help to accelerate the turbocharger, thereby reducing the turbo-lag and pumping loss. Arise et al. (Arsie *et al.*, 2014) built up a simulation model for this system. There is a 4.6% CO2 reduction for the NEDC cycle compared with similar turbocharged engine models. Dimitriou et al. (Dimitriou *et al.*,

2017) studied the transient performance of an electrically-assisted system with regard to the step load and drive cycles. There was a 70% to 90% time improvement in the transient process for specific engine torque and power targets, and more than 1kW average power can be generated in different drive cycles. Tough electric losses were not considered in this simulation. This boosting system needs less energy input than an EDC because it can recuperate energy itself, which will significantly reduce the burden of the vehicle battery. Ibaraki et al. (Ibaraki *et al.*, 2006) announced that, in their experiments, the turbo transient response time was reduced by 40% to reach the target pressure. When the engine was at 1000 and 1200 RPM, the torque was improved by 17%. They confirmed that an electrically-assisted turbocharger has better or equal performance compared with VGT; however, in their tests, the input voltage of the inverter is 72V, which is much higher than daily vehicle batteries, so the energy balance needs to be carefully designed. Katrašnik et al.(Katrašnik *et al.*, 2005) developed an EAT model based on a 6.9L six-cylinder diesel engine which has been calibrated and validated with experimental data. This 0-D simulation result shows that, for different electric motors with various power levels, the turbocharger transient response can be increased from 3.9s to 1.7s for a 25% to 100% load step at 1500 RPM. Zhao et al. (Zhao *et al.*, 2019) developed a two-level energy management framework for a 6-cylinder 7.01L ETA diesel engine, which is faster and more accurate in both the transient and steady state process. They also announced that, by applying EAT, the engine system had a better transient response.

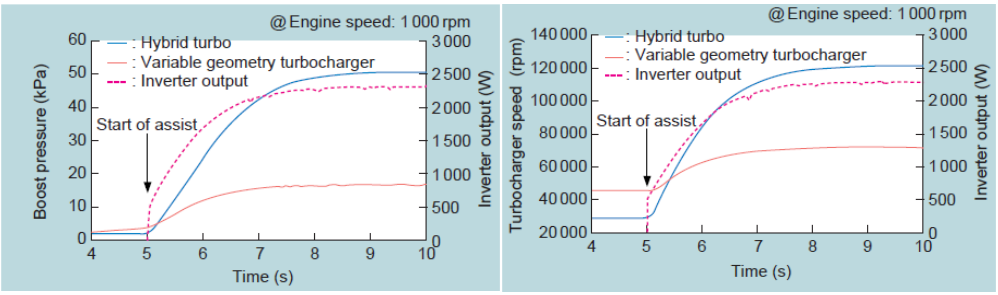

Figure 2.12 Comparison between the transient response of the turbocharger speed and boost pressure with the use of a hybrid turbo and VGT (Terdich, 2014)

Terdich (Terdich, 2014) showed that, by using an electrically-assisted turbocharger, waste-gate and variable geometry turbine devices are no longer needed, because the motor/generator can control the turbocharger speed. When the exhaust energy is sufficiently high, the device can work as an electric turbo compound device. The major

challenge with such a device is the design and packaging of the electric machine that must operate at high rotational speeds, without adding significant inertia and surviving the high temperatures caused by the exhaust gases.

There are two challenges associated with this type of design. The first is the balance between the output performance and packaging. The turbine and compressor have a high rotating speed, and also need to a motor with an excellent transient driving ability to accelerate or decelerate the turbo, so the requirements of this motor/generator are high (Balis *et al.*, 2003). The size of this electric motor will also greatly affect how it is packaged into the turbocharger house and also increase the inertia of the turboshaft, so the transient response benefit is lower than that with other electric boost systems (Katrašnik *et al.*, 2005). Last, when the electrical motor is working, considerable heat transfer will occur between them, so the heat transfer management inside the boosting system needs to be carefully designed (Balis *et al.*, 2003; Ryder, 2006). Induction switched reluctance, and a flux-switching permanent magnet machine can be used for this device (Lee *et al.*, 2016b). BMW developed clutches to connect and disconnect the shaft, which means that the e-motor is mounted outside the turbo-housing (Kresse *et al.*, 2011).

2.2.3 Mechanically decoupled turbocharger

The third type of e-boosting technology is the mechanically-decoupled electric turbocharger. As shown in Figure 2.13, the compressor and turbine are mechanically decoupled and connected to an individual motor and generator respectively. This system removes the shaft connecting the compressor and turbine, which reduces the overall efficiency from the turbine to the compressor (as the bearing system generally has 10 to 20% power losses), as two separate mechanical/electrical energy conversions must be performed (60% to 80% total energy conversion efficiency). The benefit of this decoupling is the fact that it makes it possible independently to control the turbine and compressor speed (Divekar *et al.*, 2010):

- In steady state operation, this means that the high efficiency of both devices can be achieved.
- In transient conditions, the engine boost pressure delivered by the compressor can be controlled independently of the exhaust backpressure caused by the turbine.

The Aeristech (Aeristech, 2016) company has studied the full electric turbocharger technology. They announced that a decoupled electric turbocharger could reduce the pipework under the bonnet, which will reduce the manufacturing cost. Also, this system has lower energy loss and costs compared with the multistage and VGT turbocharger. Besides, it allows the turbine to generate energy when a traditional turbocharger uses a waste-gate to split the gas.

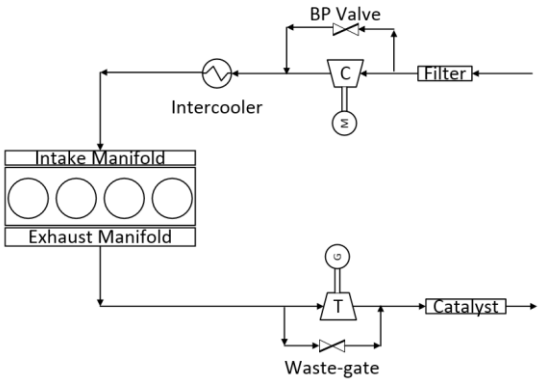

Figure 2.13 Decoupled electric turbocharger

Research on decoupled electrical turbochargers is less common, and this technology remains in its initial stage. Lee et al. (Lee *et al.*, 2016b) compared all of the current hybrid turbochargers and provided a summary of them. In their opinion, the decoupled electric turbocharger (which was called the electrically split turbocharger in their paper) has a very high-level degree of freedom, which allows this system to be controlled easily, and flexibly installed. The heat transfer effect can also be reduced to the lowest level compared with other systems due to its separate installation. The air path can also be easily optimised. The transient response of this system is not discussed. Liu et al. (Liu *et al.*, 2017) studied the performance of such a decoupled electric boosting system based on a validated 2.0L gasoline engine model. The whole system's efficiency can be improved up to 1.5% and the average power generated during different driving cycles can rise to 0.23kW; however, the drive cycle model in this research did not consider the transient process, so the conclusion regarding the energy saved by using this system is over-optimistic.

This kind of design has no additional inertia involved, but it has enough potential to improve the transient response. However, this system needs an extra electric motor, generator, and other electric devices, which means that this will increase the system's weight and size, and the overall efficiency will be significantly reduced. Whether the energy generated is enough should be carefully discussed.

All of the different types of hybrid turbochargers have their own advantages and disadvantages. It is important to understand how these electrical boosting systems will behave in real driving. The net electric energy requirement is important as it will affect the amount of electrical energy storage required and determine if there is a net surplus or shortfall in electrical energy. Any surplus can be considered as an increase in the efficiency of the overall system as the energy could be used to reduce the alternator load. Any shortfall would reduce the system's efficiency or compromise the system's performance if electrical energy is unavailable when required.

In this thesis, the research will discuss both EDC and decoupled electric turbochargers to see which has the most flexible control and installation modes. EDC-only system has a simpler design and the potential to improve system transient performance, it is also valuable to discuss if an extra turbine can help cover the electricity consumption by EDC without making the system performance worth. This superiority can greatly assist future internal combustion or mild hybrid vehicle powertrain manufacturing. Besides, due to energy conversion, its low total efficiency can also be optimised in the future.

2.3 Challenges related to turbocharger matching

The turbocharger system is considered the best choice for improving engine efficiency and power output, considering the cost. Turbocharger performance highly depends on the mass airflow, pressure ratio and thermodynamic parameters. Since internal combustion engines can be operated over a wide speed and flow range, clearly, there is no ideal solution for the conjunction of the turbocharger and engine itself. For manufacturers and researchers, the final objective then is to fit a turbocharger to an engine with the most suitable characteristics and try to achieve the best overall system

efficiency and performance(Watson *et al.*, 1982). Turning to automotive engine applications, turbochargers cannot be operated at the high efficiency flow area over the whole working range of the engine. In most of the matching tasks, although turbocharger matching is the basis, there are still some other changes necessary; for example, fuel injection system adjustment, and engine valve timing optimisation. Different components matching has been reviewed by Watson and Janota (Watson *et al.*, 1982), who summarised the procedures of different types of engine matching with turbochargers. For automotive engines, since the speed and load range is broad, typical duty cycles and load speed high torque cases are generally considered because the acceleration and deceleration is important for vehicle performance. Assanis et al. (Assanis *et al.*, 1985) introduced the simplified single-stage matching process in their research, which is also a typical design for the matching process. Determining the compressor pressure ratio and turbine pressure ratio is the first step; the turbomachinery could be chosen after this. With the given compressor maps and turbine maps, the mass flow rate and efficiency of each component can be determined. Hence, the compressor power and turbine power can be calculated. The exceeded power results in a change of turbo rotor speed. The last step is to consider all of the variables based on the solutions outlined above and find suitable turbomachinery.

2.3.1 Single stage matching

During matching, as the turbocharger is required to deliver a certain amount of boost pressure to the engine, there will be many constraints on the matching between the turbocharger and engine. Figure 2.14(a) shows a typical compressor map. The left side bold line is the compressor surge line, which means that, when the mass flow through the compressor is lower than the operating point on this line, the boost target is too high to achieve, and the compressor will be in surge and become unstable so mechanical damage may occur. Besides, if the mass flow is too large for the compressor to deliver, it will be unable to deliver the mass flow and attain the target boost pressure. When the compressor choke happens, the compressor speed will increase rapidly and over limit, compressor efficiency will plunge and lead to a very high compressor outlet pressure, makes the compressor behaviour unpredictable. The last limitation between the turbocharger and engine is that a turbocharger can only

work under an acceptable rotational speed, gas temperature and pressure. If these factors are outside the range, the potential for mechanical damage will rapidly increase. Figure 2.14(b) shows a typical turbocharger turbine map from BorgWarner (BorgWarner, 2017). Generally, the turbine can only work under the permitted speed and pressure ratio range shown on the map. The other factor that needs to be considered in turbine design is its area-radius ratio, which means that the inlet cross-sectional area is divided by the radius from the turbine centreline to the centroid of that area. This factor is used to describe the geometric characteristics of the turbine housing. A smaller A/R ratio will increase the exhaust speed passing through the turbine wheel which can make the turbine generate more power at low engine speeds, but will lead to a high speed boost rise on the compressor's side. Also, a smaller A/R ratio will reduce the flow capacity of the turbine wheel and increase the engine backpressure in the same operating points compared with a turbine with a bigger A/R ratio but, if the A/R ratio is too big, this will lead to a power loss in low speed regions because of the scavenging effect. Picking a suitable turbocharger for an engine which can not only deliver a target boost as required but also work in a safe and high efficiency region is one of the most significant processes within system design (Watson *et al.*, 1982).

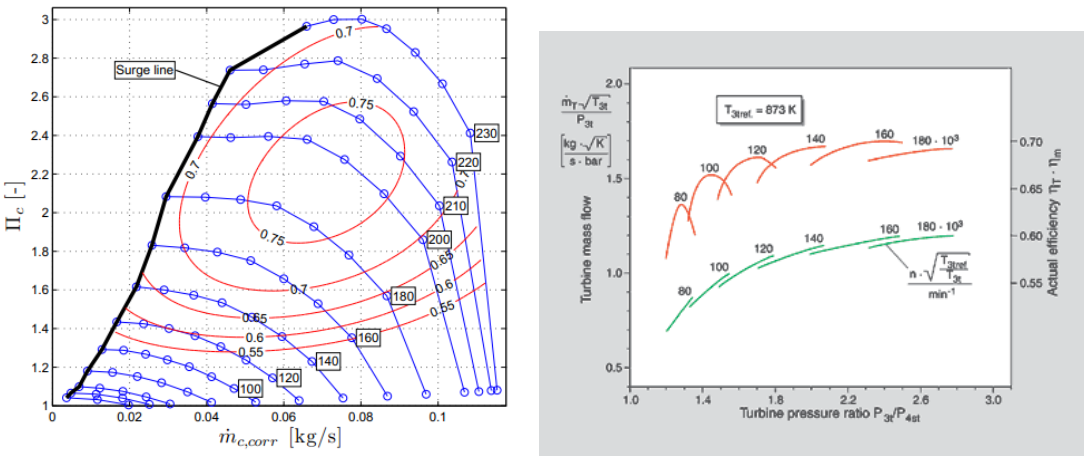

(a) (b)

Figure 2.14 (a) Compressor Map (Leufvén, 2010). (b) Turbine Map (BorgWarner, 2017)

Another problem is the matching between the compressor and the turbine for a specific turbocharger. The matching between the turbine and compressor has to be compromised. When the engine starts running, the exhaust needs time to fill the

manifold, and the turbine needs time to spin up and drive the compressor for the target boost pressure. During this period, driving in this condition will lead to a torque-leak, which is called Turbo-Lag. The turbine and compressor size will affect the engine torque and power output, transient response and peak efficiency. In order to avoid compressor surging and choking, a standard turbocharger is restricted to work at specific engine operating points (Watson 1982), and smaller turbines have a better transient response due to their low inertia, which makes turbocharger accelerate fast and deliver power to the compressor in a short time, but display poor characteristics when the engine runs under a high load and high speed condition, since the smaller turbine rotates faster for the same boost target, and can only transfer less energy to the compressor. If the speed of the turbine is too high, it will struggle in the low efficiency region and even over-speed without a turbine waste-gate. The engine pumping loss will also increase because a smaller turbine leads to bigger backpressure in the same work status. The bigger turbine will have higher efficiency and better performance in the high engine speed and load region, but the worse transient response and efficiency in the low speed region due to the high inertia.

The turbo matching method for the single stage system was a popular research topic in the past (Assanis *et al.*, 1985; Watson *et al.*, 1982; Mizythras *et al.*, 2019; Nelson *et al.*, 2003; Pesiridis *et al.*, 2012; Tancrez *et al.*, 2011). The matching procedures for the automotive single stage turbo system are quite common, and people pay more attention to other areas. The modelling method of using a compressor and turbine in a simulation tool (Müller *et al.*, 1998; Yang *et al.*, 2019a; Gurney, 2001; Zeng *et al.*, 2016; Thomas *et al.*, 2018) developed more, based on a fixed compressor map and turbine map, and is now starting to solve the problem of an unsteady flow, variable geometry turbine and, furthermore, the heat transfer effects. The measuring and fitting technologies of the turbine and compressor maps are also quite important (Galindo *et al.*, 2019; Avola *et al.*, 2015; Bell *et al.*, 2016; Tancrez *et al.*, 2011; Pesiridis *et al.*, 2012), since the compressor and turbine maps are entered into the model by look-up tables, which have a limited range of operating area. These topics lie outside the scope of this thesis but are quite crucial in turbocharger research.

2.3.2 Two-stage turbocharger and electric boosting system matching

The two-stage turbocharger, as stated above, offers many benefits over the single stage turbocharger under certain conditions. In automotive applications, systems in the parallel configuration has a broader flow range but lower boost pressure (Lee, 2009). The series two-stage configuration is more practical as it has two different sizes of the turbocharger and a higher low speed boost, so the system's efficiency and transient response can be improved (Backlund *et al.*, 1991). By matching the two turbochargers properly, the flow range can also be extended in a series configuration. Zhang (Zhang, 2015) in his thesis discussed the HP and LP turbocharger matching based on the scaling method; Figure 2.15 shows how different size of the compressors affect the boosting system flow range and surge margin.

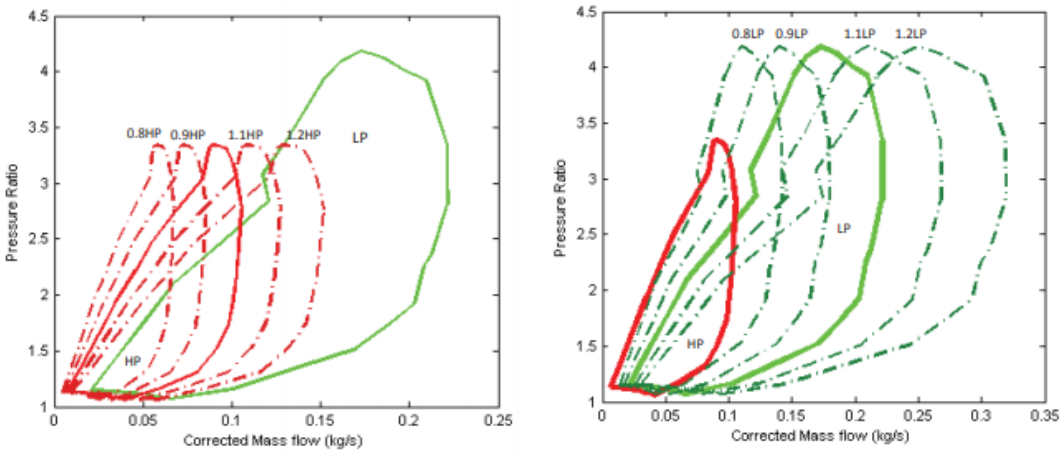

(a) (b)

Figure 2.15 (a) HP compressor map with several scaled units overlaid on the LP compressor map. (b) LP compressor map with several scaled units overlaid on the HP compressor map. (Zhang, 2015)

This thesis will focus on the series layout two-stage turbochargers. Unlike single stage turbocharger matching, which is quite straightforward (determining the pressure and temperature condition and selecting a suitable compressor and turbine with the given efficiency), for the two-stage turbocharger, it is impossible to calculate the first stage outlet pressure and temperature (P2 and T2) directly, as the pressure ratio for each stage is unknown.

The general procedure is to assume the pressure ratio for each stage and calculate the remaining parameters. The rough procedures are introduced by Watson and Janota (Watson *et al.*, 1982). However, this method is insufficient to ensure that the turbochargers operate at high efficiency on vehicle engine systems, because of the high engine speed, load and flow range ((Zhang, 2015; Lee *et al.*, 2009b). The HP turbocharger is always smaller than the low pressure one due to the exhaust energy level difference. It mainly takes responsibility for the increased engine transient performance in the low speed region (Galindo *et al.*, 2010; Watson *et al.*, 1982). The size ratio or the optimal turbine area ratio for the LP and HP turbo is generally 2:1 on marine engines (Watson *et al.*, 1982), to ensure that the boosting work is shared equally by the two compressors; however, it is not applied on automotive engines, which have variable operating conditions (Lee *et al.*, 2009b; Zhang, 2015). Due to the reasons outlined above, the matching for the two-stage turbocharger system becomes much harder.

Benson and Svetnicka (Benson *et al.*, 1974) introduced the matching procedure for the two-stage internal combustion engine based on an experimental study conducted in 1974. Based on his matching method, Lee (Lee *et al.*, 2009a; Lee, 2009; Lee *et al.*, 2009b), in his research, developed a new method that involved using turbomachinery scaling and the thermodynamic relationships to match two turbochargers. This method can conduct the matching without a particular turbine and compressor maps, which reduces the cost and evaluation time. The simulation results are more precise (increased power density from 31kW/L to 40kW/L based on a 4.5L engine) as the simulation was performed without turbocharger speed correlation curves; however, this research was not verified by an experiment. Watel et al. (Watel *et al.*, 2010) introduced a new concept that matched the two-stage turbochargers under the part load condition and obtained a high charging capacity. The whole air path achieved a reduced NOx emission with high burned gas rates on the intake side; however, this result was based on a high air excess to ensure low PM emissions. Yanbin et al. (Yanbin *et al.*, 2015) built a calculation model for the two-stage turbocharger system, considering the compression ratio, turbine flow capacity, more cooling efficiency and bypass flow contribution, which can help to increase the matching benefit. Wu et al. (Wu *et al.*, 2019) proposed a method for two-stage turbocharger matching and achieved high efficiency over the entire range of operating conditions. The torque

under a low-speed full load condition was 10% bigger than with the original engine, and this is also a simulation-based study.

Since the electric boost system is involved, more degrees of freedom are allowed during matching. For the electrically-driven compressor with a single turbocharger system, the compression work share can be more flexible; however, the electricity consumption needs to be considered. Liu et al. (Liu *et al.*, 2017) matched an electric compressor with an electric turbine, in a single stage condition, and compared eight different sizes of turbochargers' performance using the scaling method. Compared with the conventional turbocharger, it can generate 0.38kW of average power in the different drive cycles; however, negative total energy efficiency will arise if the electronic system's efficiency is lower than 72%. Yang et al. (Yang *et al.*, 2019b) matched an electrically-assisted turbocharger for a two-stroke marine engine by adjusting the electric motor's generator. Higher compressor and turbine efficiency can be achieved at the same time, and about a 2-3% BSFC benefit was achieved. A hybrid boosting system has been proven to have better transient response and fuel economy (Lee *et al.*, 2016a; Lim *et al.*, 2016; Ekberg *et al.*, 2017).

Since the 48V system has been introduced to the modern internal combustion vehicle in order to meet the Euro 6 emission regulation, electric boosting systems are now a hot research topic. Most of the matching on electric turbo systems focuses on the transient response, engine peak power and fuel economy, while limited literature discusses the energy (or electricity) balance of the system. As another phase of power source, electricity (from a battery or engine) is involved in the 48V system. Liu et al. (Liu *et al.*, 2017) demonstrated that the benefit of a decoupled electric turbo system in their paper, assuming that an electronic system's total efficiency is higher than 72%. Stoffels et al. (Stoffels *et al.*, 2017) discussed how electric power could be generated by an EAT for a 1.0L three-cylinder SI engine in WLTC. The results showed that the energy recuperated can be 87000J over 263s out of a 1800s whole cycle. The system fuel economy underwent about a 0.35% benefit. Dimitriou et al. (Dimitriou *et al.*, 2017) studied EAT performance using the scaling method. The whole system can have a 70% to 90% transient benefit, depending on the power supplied to the electric motor, also. They mentioned that, in the US06 cycle, the system could generate 3.8 kWh energy, although without considering the electrical loss. As the electronic system and

turbocharger system are the cross area, in which the matching and controlling are more complicated, as the 48V mild hybrid vehicle develops rapidly in recent years, more and more electronic systems can be introduced to improve the whole system's efficiency and reduce emissions; for example, belt starter generator technology (Atzler *et al.*, 2015), an electrically-heated catalyst system (Kirchner *et al.*, 1996), and VGT turbochargers. The 48V system generally can deliver 10 to 20 kW (Drury *et al.*, 2019) of power and around an 8 Ah capacity (BOSCH, 2019).

Controlling and distributing electricity usage becomes important for those systems and electric boosting devices (Burke *et al.*, 2019), and this can never be ignored during the matching process. Another issue in electrically-driven compressor matching is the configuration design in two-stages: for diesel engines, the electric compressor can be located at both the downstream and upstream turbocharger compressor, since it does not need the exhaust turbine. Also, the EGR route design and intercooler location will affect the compressor and engine performance, as they will affect the compressor inlet and outlet temperature. Surprisingly, the current research rarely comments on these issues (many papers discussed the two-stage layout, as already mentioned). Burke (Burke, 2016) mentioned in his research that both topologies are applicable, but there was no further discussion. Lee et al. (Lee *et al.*, 2016a) announced that a downstream electric compressor design has a faster transient response, as the upstream design has a larger volume to pressurise which is a big burden for a small compressor. However, there are no evidence that demonstrate that in his paper.

The electric boosting system still needs more research to deal with the topology design and matching issue. The challenges can be summarised here:

- The pressure ratio sharing design between multi-stage turbochargers.
- Transient response optimisation based on the size of the boosting devices.
- Hardware mechanical constrains (engine peak cylinder pressure, exhaust temperature et al.)
- Electricity distribution between different electronic devices.
- System topology consideration (Electric booster, turbocharger, EGR, intercooler)

2.4 Consideration in modern engine air path boosting system design.

A turbocharger can be applied on both a diesel and petrol engine, as it can supply compressed air to the combustion chamber and increase the fuel economy. Since the modern engine systems become more complicated, engineers attempt to explore more efficient technologies for optimising the system performance.

For petrol engines, also called spark ignition engines, the opening of the throttle will increase the engine's workload, forcing the pistons to pull air in from a low-pressure area on the intake. using a turbocharger allows the intake throttle valve to reduce its opening rate, which can help to reduce the engine's efficiency (Watson *et al.*, 1982). With the help of a throttle valve, a petrol engine can operate at a much higher and broader RPM range. Under a high load condition, the increasing air pressure generated by the turbocharger increases the chance of knocking and pre-ignition (Amann *et al.*, 2011; Zhen *et al.*, 2012; Hudson *et al.*, 2001). Moving the combustion phase to later in the expansion stroke can prevent knocking; however, there will be penalties in terms of thermal efficiency and BSFC. Direct injection helps to improve the knocking resistance. As it injects the fuel into hot compressed air, the fuel vaporisation process will decrease the mixture's temperature (Lecointe *et al.*, 2003). Other technologies, such as water injection (De Bellis *et al.*, 2017) and homogenous charge compression ignition (Hyvönen *et al.*, 2003), also help turbochargers to be applied to petrol engines by dealing with knocking or fuel economy issues. In this thesis, there is a case study about turbocharger performance with regard to a petrol engine. The combustion system for the petrol engine was not studied.

2.4.1 Importance of exhaust temperature on the engine exhaust air path

For turbocharged diesel engine systems, emission reduction is the most significant challenge that manufacturers should overcome (Mock *et al.*, 2014). Internal combustion engines have to be more efficient, and the introduction of real driving emission (RDE) driving cycles considers the arbitrary engine speed and load condition

(Franco *et al.*, 2015). This will lead to arbitrary temperature and pressure distribution for the engine and air path components (Burke *et al.*, 2019). The exhaust gas aftertreatment systems (EGAS) need to find new methods to increase the efficiency of pollution (NOx, HC, CO) conversion within these cycles (Hamedi *et al.*, 2019; Ramanathan *et al.*, 2004). Reducing the EGAS light-off time is important, and these methods have been incorporated by current engines (Ramanathan *et al.*, 2004; Korin *et al.*, 1999; Luján *et al.*, 2015). By delaying the combustion time, the exhaust temperature will drop, but this leads to an engine efficiency reduction. Throttling the intake air to reduce the air fuel ratio can also help, but it will increase the engine pumping loss. Burning additional fuel during diesel particulate filter regeneration is another way to obtain exhaust temperature benefit but, obviously, there will be a penalty in terms of fuel. All of these approaches can increase the exhaust temperature effectively but also lead to undesirable compromises regarding engine performance. Another method is to reduce the heat loss in the exhaust path upstream the EGAS, including the exhaust manifold (Knoll *et al.*, 2018) and turbocharger (Burke *et al.*, 2019).

To enhance the exhaust temperature at the EGAS inlet side, the first way is to relocate the EAT upstream of the turbine (Luján *et al.*, 2015; Serrano *et al.*, 2014). However, the cold transient response with a pre-turbo configuration is greatly slowed (which can be solved by E-heating or a two-stage turbo system), so the boosting system needs to be redesigned. The EGAS can also be relocated to the turbine bypass route; in this way, the exhaust flowing through the EGAS is not expanded. The third way is to use an active turbine bypass valve which divides the high power exhaust pulse to go through the turbine and the low power one to go through the EGAS (Hu, 2016). Finally, it is possible to reduce the heat loss between the exhaust port and the EAT through an insulation exhaust manifold or turbine housing (Ramanathan *et al.*, 2004; Kunde *et al.*, 2010; Fricke *et al.*, 2016). Turbine insulation will be discussed here, including the heat transfer modelling method.

2.4.2 Turbine Insulation technology and turbocharger heat transfer modelling

Turbochargers with an insulation design are an alternative, passive technology, designed to reduce the exhaust loss. This has been investigated in the last few years, and is quite a new but useful technology, as it means that there is no need to redesign the engine system; only provide a slightly larger space for the packaging. Fricke et al. (Fricke *et al.*, 2016) studied the thermal benefit of insulated exhaust manifolds and turbine housing. With this system, a range of 20% to 50% emission reduction is achievable with SDPF (SCR coated DPC) for the WLTC and FTP-75 cycles. The engine and insulation thermal performance have been verified by experiments, and the drive cycles performance is achieved by simulation. Lujan et al. (Luján *et al.*, 2019) discussed the thermal effects of the turbine and exhaust manifold insulation, including the cooling system. They considered a lumped capacitance model as the basis for simulating the performance of insulation, ignoring the detailed geometry effects of turbine housing. The steady state performance has been discussed, and a remarkable T4 benefit and BSFC reduction have been achieved.

This literature demonstrates that turbine insulation benefits exhaust temperature. During the simulation process, the modelling of T4 is one of the challenges that need to be overcome. A one-dimensional simulation is a standard method for evaluating engine performance and the matching of the selected boosting system. Turbine and compressor maps are used to define the isentropic efficiency characteristics. From the manufacturer's side, these maps are usually mapped onto a hot gas test facility under steady state conditions (Marelli *et al.*, 2017). Since the turbine outlet temperature is hard to measure, the turbine's actual work is calculated based on the temperature rise of the compressor gases. Although they research advanced measurement techniques that can directly measure the outlet temperature (Marelli *et al.*, 2019; Marelli *et al.*, 2016; Baar *et al.*, 2014), however, this method is rarely applied to current engine applications due to space and access limit. Current turbine maps ignore the heat transfer effects, which has a negligible impact on engine performance prediction, especially in high load research, as they have a higher exhaust temperature and

pressure. Also, this kind of model cannot predict the turbine outlet temperature (T4)(Serrano *et al.*, 2013; Romagnoli *et al.*, 2009).

In the simulation, it is critical to model the heat transfer of the turbocharger if the turbine outlet temperature is to be correctly predicted. Three-dimensional simulation can help to generate the detailed flow properties of all of the individual components and interfaces, based on the specific boundary conditions from the experiment (Baar *et al.*, 2014). This will lead to increased cost and time as computation fluid dynamics (CFD) simulation for thermal effects is usually complicated, and of limited practical benefit in a full system simulation. 1D simulation is cheaper and faster, although it cannot provide as much detail as the 3D method, with the appropriate modelling methodology, the temperatures and heat fluxes between different components can also be predicted. Lumped capacitance modelling is widely used in this area (Burke *et al.*, 2016; Olmeda *et al.*, 2013; Serrano *et al.*, 2017; Baines *et al.*, 2010; Romagnoli *et al.*, 2012). It assumes that the turbocharger's work and heat transfer happen independently and that the heat transfer will be divided into before and after the compression and expansion processes. The typical error in the turbine outlet temperature achieved by this type of model is around 10°C (Romagnoli *et al.*, 2017).

Serrano et al. (Serrano *et al.*, 2015) introduced a lumped capacitance model to predict the turbocharger inner heat fluxes. The convective heat transfer coefficient is well evaluated and considers the heat transfer between the compressor, turbine and cooling inside. Bohn et al. (Bohn *et al.*, 2005) derived the Nusselt number to predict the heat transfer coefficient with different geometry and operating points. Burke et al. (Burke *et al.*, 2015) compared the Nusselt number calculated by different researchers. The plot of the Nusselt number and Reynolds number are shown in Figure 2.16. The Nusselt number strongly depends on the flow density and gas composition.

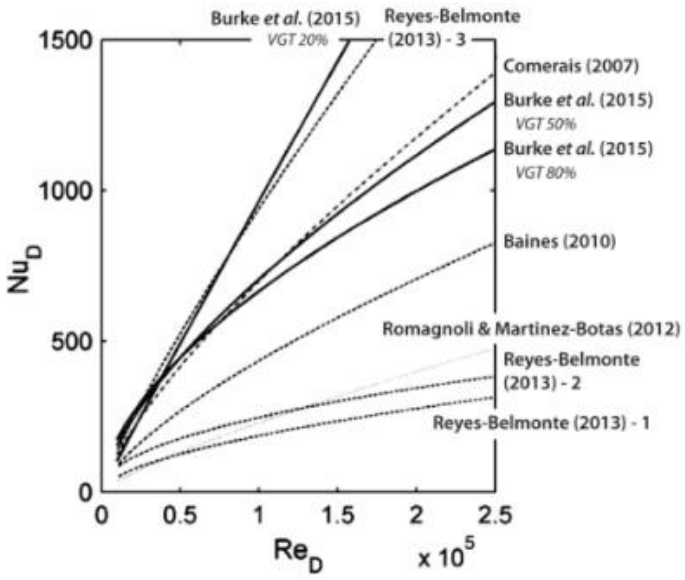

Figure 2.16 Nusselt Number Vs Reynolds number (Burke et al., 2015)

Since the heat transfer on the compressor side is small, because of the low inlet and outlet compressor temperature (Baines *et al.*, 2010; Olmeda *et al.*, 2013), the major heat transported to the compressor is mainly by the bearing housing, which takes about 2/3. This value is related to the oil temperature (Sirakov *et al.*, 2013). The turbine heat transfer effect is more important since predicting the T4 accurately is more critical nowadays. It has been found by Romagnoli et al. (Romagnoli *et al.*, 2009) that the inner and outer wall temperature of the turbine can have up to a 50K difference, which leads to a miscalculation of turbine efficiency. Turbine heat transfer generally needs to consider the heat loss from the turbine to the ambient, as this will take about 50% of the heat loss (Payri *et al.*, 2014; Baines *et al.*, 2010). Radiation is another aspect that needs to be investigated. Serrano et al. (Serrano *et al.*, 2007) calculated the radiated power, considering the compressor as a white body with an emissivity of 0.1 and the turbine as a black body with an emissivity 0.9. The power lost by the turbine takes up 10% to 20% of the compressor's effective power.

Given the increasing need for emission reduction and energy saving, heat transfer modelling of turbochargers can never be neglected when predicting the exhaust temperature for exhaust aftertreatment systems (Dalby *et al.*, 2019).

For modern engines, people are concerned more about the whole system's performance, considering an environmentally-friendly design, drivability and safety.

The air path design for engines with a boosting system becomes far more significant. The design of an airflow route and different pipe junction impacts the system's packaging, gas pressure drop and heat transfer; in the design of the boosting system, the fuelling components will affect the vehicle's NVH (Noise, Vibration and Harshness) level (Stoffels *et al.*, 2003; Evans *et al.*, 2005; Teng *et al.*, 2009). Each component of the vehicle is never independent, so the air path system control and design will become more important.

2.5 Summary and potential improvements

Turbochargers have been commonly applied to vehicle engine systems, as they can increase the engine's specific power and reduce fuel consumption. Electric boosting systems are a new design of modern powertrain which uses electrical energy to provide some or all of the engine air-flow. This increase in airflow allows a higher quantity of fuel to be burnt in the combustion chamber, meaning that the electrical energy used in the air-path results in additional power at the crankshaft. The system can ultimately result in higher efficiency vehicles through downsizing or down-speeding.

The matching problems between the boosting system, engine and other components become more complicated after electric systems become involved. For two-stage hybrid boosting systems, there is the potential to increase the engine's transient performance and fuel economy by matching the two-stage boosting devices properly. If further considering the energy consumption of the whole engine system, the fuel economy is allowed to be further optimised by re-designing the control of the electric boosting device. The matching and optimisation process for multistage boosting system is generally undertaken by the 1D simulation method because this kind of method can provide precise results based on well-defined models, without costing much time and money. However, researchers need to consider both the accuracy of the model and the effects of new technologies, how to justify the relationships and calculation during this stage becomes more crucial in modern engine system.

The fast development of a 48V mild hybrid system offers the chance to use an electric boost system and electric aftertreatment system. The heat transfer effects between the turbine and EAT then become a critical issue. A lumped capacitance model is a

common method for 1D heat transfer simulation. By combining insulated turbocharger technology with an accurate turbocharger hear transfer model, the exhaust temperature can be increased and predicted, which helps to advance the activation of EAT and reduce emissions.

In the modern engine air path, every single component plays an important role which helps to improve the whole system. Based on the literature review in this chapter and the research accomplished by the author in the last few years, the potential improvements in this area can be concluded as follows:

1. The matching process and optimising methodologies for a two-stage electric boost system.
2. Insulated turbocharger applications and related research for enhancing the turbine outlet temperature, helping the EAT system to be activated earlier.

3. Optimising and controlling the system's air path (pipe geometry, EGR, VGT et al.), to increase the system's performance, and reduce the energy loss and engine emissions.

In the following chapters, the author will discuss different electric turbocharger systems with some components case studies, focus on the transient optimization, energy consumption analysis and components operations.

Chapter 3 – Test facilities and modelling methods

This chapter will introduce the experimental instrumentation and test procedures and the modelling methods used in this thesis. There are four sections in this chapter

The first section is about the installation of the test rig (engine gas stand). The test rig components will be introduced, including the details of measurement sensors, the data acquisition system and control methodologies. Engine gas stand is a gas stand at compressor side combining with an exhaust generator (2.2L Diesel engine in this thesis) and turbine, and researchers can control the compressor boundary condition and engine intake characteristics.

The second section will mainly focus on the test procedures, calibration and validation tests will be described in this section, for demonstrating the reliability of future simulation works.

The third section is the introduction about the simulation tools, methodologies and supposed results that can be generated from this thesis. This section is a summary of all the simulation works in this thesis, which focuses on different research topics; however, they are all strongly related to the mild hybrid boost system air path design.

The last section is a summary of the whole chapter.

Work in this chapter has been published in: Vijayakumar, R., Burke, R., Liu, Y., & Turner, J. W. G. (2018, November). Design of an Advanced Air Path Test Stand for Steady and Transient Evaluation. In ASME 2018 Internal Combustion Engine Division Fall Technical Conference. American Society of Mechanical Engineers Digital Collection.

3.1 Test rig setup.

For turbocharger testing purpose, there are generally two types of rig design, engine stand (ES) and gas stand (GS). Figure 3.1 shows the simple structure of these two rigs, related components (cooling, pumps, heater, wastegate and so on) and measuring sections were not plotted here. Engine stand rig is performed as the system is in a real vehicle; the compressor pressurises the air and pumps it into the engine. The exhaust from the engine outlet will supply energy to the turbine which connected with the compressor at the inlet side. This rig is mainly for engine and turbocharger matching targets; it can test and evaluate the engine performance, generate the results for the effects of turbocharger on the engine. However, this system is hard to control the turbocharger boundary condition, as each component and factor in this rig is affected by the others.

Gas stand rig is the turbo only rig, which is mainly for evaluating the compressor and turbine performance, including turbocharger mapping, turbine pulsation testing and turbocharger matching. The hot gas is generally produced by a pump and heater so that the turbine inlet boundary condition can be controlled and not affected by the compressor and another air path (which is different from ES rig). However, this kind of rig cannot do the test related to the engine, so if there is request about how engine exhaust or engine-related components affect the turbocharger performance, this rig is not able to achieve that.

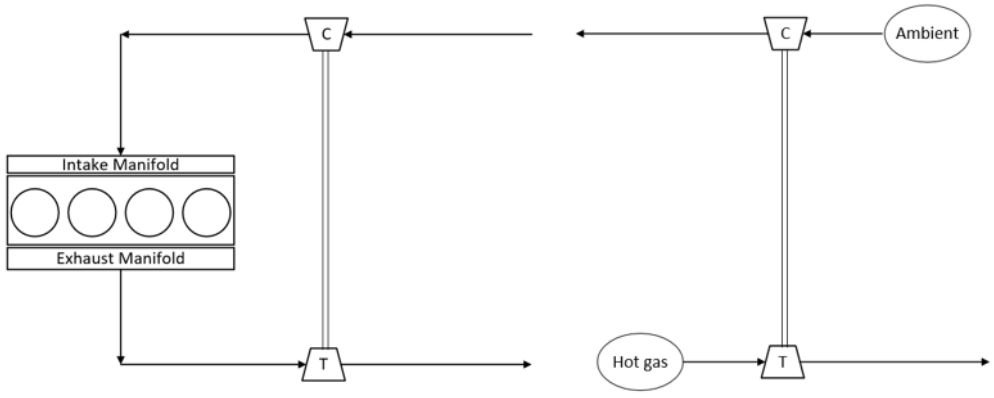

Figure 3.1 (a) Simple structure of engine stand rig. (b) Simple structure of gas stand rig.

In this thesis, a new test facility has been constructed by the colleagues and the author, called engine gas stand (EGS), with the intention to undertake steady flow and transient characterisation for a complex air path system and investigate potential future system layouts and control strategies. Figure 3.2 shows the simple structure of EGS, this is a combination of ES and GS rig, the compressor is on the individual air path, there will be a compressor backpressure valve controlling the compressor outlet pressure and flow. The engine absorbs the boosted flow produced by the boost rig and generate the exhaust to drive the turbine. In this way, this rig can measure both turbine and compressor individually, also has the ability to do a part of engine related testing (for example, EGR test). The test facility is flexible and allows for the study of individual components and full systems. The facility also allows for the replication of realistic, on-engine boundary conditions but also separating physical phenomena to promote the scientific study of the system behaviour.

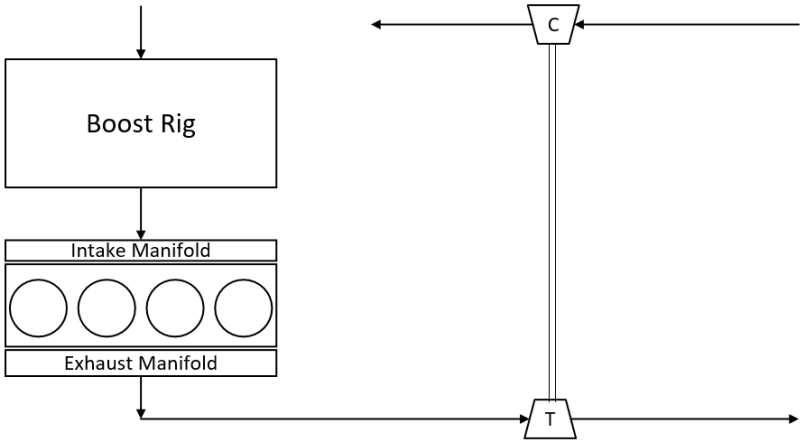

Figure 3.2 Engine gas stand test rig structure.

3.1.1 Engine gas stand test rig overview

The design principle of the test facilities in this thesis is to take an engine and introduce new hardware modules that promote measurement accuracy and allow for isolating different physical effects. A 2.2L diesel engine is used with an external boost supply module one the intake side to provide boost air. The schematic of the engine gas stand (EGS) test facilities are shown in Figure 3.3.

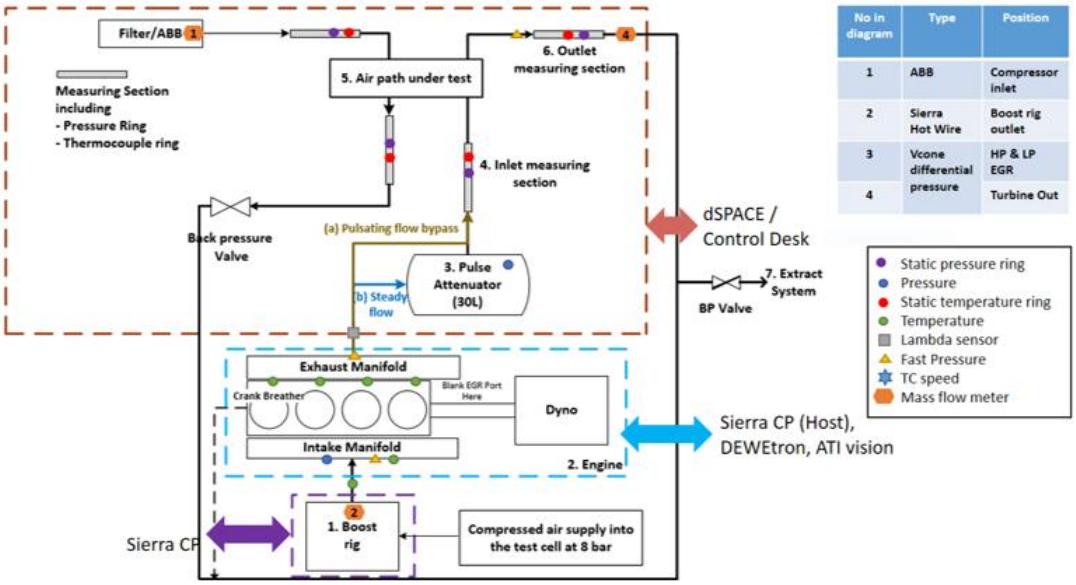

Figure 3.3 Schematic of the EGS experimental setup

The whole rig can be classified into three parts:

- The boost rig which supply boost air to the engine.
- The engine which generates required exhaust gas.
- Gas stand which is created for measuring compressor and EDC.

As the compressor outlet is disconnected from the engine intake system, the boost rig can independently supply air at required conditions, the turbine operating point can be controlled with more freedom than on and engine test bench. Meanwhile, the compressor is driven by the turbine in a turbocharger which is powered by the turbine and the flow through the compressor is controlled by the compressor back pressure valve. Figure 3.4 shows the picture of the experiment test facilities, and each module will be described in more details.

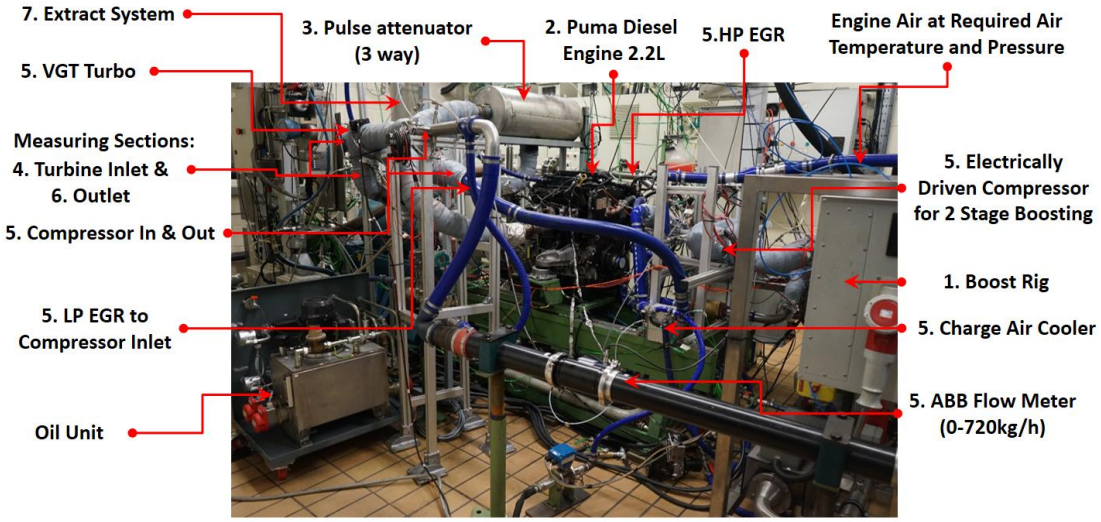

Figure 3.4 Experiment test facilities

The engine gas stand test rig is developed by IAAPS (The Institute for Advanced Automotive Propulsion Systems) in University of Bath. The facilities are designed for mapping turbines and compressors, with the provision of a second stage EDC (electrically driven compressor) and the use of HP, LP EGRs, and the rig is operated under real exhaust gas generated by the engine. From the very beginning, the requirements of the test rig with advanced air path design is shown below:

1. Produce gas flow rates covering a similar steady-state mapping region of turbine, compressor and EDC to conventional steady flow gas stand. The operating ranges are required for turbine and compressor are specified in Table 3.1

		Turbine	Compressor	EDC
Maximum mass flow	**Kg/h**	600	600	600
Inlet pressure	**bar**	Up to 4bar	~1bar	1-2bar
Outlet pressure	**bar**	1-1.3bar	1-3bar	1-3bar
Maximum Inlet temperature	**°C**	800	30	100
Maximum outlet temperature	**°C**	600	250	250

Table 3.1 Maximum steady flow specification requirements of advanced air path test facility

2. Allowing independent control of turbine inlet temperature (TIT) and mass flow.

3. Be able to test a turbine and compressor under steady and engine load-like transient conditions (engine warm-up or engine load change) with and without pulsating flows.
4. Be able to test a full air path system with different air path routings, including the recreation of different EGR paths (Low and High pressure).
5. Provide 48V electric power up to 5kW for EDC testing.
6. Provide independent conditioning of lubricating oil and cooling water for the air path components.
7. Incorporate adequate safety systems in line with the prototype nature of the test facility.

3.1.2 Test facilities.

3.1.2.1 2.2L Diesel engine

The rig is built based on a diesel engine rather than a gasoline engine as this provides the possibility to adjust fuel flow independently of airflow and control exhaust gas temperature and airflow independently. The engine at the centre of the advanced test facility is a 2.2 l diesel engine which is in series production and therefore a robust platform. The series production engine is turbocharged and uses common rail fuel injection. By selecting an engine with larger displacement, it can deliver the required range of mass flows and ensures an engine-independent metric of the turbocharger performance. The overall engine characteristics are listed in Table 3.2.

Parameter	Value
Peak exhaust gas mass flow	500kg/hr
Max exhaust gas temperature from engine	850°C
Exhaust gas temperature limit due to operating range of the settling tank	650°C
Engine peak power	114kW
Engine peak torque	385Nm

Table 3.2 Summary specifications of the 2.2L Diesel engine used in the test facility

3.1.2.2 External boost rig (CAHU)

The external boost rig provides boost air to the diesel engine. The boost facility is supplied by an industrial screw compressor that provides up to 1000kg/h or dry and cooled air at 8 bar pressure. The boost rig is located between this supply and the engine

intake manifold with the use of a series of control valves, heaters and coolers to control the delivery pressure and temperature of the air to the engine. The layout of the boost rig is shown in Figure 3.5. The flow pressure from the supply will be reduced controlled by a pressure regulator to 4 bar. Then it will flow through a parallel loop which has a cold flow, a hot flow and a mixing valve. Before it was pumped into the engine, there is a dump valve, to control the final pressure request. The arrangements allow the boost rig has fast transient control with inlet temperature and pressure; it is designed to respond approximately ten times faster than a turbocharger allowing for engine-like transients. The operating range of the boost rig is summarised in Table 3.3(Zhang, 2010).

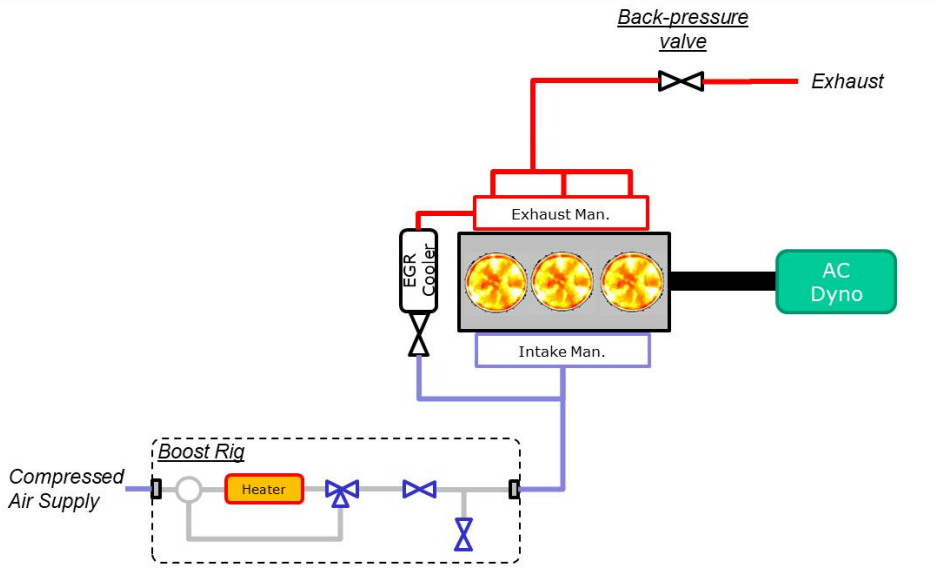

Figure 3.5 Schematic of the boost emulation facility.

Parameter	Value
Air delivers pressure	1.2-6bar
Pressure control accuracy	+/-0.5%
Maximum flow rate	700kg/hr
Maximum temperature	60°C
Minimum Temperature	20°C
Temperature accuracy	+/-1°C

Table 3.3 Summary specifications of the boost rig.

3.1.2.3 Pulse attenuation tank (previous work by colleagues)

Because of the limitation in the availability, cost and accuracy of specific instruments, it is difficult to measure the instantaneous turbine flow and inlet temperatures with pulsating conditions. The unsteady flow will create an operating profile which varies the turbocharger (turbine and compressor) temperature and pressure, on gas stand situation, the turbocharger will be operated at a constant speed for a single operating point. For some aspect, part of the typical operating profile of the turbine tends to be run outside of the turbine map. For this reason, it is advantageous to remove the pulsations from the engine exhaust flow and this is the motivation behind the pulse attenuator. With this installation, the test rig can still provide thermally transient boundary conditions such as those seen on the engine; however the turbine flow rate can be measured using conventional mass flow meters.

The pulsation attenuator is a stainless steel settling tank located between the engine exhaust and the turbocharger inlet. The size and design of the tank was undertaken in a 1D simulation environment, and a 30L tank with 90° angle between the inlet and outlet is shown sufficient to dampen the pressure pulsation at the tank outlet and making the flow nearly steady within acceptable levels as shown in Figure 3.6.

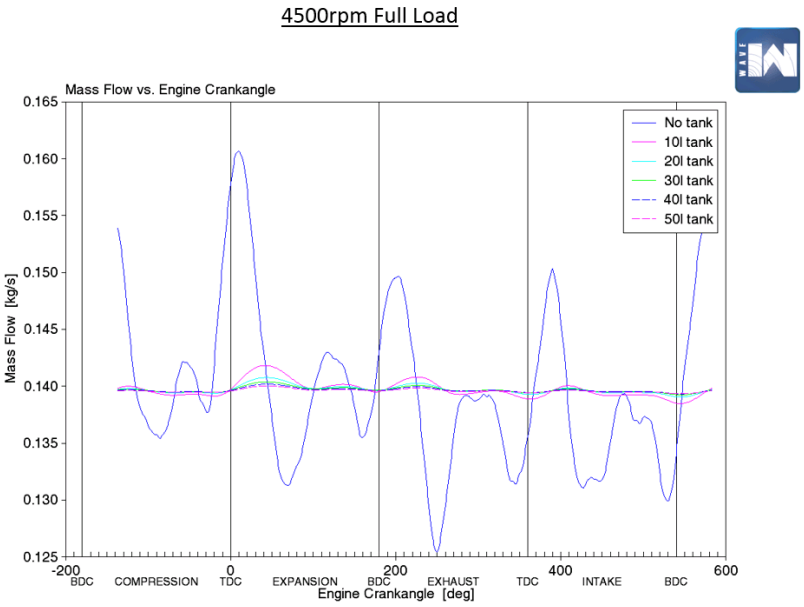

Figure 3.6 1D simulation showing the effect of tank volumes on the pressure pulsation at the tank outlet

The tank was designed by previous researchers, as shown in Figure 3.7, the manufacturing was outsourced. The tank could be described as an oversized t-piece the intake flow comes from the engine exhaust gas. For the rest two ends, one is connected to the measuring section and feeding the turbocharger turbine, the other to the HP EGR circuit. The settling tank is insulated with a high temperature material which is supported by an external cladding.

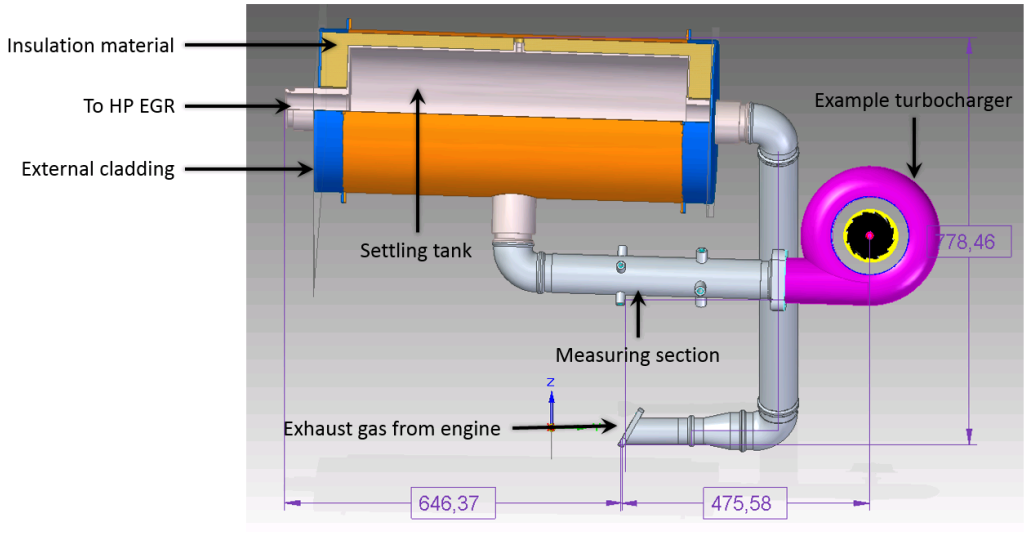

Figure 3.7 3D design of the settling tank used for dampening flow pulsation.

3.1.2.4 Turbocharger and EDC measurement unit

The turbocharger is the first stage of the two-stage boosting system, was supplied by BorgWarner for THOMSON project. A 3D model of the turbocharger is shown in. The turbine inlet and outlet flanges are mounted at the end of a measuring section which is connected to the settling tank, as shown previously in Figure 3.8. Hot exhaust gas at typical engine conditions powers the turbocharger turbine which in turn powers the compressor.

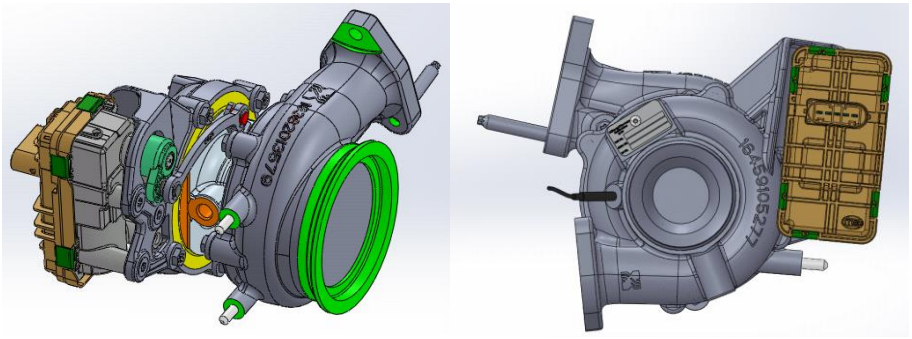

Figure 3.8 3D model of the turbocharger (supplied by BorgWarner)

The turbine inlet and outlet flanges are mounted at the end of the measuring section, this is connected to the settling tank. The compressor inlet stub and outlet flange are also connected to 2 measuring sections. The four measurement sections are straight pipes with an array of temperature and pressure sensors. Each of the four measurement sections has four ports for thermocouples or PRTs at 90° to each other. Four radial taps at a 45° angle to the temperature taps were connected by a monomeric ring to measure the average static pressure. This eliminates the difference in pressure in the pipe across the measuring section. The number of thermocouples/PRTs and their lengths inside the measuring sections are specified in Figure 3.9 and Table 3.4.

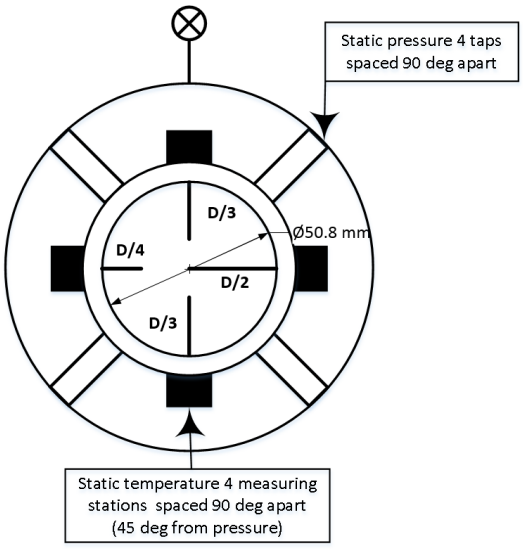

Figure 3.9 Thermocouple lengths and pressure ring orientation in the compressor outlet and turbine and inlet and outlet measuring sections

Measurement sections location	**Static pressure type**	**No of static temperature ports**	**Lengths of thermocouples/PRTs**
Compressor and EDC inlet	Static pressure ring with four ports spaced at 90° interval to measure the average static pressure and 45° from temperature ports	2	1/3 diameter of the tube at 180° relative to each other and perpendicular to tube walls
Turbine inlet		4	1/3 diameter at 0° and 180°, 1/2 diameter at 90° and 1/4 diameter at 270°
Turbine outlet		4	
Compressor and EDC outlet		4	

Table 3.4 Specification of pressure and temperature measurement using test sections

The second stage of the boosting is the EDC. A 3D model of the supplied electric compressor is shown in Figure 3.10. The EDC is powered by a 48V system with a DC power source which is controlled by dSPACE control system. A CAN signal from dSPACE with an appropriate speed input will be used to control the EDC speed. The EDC inlet port and outlet flange will be connected to 2 measuring sections, similar to those used for the compressor. The EDC requires conditioned water at a specific temperature for cooling which will be supplied by a Regloplas P140smart unit; no external lubrication system is needed.

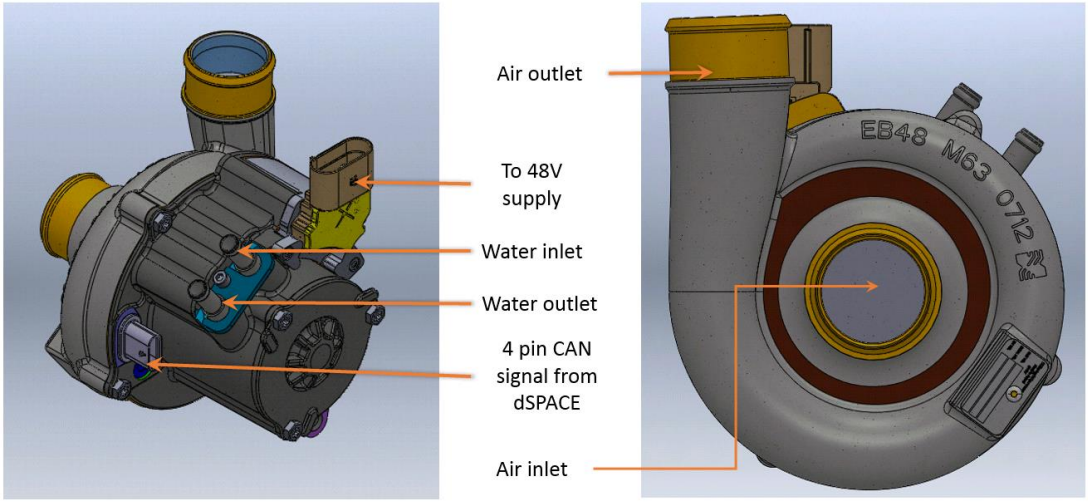

Figure 3.10 3D model of the EDC (Supplied by BorgWarner)

3.1.2.5 Other mechanical and hydraulic systems

Besides the mechanical systems described above, the rig includes a flexible EGR system including HP and LP EGR. This system has water-cooled poppet EGR valves, can supply one or two EGR heat exchangers based on the requirements (shown in Figure 3.11). The EGR valves are controlled from dSPACE with a 0-5V analogue voltage signal proportional to the opening position. The engine coolant flow is extended by coolant manifolds (feed and return) as shown Figure 3.11, used as a source of cooling for the EGR valves and heat exchangers which are conditioned to approximately 90°C.

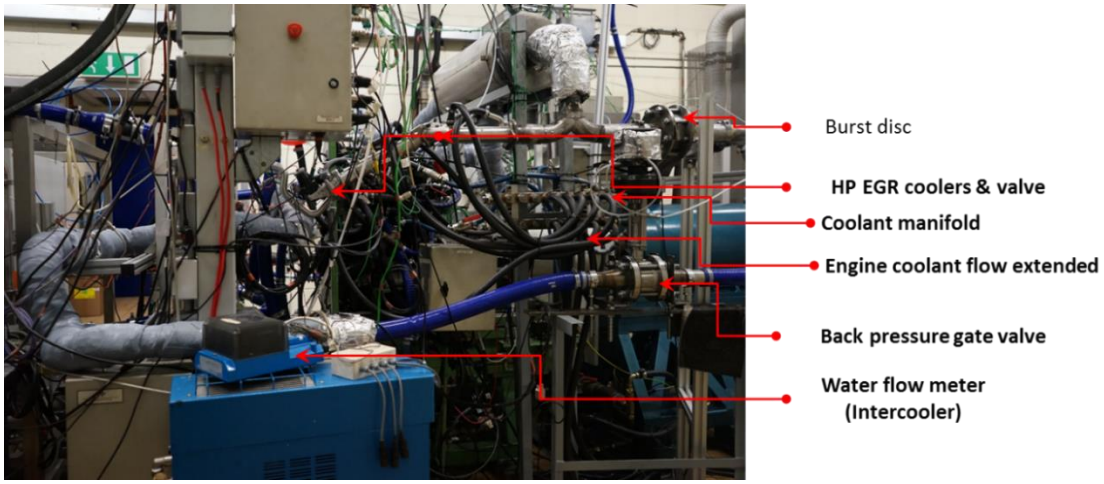

Figure 3.11 HP EGR cooler and pipework to be connected to valve and silicone hoses

The flexible EGR systems allow the researchers to adjust the routing of EGRs, four EGR layouts are able to be achieved, shown in Figure 3.12. The purpose of this study is to mainly observe the change in compressor and turbine efficiency with different proportion of LP and HP EGR. A brief description of the purpose of different EGR routes are given in Table 3.5.

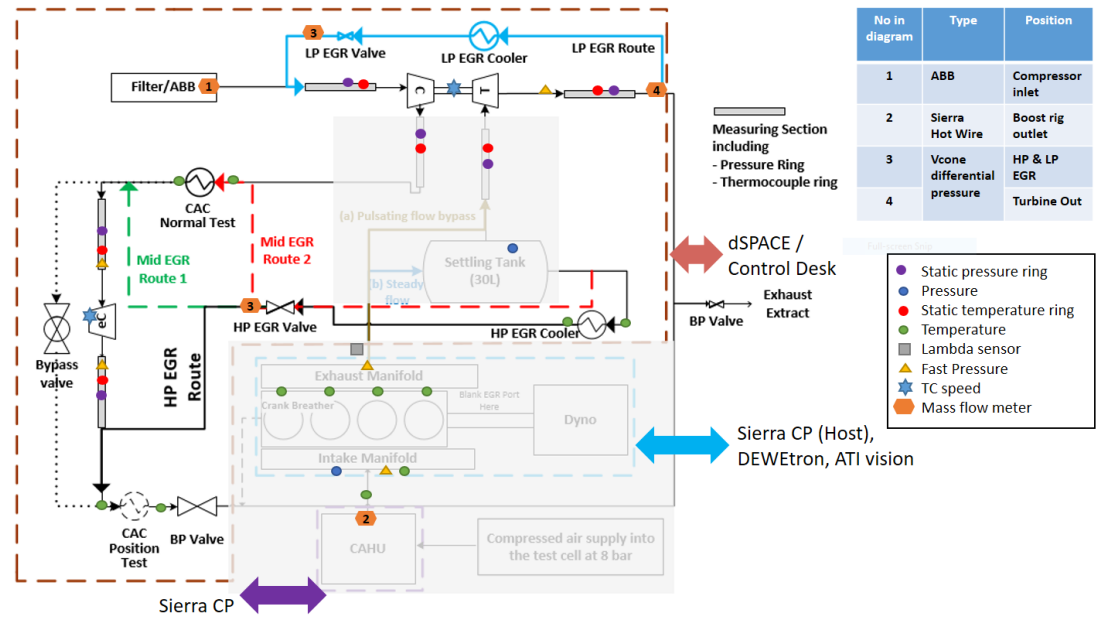

Figure 3.12 Example flexible air path layouts used in THOMSON project.

EGR type	Purpose
LP EGR route	Effect of LP EGR proportion on compressor and turbine efficiency for different turbocharger speed and engine operative conditions
Mid EGR route 1	Effect of single stage EGR cooling (HP EGR cooler only) combined with studying HP EGR proportion on EDC and turbine efficiency and turbocharger compressor surge characteristics for different turbocharger speed and engine operative conditions
Mid EGR route 2	Effect of two-stage EGR cooling (both HP EGR cooler and CAC) combined with studying HP EGR proportion on EDC and turbine efficiency and turbocharger compressor surge characteristics for different turbocharger speed and engine operative conditions
HP EGR route	Effect of high back pressure from EGR introduction on EDC surge and efficiency and also turbine efficiency characteristics for different turbocharger speed and engine operative conditions

Table 3.5 Purpose of different EGR routes

Cooling systems are used to maintain the temperature of engine components, EDC, EGR valve and EGR heat exchanger. Overall cooling is provided by a central water cooling supply for the building facilities. A proportional Kinetrol valve (electro-pneumatic servo valve) is used to maintain the engine components within a specific temperature, and this is controlled through the Sierra CP software via a PID loop to a set point (temperature). A Regloplas P140 smart coolant system with user specified temperature regulates the turbochargers and EDCs operating temperatures. It uses the central pond water supply to maintain the coolant supply temperature, top up the cooling water for those lost in evaporation.

The lubrication oil for the turbocharger bearings is supplied by a standalone unit. The position of it within the test cell is shown in Figure 3.4. A screw pump sends oil from a 7 gallon mild steel tank fitted with three 1kW heaters and can supply up to 10 L/min. The oil is pumped from the tank via a plate water cooler, an in-line filter with a bypass and an electrical clogging indicator. The oil flow can be supplied to two branches, each of which incorporates a flow control valve and flow meter. The water-side cooler includes a solenoid-operated valve to regulate water flow through the cooler. This valve splits the mainline into two feeds in order to obtain individually adjustable output in each leg. The main pressure lines also include a temperature indicator which works in conjunction with the cooler and the heater fitted in the tank to maintain the required temperature. The tank also includes a visual level gauge, a filler/breather, a drain valve

and the oil return. The control system is housed in an enclosure and comprises of a Danfoss +1 controller. The outside of the enclosure incorporates an e-stop and the motor start/stop buttons. Inside of the enclosure, the controller, switchgear for heaters, motor and cooler solenoid valve and a 24V DC supply is housed. The control system monitors and maintains the oil temperature by switching the heater and cooler as required.

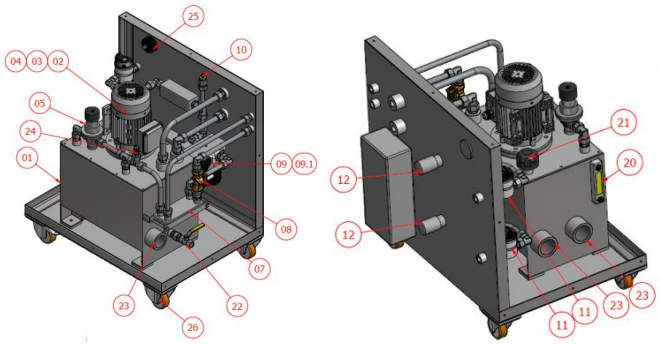

Parts List			
ITEM	QTY	STOCK NUMBER	DESCRIPTION
26	4		90kg Castors
25	1	PG-2GS-B160-DC	Pressure Gauge
24	1	PTP2103-01-18.55	Test Point
23	3	HEAT-HR1116B	1kW Heater
22	1	BV-LP-D	Drain Ball Valve
21	1	UC-SAB-5101	Filler Breather
20	1	FSA127-2-1-12	Level Gauge
12	2	BHS-08-05623	Pressure Compensated Flow Control Valve
11	2	BHS-08-5622	Positive Displacement Flowmeter
10	1	BHS-08-05123	Temperature Senor
09.1	1	MP-DEA20HA50P01	Electrical Indicator
09	1	LMP1101BVA2A10NP0	In-Line Filter
08	1	BHS-09-00124	Water Solenoid Valve
07	1	ABC-LA14-10-3/4"	Cooler
05	1	BHS-08-05383	Pressure Relief Valve
04	1	GR20SMT16B20LGVHA	Screw Pump
03	1	MP-AKM-M01Z0212FG0	Bellhousing
02	1	EM-0.55-FF-3	0.55kW Electric Motor
01	1	BJ008373-04	Reservoir

Figure 3.13 3D model showing the components of the oil conditioning system (supplied by manufacturer)

3.1.3 Measurement, controlling and data processing system

For generating data in steady and unsteady flow experiments, some specific data acquisition software is used. A schematic of the parameters recorded and the software used are shown in Figure 3.14. The steady flow data required for mapping the turbine and compressors will be recorded at low frequency (10 Hz) using proprietary software by Sierra CP. The pressure, temperature, mass flow rate and turbocharger speed sensor measurements are made in the software with pre-calibrated physical channels. Also, the control of engine speed and load and the CBPV (used to vary the flow rate) are done through this.

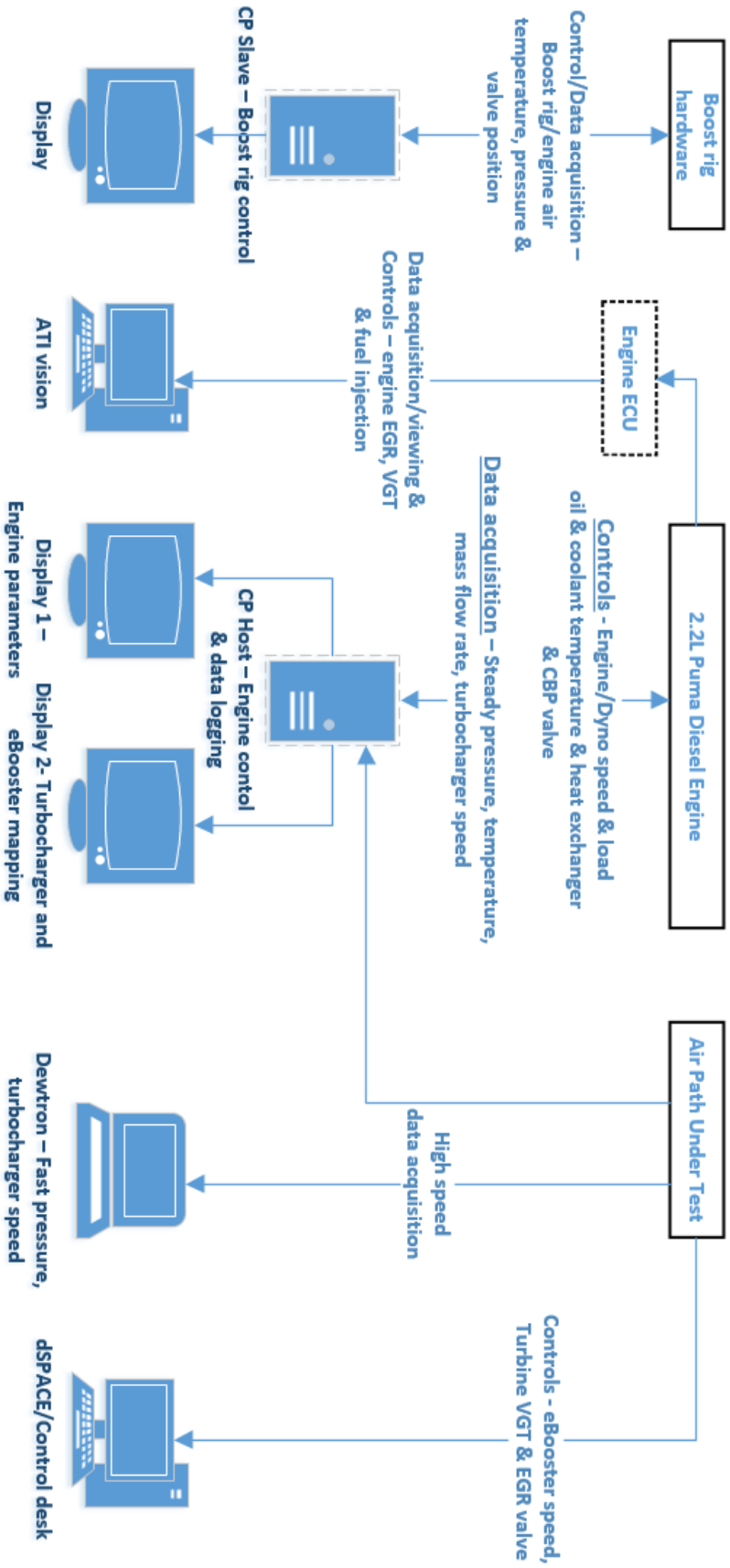

Figure 3.14 Communication diagram of the test facility

High frequency measurements are made using proprietary hardware and software from Dewetron. For example, the compressor surge characteristic study requires high frequency pressure measurement at the compressor outlet, and this will be recorded by the Dewetron equipment. Also, experiments that involved any pulsating flows and engine transients with fast changing conditions will need fast data acquisition. For example, instantaneous exhaust pressure pulsations and turbocharger speed data are required in the above experiments, are connected to the Dewetron. This has the capability to measure data up to 200 kHz but is usually limited by the response time of the sensors. ATI vision is a robust software solution that can acquire the ECU data and modify closed-loop controls. In this work, it will be used to control and regulate the exhaust gas temperature at the turbine inlet. This is usually achieved by changing the amount of fuel injected into the engine.

To operate the test facility, the user controls the engine/dyno speed and load, EDC speed, turbine VGT position, valves and other important parameters. A schematic of the control software and the parameters controlled are shown in Figure 3.14. A central CP Engineering system acts as a host system and sends commands to a CP slave, controlling the boost facility. Besides this, the ATI vision system monitors and adjusts ECU parameters manually (can also be controlled by CP, if the transient test is required), the dSPACE system controls the prototype air path. Most of the controls related to the gas stand are controlled using dSPACE, a robust and compact proprietary hardware that includes a comprehensive I/O interface including Controller Area Network (CAN), Ethernet etc. The CAN interface allows two-way communication and control between the microcontrollers and the devices without a host computer. The Simulink-based field-programmable gate array (FPGA) offers programming features to achieve the required functionality. The embedded PC (Windows based) and the Control Desk (graphical user interface) are easily programmable and are made to suit the project requirement. Various I/O interfaces allow the control of different hardware as summarised in Table 3.6. The EDC speed is controlled between 0 to 70000 rpm via a CAN signal from dSPACE. The EDC requires 48V and a 5kW power DC power which is supplied by a Magna Power programmable DC supply (TDS50-300/415 + LXI). It can supply up to 50 V dc, 300A dc and 15kW. The input power required is a 3-phase supply, 374-457V ac and 30 A ac at 50-400 Hz. EGR valves (poppet type) are controlled with a 0 to 5V analogue signal from dSPACE. VGT vane angle is regulated

by an aftermarket regulator (VNTT pro). The change in VGT angle also brings a change in pressure ratio (PR) across the turbine. The CBPV regulates the back pressure from the turbocharger compressor or the EDC (depending on the configuration) and is controlled by a 0 to 10V analogue signal from Sierra CP. This controls the flow and PR across the turbocharger compressor or EDC.

Control parameter	**Variable**	**Communication type**	**Signal Range**	**Range**	**Power Supply**	**Software**
EDC speed control	EDC speed	CAN	-	0 to 70000 rpm	48V	dSPACE
VGT vane angle control	Turbine vane angle and PR	Analogue voltage	0-5 V	0 to 100%		
HP and LP EGR valve lift	EGR %	Analogue voltage				
CBP valve	Compressor PR	Analogue voltage	0-10 V			Sierra CP

Table 3.6 Control parameters and specification

3.1.4 Sensors

Different fluid types are involved in operating an EGS for specific purposes, and their flow rate has to be measured precisely. The types of fluids used, purpose, location in the test rig, flow meter and measurement principles are described in Table 3.7.

Measurement fluid type	**Purpose or location on the test rig**	**Flowmeter used**	**Measurement principle**
Compressor airflow	Compressor inlet	ABB	Hot film anemometer
Engine airflow	Boost rig outlet	Sierra	Immersible Thermal Mass Flow Meter
Exhaust gas	Turbine outlet	Vcone	Differential pressure

Lubricating oil	TC lubrication system (bespoke unit)	SKF	Gear flow monitors
Cooling water	EDC cooling system (Regloplas P140smart)	Inbuilt	-

Table 3.7 Flowmeters used, principle, medium and location on the test rig

Airflow through the compressor is measured using an ABB hot wire flow meter at the compressor inlet; this will be corrected later based on the inlet total temperature and total pressure measured. The airflow via the boost rig is measured using a Sierra hot wire flow meter before it enters the engine. The exhaust gas flow through the turbine and the EGR path are measured using Vcone differential pressure flow meter. The oil flow through the turbocharger is measured internally inside the oil conditioning unit using SKF gear flow monitors. The cooling water flow rate through the EDC is measured internally in the Regloplas P140smart unit.

Pressure sensors, both absolute and gauge, are used in recording static pressures in different sections of the gas stand and the engine. As mentioned earlier, a pressure ring measured the average static pressure across the test section pipe. The location of the different pressure sensors are specified in Figure 3.12. The range of the sensors used and their accuracy are specified in Table 3.8.

Static temperature measurements are done at the inlet and outlet of the turbocharger compressor and the turbine and the EDC in a measuring section. The place where the air/exhaust gas temperatures are below 200°C, PRTs are used in the measurement and in locations where the temperatures are above this, K-type thermocouples of 1.5mm diameter have been used. Except at the inlet of the compressor and the EDC which have two temperature measurement ports, all of the remaining sections have four measurement ports. The lengths of the thermocouples and PRTs used in the compressor and EDC outlet and turbine inlet and outlet sections are the same and are represented in Figure 5. Their range and accuracy are specified in Table 3.8.

Sensor	Range	Accuracy
PRT	-50°C to +200°C	0.3 + 0.005*T
K type TC	-200°C to 1260°C	0.0075*T
Fuel flow	0 to 200 Kg/h	±0.05%
Pressure transducers	-1 barA to 6 barA	0.25%
Turbo speed	0 to 400,000 rpm	0.1%
Exhaust gas mass flow	30 to 300 kg/h 50 to 750 kg/h	±0.5% of the measured value
Air mass flow	0 to 700 kg/h	< 1% of measured value

Table 3.8 Sensor types, range and accuracy

Turbocharger speed is monitored using an eddy current sensor positioned in the compressor housing. By setting up a jumper in a position that corresponds to the number of blades on the compressor wheel, the sensor measures the number of passing blades. The turbo speed is derived by correlating the blade setting with the number of passing blades over a given period. The accuracy of the sensor is ±0.5%.

There are also safety systems, including burst disk which ensure the safety pressure release from connected components; the emergency stop which ensure the rig can stop running immediately when the accident happens; fire suppression system, which will sensor the temperature and smoke to avoid fire accident.

3.1.5 Experimental uncertainty

Researchers need to know how confident they are with the experiment results; the measurements uncertainty analysis is necessary for people to get this information. Every measurement has its errors and will lead to the change of the system uncertainty. For turbocharger related experiment, the main uncertainty of data generation mainly happens during the map generation process.

There was no specific uncertainty test in this thesis, since the experiment is not the key part of the output. However, a discussion of how different sensors affect the system uncertainty is still necessary. Four factors are important here: temperature, pressure, flow measurements and rotational speed. The properties of the measuring sensors have

been introduced in Table 3.8. The accuracies exist will bring in the increasing uncertainty of the system, these measuring errors at last will be observed on the efficiency and pressure ratio differences (efficiency difference around 10% at most, pressure ratio differences 3%), since the mass flow rate parameters were calibrated in advance.

Another issue is the test bench design in this thesis, EGS test rig is used for mapping the compressor and turbine, different from gas stand, this involved the corrected mass flow parameter uncertainty, and also brings in heat transfer effects. The accuracy of turbocharger efficiency will be affected by the heat transfer inside the body (The results can be seen in the next section). The heat transfer errors are more critical in low flow region measuring.

Mass flow and temperature measuring frequency is another issue that brings uncertainty to the system, the mass flow sensors in this research have 40Hz frequency, which is capable for steady state tests and slow transient tests, however, for highly changed transient tests, the sensors are too slow (for example, the EGR rate measuring in Chapter 5), although the results can still be used as an explain of the fast transient trade-offs, the author is not confident with the specific values the sensors generated. Besides of the measuring frequency problem of mass flow and pressure sensor, the response of thermocouples is another issue exists in transient temperature measuring. Figure 3.15 shows the thermocouple 95% response time with diameters and turbine flow Reynolds number. When the diameter is 3mm and the flow is low (low Reynolds number), the transient response time can be as much as 27s for turbine measuring. If the thermocouple diameter is small and the flow is high, this time can be reduced to less than 5s. Coming to the designed tests in this thesis, for those cases with low flow rate (EGR measuring for example), the temperature measurements are not that trustable anymore.

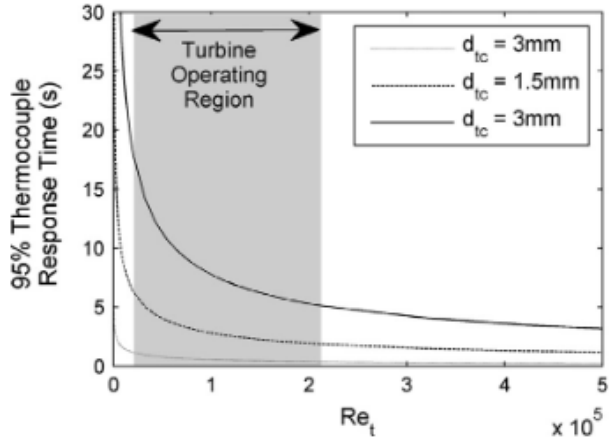

Figure 3.15 Estimated thermocouple 95% response time for thermocouple diameters0.5–3 mm as a function of turbine Reynolds number(Burke et.al. 2015).

There is another specific point in error controlling in this experiment design. The calibration of the turbine VGT controller. Since the rate of turbine VGT will significantly affect the turbine performance, the calibration of it becomes much important. The VGT actuator used in this experiment is a third-party designed tune-box. In order to reduce the error, the actuator and the VGT brings in. The Turbine VGT position is re-calibrated and verified in each test with different boundary conditions, before recording the results.

3.1.6 Rig design summary

The rig was constructed based on the 1D model input of having a 30 litre pulse attenuator to dampen any flow pulsation with a steady mass flow at the turbine outlet. This eventually allowed steady mass flow measurement and hence characterising the turbocharger under steady flow conditions. Following this, the EGS was built up. An oversized 2.2 L diesel engine has been chosen in order to provide enough energy to the turbocharger turbine across the entire speed range while accounting for heat loss from the pipe and settling tank. The air path for this rig includes a VGT turbocharger, EDC, Charge air cooler, LP and HP EGRs, shown in Figure 3.12. The engine is supplied with boost air from CAHU and the exhaust gas coming out of the engine goes via the pulse attenuator (bypassed for pulsating/transient tests) before powering the turbine. The EDC is the second-stage boosting system, the airflow goes through the turbocharger compressor and EDC back pressure is controlled by the CBPV. The

exhaust gas for EGR can be taken from HP and LP EGR using manually-actuated poppet valves. Depending on the requirement, individual components can be characterised or could be combined to do the system level mapping. This is a flexible air path system, each of the components mentioned (VGT, EDC, EGRs, pulse attenuator) can be bypassed as required.

3.2 Demonstration tests

3.2.1 Compressor mapping

The compressor is powered by the turbine, driven by the exhaust gases from the engine. The compressor flow is then controlled by the CBPV. For compressor mapping, a number of elements of the prototype air path that are not needed are removed (EGRs, EDC).

A typical mapping method to get to a single operating point is illustrated by:

- Starting at point A, the reduction in compressor mass flow shifts the operating point to point B
- Adjustments in the turbine power return to point C, which has the same speed as point A

When conducting a complete speed line, the process is shown in Figure 3.16. The compressor operating point was varied from choke to surge for four compressor corrected speeds. The compressor efficiency was calculated based on the SAE recommendations (1995). The process is more complicated than using a conventional steady flow GS, and, if only steady flow maps are required, this new facility is not the most efficient tool available.

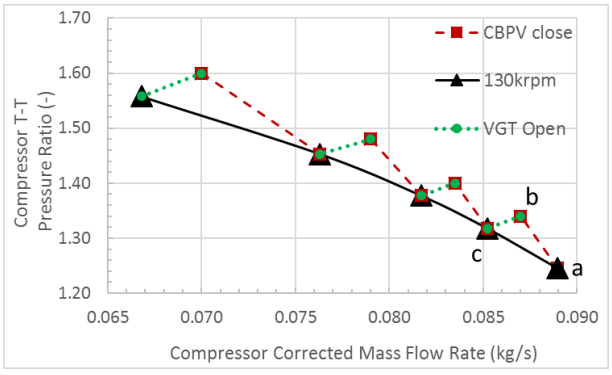

Figure 3.16 Compressor mapping procedure

The measured map of the compressor is shown in Figure 3.17. In any configuration, different compressor operating conditions are achieved by closing the CBPV or increasing the flow from the boost rig or the engine speed. Closing the CBPV allows a reduction in mass flow through the compressor. As this mass flow is reduced, typically, the TC speed increases as the compressor power absorbed is reduced while the turbine power remains the same. To maintain a constant speed line, the turbine power must be adjusted by either adjusting the VGT or wastegate or reducing the turbine mass flow rate. However, changes in the mass flow rate are coupled to the gas temperature in this facility, which needs to be carefully managed. The turbine inlet temperature (TIT) was kept constant at 823K by varying the intake boost and the throttle signal, which is linked to the fuel injection in the engine's ECU AFR (air-fuel ratio) control.

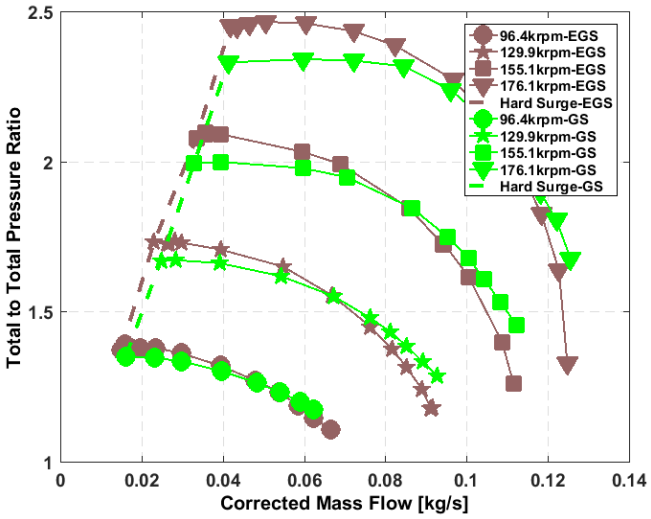

Figure 3.17 Steady flow compressor map obtained from the engine gas stand

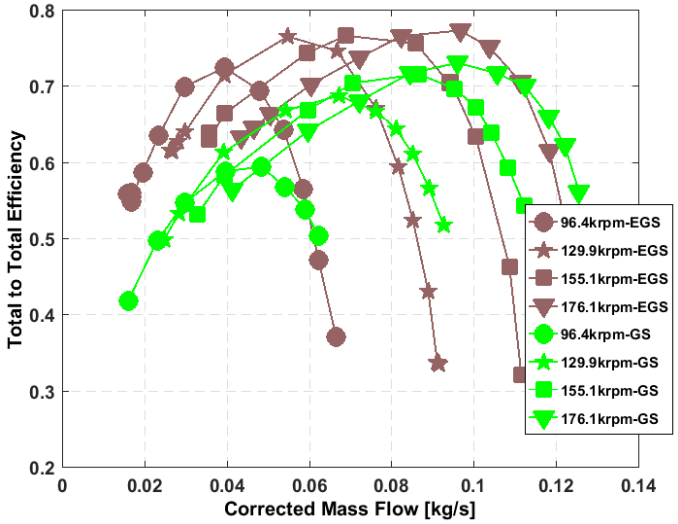

Figure 3.18 Steady flow compressor efficiency obtained from the engine gas stand

.

Figure 3.17 and Figure 3.18 show a comparison of the steady flow compressor map obtained from the EGS and conventional GS (obtained on a conventional turbocharger gas stand rig). The compressor PR on the EGS is higher (Figure 3.17) at a lower mass flow rate than the conventional GS and lower at a high mass flow rate. The reason may be the change in the pipe sizes and bends at the compressor inlet and outlet. The change in PR seems to have a similar effect on the compressor's efficiency, as shown in Figure 3.18. This is not entirely due to the change in PR but also the change in the TIT (823K on the EGS and 873K on the GS), so it makes sense that cases with lower TIT have higher efficiency.

3.2.2 Turbine mapping

The turbocharger has a VGT, the position of which was adjusted by an aftermarket VGT regulator. The regulator has a target and an actual position on its display which can be manually varied by the test cell operator. Turbine mapping can be performed under pulsating or steady conditions through the inclusion or bypassing of the settling tank. In this thesis, only steady state mapping is studied.

Turbine mapping is undertaken in the opposite manner to compressor mapping, where the VGT or closed waste-gate conditions are held constant throughout. To explain this, the operating point is moved from the highest PR and corrected mass flow point P1 to

the lowest PR and corrected mass flow rate point P5 without changing the VGT position. From point P1, the CBPV is opened and this drops the TC speed. In order to achieve the target turbo speed and TIT, the boost pressure (CAHU) and engine speed and/or torque (fuel quantity) are reduced. This reduces the PR and mass flow rate across the turbine when moving to P2. The process is repeated to obtain the remaining points and all six rack positions were characterised over a range of turbo speeds.

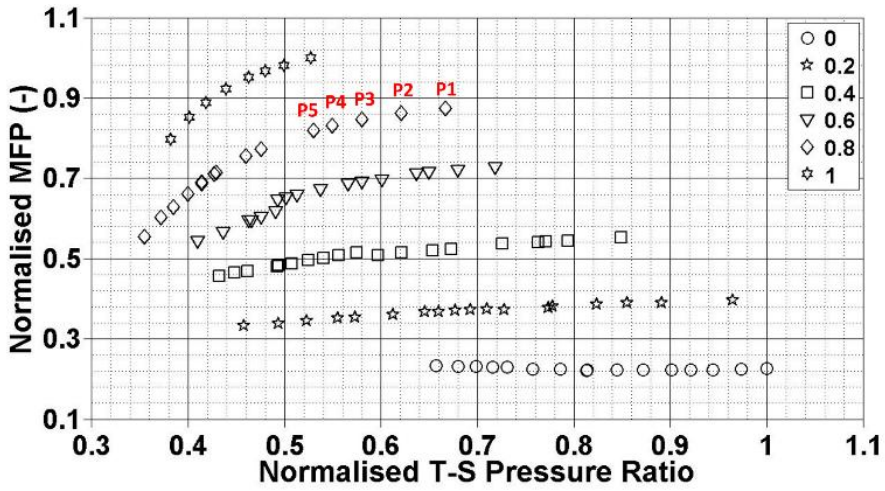

Figure 3.19 Turbine mapping procedure

The turbine characteristics map obtained on the EGS while using the settling tank (to steady the flow) is compared with that obtained using the conventional turbocharger GS, as shown in Figure 3.20 and Figure 3.21. There is good agreement in terms of the turbine mass flow parameter (MFP) and total-to-static (T-S) PR across the turbine for all of the rack positions except at low PRs, where there is a small difference. The turbine efficiency obtained on the EGS is lower compared to that obtained on the GS. This is mostly due to the difference in TIT (823K on EGS Vs 873K on the conventional GS) and the associated heat transfer characteristics.

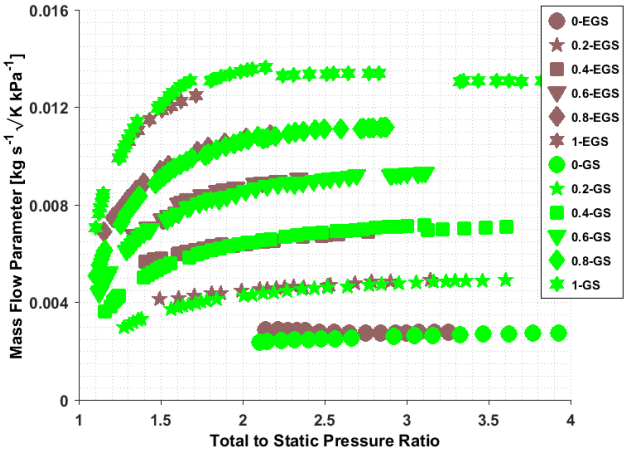

Figure 3.20 Steady flow Turbine map

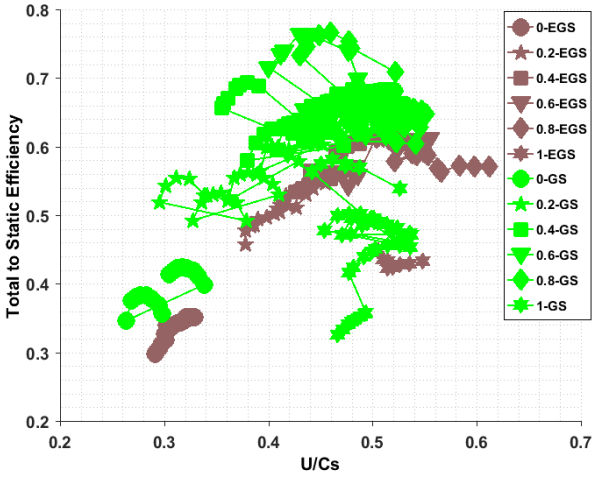

Figure 3.21 Turbine efficiency map

3.2.3 EDC mapping

EDC Mapping is conducted essentially on an EDC test stand which is made by isolating certain parts of the system. The EDC is connected to the inlet and outlet measurement sections, upstream mass flow sensor and flows against the CBPV. This layout is shown in Figure 3.22. The EDC is connected to a 48V power supply system and a proportional CAN signal from the dSPACE/Control Desk maintains a steady EDC speed even when the CBPV is closed. This makes the mapping process relatively simple. The mass flow rate was varied from choke to surge while allowing sufficient settling time before logging the data. The air filter/ABB assembly can also be replaced by the boost rig to test the EDC with a higher than ambient inlet pressure which is closer to its operation within the air path.

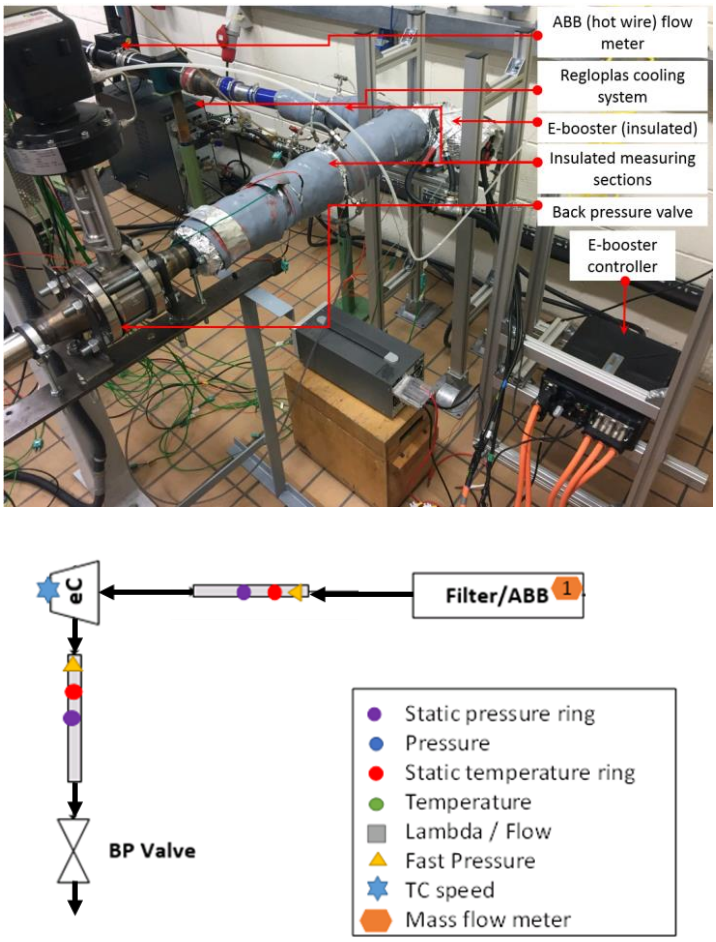

Figure 3.22 Test rig for characterising EDC in standalone conditions

A comparison of an example map obtained from the EDC setup and that from the manufacturer is shown in Figure 3.23 and Figure 3.24. There seems to be a significant shift in the location of the surge and the shape of the line going into surge. On the test conducted on the facility (EGS), it surges earlier whereas that from the manufacturer has a dip in PR before the surge. The compressor efficiency is sensitive to PR. Again, the difference in pipework could account for this change in surge behaviour and also cause a difference in compressor efficiency.

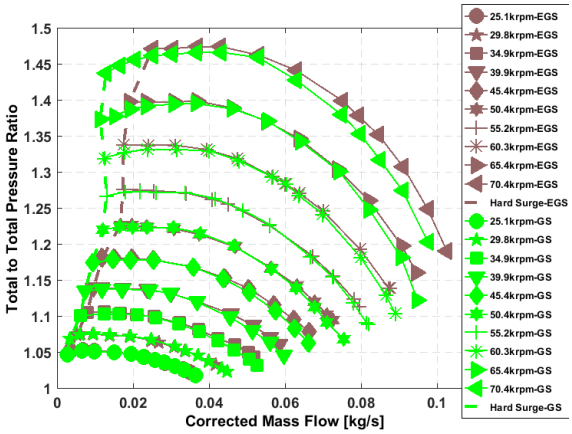

Figure 3.23 Steady flow EDC map

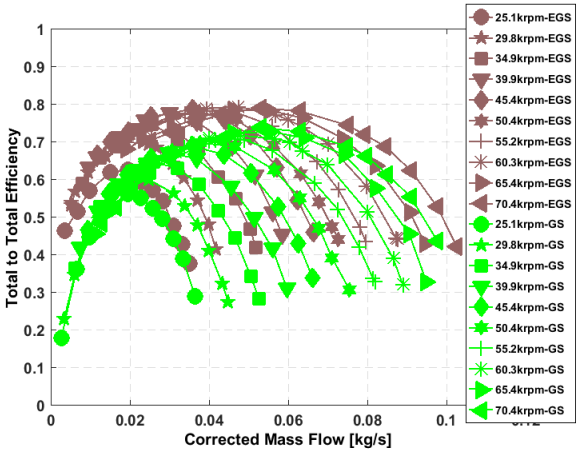

Figure 3.24 Steady flow EDC efficiency map

3.2.4 Two-stage testing

The objective of these tests is to validate the system level model and use it to study the effect of different configurations. The two-stage mapping essentially uses the configurations of the complete test rig already shown in Figure 3.12. These configurations involve the first-stage turbocharger compressor and the second stage EDC with the CBPV positioned after the EDC. The target or test points were supplied by a validated 1D model. The test point discussed here comes from a low engine speed full load condition where the EDC operates close to its full potential.

The test was performed by running the engine at a certain speed and loading it with the boost rig, thereby supplying sufficient mass flows and boost pressure. The turbocharger speed was matched by adjusting the factors above and the VGT position. The EDC speed was increased in 5000 rpm steps as the turbocharger speed increases.

The CBPV is closed gradually along with the above steps. The air mass flow rate through the turbocharger compressor and the EDC are the same. When the target turbocharger speed, EDC speed and air mass flow were achieved, the entire system was left to reach a thermally steady condition before logging the data.

The inlet pressure of the EDC is changed by running the turbocharger at different speeds, and mapping is performed at different upstream conditions characterizing the EDC by varying the CBPV position at different EDC speeds. The resulting data could be used in 1D modelling studies and also to analyse the influence of the first stage on the EDC's performance.

Example test points from a system test on the THOMSON layout are discussed. The test points from a 1.6 l downsized diesel used in the THOMSON project are taken at the following engine speeds where the EDC operates close to its full potential: 1000 rpm and 1500 rpm. An example dataset of the EDC and turbocharger compressor operating points from the EGS for a two-stage boosting system is shown in Figure 3.25 and Figure 3.26, respectively. To negotiate the effect of temperature and pressure, the mass flow terms have been corrected for temperature and pressure. The figures show that there is a good match between the 1D modelling and the test results in the above configuration. The EGS can be used for system level tests with good accuracy and, in this case, it replicates the THOMSON layout.

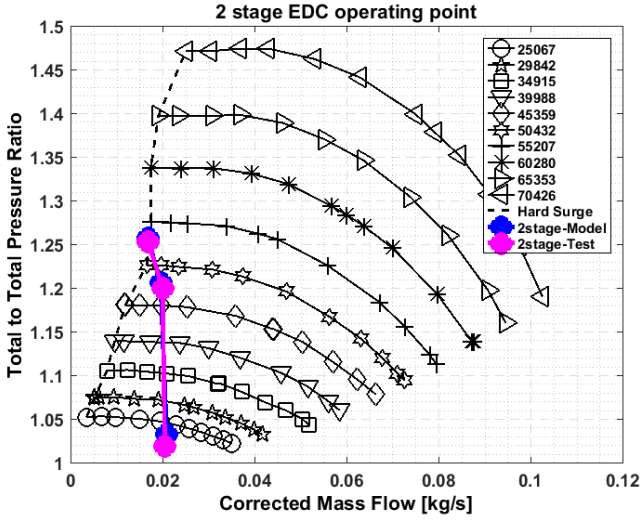

Figure 3.25 EDC operating point in the EGS under a steady state condition

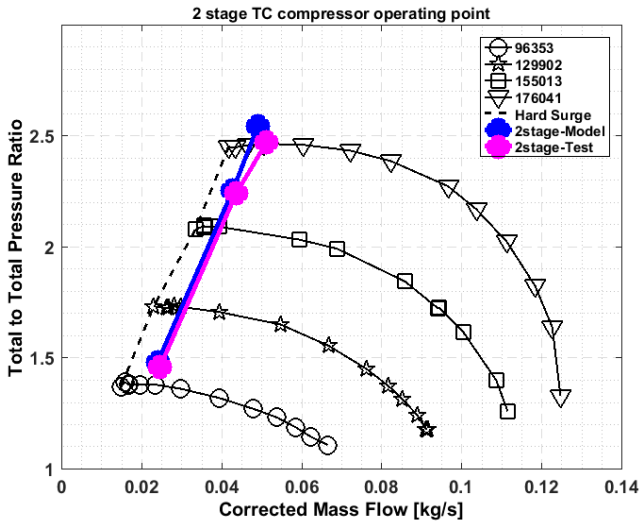

Figure 3.26 Turbo Compressor operating points in the EGS under a steady state condition

3.2.5 Intercooler position tests

The intercooler (CAC) for cooling the compressed air from the turbocharger compressor or the EDC compressor could be positioned either between or after the two-stages. To compare the effect of its position, the CAC was moved to after the second stage. Identical test points were compared with tests having the CAC between the two-stages. The operating procedure remains the same, as described above. The TC and EDC were run under physically the same conditions (in terms of VGT position, PR, mass flow rate and TC speed) in order to observe the thermal effect.

The air path considered in this case study is flexible. Positioning the CAC hardware is one of the key decisions to be made. Thus the intercooler was positioned between the two boosting systems (1^{st}-CAC) and after the two boosting stages (2^{nd}-CAC). Similar test conditions were maintained when testing it at two locations. For example, the turbocharger and the EDC speeds were similar, as shown in Figure 3.27. An identical air mass flow rate was maintained in the two cases across the EDC and the turbocharger compressor, as shown in Figure 3.28. The PR across the EDC dropped marginally when the intercooler was positioned after the EDC, mainly due to the higher EDC inlet and outlet temperature reducing the outlet pressure.

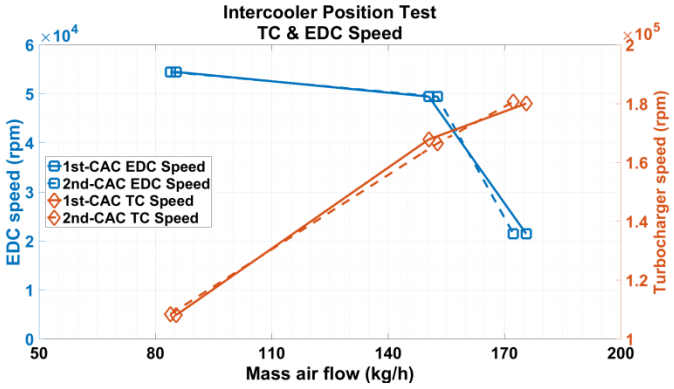

Figure 3.27 Similar turbocharger and EDC speed maintained in the two sets of tests

Another important observation made was that the EDC acts as a sink for heat rejection when the turbocharger operates at high speed. This may be seen from the lower EDC outlet temperature compared to the inlet temperature in Figure 3.29. This significant cooling effect of the EDC is not typically modelled (this lies outside the scope of this thesis).

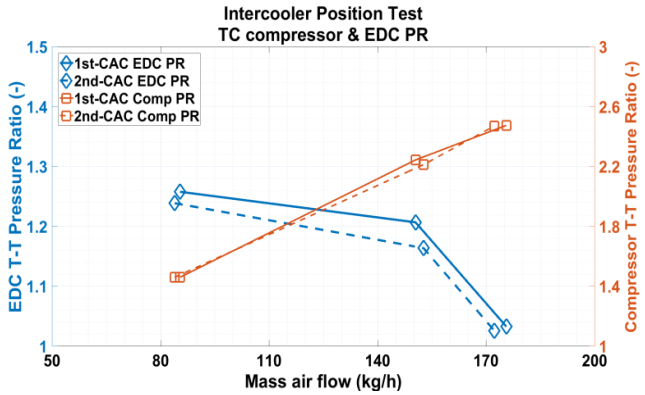

Figure 3.28 Identical mass flow rate but different EDC PR observed

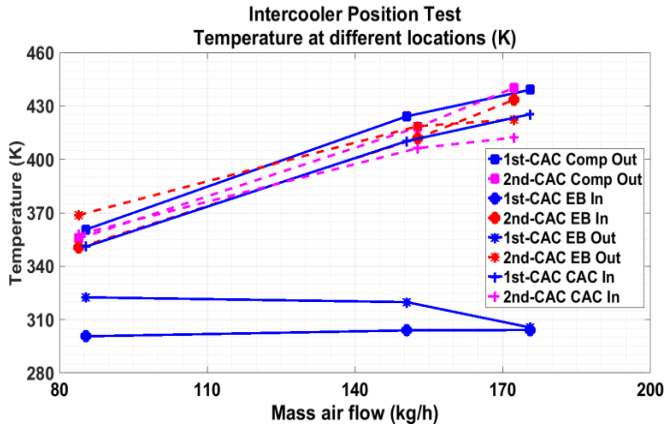

Figure 3.29 Temperature at different locations in the 2-stage system test

3.2.6 Transient testing

The test rig will be used for the transient characterisation of the boosting system with 3 major purposes of research:

1. Evaluating the time to boost by stimulating the turbine inlet enthalpy and the major air path control actuators
2. Evaluating the EGR transient performance in mixing process.
3. Evaluating the thermal behaviour of the air path from cold start and during load transients

The transient process will be achieved by applying the following methods:

1. Known engine exhaust flow profiles will be used as boundary conditions for cycles such as WLTC and from some real driving conditions. These will allow the boosting performance to be evaluated in a realistic scenario. The results will be used to validate the performance of turbocharger models and other experiment results.
2. Dynamic system identification approaches will be used where the system inputs (turbine enthalpy and all control actuators) will be excited using sinusoidal or step signals to perform a complete dynamic identification of the system.

An example of such excitation is shown in Figure 3.30, which was applied in a previous thesis at the University of Bath for only a fixed geometry turbocharger. Here it will be expanded to the full air path system including e-booster, VGT, e-booster bypass valve and EGR valves.

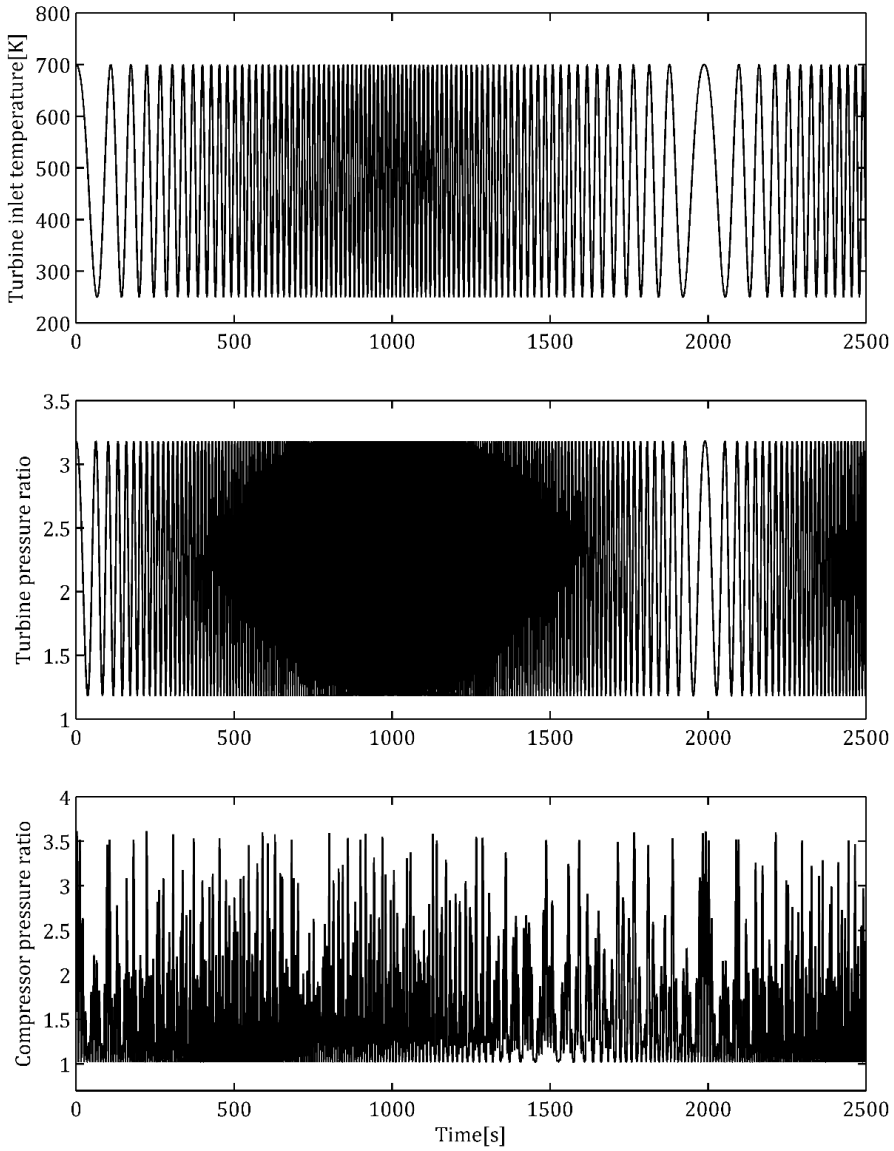

Figure 3.30 Example sinusoidal excitation of turbocharger boundary conditions

3.3 Simulation tools and models

In this thesis, both 1D and 3D modelling tools were used. 1D simulation mainly focuses on predicting and optimising the system performance, components characteristics and its influence on other facilities. 3D simulation is applied in the case study for optimising the inlet air path pressure drop and flow uniformity, further increase the system efficiency.

3.3.1 1D modelling tool and basic model

In 1D simulation, both single stage decoupled turbocharger system and two system EDC system are discovered. The boosting system of the baseline engine was a single-stage turbocharger. The model was configured within the GT-Power (Gamma Technologies, LLC, Westmont, IL, USA, 2014) simulation tool. The component templates are based on the built-in functionality of GT-Power, for all of the engine simulations. The author targets on creating the models for specific two-stage system, which will be described in subsequent chapters.

3.3.1.1 Decoupled turbocharger engine model

This model is based on a four cylinder, gasoline turbocharged direct injection 2.0L engine with a rated power of 176kW. An experimentally validated gas dynamics model of the engine provided the basis for this work. The boosting system of the baseline engine was a single-stage, fixed-geometry, waste-gated turbocharger. Following key sub-models are used (Tang, 2016):

- Imposed heat release profiles derived from measured data at 46 operating points across the full engine speed and load map.
- 1D representation of manifolds and ducting validated against crank angle resolved measurements of pressure pulsations within the intake and exhaust system
- Experimentally tuned heat transfer coefficients validated against experimental data.

Further details on the baseline engine model can be found in(Dimitriou *et al.*, 2017; Tang, 2016) and a summary of the model accuracy is provided at full and part load in Table 3.9 and Table 3.10 respectively.

	Cylinder number			
	1	**2**	**3**	**4**
Measured total mass airflow (kg/h)	258.69			
Simulated total mass airflow (kg/h)	263.65			
Error in total mass airflow (%)	1.92			
Measured net IMEP (bar)	20.71	21.19	20.75	18.29
Simulated net IMEP (bar)	20.44	20.76	20.30	18.02
Absolute error in net IMEP prediction (bar)	0.39	0.43	0.45	0.27
Error in net IMEP prediction (%)	1.87	2.05	2.15	1.47
Averaged absolute error in net IMEP (bar)	0.36			
Averaged error in net IMEP (%)	1.89			

Table 3.9 Model accuracy at full load conditions

	Low-Load	**Medium-Load**	**Full-Load**
Error in total mass airflow prediction (%)	0.69	3.26	1.92
Averaged error in net IMEP prediction (bar) (Cylinder 1)	0.19	0.39	0.39
Averaged error in net IMEP prediction (%) (Cylinder 1)	7.39	2.56	1.87

Table 3.10 Model accuracy at different load conditions at 2000rpm

The standard model was modified to incorporate a mechanically decoupled electric turbocharger, as shown in Figure 3.31. The compressor is connected to an electric motor which will drive the compressor to create boost pressure. Within the model, the motor is controlled by a PID controller, by varying the compressor speed to reach different levels of brake mean effective pressure (BMEP). The turbine is connected to a generator which is controlled by a second PID controller that adjusts the turbine operating point. A compressor bypass valve and turbine waste-gate are also considered (not shown here); however both are closed when boost pressure is demanded. Though electric motor and generator are included, other electrical devices are not modelled in detail (inverter and battery) and are represented by simple efficiency terms. Each of these efficiency terms is illustrated in Figure 3.31 and Table 3.11. What should be noticed here is that the efficiency of battery needs to be discussed respectively in charging and discharging situation, it will be affected by different factors, for example, voltage, current, temperature. In order to simplify the mathematic model in this simulation, the total energy conversion efficiency of battery and inverter is regarded as μ_B, $\mu_{TB}$and μ_{BC}represent the efficiency that power transmitted between battery and turbine/compressor (due to the energy losses in inverter and other electric components). Those electric components in the 1D model can be regarded as an energy

generator and consumer, the use of electric power will impact the performance of E-turbo system.

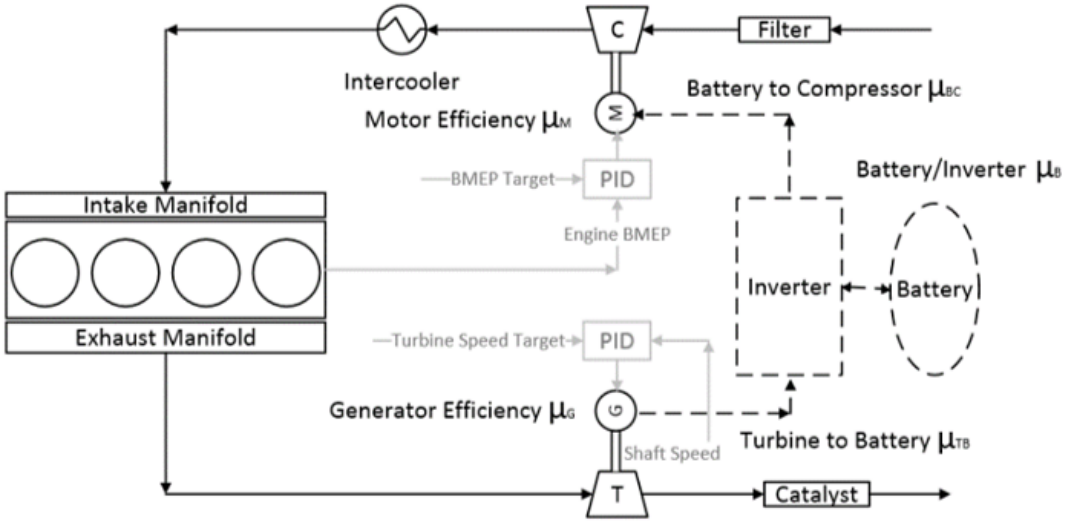

Figure 3.31 Engine model layout including the mechanically decoupled electrically assisted turbocharger

Efficiency Factor	Description
μ_M	Compressor Motor Efficiency
μ_G	Turbine Generator Efficiency
μ_{TB}	Electricity from Turbine to Battery
μ_B	Battery Energy Conversion Efficiency
μ_{BC}	Electricity from Battery to Compressor

Table 3.11 Efficiency Factor assumptions in the system

3.3.1.2 Two-stage EDC engine model

This model is based on a multi-stage electric boosting system for a 1.6L Diesel engine which has been downsized from a 2.0L baseline engine. The 1.6L engine air-path is composed of two EGR loops (low and high pressure) and a two-stage boost system, comprising an EDC and a VGT turbocharger. The air path layout is summarised in Figure 3.32. The electrical energy needed to drive the EDC can be taken from the

battery or the engine alternator. Engine inlet intercooler location (pre- or post- EDC) is also a design variable to be discussed. The main target for this paper is to investigate how the system configuration and control affect engine performance.

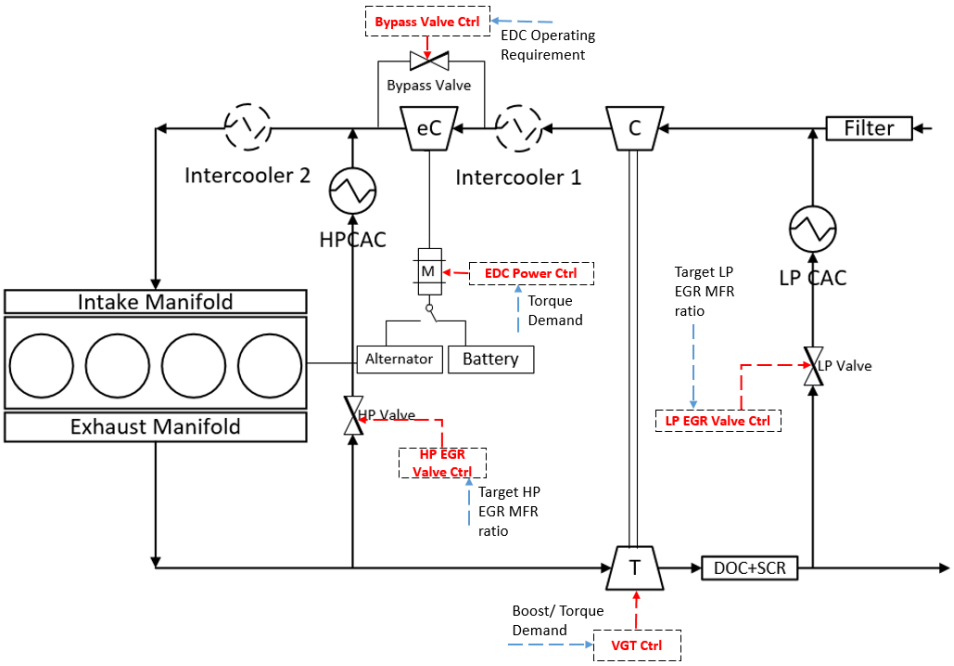

Figure 3.32 Engine air path Layout

The air path model included characteristic maps for the VGT, turbocharger compressor and electrically driven compressor. The electrically driven compressor is driven by a simple electric motor model. A simple alternator model is included in the case of energy being drawn from the crankshaft. An EDC bypass and control valve is also included. Boost is delivered according to the following control principles:

- At high engine speeds, the turbocharger compressor boost target was set to achieve the desired engine torque and EDC was bypassed.
- At low engine speeds, turbocharger compressor was set with consideration of compressor surge. This introduces a trade-off between reducing the electrical load of the EDC by operating the turbocharger compressor closer to surge or increasing the surge margin but requiring higher EDC power.
- During transients, the EDC can be used to reduce the boost error during periods of turbo-lag.

There is some level of flexibility in the control of the boosting system as the total boost pressure can be provided either from the turbocharger compressor or from the electrically driven compressor. The turbocharger compressor is controlled by the VGT guide vanes and must be selected with attention on possible surge. The VGT position will also affect the engine backpressure. The EDC is controlled using electrical power but does not affect engine backpressure. In this paper, the trade-off between VGT and EDC operation will be discussed in full load and low speed condition.

This air path model was controlled based on the following principles, the controlling structure is shown in Figure 3.32:

- VGT guide vanes were controlled using a PID controller targeting a specified compressor outlet pressure and respecting the compressor surge limit.
- The fuelling was determined based on an Air Fuel Ratio limit which also sped dependent.
- EDC controller adjusts the EDC speed for engine torque demand by increasing inlet pressure.
- Three valves, including two EGR valves and EDC bypass valve, are used for controlling the flow through each path.

In summary, the engine output power is adjusted by changing target boost pressures for both turbocharger compressor and EDC.

3.3.2 3D Modelling tool and basic model

In 3D modelling section, the optimisation of the two-stage turbocharged engine inlet air path has been investigated. By applying Computational Fluid Dynamics (CFD) to the individual component, the inflow of turbocharger can be potentially optimised and improve the turbocharger efficiency.

The baseline model is supplied by Ford, which is a CAD model for a gasoline engine inlet air path. The design target is the T-piece (TP) junction between EDC (Upstream) and turbocharger (Downstream). The boundary conditions were taken from a 1D model or the two-stage boosting system. In this thesis, a combined optimisation

methodology with ANSYS Fluent and Tosca Fluid is presented, modified the shape of T-piece junction for reducing its pressure drop and curling flow.

3.3.2.1 Model introduction

The Simulation focused on a TP junction in two-stage turbocharged engine inlet air path. Figure 3.33 shows the fundamental structure of the engine inlet air path, the TP junction between EDC and Compressor is the optimising object.

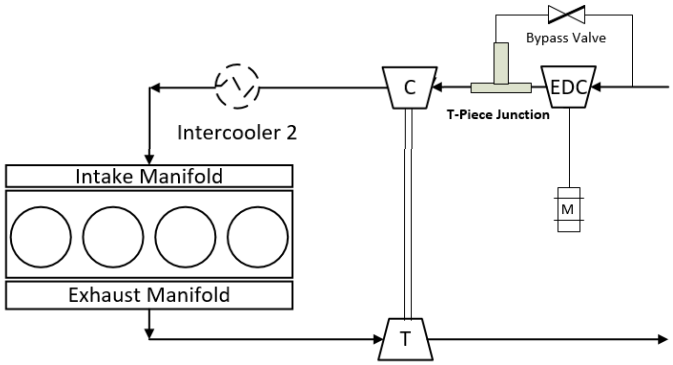

Figure 3.33 System layout

Figure 3.34(a) shows the whole air path system CAD model (excluding the engine block) and the extracted components need to be designed with. In order to further simplify the model, the EDC inlet pipes and small flow area (pressure control valve etc.) are deleted, the baseline model version for the start of CFD simulation is shown below in Figure 3.34(b), with the flow direction.

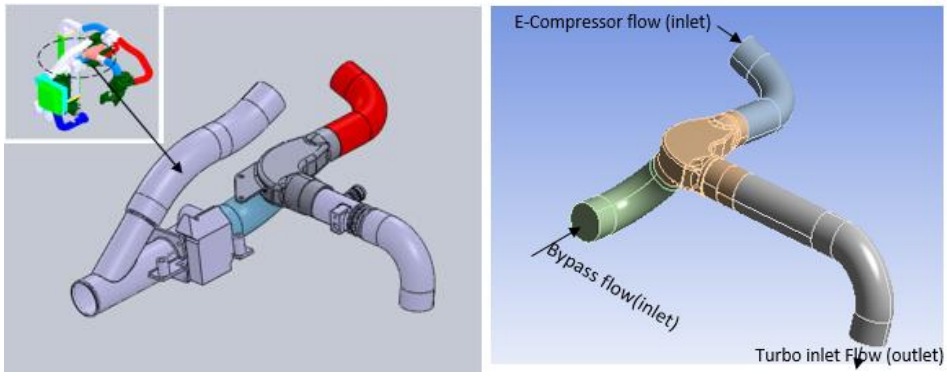

(a) (b)

Figure 3.34 (a) Engine system CAD model and components, (b) Simplified air path flow domain for simulation and optimisation.

Based on a previous study (results shown in Figure 3.35) the 90-degree bend of that airbox outside will lead to pressure drop; however has little effects on the pressure drop in the TP junction.

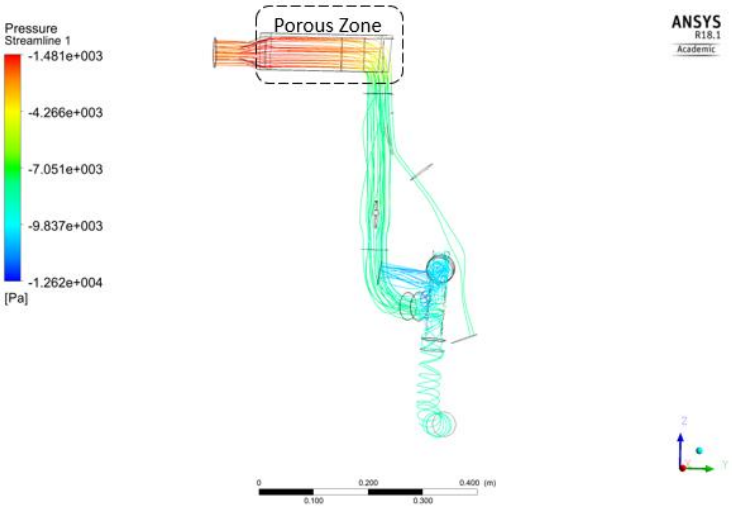

Figure 3.35 Porous Zone setting and pressure flow on the whole air path including air box.

Figure 3.36 shows the fluid domain, including the flow path, and the TP geometry extracted by ANSYS. There are two cases that need consideration and the optimisation problem needs to determine a design for the TP which can satisfy performance in both these cases.

- EDC bypassed case (Turbo only shown in the graph) representing high engine speed operation.
- Two-stage case (EDC and turbocharger) which represents low engine speed operation.

The research in this thesis is an initial study on the model, the boundary condition is taken from a 1D model of the engine layout (the model used: V-Charge simulation model from University of Bath). In the following simulations, only two-stage case was discussed, as it can fully explain the TP junction performance. One thing that needs to be mentioned here is that in V-charge 1D model, EDC is never bypassed; it does not supply boost but maintain the pressure go through it in some cases. The boundary conditions for each of the operating points are taken from a 1D engine performance model. These boundary conditions are summarized in table 1 with the ports and flow directions indicated in Table 3.12. The thermal effects of fluid will be ignored, flow

velocity, pressure, swirling and compressor efficiency are the main factors to be discussed.

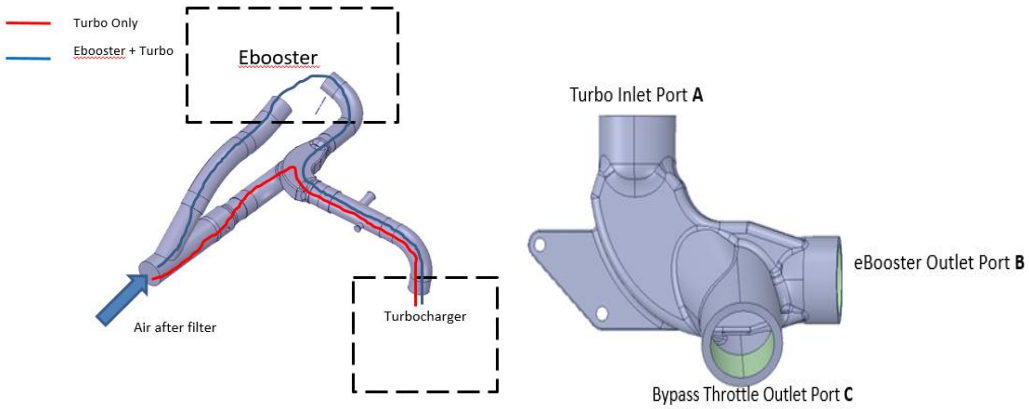

Figure 3.36 Fluid Domain and the flow path.

	Boundary status	Pressure (Pa)	Mass flow (kg/s)
Bypass Outlet (C)	Inlet1	absolute 97,000	0.0534
EDC Outlet (B)	Inlet2	absolute 97,000	0.0405
Turbo Inlet (A)	Outlet	relative -5300	0.0939

Table 3.12 Simulation boundary setup

3.3.2.2 Simulation tools

This research in this part is mainly 3D simulation based study. ANSYS and related optimisers are undertaken. ANSYS is used for modelling and fluent simulation, calculating the flow properties, other optimizers are mainly focused on the geometry optimisation and DOE literation optimisations.

A typical turbocharger model (supplied by group colleagues) is connected to TP outlet, this is mainly to study if the reduction of pressure drop and the swirl flow optimisation can help increase the compressor efficiency or isentropic power. What should be noticed here the compressor CAD model is not the model existed in the baseline engine system model, as that model is an STL format file, the compressor geometry data was not supplied. The compressor model used in this study is a small size model, which can suit with 1.6L engine inlet air path. The results generated in this part can only be

used for analysing the TP performance briefly but not on data validation or other jobs in detail. Figure 3.37 shows the CAD model of the turbo-compressor (Blade geometry and volute) in ANSYS.

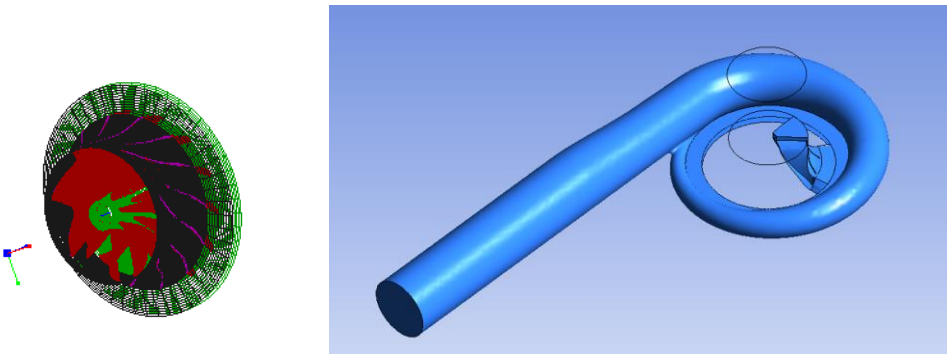

Figure 3.37 Compressor Blade Geometry and volute.

In this report, the TP geometry design space is limited, as there is a design requirement here:

-In respect for engine rock, it is min. 25mm + 10mm package safety clearance required for all body mounted components in X and Z direction (X cooling pack direction)

-Regarding engine rock in Y direction (to body side rail) it needs min. 12mm package clearance

-Engine mounted static components required min. 3mm clearance from part to part

-Engine mounted components under dynamic condition (drive shafts) are min. 8mm clearance required

The shape of TP, the angle of inflow and outflow will not be changed too much, to ensure the final design meets these requirements. Further comparison will be displayed in the result part. Figure 3.38 shows the engine rock packaging limit in three-dimensions and the local minimum distance between optimised TP fluid and engine rock. As the TP inlet and outlet pipe will not be changed, so those geometries were using the pipe shells instead of extracted fluid geometry. The local minimum distance is around 10mm, considering the width of the outside pipe, it is allowed in design. This value can also be reduced further by changing the initial design space of TP. One thing needs to be noticed here is that, as there is some simplification in 3D geometry of the fluid domain, so current TP is not perfectly matched with the inlet and outlet pipe (There are some overlapping in the area in the model), though it still can be used for characteristics analysing.

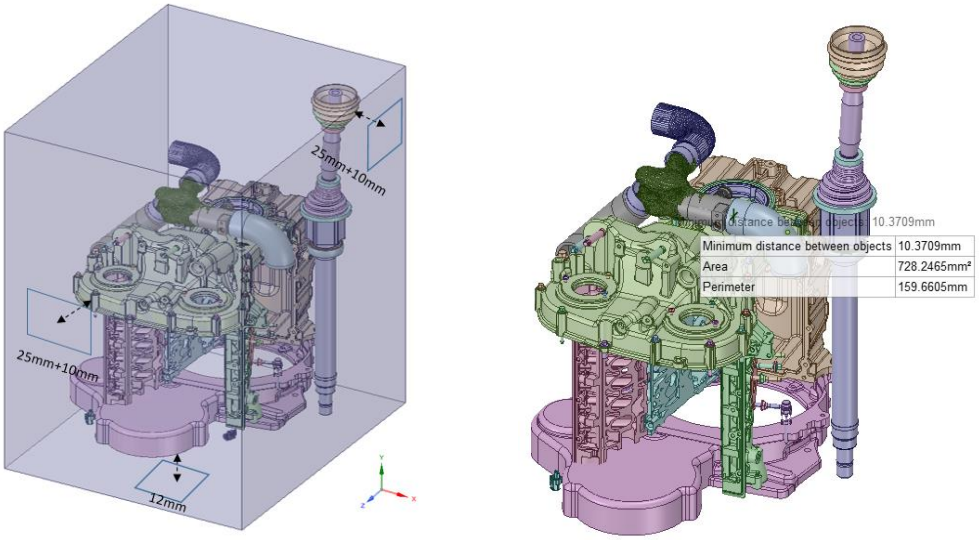

(a) (b)

Figure 3.38(a) Engine rock packaging limit space. (b) Local minimum distance between optimised TP and Engine rock.

3.4 Summary

This chapter introduced the test rig design and experimental setup of the research in this thesis. A two-stage engine gas stand test rig has been constructed, in order to undertake the steady and transient study of two-stage electric boost system. This test rig also can investigate the characteristics of the components in the air path. The test facilities are flexible, the air path configurations of the 2.2L diesel engine can be adjusted based on the research requirements. In this thesis, the rig is mainly for validating the steady state performance and investigate the transient performance of the two-stage system. The 1D and 3D simulation models and tools have also been introduced in this section, including 1D system simulation and 3D air path flow optimisation. In this thesis, both decoupled turbocharger and two-stage EDC boosting system are investigated. The decoupled turbocharger research is based on a 2.2L gasoline engine system; this work mainly focuses on the energy balance and optimisation control of the turbocharger. The research on two-stage EDC system is based on a 2.2L Diesel engine, which is correlated with the experiments, discovering the performance of hybrid boosting system and insulated turbocharger technology.

Chapter 4 – Research methodologies for specific mild hybrid air path applications.

This chapter introduces four air path applications that form the basis of the investigations within this thesis. For each application, the modelling methodologies and related experiment designs will be presented. In the first section, a turbocharger with an electrically-driven compressor test rig was introduced in Chapter 3, which will also be further used as a model resource for the THOMSON 1.6L engine model. A brief matching process of this system will be explained, then the transient study of components' sensitivity is conducted.

The second section introduces the 1D model of a decoupled electric turbocharger (DET) system, focuses on transient and drive cycle simulations. This part aims to identify the potential benefit of the DET, focusing on system energy balance and compressor size matching.

The next section will focus on the modelling and research for the inner-insulated turbocharger, investigating its thermal benefit regarding the turbine outlet temperature and its transient thermal performance. This part concludes the 1D heat transfer modelling work and related experiment planning.

The last section will discuss the 3D optimisation of the T-piece junction at engine inlet side for the two-stage system The aim of the 3D study is to demonstrate the potential for increasing the compressor efficiency and flow condition without changing the hardware of the whole system very much.

Work in this chapter has been published in: Liu, Y., Vijayakumar, R. and Burke, R., 2018, November. Analysis of the opportunities and trade-offs for a 48v electrified air path.Liu, Y., Burke, R.D., Akehurst, S. and Zhang, Q., 2017, October. Numerical Investigation Into the Performance and Efficiency Trade-Off for a Mechanically Decoupled Electric Boosting System.Burke, R., Liu, Y., Vijayakumar, R., Werner, J. and Dalby, J., 2019. Inner-Insulated Turbocharger Technology to Reduce Emissions and Fuel Consumption from Modern Engines (No. 2019-24-0184).

4.1 Modelling of the electrically driven compressor for a two-stage turbocharged Diesel engine system

The work presented in this part is devoted to systems level modelling of the experiment test rig and CRF 1.6L diesel engine from the CRF Company for project THOMSON. The aim of the research is to provide the predicted operating conditions of the boosting system to provide the specifications for the operating conditions of the turbocharger and EDC to enhance the component level design. This base model was controlled in the following manner:

- VGT guide vanes were controlled using a PID controller targeting a specified boost pressure for each engine speed.
- The fuelling was determined based on an Air Fuel Ratio limit which was also speed-dependent.
- The combustion model is a profile model, apparently based on measured heat release profiles.

In this way, the engine output power is adjusted by changing the target boost pressure to change the airflow through the engine. The work makes extensive use of the modelling environment's GT power to explore the different configurations and control the air path system.

4.1.1 Two-stage mild hybrid boost air path modelling

The modelling work for this section is based on a 2.2 L diesel engine, and the baseline engine model has already been calibrated and validated (Avola *et al.,* 2016; Avola *et al.,* 2015). The system layout is shown in Figure 4.1. The model has been validated based on a single-stage turbocharger engine stand test rig. As the whole rig is updated for the two-stage unsteady experiment, the air path model for the updated system had to be re-designed. Figure 4.2 shows the configuration of the two-stage test rig, which has already been introduced in Chapter 3. The area in the red dashed polygon is the air path that needs to be re-modelled.

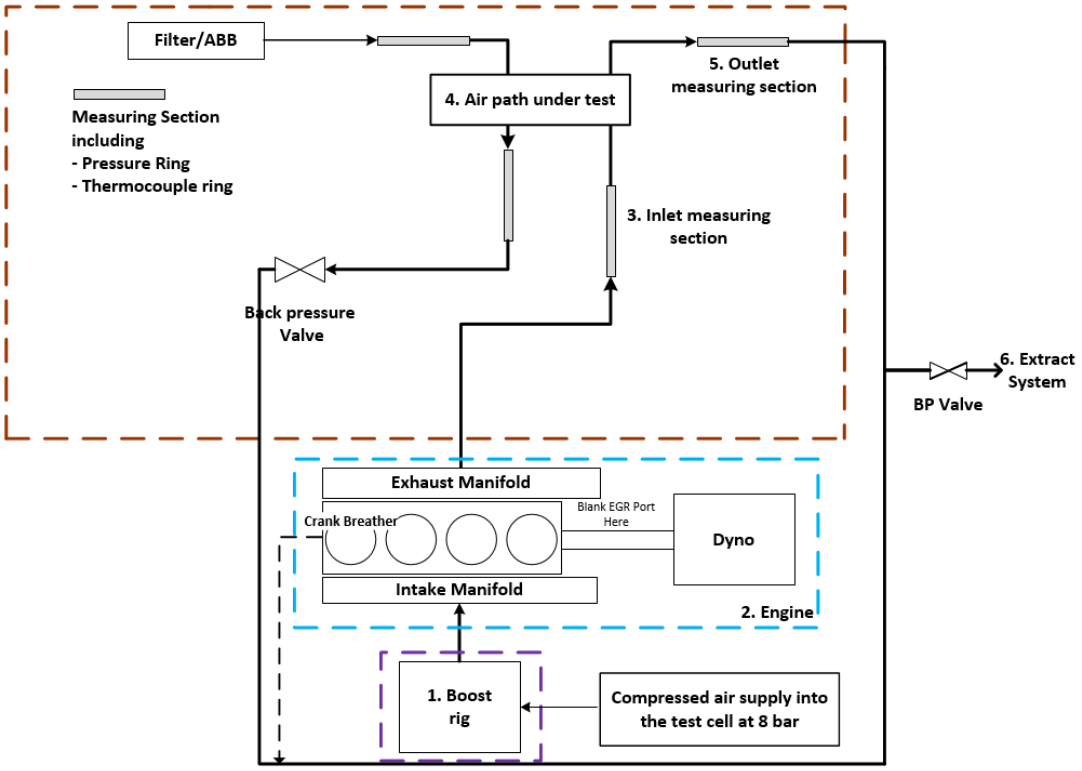

Figure 4.1 The schematic for the two-stage engine gas stand test rig.

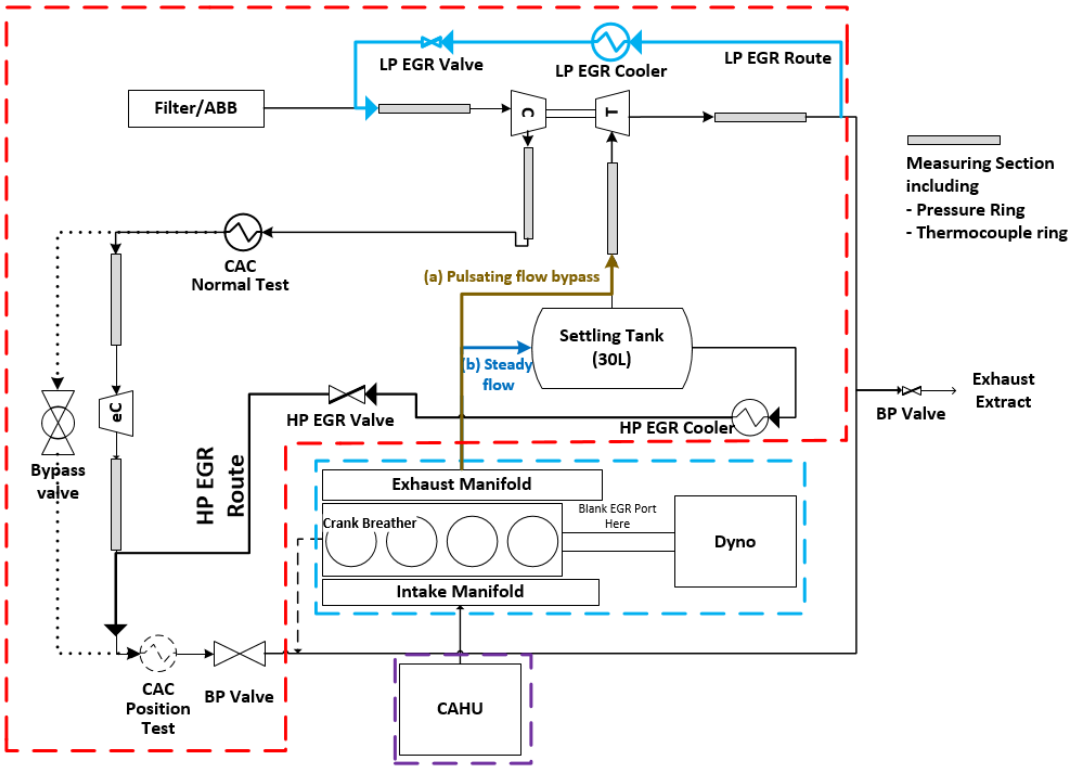

Figure 4.2 The structure of the updated test rig for modelling.

The GT-Power 1D model for the two-stage air path is shown in Figure 4.3. The VGT turbocharger and EDC maps are mapped by BorgWarner and the University of Bath, in both the gas stand and engine gas stand, as validated in Chapter 3.

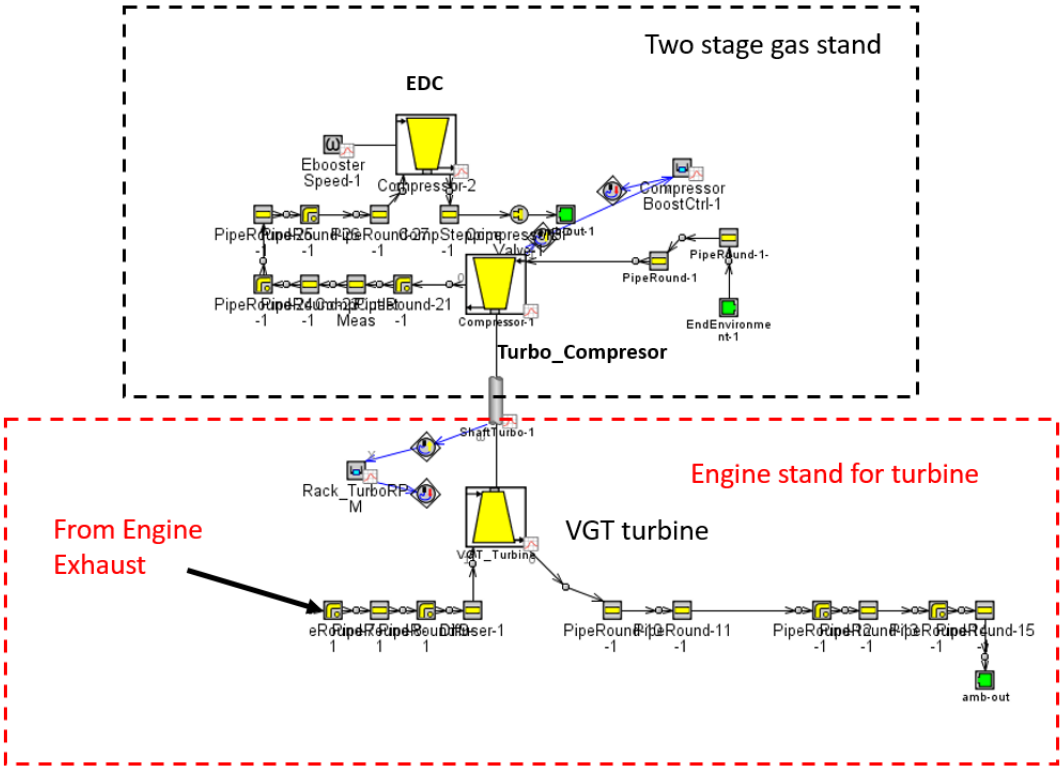

Figure 4.3 1D model for the experimental air path

The modelling for the air path includes:

1. The modelling of the pipework, turbocharger and EDC.
2. The calibration of the temperature, mass flow rate, pressure drop and boosters' speed.
3. The calibration of the turbine VGT and backpressure valve after the EDC.

The VGT and compressor backpressure valve are calibrated by applying PID controllers to the turbine VGT guide vane and backpressure valve, adjusting them to match the mass flow rate. A polynomial calibration was applied between the simulation results and experiment value for these two components after that.

The intercooler model was not applied here, and a simplified large heat transfer multiplier is added into the pipe wall heat transfer calculation to enable the gas temperature directly to reach the target value since the intercooler in the experiment is

oversized which will cool down any hot gas to the same temperature (approximately 80~90°C). EGR modelling is not conducted here, due to the failure of the EGR mass flow sensors in the early stage; besides, since the engine in this experiment is regarded solely as an exhaust generator, a back to back comparison is unnecessary for this part. The EGR investigation is mainly experiment-based in this thesis.

The designed operating points cover most of the available test region for the boosting air path, in regard to the range below:

Factors	**Lowest Value**	**Highest Value**
Turbo Speed	61.9 kRPM	157.8 kRPM
Turbine mass flow	0.0393 kg/s	0.0639 kg/s
Turbo Inlet pressure	118.2 kPa	289.4 kPa
Compressor outlet pressure	110.6 kPa	177.4 kPa
Compressor mass flow	0.0245 kg/s	0.0706 kg/s
Turbine inlet temperature	556 K	712 K

Table 4.1 Air path factors range in calibration

Thirty-five simulation cases were performed according to the experiment boundary condition. The compressor and turbine-related calibration results are shown in Figure 4.4 and Figure 4.5. All of the parameters between the simulation and experiment have proper alignment; however, there are some errors (shown in Table 4.2) and point shifts in the high speed high flow range, due to the difference between the simulation and reality, which lie in an acceptable range.

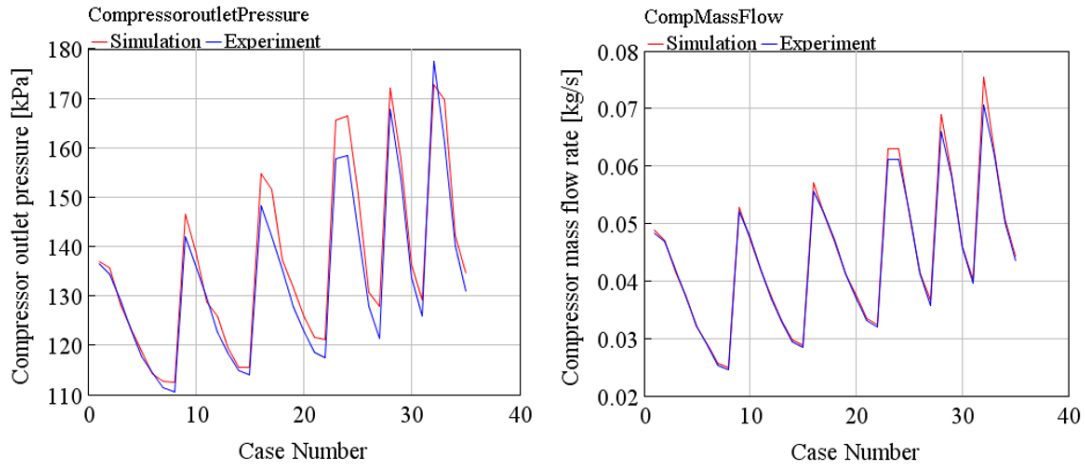

Figure 4.4 Compressor-related calibration

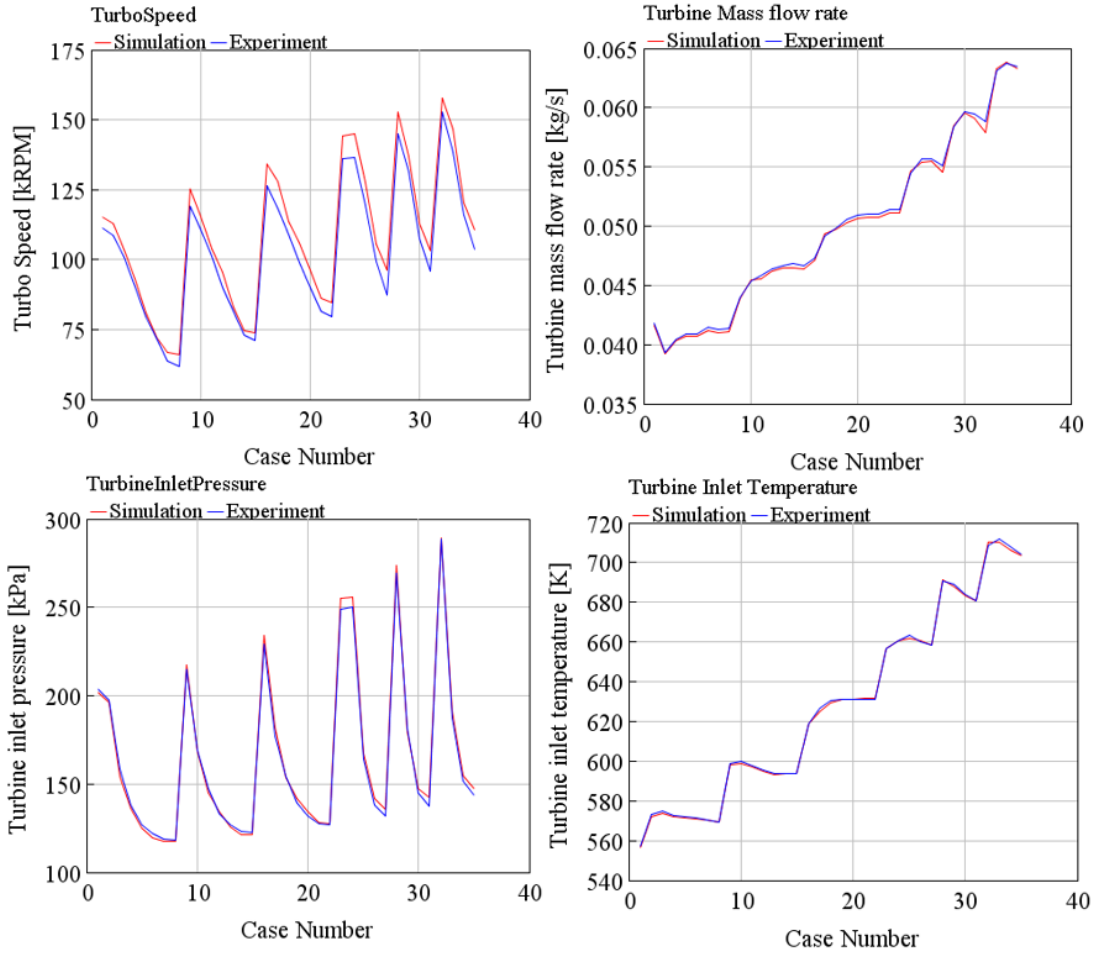

Figure 4.5 Turbine-related calibration

Comparing measurements	Root mean square error(RMSE)	Mean error	Maxium error
Compressor outlet pressure	4.261	2.10%	2.70%
Compressor mass flow rate	0.001	0.01%	0.07%
Turbocharger speed	5.693	4.70%	9.20%
Turbine mass flow rate	0.0003	0.40%	1.60%
Turbine inlet pressure	3.074	0.50%	2.90%
Turbine inlet temperature	0.794	0.06%	0.26%

Table 4.2 Errors of each measurement

4.1.2 Two-stage mild hybrid boost system model

The same air path design for the two-stage system mentioned in the last section has been applied to an engine model, in order to assess the engine performance with a mild

hybrid air path. This research used the turbocharger with an EDC air path model, the two-stage boost system then was applied on a 1.6L Diesel engine which has been downsized from a 2.0L baseline engine, as introduced in Chapter 3, section 4.1.2. The system configuration is shown in Figure 4.6. The results of this part will be illustrated in Chapter 5.

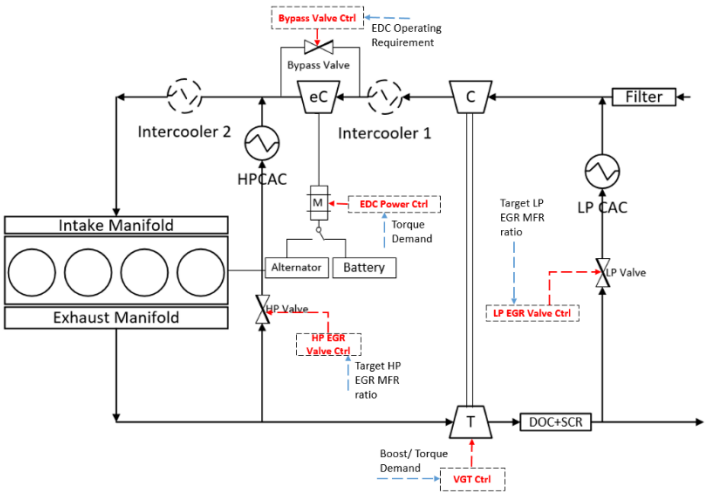

Figure 4.6 Engine air path layout

The modified GT Power model is illustrated in Figure 4.7(a), and the alternator model in Figure 4.7(b).

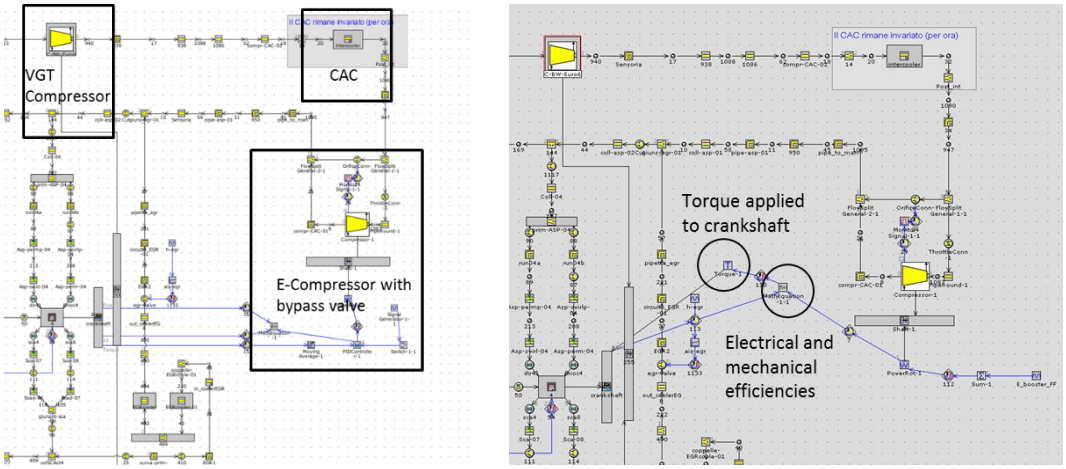

(a) (b)

Figure 4.7(a) Air path Model layout including EDC; (b) Integration of a simple alternator model

The air path model included characteristic maps for the VGT, turbocharger compressor and electrically-driven compressor. The electrically-driven compressor is driven by a simple electric motor model. A simple alternator model is included in the case of

energy being drawn from the crankshaft. An EDC bypass and control valve is also included. Boost is delivered according to the following control principles:

- At high engine speeds, a turbocharger compressor boost target was set to achieve the desired engine torque and the EDC was bypassed.
- At low engine speeds, the turbocharger compressor was set with a consideration of compressor surge. This introduces a trade-off between reducing the electrical load of the EDC by operating the turbocharger compressor closer to surge or increasing the surge margin but requiring higher EDC power.
- During transients. The EDC can be used to reduce the boost error during periods of turbo-lag.

There is some level of flexibility in the control of the boosting system as the total boost pressure can be provided from either the turbocharger compressor or the electrically-driven compressor. The turbocharger compressor is controlled by the VGT guide vanes and must be selected paying attention to possible surges. The VGT position will also affect the engine backpressure. The EDC is controlled using electrical power but does not affect the engine backpressure. Its operation should be selected bearing in mind the maximum electrical power available. In this paper, the trade-off between VGT and EDC operation will be discussed under full load and low speed conditions.

This air path model was controlled based on the following principles. The controlling structure is shown in Figure 4.6:

- VGT guide vanes were controlled using a PID controller targeting a specified compressor outlet pressure and respecting the compressor surge limit.
- The fuelling was determined based on an Air Fuel Ratio limit which was also speed-dependent.
- The EDC controller adjusts the EDC speed for engine torque demand by increasing the inlet pressure.
- Three valves including two EGR valves and the EDC bypass valve, are used to control the flow through each path.

In summary, the engine output power is adjusted by changing the target boost pressure for both the turbocharger compressor and the EDC.

4.1.3 System steady state modelling

The downsized 1.6L engine is an evolution of a lower power, 1.6L engine which provided the basis for the new air path. The turbocharger on the older engine was replaced by a larger device which allows for the increase in engine power. However, the larger turbocharger reduces the low speed, thereby limiting the torque due to the larger turbine being unable to create sufficient backpressure. Therefore, for the engine speed range of 1000-1500rpm, the EDC provides the additional boost pressure. The control methodology is based on the assumption that VGT is always controlled to deliver the largest pressure ratio it can achieve. For a given engine airflow requirement, this limit is effectively defined by the surge line of the turbocharger compressor. The rationale for this approach is that the thermal energy in the exhaust is free and so its use should be maximised. The maps and engine operating points with speed are shown in Figure 4.8. As can be seen, for engine speeds of 1500rpm and below, the turbocharger compressor is operating along the surge line and therefore limited in terms of pressure ratio.

The electrical power for the EDC can be obtained from a battery (without loading the engine crankshaft) or provided from the alternator (which increases the load on the engine crankshaft). The structure can be seen in Figure 4.6. If the alternator is used, then to maintain the same brake torque, the engine must produce a higher indicated torque which is achieved by burning more fuel, and therefore increasing the airflow requirement for a fixed limiting air-to-fuel ratio. An unexpected consequence of this is a reduction in the amount of electrical power required to drive the electrically-driven compressor. This is because, when using the alternator, the higher airflow shifts the operating point on the turbocharger compressor towards the higher mass flows (towards the right). This, in turn, means that a higher pressure ratio can be achieved within the surge limit (Figure 4.8).

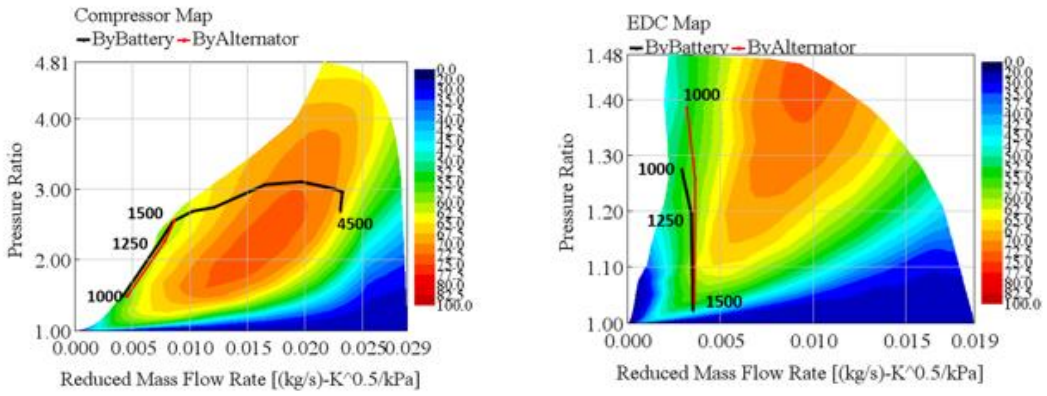

(a) (b)

Figure 4.8 (a) Compressor operating points. (b) EDC operating points

Despite the lower electrical power, the specific fuel consumption is naturally increased when using the alternator because the electrical energy is no longer "free" as in the case of the battery (Figure 4.9). When the EDC is driven by an alternator which is connected to the crankshaft, the system's BSFC will decrease as the EDC delivers more boost. When the EDC is driven by an E-motor, the energy comes from the battery, and electricity of about 0.5 to 2kW is needed in this case. It is justified to consider that the electrical energy is free in the case of the battery system as, unless the full drive cycle operation is considered, it is impossible to determine the origin of this energy. In a 48V hybrid vehicle, it is reasonable to assume that kinetic energy recovery will be available during braking and, if this is used subsequently to drive the EDC, then it is effectively free.

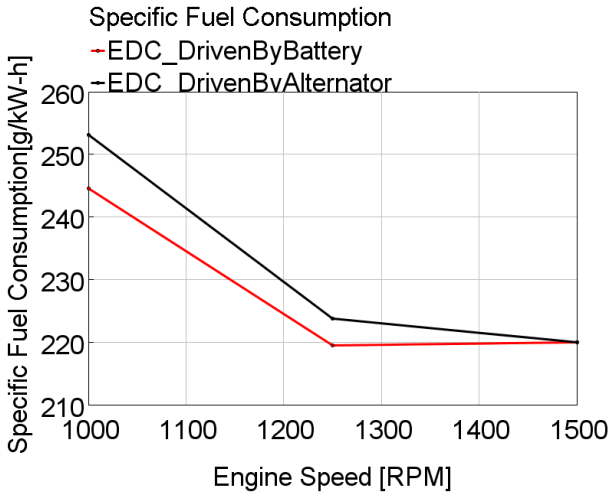

Figure 4.9 System's BSFC under different EDC energy source.

4.1.4 System transient modelling

The transient simulations are all performed, ignoring the electrical load of the alternator on the engine crankshaft. This is a reasonable assumption as a transient event is, by definition, short-lived and could sensibly be used based on energy storage. Firstly, the baseline transient model performance will be presented in the results chapter, followed by a series of three results, covering:

- The inertia of the turbocharger
- The sensitivity to the EDC power strategy
- The sensitivity to the VGT control strategy

For transient simulation, the engine heat release model, combustion rate, and heat transfer model have been changed into the transient mode. The transient operating points are from the 2000RPM 5bar part to the 2000RPM full load condition. It is important to note that the model has not full transient capability. In particular, the Water Charge Air Cooler does not include any transient aspects as, in this system, the CAC is an oversized design, to guarantee the cooling effects. The transient thermal behaviour of the engine block and exhaust manifold also lie beyond the scope of this thesis.

During the transient. A number of control actuators are available to influence the transient response of the engine:

- The EDC power level (kW used and duration of activation)
- The EDC bypass valve (duration of time spent using the EDC and bypassing it include the delay before closing)
- The Turbocharger VGT (position and duration in an over-closed position)
- The EGR valve closing times (both HP and LP valves)

Turbocharger inertia is a key factor in turbo lag during the load steps and will be analysed later. The transient results of this part will be introduced in Chapter 5 section 2.

4.1.5 Engine intercooler modelling with different intercooler layouts

Another interesting topic is the position of the intercooler. The intercooler's location will affect the EDC inlet temperature so that the EDC's efficiency and boost requirement will change. It is necessary to study how different intercooler locations change the EDC's work status and engine inlet temperature. The intercooler can be:

- In between the turbocharger and EDC.
- Downstream of the EDC and turbocharger.

In the previous engine model, the inlet air cooler model is an implementation designed to replicate the experimental boundary conditions. The heat transfer in different cases is not modelled in a physical sense. The wall temperature of the intercooler was set at:

$$T_{wall} = T_{intercooler\_outlet} - T_{post\_intercooler} + T_{input} \qquad (18)$$

The intercooler outlet temperature$T_{intercooler_outlet}$ and the pipe temperature after intercooler $T_{post\_intercooler}$ is almost the same, and the heat transfer multiplier is set at 100 (very large), so whenever the air comes through the intercooler, the temperature will be reduced to the set valueT_{input}. This method can help to match the simulation results with the test data, but cannot be used to predict the simulations in different situations.

A theoretical heat transfer model is built in order to predict the engine inlet temperature more accurately, which is mainly used for discussing the effects of the intercooler location. The approach adopted was to create a heat transfer-based model that exhibits similar behaviour to the imposed wall temperature approach when it is located in the same position within the air path. After moving to an alternative location, it will provide a better estimate of the performance with the modelled heat exchanger.

For the condition when the heat flow is steady, the heat transfer between the cooling fluid and engine inlet air is shown in Figure 4.10.

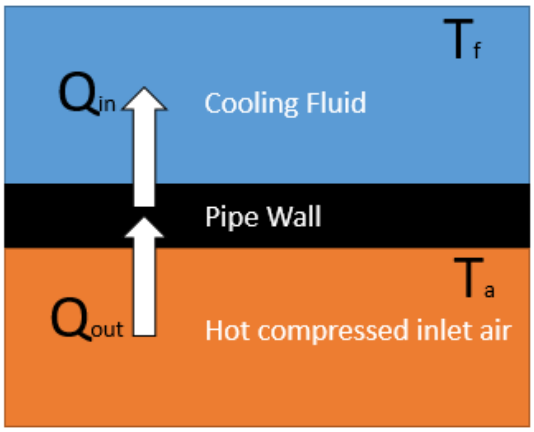

Figure 4.10 Heat transfer between the compressed inlet air and cooling fluid

Using Newton's law of cooling, some assumptions can be made:

The heat transfer between the inlet air and wall Q_{out} is equal to that between the wall and cooling fluid Q_{in}

In which:

$$Q_{out} = qA = hA(T_a - T_{wall}) = h_{a\_w}\pi DL(T_a - T_{wall}) \quad (19)$$

$$Q_{in} = qA = hA(T_{wall} - T_f) = h_{f\_w}\pi DL(T_{wall} - T_f) \quad (20)$$

$$Q_{out} = Q_{in} \quad (21)$$

Where

Q_{out} is the heat transfer between the engine inlet air and cooling pipe wall

Q_{in} is the heat transfer between the cooling fluid and cooling pipe wall

q is the heat flux (W/m^2)

A is the fluid/solid "wetted" area (m^2)

h_{a_w} is the convective heat transfer coefficient between the engine inlet air and cooling pipe wall (W/m^2K)

h_{f_w} is the convective heat transfer coefficient between the cooling fluid and cooling pipe wall (W/m^2K)

D is the cooling pipe diameter

L is the cooling pipe total length

T_a is the engine inlet air temperature

T_{wall} is the cooling pipe temperature

T_f is the cooling fluid temperature

Also, as the pipe wall is metal made, it can be assumed that the heat transfer inside the pipe wall is far bigger than the outside and that the temperature of the pipe's inner and outer surface is always the same.

Based on those three equations, it can be inferred that:

$$Q_{out} = Q_{in} = \pi DL(T_a - T_f)h_{a\_w}h_{f\_w}/(h_{a\_w}+h_{f\_w}) \quad (22)$$

$$T_{wall} = (h_{a_w}T_a + h_{f_w}T_f)/\,(h_{a\_w}+h_{f\_w}) \quad (23)$$

These formulae are used to define the intercooler's wall temperature and heat transfer rate. A steady state simulation will be performed based on the heat transfer model above, in order to investigate how this will affect the engine inlet temperature and EDC operation. The compressor operating conditions and the boundary conditions of the simulation is related to the full load engine operating curves.

4.1.6 System's performance with different EGR layouts

The ability to flow EGR near the limiting torque curve is investigated due to its importance in emissions control regarding the Real Driving Emissions legislation. In this engine system, the EDC boosting effects and CAC cooling will affect the HP EGR mixing speed and the air path flow condition. It is necessary to study how different HP EGR locations change the system's performance. The different HP EGR location layouts are shown in Figure 4.11 (mid route 1 and 2). The HP EGR can be:

- Between the turbocharger and CAC. (Mid route 1)
- Between the EDC and CAC. (Mid route 2)

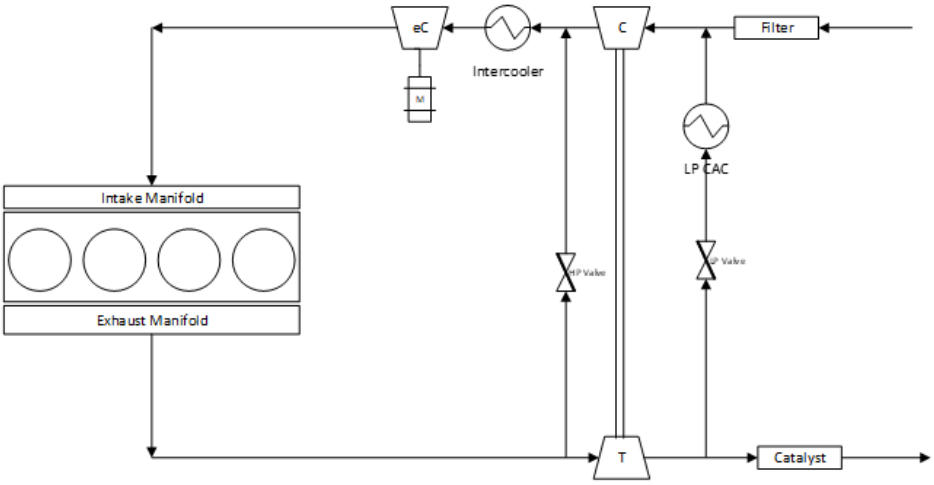

(a)

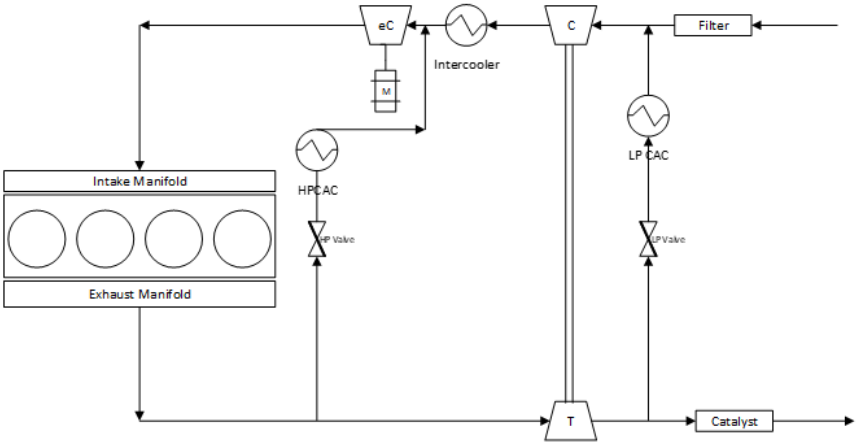

(b)

Figure 4.11 (a) Mid route 1 EGR layout. (b) Mid route 2 EGR layout.

As the transient process of EGR mixing is quite fast, it is difficult to capture using current engine models. Conducting a back to back comparison between the experiment and simulation for this kind of research currently remains a challenge. For this research, an experiment-only research design is used, designed to identify the transient effects of EDC and turbine VGT on HP EGR mixing under different EGR routing conditions (Mid route 1 and 2). The controlling factors vs the time design is shown in Figure 4.12. The transient start to end time for the engine speed is 5s, which is the same if adjusting for EDC speed, VGT position and those valves. However, in order to see how the EDC and VGT affect the EGR mixing, they will be held at the adjusted value for 5s longer and then restored to the baseline value in another 5s. The whole transient lasts 160s, as the system needs time to heat up or release the extra heat.

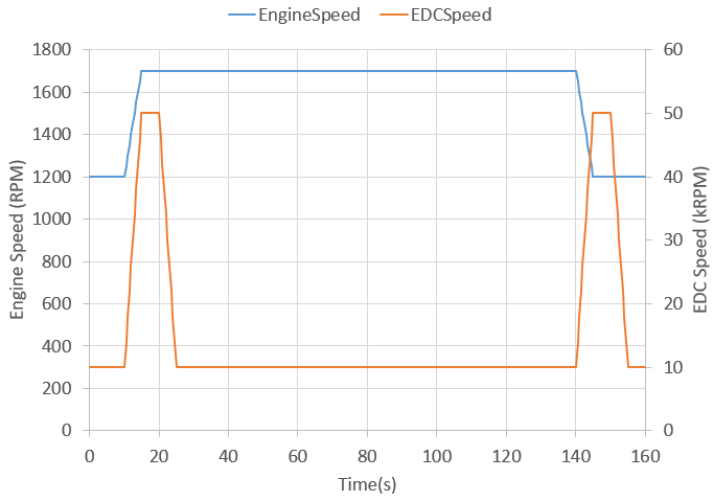

(a)

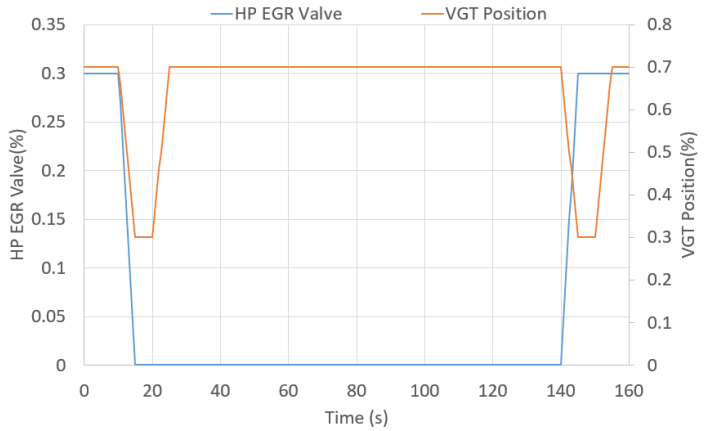

(b)

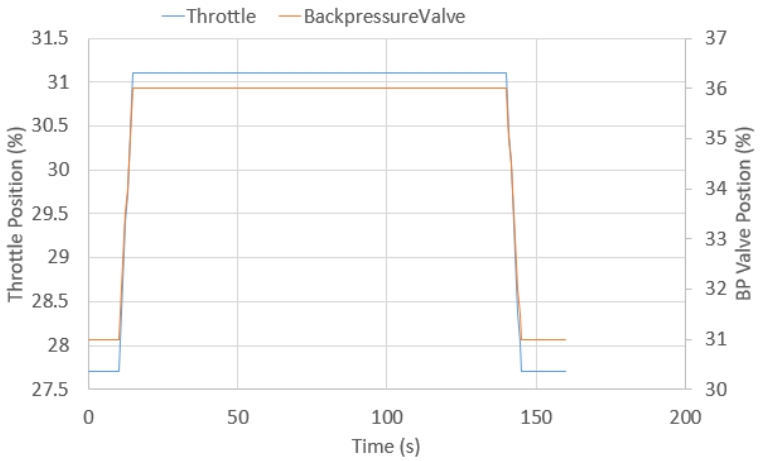

(c)

Figure 4.12 Transient schedule of the EGR mixing test (a) Engine speed and EDC speed. (b) HP EGR Valve and VGT position. (c) Throttle and BP Valve position.

4.2 Modelling of the decoupled electric turbocharger for a gasoline engine.

After the study of the two-stage system, the performance of another electric boost systems was also be investigated, using a similar methodology. With a decoupled electric turbocharger (DET), more attention should be paid to the control between the electric turbine and compressor, to find the internal energy balance. The simulations work steps for DET is shown below:

1. Modelling a DET: In this step the base GT Power model is constructed that captures the air path and a simplified representation of the electrical components.

2. Turbine Scaling Analysis: A simple scalable model of the turbocharger is implemented to assess the trade-off from the choice of compressor and turbine mass flow capacity in a DET layout.

3. Electric turbocharger power analysis: In this step the power consumption/generation of the DET will be analysed in the engine full load and part load condition with scaling factors, which will then be applied to different drive cycles.

4.2.1 The Decoupled Electric Turbocharger (DET) Model

The turbocharger model is based on a given gasoline turbocharged direct injection 2.0 litre engine with 240PS. The model is based on GT-Power, a mechanical engineering simulation software.

The standard model was modified to incorporate a mechanically-decoupled electric turbocharger, as shown in Figure 4.13. The compressor is connected to an electric motor which will drive the compressor to create boost pressure. Within the model, the motor is controlled by a PID controller, by varying the compressor speed to reach different levels of brake mean effective pressure (BMEP). The turbine is connected to a generator which is controlled by a second PID controller that adjusts the turbine operating point. A compressor bypass valve and turbine waste-gate are also considered (not shown in Figure 4.13); however, both are closed when the boost pressure is

demanded. Although an electric motor and generator are included, other electrical devices are not modelled in detail (inverter and battery) and are represented by simple efficiency terms. Each of these efficiency terms is illustrated in Figure 4.13 and Table 4.3. Notice that the efficiency value for each factor is the baseline setting for the simulation, which will be adjusted later to see how much efficiency the system needs to get benefit.

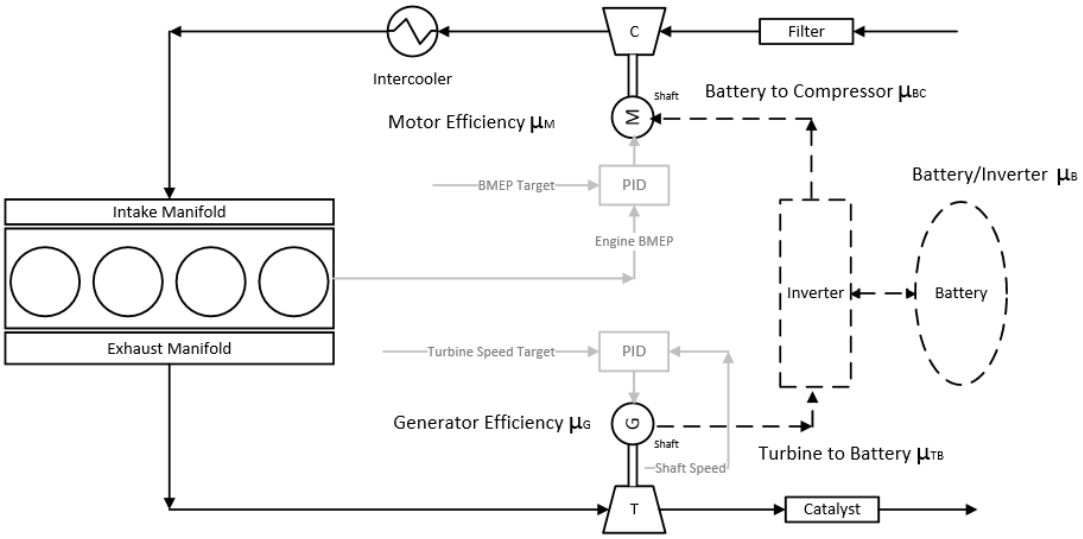

Figure 4.13 DET controlling layout

Efficiency Factor	Description	Value (%)
μ_M	Compressor Motor Efficiency	85-95
μ_G	Turbine Generator Efficiency	85-95
μ_{TB}	Electricity from Turbine to Battery	85-95
μ_B	Battery Efficiency	80
μ_{BC}	Electricity from Battery to compressor	85-95

Table 4.3 Efficiency factor assumptions in the system

The model was used to analyse the efficiency of the engine system operating under steady state conditions.

As the engine now incorporates two power outputs (the engine crankshaft and surplus electrical energy in the inverter), the system's efficiency rather than the engine's efficiency is considered, as described in equation (1).

$$P_{total} = P_{engine} + P_{turbine} \times \mu_G \times \mu_{TB} \times \mu_B - P_{compressor} \div \mu_M \div \mu_{BC} \quad (1)$$

We define the electrical efficiency on the turbine side as:

$$\mu_T = \mu_G \times \mu_{TB} \times \mu_B \quad (2)$$

And the electrical efficiency on the compressor side as:

$$\mu_C = \mu_M \times \mu_{BC} \quad (3)$$

For the steady state investigations, the battery's efficiency was assumed to be 80%, whilst the motor, generator and invertor's efficiency was assumed to be 95%. In this way, the power output of the electric turbocharger and the whole engine system can be calculated, as well as the combined system's specific fuel consumption. Combined with driving cycles, the ability regarding electric turbocharger power generation can be shown.

$$bsfc = \frac{m_{fuel}}{P_{total}} \quad (4)$$

The effect of turbine size was investigated by introducing a simple turbine scaling factor (which will be introduced Section 2.2). For each size, simulations were performed at 46 different engine operating points to produce an overall engine efficiency map. The turbine speed and turbine pressure ratio are fixed to be the same for different turbines at the same operating point.

4.2.2 The turbocharger scaling methodology

Within the model, the scaling of the turbine size is critical to the validity of this study. To avoid the need to introduce a range of maps representing different-sized devices, a simple scaling method is proposed. However, it is important to assess how well the scaling methods capture the flow and efficiency characteristics of real turbochargers as this will give a perspective on the expected error induced by this method.

The research in this section is aimed at giving a simple mathematical method to assess a wide range of turbine and compressor sizes without the need to replace specific maps within the simulation. There will be some level of inaccuracy here, due to the geometry design and inner roughness differences between turbochargers, but the aim is not to find a specific turbine and compressor, but rather the sensible size range, also to get the trade-offs between turbocharger size and the system performance.

Various scaling methods have been proposed for scaling the turbine: Kurzke et al. (Kurzke *et al.,* 2000) applied three characteristic numbers which describe the highest efficiency region, mass flow-speed relation and the shape of speed lines. They compared the points with 70% and 10% turboshaft power while the compressor is at a 90% design speed, and the new method can cover the most typical map data. Kern et al. (Kern *et al.,* 2011) used this method in his simulation to discuss the injection system's effect on turbo components' surge margin, but this method can only be used when the compressors have similar maps, and the geometry design is known in detail (Misté *et al.,* 2012). A more practical method has been provided by Dufour et al. (Dufour *et al.,* 2006), who summarised the classical scaling method given by the Buckingham Π-theorem (Buckingham, 1914), and applied this to the rotating speed, diameter, and mass flow rate. For a specific scaling target, the ratio of the mass flow rate between two turbines can be named the mass flow multiplier, which is:

$$Massflow\ Multiplier = \frac{m^{scaled}}{m^{baseline}} \qquad (5)$$

Then the speed relationship can be given as:

$$\frac{N^{baseline}}{N^{scaled}} = \frac{(\frac{m^{scaled}}{m^{baseline}})^{0.5}}{(\frac{RT_{inlet}^{Scaled}}{RT_{inlet}^{baseline}})^{0.25}(\frac{p_{inlet}^{Scaled}}{p_{inlet}^{baseline}})^{0.25}} \qquad (6)$$

When the turbines are operated under the same condition, R and T are the same. This equation can be written as:

$$Speed\ Multiplier = \frac{N^{scaled}}{N^{baseline}} = \frac{1}{\sqrt{Massflow\ Multiplier}} \qquad (7)$$

Which can be simply applied in various simulation models. Dufour et al. (Dufour *et al.*, 2006) also considered the effect of the Mach number effects and efficiency scaling. Ernst et al. (Ernst *et al.*, 2011) further developed this scaling method by including trim scaling, which gave a better correction between the scaled and measured nominal maps. They concluded that this method still has many limitations but can be used. Efficiency scaling is one of the problems, as a compressor or turbine will have considerable energy loss due to its geometry design, and different designs will have very different efficiency trends. Ernst et al. (Ernst *et al.*, 2011) summarised the efficiency scaling method from Casey (Casey, 1985), shown in equation (8) (where n is an empirical factor which is related to the specific compressor geometry design and lies in the range of 0.1 to 0.675). In this thesis, the efficiency multiplier is calculated by dividing the two peak efficiency of the baseline-turbine and target turbine because, in later research on the e-turbo, it was assumed that the turbines scaled had a similar design and peak efficiency.

$$\eta_{scaled} = 1 - \frac{1 - \eta_{baseline}}{(MFM)^{\frac{n}{2}}} \qquad (8)$$

For transient simulations, the turbocharger inertia is also important. The scaling of the inertia is assumed to vary to the power 2.5 of the mass flow. This is calculated because the inertia of the rotor is proportional to the wheel radius to the power 2:

$$I = \int r^2 dm \propto r^2 \qquad (9)$$

But the mass is proportional to the volume of the rotor, such that the inertia is, in fact, proportional to the rotor radius to the power 5:

$$I \propto mr^2 \propto \rho r^5 \propto r^5 \qquad (10)$$

Mass flow is proportional to the cross-sectional area of the flow passages within the device, and hence related to the rotor radius to the power 2, assuming that the air speed in the device is similar:

$$\dot{m} \propto Av \propto vr^2 \propto r^2 \qquad (11)$$

Therefore, the relationship between the mass flow and inertia is given by:

$$I \propto r^5 \propto \dot{m}^{5/2} \qquad (12)$$

Finally, it is assumed that the contribution to the total rotor inertia of the turbine is approximately four times that of the compressor, i.e.$I_T \approx 4I_C$:

$$I_s = 0.2I_b * (MFM_C\text{^}2.5) + 0.8I_b * (MFM_T\text{^}2.5) \quad (13)$$

To quantify the uncertainty introduced by this method, the scaling results are analysed for eight different turbines with a range of sizes. Table 5 shows the turbine wheel diameters and the scaling factor to the reference turbine (#1).

Turbine Number	**Wheel Diameter (mm)**	**MFM**
1	64.4	1
2	50.9	0.49
3	51	0.54
4	48	0.58
5	55.8	0.78
6	55.9	0.79
7	59	1.18
8	72	1.40

Table 4.4 Turbine Mass flow multiplier and diameter comparison

Each of the turbines was scaled back to the same size as turbine #1 by applying equations 6-8. Figure 4.14 compares the scaling results for mass flow and efficiency:

Figure 4.14(a) shows the mass flow rate comparison between turbine 1 (baseline turbine) and other turbines. The smaller turbines were better matched with baseline data, while the bigger turbine has a larger error. The results in Figure 4.14(b) used only the mass flow and speed multiplier (i.e. without the efficiency multiplier), and Figure 4.14(c) shows the efficiency results when scaling with the mass flow (MFM), speed (SPM) and efficiency multiplier (EFM).

In Figure 4.14(b), all of the other turbines are scaled to turbine 1. Clearly, those turbines have a different turbine geometry design and totally different sizes (which makes their map shape and peak efficiency different from others). Scaling with the efficiency multipliers improves the correlation between the devices.

When MFM, SPM and EFM are all considered, the central region of most turbine maps will be well matched, as shown in Figure 4c. However, for turbine 2 and turbine 3, which have the smallest multiplier value, this method has a significant error. Turbine 4 is also small but has a bigger scaling factor than 2 and 3 which means that it has the ability to allow more exhaust to pass through. One conjecture is that both of these turbines have a totally different size with different turbine map shapes, which makes the scaling results poor. Besides, the scaling results will be inaccurate when the operating points are close to the map boundary.

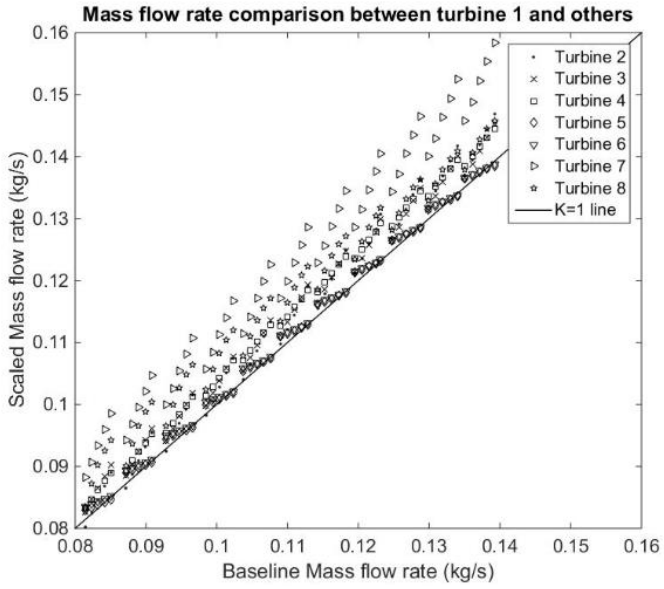

(a)

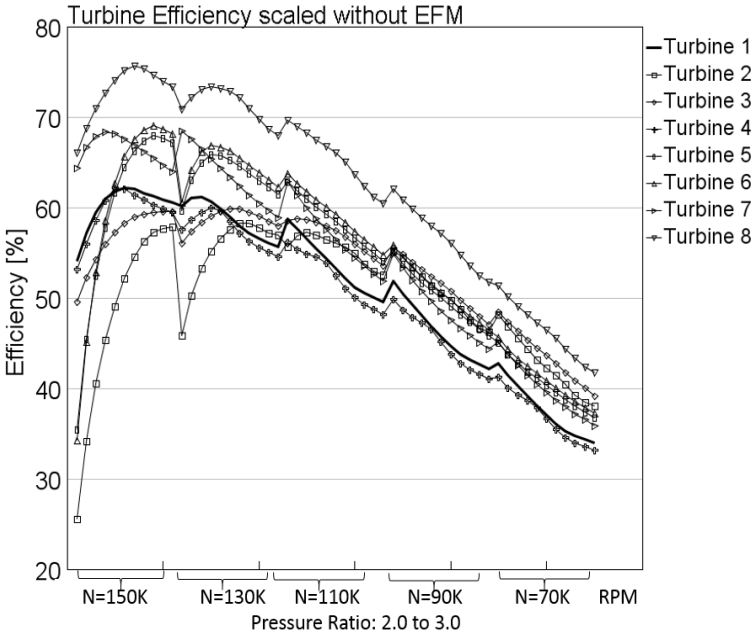

(b)

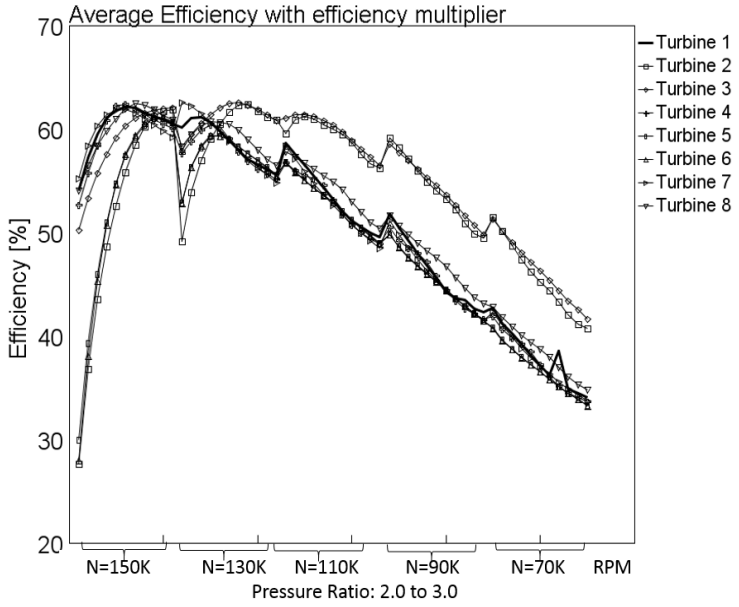

(c)

Figure 4.14 Comparison of efficiency for all turbines after scaling; (a) scaled mass flow rate vs baseline mass flow rate (b) ignoring efficiency scaling and (c) with efficiency scaling

As mentionsed in section 2.1, the EFM is generated by calculating the average efficiency difference with two turbochargers. In Figure 4.14(c), EFM failed to scale all the turbine maps to the reference, especially for the two small turbines 2 and 3. However, there is still a trade-off between EFM and turbine size, Figure 4.15 shows the relationship between EFM and MFM, it can be found that as the turbine size

increasing, the efficiency multiplier will drop, which means the average turbine efficiency will increase. Turbine 7 is an exception, because this turbine is designed for the two stage high pressure located turbocharger, which has a different geometry design. Another point can be found is that as the scaling factor is becoming far away from 1, the scaling accuracy will drop fast. This is also the reason why the methodology in this chapter can only used for scaling the turbine in simliar size and the results can only be used for estimating the system performance but can not be used for predicting the real turbocharger measurements.

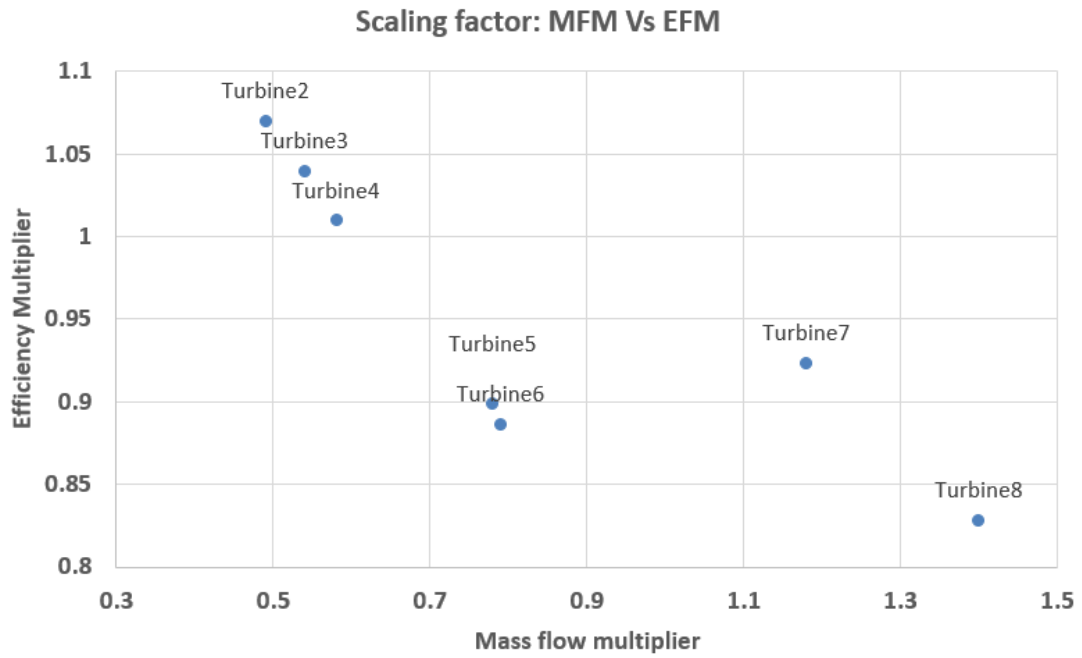

Figure 4.15 Relationships between MFM and EFM

4.2.3 System simulation procedures

The original engine map has boost regions where a compressor is needed to supply the boost pressure and a natural aspiration region where the compressor is bypassed. The map shown in Figure 4.16 is supplied by Zhang (Zhang, 2015). Both full and part load conditions will be discussed.

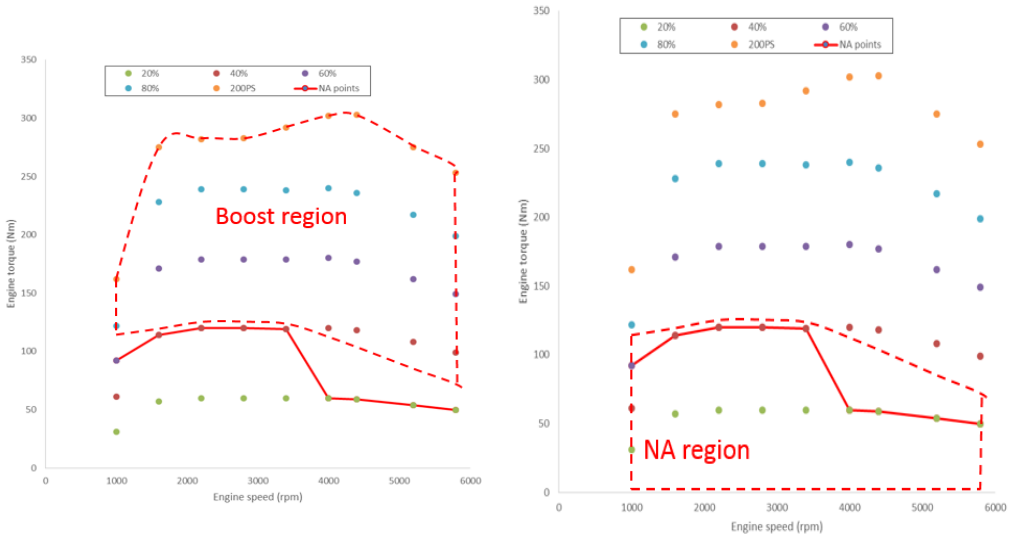

Figure 4.16 Boost region on the engine map (Zhang, 2015)

In order to discuss how turbine size affects engine performance, PID controllers here are used to adjust the BMEP value to make it equal to the original engine BMEP. The turbine speed is set to work in the most efficient region. The throttle is fully open, and the turbine waste-gate is fully closed, which ensures that the exhaust energy is used by the turbine completely.

For the vehicle-level study, a simple vehicle model was implemented where measured data from the different driving cycles were used to impose the engine speed and torque requirements on the engine. A basic driveline model was used to calculate the vehicle gear ratio and tractive force requirements.

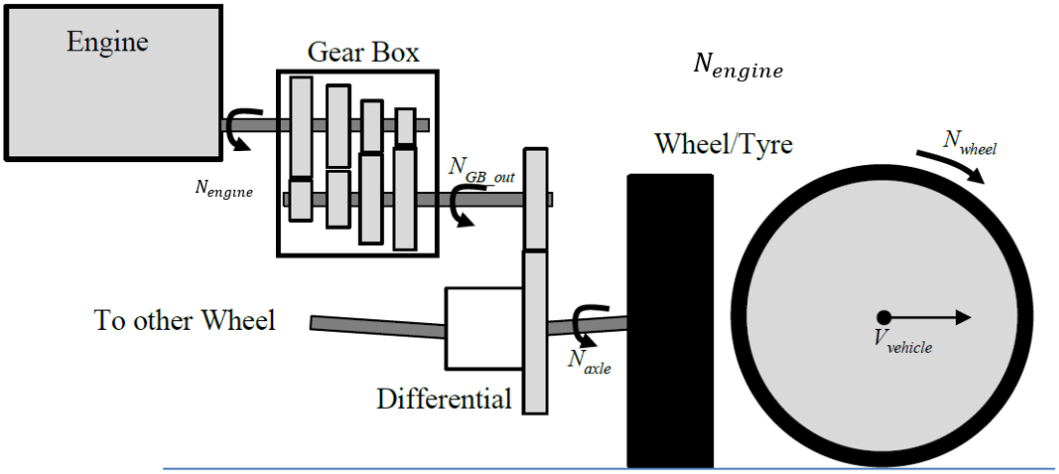

Figure 4.17 Vehicle driveline schematic

$$F_{wheel} = F_{traction} = \tau_{engine}\mu N_{engine}/(D_{wheel}N_{wheel}) \quad (14)$$

$$\pi N_{engine}D_{wheel} = V_{vehicle}k_{gear} = \pi N_{wheel}D_{wheel}k_{gear} \quad (15)$$

$$N_{engine} = N_{wheel}k_{gear}$$

For different engines driving the same vehicle, the gear ratio needs to be varied.

$$N_{engineX} = N_{engine}k_{GRmulti} = N_{wheel}(k_{gear}k_{GRmulti}) \quad (16)$$

$$\tau_{engineX} = \tau_{engine}/k_{GRmulti} \quad (17)$$

The efficiency and net electrical power were obtained from the engine efficacy maps obtained from Chapter 3 and analysed over the full driving cycle. The measured data time step is 0.5s, which is regarded as a uniform linear motion. By applying these points to the engine maps, for each single measured point, the power consumed and output from the system are numerated, so the energy for each cycle is:

$$W_{cycle} = \sum P_{total\_i}t_{step} \quad (18)$$

$$P_{average} = W_{cycle}/t_{total} \quad (19)$$

$$P_{benefit} = (\sum(P_{total_i} - P_{engine_i})t_{step})/t_{total} \quad (20)$$

Three driving conditions were considered: the NEDC, WLTC and eight different on-road trips. The engine speed and BMEP operating points for NEDC and WLTC are shown in Figure 4.18.

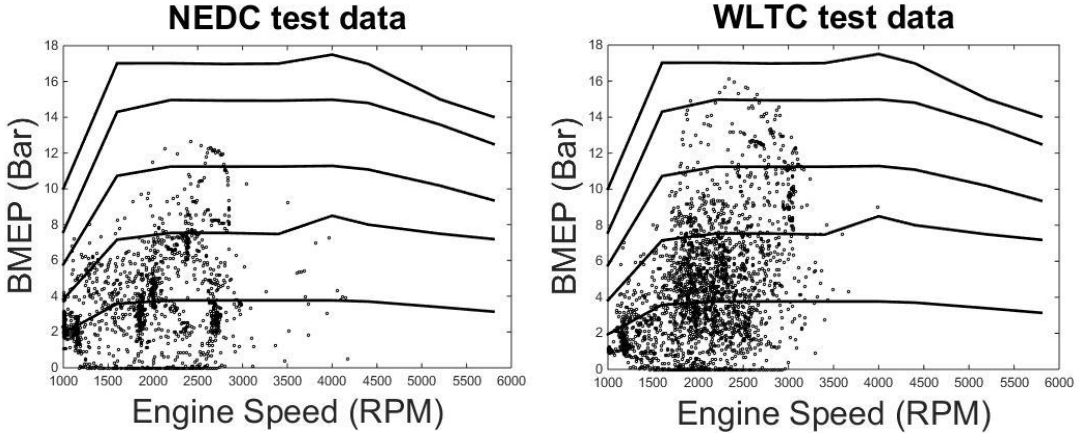

(a) (b)

Figure 4.18 Driving cycle data comparison (a) NEDC (b) WLTC

The characteristics of these routes as well as the NEDC and WLTC are summarised in:

Drive Cycle	**Average Speed (km/h)**	**Length (km)**	**Description**
NEDC	33.13	130.5	11 times NEDC tests
WLTC	46.97	23.49	
On-road 1	60.12	49.41	Driver A – Mix of City and rural driving
On-road 2	48.21	52.13	Driver A – reverse of On-road 1
On-road 3	37.72	37.88	Driver B – Rural Commute
On-road 4	60.66	117.88	Driver B – Motorway drive
On-road 5	63.41	184.52	Driver C - Long distance motorway drive
On-road 6	55.16	148.25	Driver C - Long distance motorway drive
On-road 7	54.54	134.42	Driver C - Rural commute
On-road 8	38.34	17.90	Driver C - Rural commute

Table 4.5 Summary characteristics of the different driving routes

The efficiency of the system varies significantly across the engine map as well as the net electrical energy balance. In addition, the results obtained depend on the efficiencies of the electrical components for which only assumed values had been taken. Therefore, two sensitivity studies were conducted on the electrical efficiency and the choice of vehicle gear ratios (which affect the engine operating point).

1. The efficiency of the motor, generator and inverter was varied between 85% and 95% to determine the point at which the system is no longer viable from an overall efficiency perspective.

2. The vehicle gear ratios were varied by 20% to show the possible sensitivity of the results from application to application.

4.3 Insulated turbocharger heat transfer modelling

The benefit of the inner insulated turbocharger has been discussed in Chapter 2, in this section, the design of inner-insulated turbocharger turbine will be introduced, and this design focuses on the concept that deals with minimization of the turbocharger hot end heat losses, called 'T4 Enhancement'. Both design method and actual manufactured product will be introduced. After that, the overall structure of the turbocharger thermal model will be presented. This is mainly a parameterisation study based on supplied experiment data and 3D heat transfer simulation supplied by cooperative company.

4.3.1 Inner-insulated turbocharger introduction

This section (Burke et al., 2019) (External resources) is not the output of this thesis but contributed to the author's research.

Figure 4.19(a) reveals the assembly of an inner-insulated turbine housing (T/H) design concept, consisting of a modified T/H and an insert parts (turbine inlet, volute and outlet) for enabling the insulation, to be mounted inside the T/H. The insert parts itself consist of the outer and the inner shell made out of sheet metal and a silicate insulation material in between. The outer shell is supported by bosses (highlighted with red in Figure 4.19(b)) which limit relative movement between the T/H and the insulation parts. The thermo-mechanical contact has been carried out by finite element analysis (FEA) analysis and highlights the support locations of the bosses where only conductive heat transfer can occur. No heat transfer is taking place at the other insulated shell surfaces. Figure 4.19 (c) reveals the positioning of the outer shell during operation. The manufactured components based on model design are shown in Figure 4.20. The volute has three layers, the inner and outer metal shell and the middle silicate fibre insulation. The size of the T/H will increase a little (15mm in Diameter and 0.25kg in weight) due to the insulation.

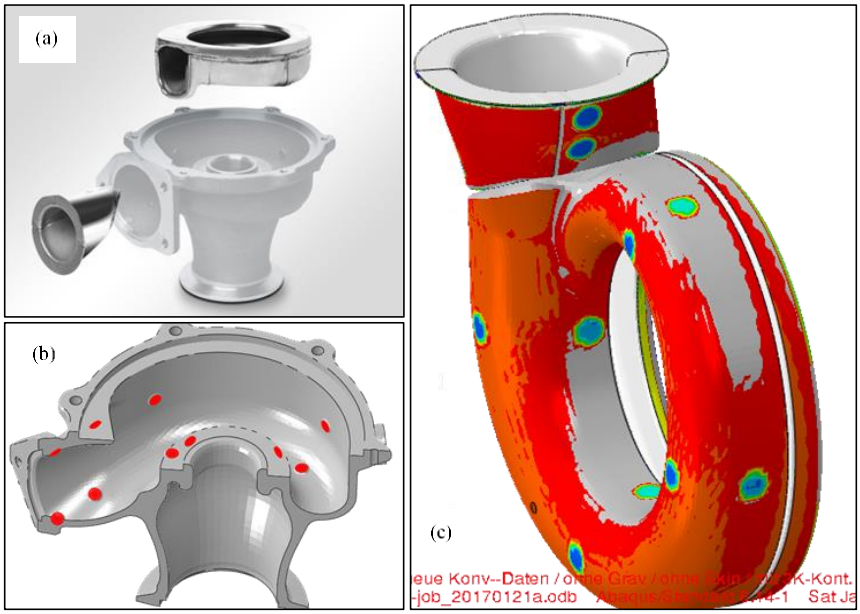

Figure 4.19 (a) Inner-insulated T/H, exploded view of T/H assembly. (b) T/H with structural mounting points of the inner-insulation and (c) inner-insulation with location of mounting points with T/H. (BorgWarner)

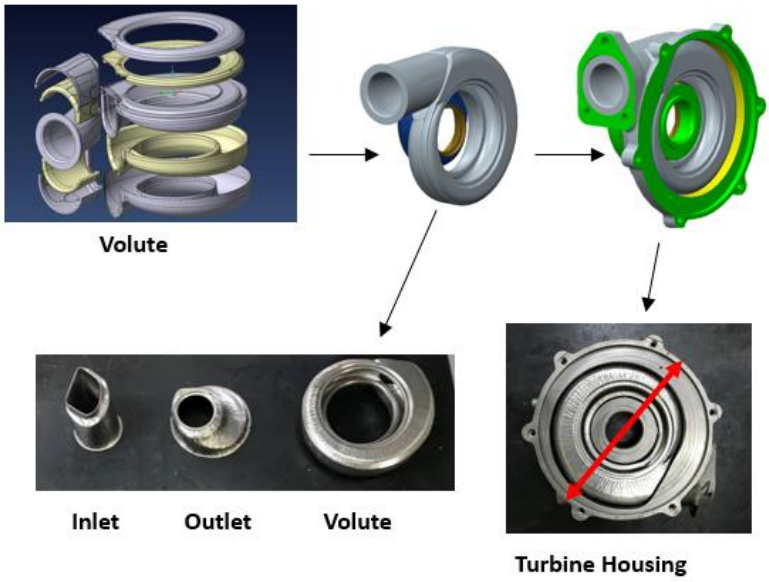

Figure 4.20 The actual design of inner-insulation (BorgWarner)

4.3.2 Modelling for the standard turbocharger heat transfer

In 1D simulation, the heat transfer effect is generally ignored at the turbine side. In practice heat transfer will occur through the turbocharger stage, however a common assumption in 1D models assumes that heat transfer and work transfer occur independently(Olmeda *et al.*, 2013); this is represented schematically on enthalpy-entropy diagrams in Figure 4.21. The actual processes undergone by the gases are shown between states 1-2 and 3-4 for compressor and turbine respectively. The split of work and heat transfer is shown by the intermediate states 1', 2', 3' and 4' such that flow through the turbine is composed of the following stages:

1. A heating or cooling at constant pressure (processes 1-1' and 3'-3),
2. An adiabatic compression/expansion (processes 1'-2' and 3'-4')
3. A heating or cooling at constant pressure (processes 2'-2 and 4'-4)

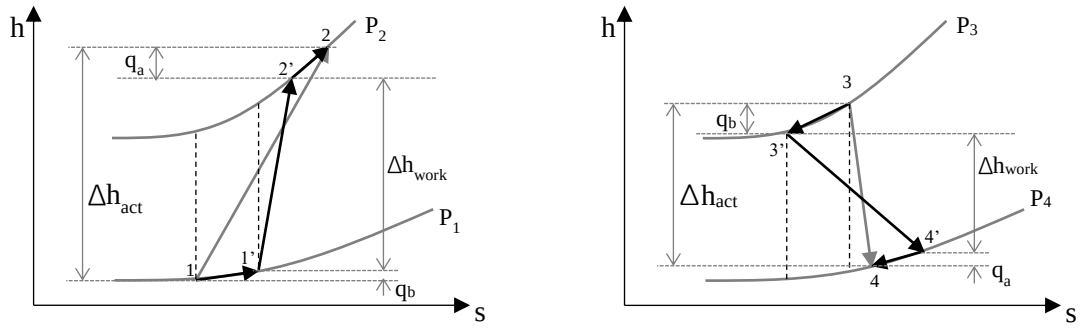

(a) Compressor *(b) Turbine*

Figure 4.21 Apparent and assumed compression and expansion processes in (a) compressor and (b) turbine

In order to consider the heat transfer for the system, a 1D lumped capacitance model is built in GT-POWER. A simplified heat transfer model method has already been studied and verified by others (Shaaban, 2004; Serrano *et al.*, 2007; Baines *et al.*, 2010; Cormerais *et al.*, 2009). The model combines two thermal nodes (the compressor and turbine housing), linked via conduction through the bearing housing. Heat transfer between the gases and housings can occur both before and after the compression/expansion processes which are important because of the different temperature gradients between the gas and the wall.

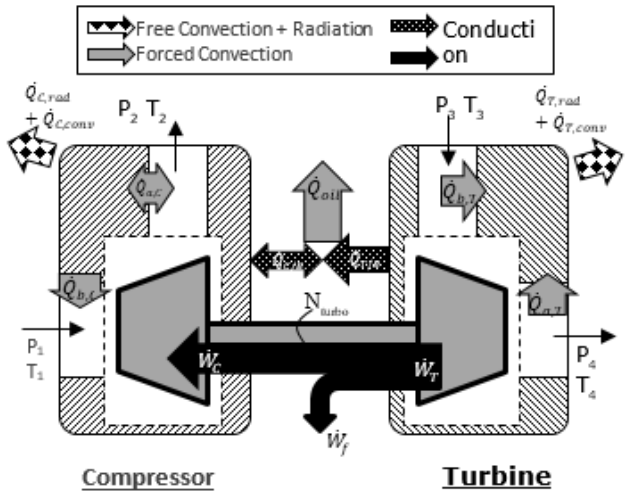

(a)

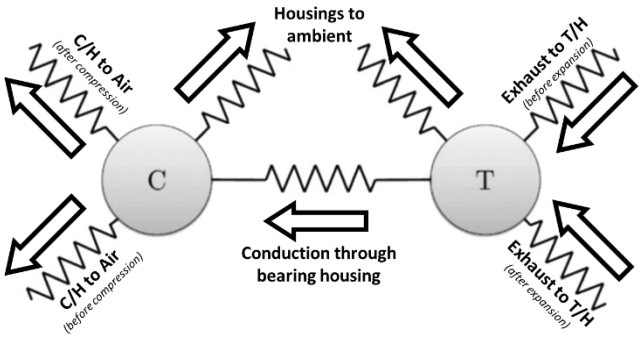

(b)

Figure 4.22 (a) Overview of the turbocharger heat transfer model. (b) the lumped capacitance thermal network (Burke et al., 2015).

The research in this thesis will focus on the heat transfer between the exhaust gases and the turbine node. This convective heat transfer is typically modelled by assuming or adapting convective correlations for the flows in the pipes such as Dittus-Boelter or Seider-Tate (Incropera *et al.*, 1985). Applying an energy balance on this node yields equation (1); the heat transfer model aims to determine each of the terms on the right hand side:

$$m_T c_{p,T} \frac{dT_T}{dt} = \dot{Q}_{b,T} + \dot{Q}_{a,T} - \dot{Q}_{T/B} - \dot{Q}_{T,rad} - \dot{Q}_{T,conv} \qquad (21)$$

It was assumed that all of the heat that comes from the gas to the wall is by convection, and the Nusselt number calculation is the following equation (22):

$$Nu = aRe^{b}Pr^{1/3}\left(\frac{\mu_{bulk}}{\mu_{skin}}\right)^{0.14} \quad (22)$$

For the radiation process:

$$Q = \sigma\varepsilon A(T_1^4 - T_2^4) \quad (23)$$

For the heat loss process,

$$Q_{loss} = 0.53(\mathrm{Gr} * \mathrm{Pr})\ 1/4 \quad (24)$$

Parameters a and b will be based on the calibration between the simulation and the experiment.

The turbocharger heat transfer model must also include heat loss to the ambient, which has been regarded as a free convection from the turbine housing to the ambient. For an insulated turbine, in a 1D simulation environment, the insulation will reduce the heat loss from the fluid to the ambient; however, using 1D modelling to describe the behaviour in the air gap between the housing and the insulation becomes difficult, as many factors are difficult to parameterise. Therefore a simpler approach is taken where an insulation factor is added to the convection process to account for the reduced heat loss from the exhaust gasses to the turbine housing. This is effectively modelled as a modification of the heat flux between the exhaust gases and the ambient by reducing the convective heat transfer from the exhaust gases to the turbine housing.

Figure 4.23 shows the structure of the turbine model, including the heat transfer effects. The model has been parameterised based on an analysis of the CAD geometry of the turbocharger and the selection of a convective heat transfer coefficient for a similar variable nozzle turbocharger system.

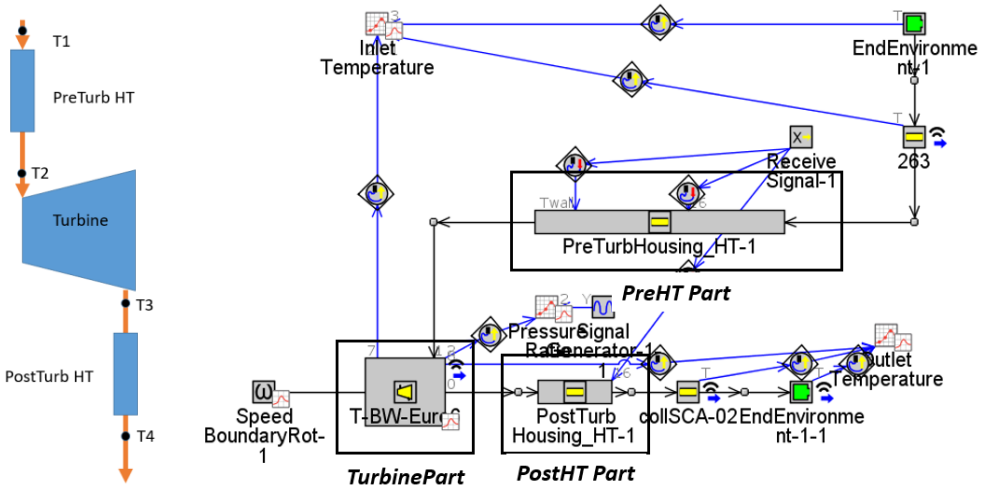

Figure 4.23 Turbine heat transfer model structure.

Since the research focuses on the thermal effects on the turbine, the turbocharger heat transfer model must include heat losses to the ambient to capture any differences between the two turbochargers. This can be seen in Figure 4.24.

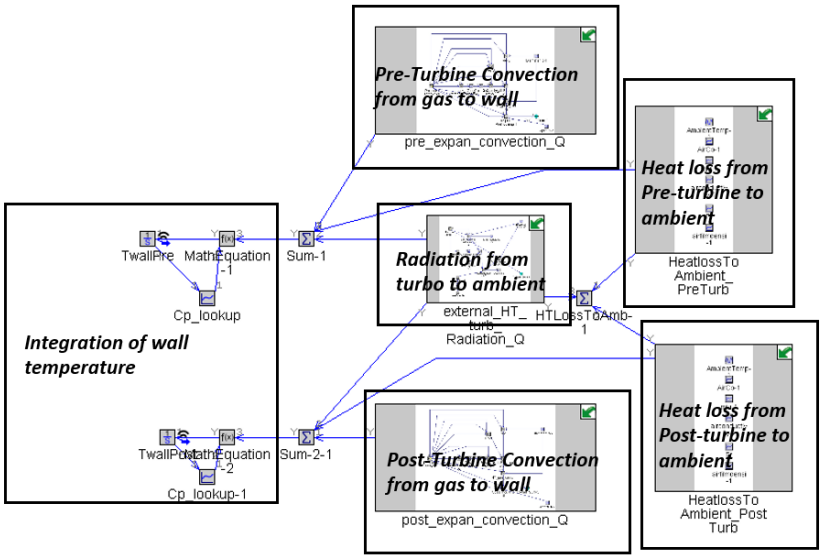

Figure 4.24 Heat transfer model structure considering the heat loss to the ambient.

This is the baseline heat transfer model that will be used in this thesis for the standard turbocharger turbine. The heat transfer modelling part attempts to parameterise the turbine heat transfer performance in the 1D model, offers an opportunity for researchers to investigate different thermal effects on the turbocharger system. The experiment study plays the main role in the demonstration work.

4.3.3 Modelling for inner-insulated turbocharger heat transfer

For inner-insulated turbine housing heat transfer, a further modification was made based on the model shown in Figure 4.24. It considered the pre- and post-turbine heat transfer individually, calculated the inner insulation temperature, then used that value to calculate the inside air gap heat transfer between the inner-insulation and outer turbine housing. An assumption has been made in this part, as the wall temperature is an average value when it was used to calculate the air gap heat transfer, as the convective coefficient is regarded as being big enough inside the metal.

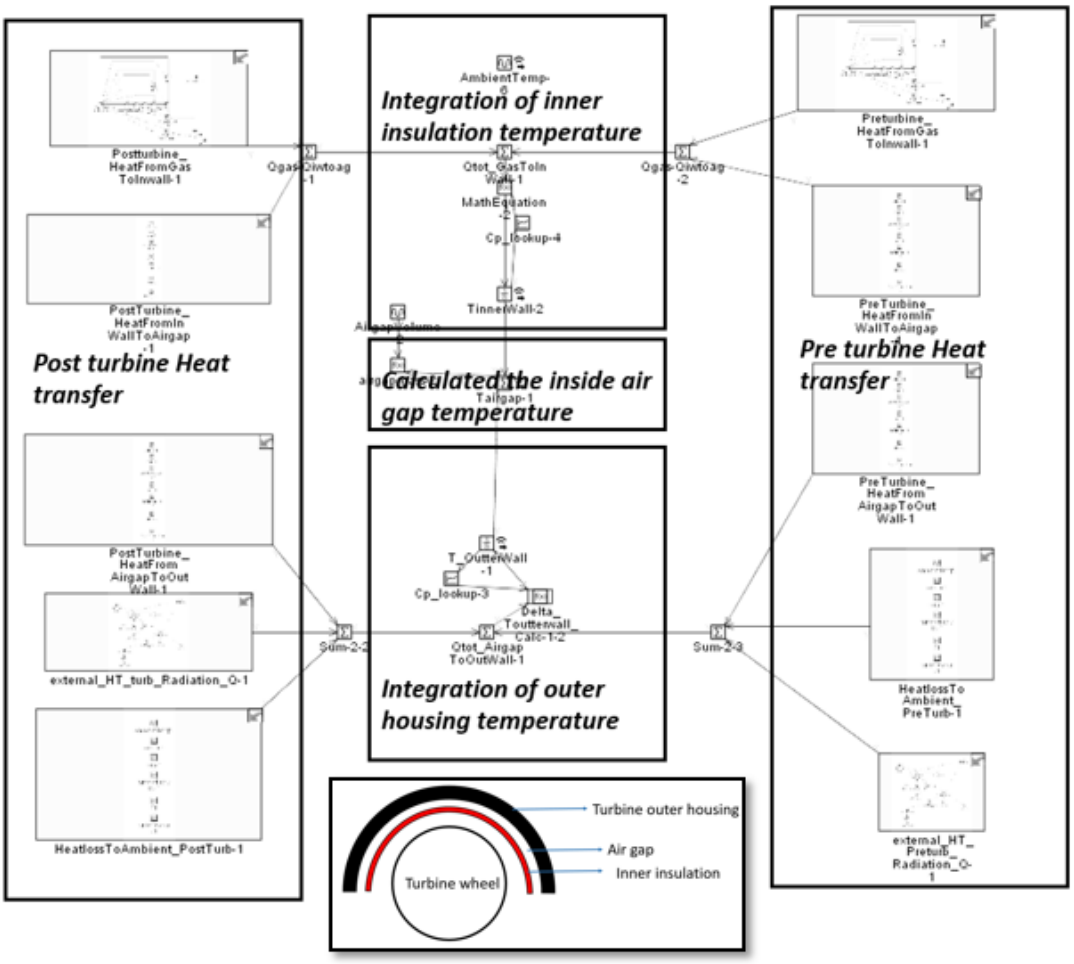

Figure 4.25 Heat transfer model for inner-insulated turbine

This approach is of course a simplification, as it introduces additional thermal resistance (two convective resistances for the gap between the inner and outer turbine

housings). However, the 1D heat transfer model is insufficient to describe the thermal effect in a complicated 3D geometry. Especially for turbine volute, the heat transfer must be optimised in a more practical way. In the 1D process, the heat transfer coefficient multipliers are turned to calibrate the model results with the experiment results.

The parameterisation process for the insulated turbine thermal properties will be accomplished under different scenarios in the following sections, with the main focus on the transient process, in order to see if the model is able to simulate the real transient heat fluxes in an acceptable way. Experiments are planned based on the related results, which are used to validate the model.

The heat transfer modelling part is trying to parameterize the turbine heat transfer performance in 1D model, offers an opportunity for researchers to investigate different thermal effects on turbocharger system, this is not the major topic in insulated turbocharger research, experiment study plays the main role for the demonstration works.

4.4 The 3D optimisation method of the T-Piece duct in the two-stage air path

Chapter 3 has already introduce the 3D air path model for a whole engine system, specified the T-Piece component between two boosting devices would affect the air flow condition. The topological optimization of bypass T-Piece geometry is a potential way to improve compressor efficiency and reduce airflow pressure drop. In this part, the optimization procedures and baseline model CFD results will be explained.

The research in this part is the optimisation of one intake path component using 3D simulation software. ANSYS and Tosca Fluid are the two software systems involved. ANSYS is used for modelling as well as ANSYS Fluent as CFD simulation solver. Tosca Fluid is used for optimising the T-piece shape with CFD topology optimisation. The research covers four stages shown in Figure 4.26. The red frames showed the

outcome of the on-going studies, and the dash frames show the opportunities for further work that are outside the scope of this thesis.

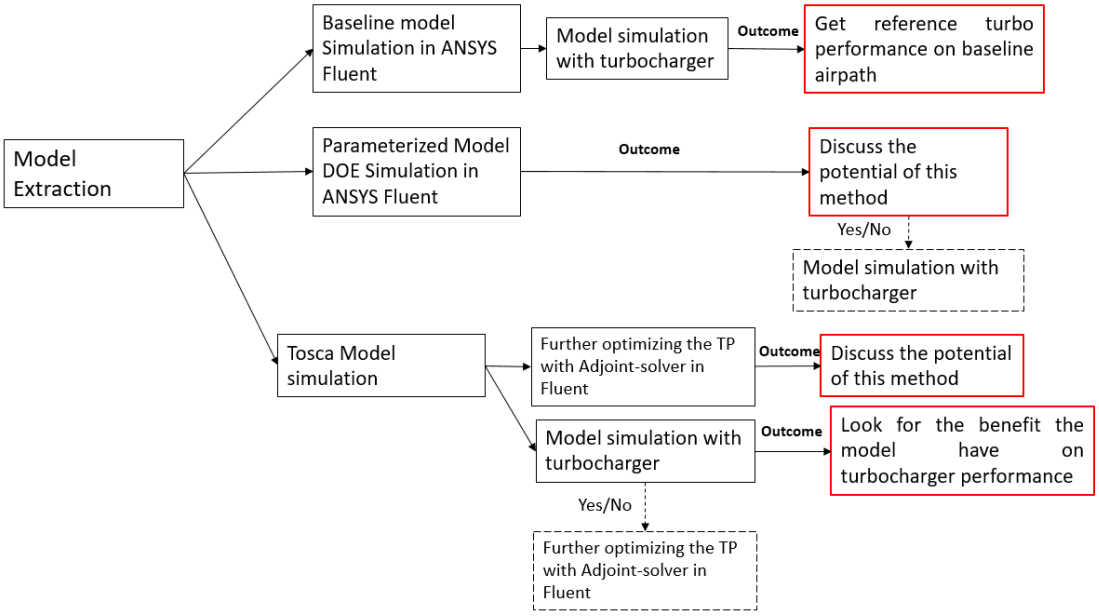

Figure 4.26 Overview of the approach using different optimisation methods

Firstly, ANSYS fluent was used to generate a baseline model with reference airflow characteristics. This result will be compared with each optimisation result to evaluate the effective reduction of the pressure drop within the T-piece junction. Three different 3D simulation methods were used in this work:

1. **ANSYS DOE parameterisation analysis**: Parameterisation is a common method in geometry optimisation. As the original T-piece was not a parameterised design, it was simplified and parameterised as a group of pipes. Figure 4.27 shows the parameters defined for simplifying the T-piece junction; however, due to the limit of the design space for the whole air path system, only some of the parameters were considered. The impact of these parameters on the shape of the T-piece is exemplified in Figure 4.28

2. **Tosca Fluid topology analysis**: The next optimisation approach is the CFD topology optimisation, which is the key part of this research, using a combined simulation between ANSYS Fluent and Tosca Fluid. A so-called design space has to be defined e.g. in a CAD system and will be imported and meshed with ANSYS, including setup of boundary conditions. Tosca Fluid will perform as optimisation solver working together with ANSYS Fluent as CFD solver.

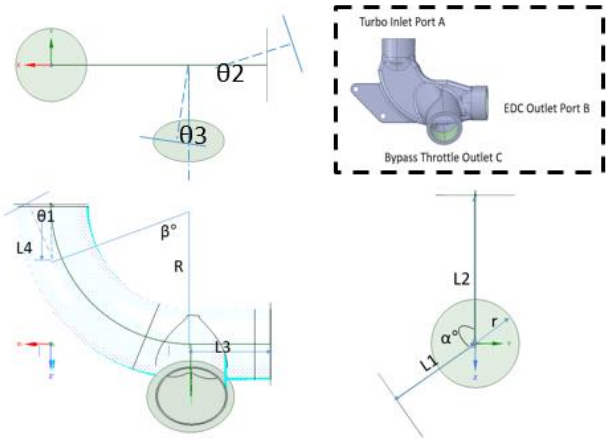

L1	Dist from C to pipe axle
L2	Dist from A to Intr plane
L3	Dist from B to Intr plane
L4	Dist from A to Arc track Starting Point
α	Angle between L1 and L2
β	Angle of Arc track
r	Pipe port inner radius
θ1	A angle betw Axle and Z Axle
θ2	B angle betw Axle and X Axle
θ3	C angle betw Axle and X Axle

Figure 4.27 Parameterisation of T-piece junction

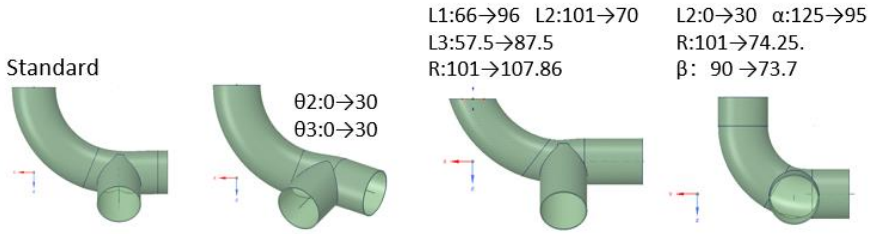

Figure 4.28 Examples of T-piece junction parameterisation

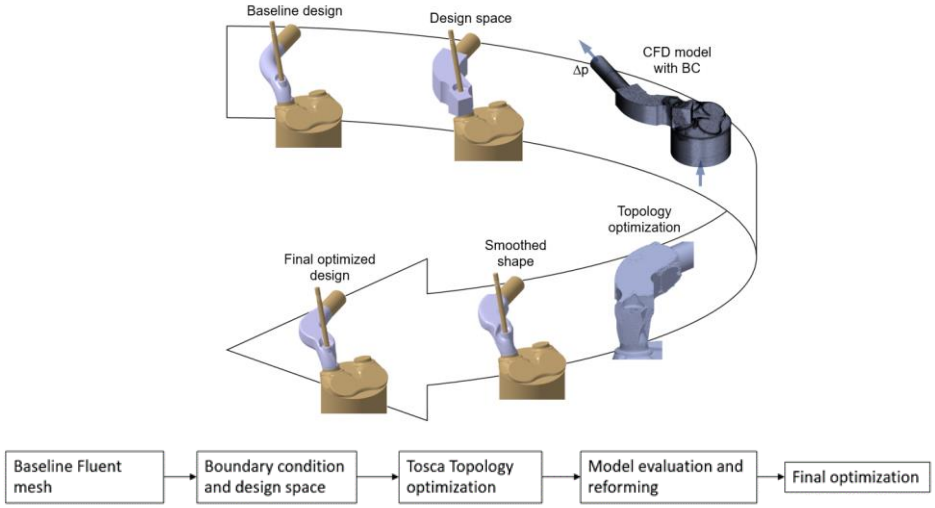

Figure 4.29 Tosca Fluid working process (Hopf et al., 2017)

During the optimisation run, the finite volumes of the design space will be switched on or off. The result is a stepped brick model, which will be smoothed afterwards. This process is shown in Figure 4.29. After the optimised fluid model generated, further CFD simulation will be done in ANSYS fluent to

validate if the new model works well, after then, the model will be slightly modified and derived by another CAD tool, make it easy to be manufactured.

3. **Adjoint Solver shape optimisation**: The Adjoint Solver is an add-in application in ANSYS Fluent. It can help to optimise the outer surface of the target geometry. The surface changes during the shape optimisation are usually very small, which can be used for optimisation in the final stage. Here, the Adjoint Solver is used as a second step after the topology optimisation driven by Tosca Fluid. Figure 4.30 shows the work process of the Adjoint Solver. Firstly, an initial Fluent result has to be solved. Then the user needs to input the variables that need to be optimised, define the surface region and morphing method. Based on the calculated adjoints/sensitivities, the application will generate a new mesh with a different shape. After that, it will evaluate the observation user set and decides if the optimisation need to be iterated until it gets to the optimum point.

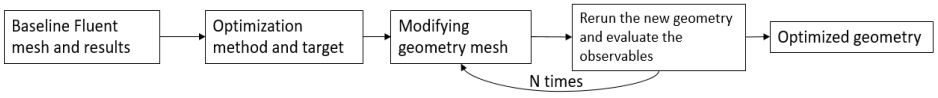

Figure 4.30 ANSYS Adjoint Solver working process

4.5 Summary

This chapter mainly introduced the methodologies and procedures for both simulation and experiment. The thesis covers different prospects in mild hybrid system. It will introduce different configurations, models and research methods. The work focuses on 4 topics:

1. The modelling and experiment of two-stage engine gas stand air path. The similar air path design will be applied on a 1D model of the 1.6L Diesel engine with Turbo and EDC layout which will explore different turbochargers and different control strategies and how these affect steady and transient performance. This will be illustrated in Chapter 5.

2. A 1D model of 2.0L Petrol engine with DET layout with a mathematical methodology for scaling turbocharger size, help to explore the trade-off in turbine and compressor size for system controlling, matching and energy balance issues. This will be explained in Chapter 6

3. An original heat transfer model to simulate the benefits of a thermally insulated turbocharger. The insulated turbocharger will also be tested on the rig in both steady state and transient phase. This will be used in Chapter 7.

4. The 3D optimization of a TP junction, which located at the inlet bypass route between EDC and turbocharger, this is for reducing the swirling flow and pressure drop of the engine inlet air, by means of topologic geometry optimization. This will be shown in Chapter 8.

Chapter 5 – Study on the two-stage electrically driven compressor system

This chapter will focus on experiment and modelling research on the two-stage hybrid boosting system, involving a turbocharger that is serially connected to an electrically driven compressor. This chapter looks at the matching methodologies (EDC). In the two-stage system, and transient performance of the engine system affected by the VGT and EDC.

Firstly the experimental study on the two-stage EDC system will be explained, introducing the test results about the characteristics of the components in this system, focusing on the VGT and EDC's controlling trade-off to deliver target boosting, and the EGR, intercooler routing studies. Then the transient study will also be presented which includes both the air path response for EGR mixing with the EDC and the thermal response of turbine outlet temperature.

After the two-stage air path characteristics have been demonstrated by the engine gas stand experiment, this system will be added to the engine stand in simulation, in order to investigate how the air path affects engine performance. The baseline model is 1.6L, single stage turbocharged Diesel engine. This model will be tuned and validated using engine stand measurements. After that, the sensitivity of the boosting system components will be investigated in the steady-state and transient conditions. In the last sub-section, initial research on the different air path design effects on engine inlet airflow was described, discussing how different intercooler and HP EGR locations performed in the steady state and transient situation.

Work in this chapter has been published in: Liu, Y., Vijayakumar, R. and Burke, R., 2018, November. Analysis of the opportunities and trade-offs for a 48v electrified air path. In ASME 2018 Internal Combustion Engine Division Fall Technical Conference. American Society of Mechanical Engineers Digital Collection.

5.1 Experimental study on the two-stage EDC air path

In Chapter 3 and Chapter 4, the test rig configurations and validated model were illustrated. The sample tests in Chapter 3 demonstrated that the engine gas stand test rig has the ability to conduct single-/two-stage turbocharger testing under the steady state and transient conditions. This section will focus more on the components' level testing. Section 1.1 focuses on the testing of VGT and EDC control, as both of them can control the engine boost, the aim of this part is to find out the compromise between these two components and how they affected the system performance in steady stage condition. Section 1.2 introduces the LP/HP EGR testing in this two-stage system, mainly to see how they will affect the engine inlet flow in steady state and transient situation, with the assistance of EDC.

5.1.1 VGT vs EDC trade-off testing

The components testing is the first step in calibrating the measurements for each sensor. Chapter 3 already described the mapping for the turbocharger and EDC, which will not be repeated here. This section focuses on the VGT and EDC's relationships in the steady state condition. The test rig configuration is shown in Figure 5.1， this test was done in HP EGR Route condition, and the EGRs were not opened.

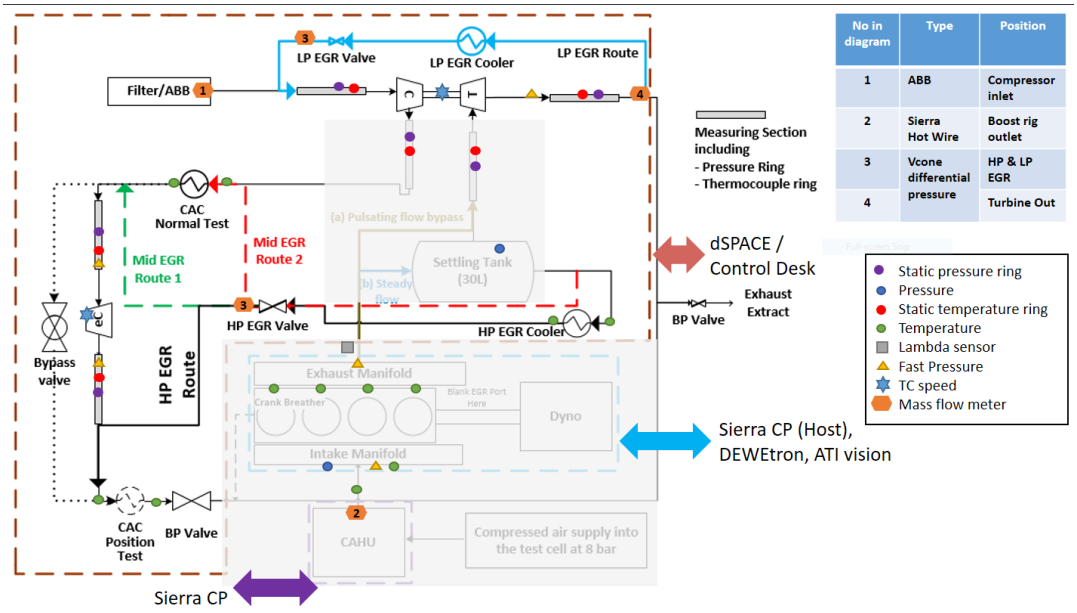

Figure 5.1 Test rig configuration

The ABB mass flow meter (Figure 5.29 1) is installed on the compressor side; this flow meter has been calibrated by the others and was regarded as a reference of mass flow calibration. The Boost rig mass flow meter and turbine Vcone mass flow meter were calibrated in this way.

A start point has been set for the test, by keeping the EDC outlet pressure the same, gradually accelerating the EDC speed but adjusting the turbine VGT. Figure 5.2 shows the controlling measurements for the EDC speed, VGT position, total boost pressure and related pressure ratio.

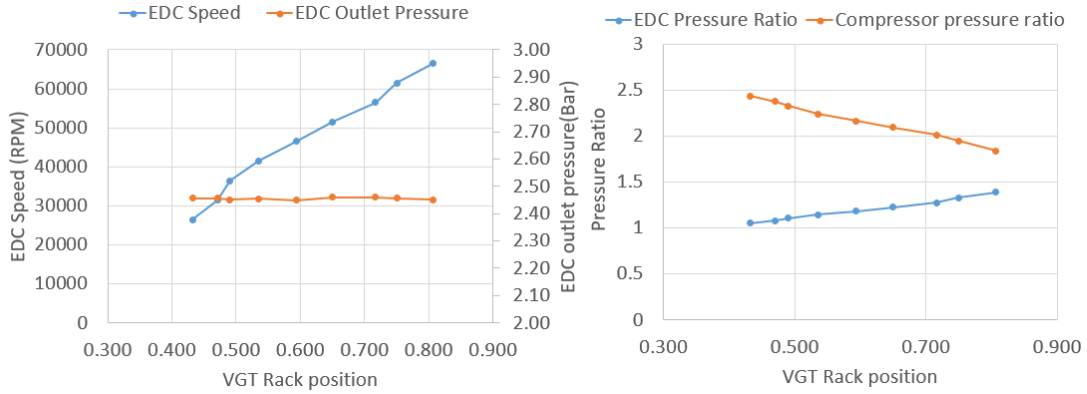

Figure 5.2 (a) EDC and VGT relationships for the same total boost pressure. (b) Pressure ratio of each component.

Figure 5.3 shows the EDC, compressor outlet temperature, mass flow situation and the EDC power consumed by the changing VGT. In Figure 5.3(b), the total mass flow rate is dropping due to the open of the VGT, because the EDC's outlet temperature increases as the EDC's speed is increasing. The EDC power increased from 0.2kW to 1.8kW. The result looks reasonable, since opening the VGT can reduce the engine pumping loss, but increase the EDC's power consumption; manufacturers need to decide the controlling methodology depending on their own requirements.

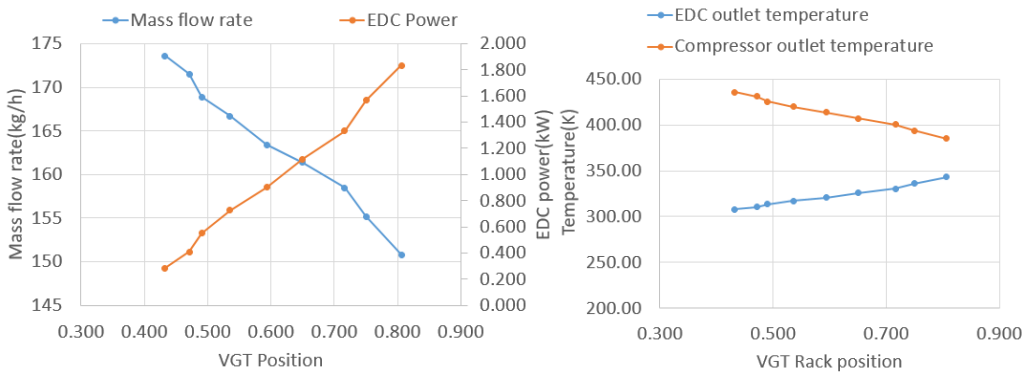

Figure 5.3 (a) Air path mass flow rate and EDC power. (b) Components' outlet temperature.

The experiments in this section shows that the designed test rig is well performed in two-stage steady state test. Either by adjusting VGT position or the EDC speed can achieve the target boost, however, for the same boost target, closing VGT more will lead to an increasing of pumping loss, but opening VGT will make the EDC power increased, and the mass flow will also change during this process.

5.1.2 EGR testing

In this thesis, two-stage EGR (LP and HP) can be applied to the test rig, in order to reduce the NOx emission for a diesel engine. Sample tests were performed for LP and HP EGR, in order to evaluate their reliability and accuracy, in a steady state condition. After that, the effects of EDC on the HP EGR mixing is measured in both the mid route 1 and mid route 2 situation (shown in Figure 5.1 and explained in Chapter 3). This chapter will take Mid route 1 as an example to analyse its transient performance.

For steady state tests, two different designs have been used to verify the reliability of the LP and HP EGR, including their relationships with turbine VGT and EDC operation.

Figure 5.4(a) shows how the LP EGR operating condition has been adjusted to the 5% and 10% rate of the total mass flow; however, the system is an engine gas stand, so the LP EGR has no considerable effect on the turbocharger speed. The target mass flow is achieved by adjusting the EGR valve position mainly, the VGT position and EDC speed are shown in Figure 5.4(b). The VGT was operated under the same condition.

The EDC speed is higher in 10% of the EGR cases due to the operation. It should be declared that, as the EGR flow is relatively low, it is hard to control the EGR valve to be exactly the same amount of the target flow, and there is measuring noise under low flow conditions. The further air path validation tests for the engine system simulation will be described in the next section.

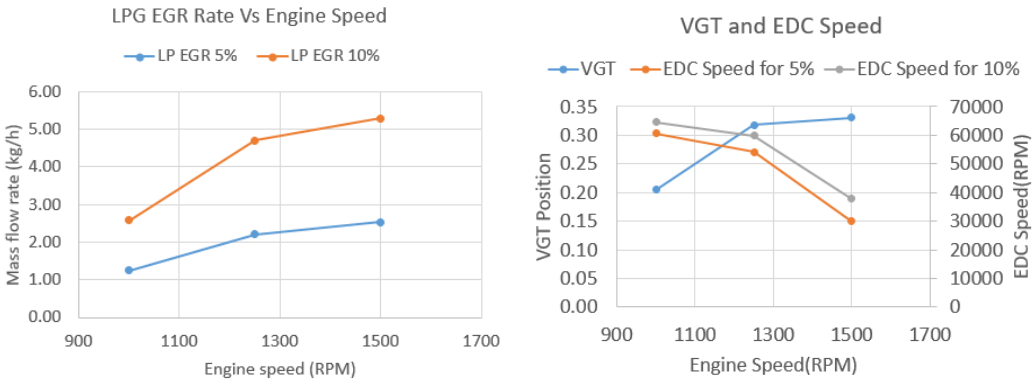

(a) (b)

Figure 5.4 (a) LP EGR operating condition. (b) VGT and EDC operating condition. (Note, VGT is the same position in different LP EGR cases.)

The HP EGR steady state characteristics are measured with the changing VGT position and HP EGR Valve position. The operating points are shown in Table 5.1.

VGT Position	EGR Valve Position	Other Factors	
0.2	0.1 to 0.4	Engine Speed	1280RPM
0.4	0.1 to 0.4	Throttle Position	30.5%
0.6	0.1 to 0.4	EDC Speed	10kRPM
0.8	0.1 to 0.4	Comp_BPValve	30%

Table 5.1 HP EGR tests' operating points

The EGR mass flow rate is shown in Figure 5.5(a); as the EGR opens, the EGR flow increases linearly. Closing the VGT helps to increase the EGR flow as the turbine inlet pressure (which is also the HP EGR inlet pressure) is increased. Compared with the LP EGR, the HP EGR is more sensitive to the VGT position.

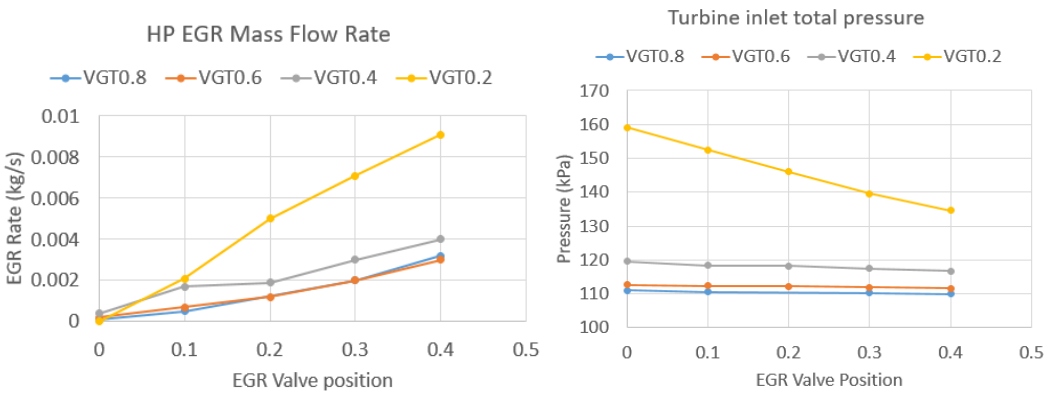

Figure 5.5 (a) HP EGR mass flow rate, (b) Turbine inlet total pressure.

A transient test was designed for HP EGR, EDC and VGT, as the EDC and VGT will affect the HP EGR outlet flow in the mixing process. Moreover, how they were operated will also have an impact on the HP EGR rate. The transient study is based on the *Mid route 1 configuration*, and the EGR outlet is between the intercooler and the EDC. Figure 5.6 shows the HP EGR transient schedule for the test. The design has three cycles. The first cycle is the reference cycle, which has a step load increase at the beginning and then a step load drop at the end; EGR is operated from 0.2 to fully close at the start then returned to 0.2 again at the end. The cycle last 160s. The second cycle has EDC assistance in the step loading period, and the speed changes from 10kRPM to 50kRPM (Figure 5.6 (a)). The third cycle has a VGT change during the process, from 0.3 to 0.7.

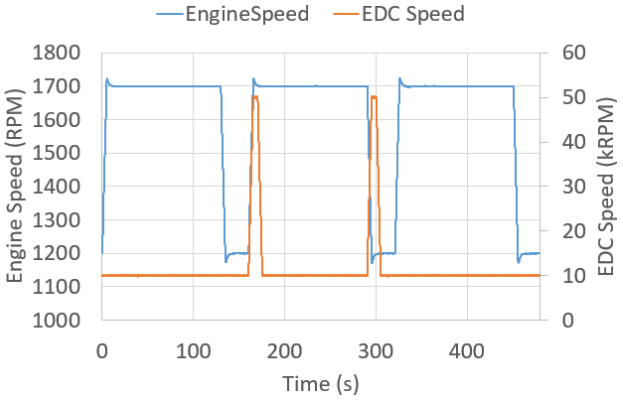

(a)

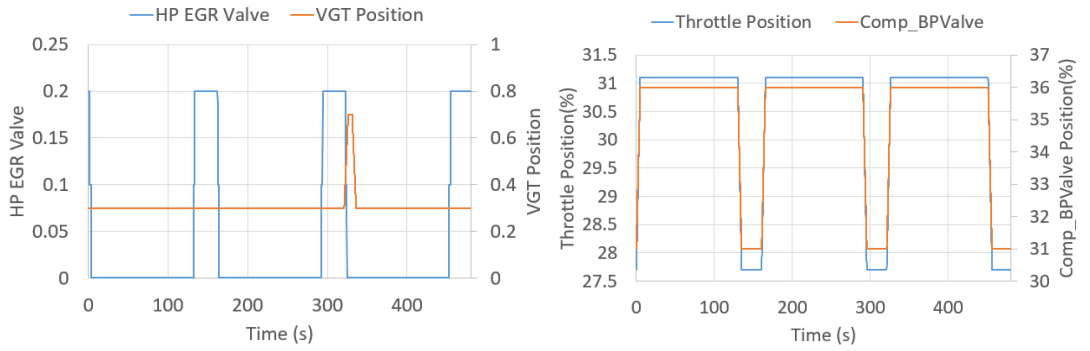

(b) (c)

Figure 5.6 HP EGR transient test schedule (a) Engine speed and EDC speed. (b) HPEGR Valve and VGT. (c) Throttle and Compressor BPValve.

Before performing a back to back comparison of the EDC and VGT effects on HP EGR mixing and its flow rate, the whole test is performed. Two lambda CAN sensors are installed on the HP EGR outlet port and the EDC outlet port, to measure the oxygen rate before and after mixing, to evaluate whether the EDC rotation can help to speed up the EGR mixing.

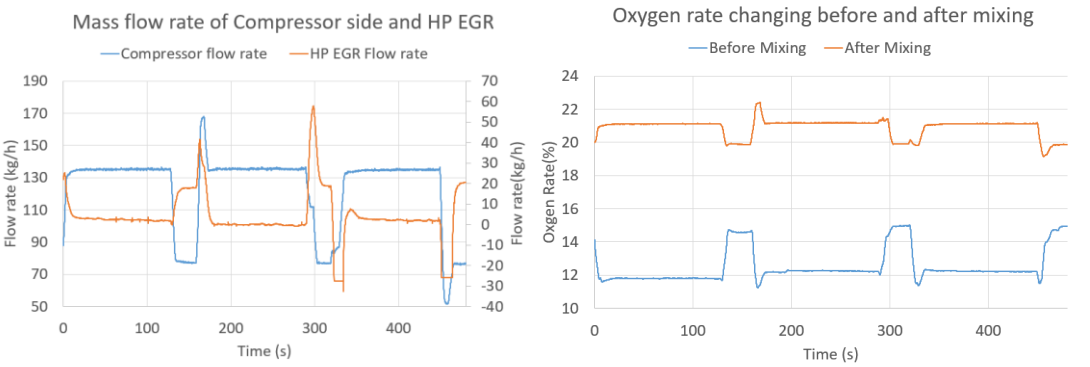

(a) (b)

Figure 5.7 (a) Mass flow rate changes to the compressor and EGR path. (b) Oxygen rate change before and after mixing.

From Figure 5.6(a), it was known that the whole test has 3 similar cycles (0 to 160s, 160s to 320s, and 320s to 480s). From 160s to 320s, EDC was accelerated to 50kRPM and then returned to 10kRPM at the beginning, the whole process last 15s and would be repeated when EGR is going to close. In Figure 5.7(a), it can be seen that last EDC will increase both the EGR and compressor flow (from a 160s to a 320s cycle), the oxygen rate also increased when EDC accelerated and pumped more air into the engine (Figure 5.7(b)).

From Figure 5.6(a), 320s to 480s, VGT position changed from 0.3 to 0.7 at the beginning, and then returned back to 0.3, this process also last 15s. In Figure 5.7(a), 320s, there was a reverse flow from the EGR outlet to the EGR inlet, because the VGT opened too fast, it leaded to the high pressure drop at the turbine inlet side. Figure 5.7(b) shows when VGT position started increasing, the oxygen rate in the mixed flow dropped a little, that also because the reverse flow coming from the compressor air path side affected that.

Both EDC and VGT can affect the oxygen rate, so back to back comparison of the transient period must be examined in detail.

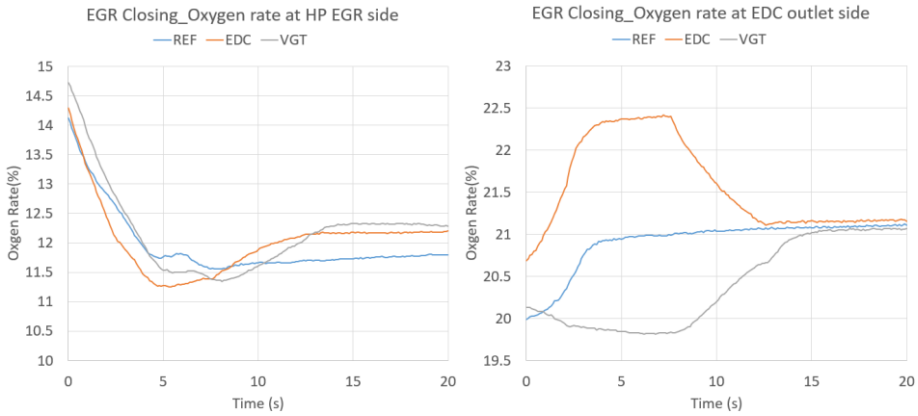

(a) (b)

Figure 5.8 Oxygen rate at the HP EGR side and EDC outlet side when the EGR is closing

Figure 5.8 shows a comparison of the 3 cycles (0~160s, 160~320s, 320~480s), and describes the oxygen rate changes when the EGR start closing. This figure is actually the enlarged view of Figure 5.7, focusing on the start and end periods in the 3 cycles.

In Figure 5.8(a), the EDC acceleration and VGT opening have little effects on the oxygen rate. Compared with the reference value, the oxygen rate has increased slightly when the EDC speed rises or the VGT opens more; however, as the oxygen rate measured by the Lambda CAN is susceptible to temperature, there are some errors within the three curves. But the whole oxygen rate keeps in the same level in HP-EGR before mixing.

In Figure 5.8(b), the differences are obvious. EDC helps to increase both the compressor and EGR flow (Figure 5.7). The increased compressor flow is higher than the increased EGR flow, and the oxygen rate change speed has been accelerated by the EDC. On the contrary, the VGT's opening leads to a reverse flow to the turbine side, which causes the oxygen rate to drop and reduces the EGR mixing speed. The same phenomena can be observed in the EGR valve opening process, in the opposite direction, as shown in Figure 5.9.

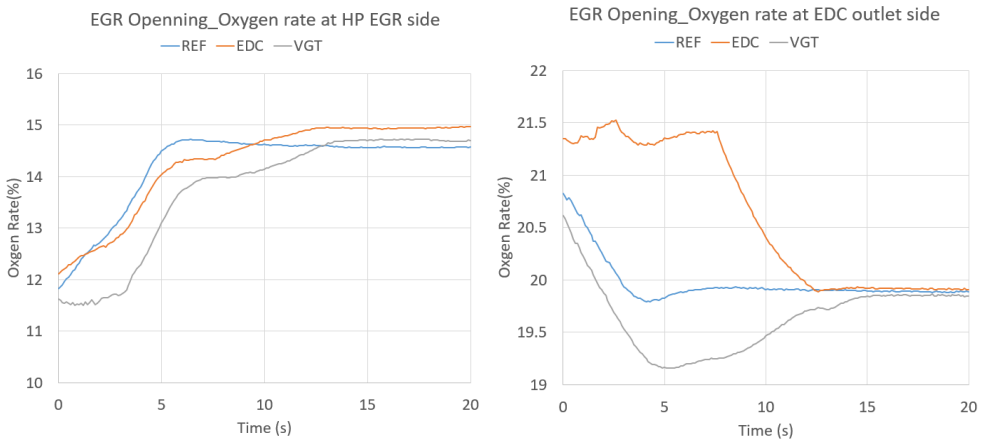

(a) (b)

Figure 5.9 Oxygen rate at the HP EGR side and the EDC outlet side when EGR is opening

This section explained the experiment results for the two-stage EGR air path. The steady state tests showed that both VGT and EDC can help increasing the engine inlet pressure and pumped more air, however, closing the VGT will increase the engine pumping loss, increasing the EDC speed will lead to more electricity consumption that is a critical point in mild hybrid system. In EGR testing, LP EGR function was validated, as it was located before the two-stage boosting device, EDC can help increase the LP-EGR rate. HP EGR was measured in transient situation, because it was located just upstream the EDC, so EDC has the ability to increasing the EGR and fresh air mixing rate and speed. The experiment results showed that EDC can help increasing the mixing speed by supplying higher boost, in the contrary, opening VGT will lead to a pressure drop at turbine inlet side, in this case, it leaded to a reverse flow from compressor side to the turbine (as the VGT opened suddenly, the EGR outlet pressure at compressor side becomes higher than the EGR inlet at turbine side.), so this will have a negative effects on EGR mixing.

5.2 1D modelling for the two-stage electrically driven compressor (EDC) system

Section 1 and Chapter 3 have already demonstrated the benefit of the two-stage EDC system; however, as the test rig is an engine gas stand design, it is hard to evaluate the engine's performance. In order to investigate further the two-stage system's effects on the engine, the same two-stage compressors and turbine air path have been applied to an engine model.

This section describes the modelling for a two-stage EDC system. The model is based on a 1.6L diesel engine, with the same air path as verified in the experiment. The matching between the turbochargers and the engine will be firstly investigated. This will also consider the turbocharger and EDC size effects on engine performance using the scaling method.

Transient study is in the third part, mainly focusing on the sensitivities of VGT and EDC controlling and discussing their transient response and power consumption.

Some of the modelling results will be analysed combined with experiment results from both engine stands (with external resources from the manufacturer; these results with be used here but will not be analysed in detail) and the engine gas stand, as these can help to validate and calibrate the model.

5.2.1 Two-stage system matching

5.2.1.1 Matching simulation

The two-stage baseline model performance was discussed in Chapter 4, section 2. The engine output was increased from 120PS to 140PS by the introduction of a turbocharger, which was achieved at 3750RPM, and the low speed torque rose to 320Nm with the help of the EDC. The study in this section discusses the performance of two different sized turbochargers on this engine, and also investigate the possibility of achieving the 140PS output under specific engine design constraints.

The baseline matching and optimisation took place during the initial stage, and the target engine output was achieved without considering the engine design limitations. However, for real engine design, there are many constrains for some factors, the factors are shown below:

Factors that have limit	Limiting range
Peak cylinder pressure	Generally upper limit 160~200 bar
Turbine inlet temperature	Generally upper limit around 1100K
Compressor outlet temperature	Generally upper limit due to the air path design
Turbocharger speed	A speed limit with design margin

Table 5.2 Design constraints of the engine.

When the EDC is bypassed, the engine torque output is shown in Figure 5.10. The engine combustion model has been verified and calibrated by the engine manufacturer, which lies outside the scope of this thesis.

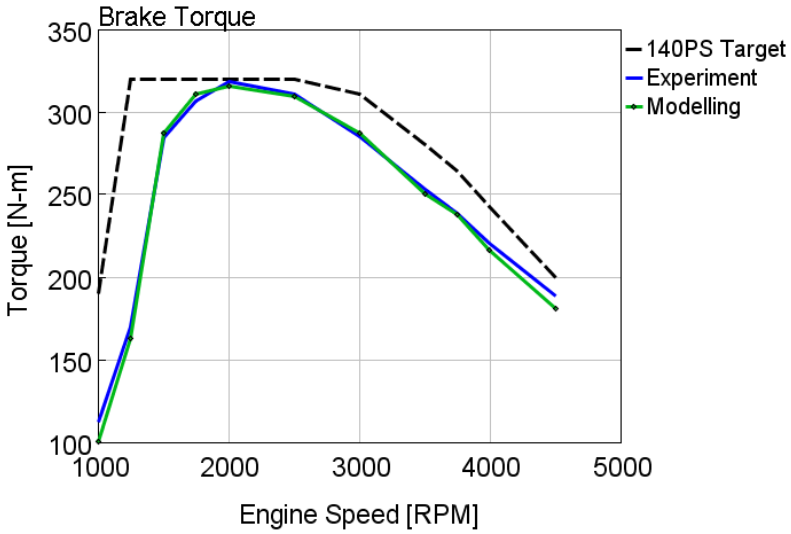

Figure 5.10 Engine brake torque under experiment and simulation conditions.

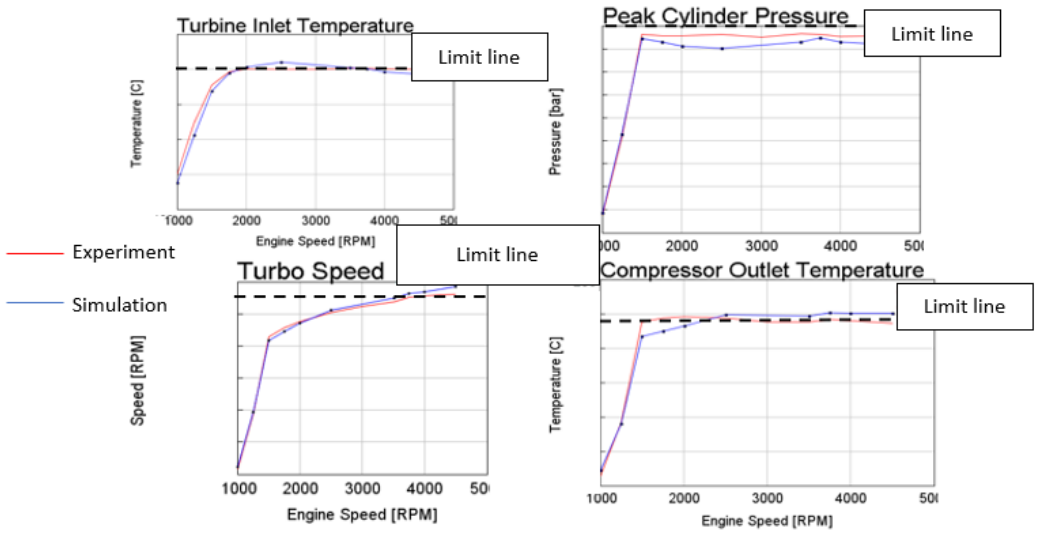

Figure 5.11 Design constraints with the system performance for both the simulation and experiment.

Figure 5.11 shows the plots of the simulation and experiment results with their related boundary conditions. All of these factors have already reached the limits even with the 125PS peak power design. There is little chance of improving the engine's performance simply by varying the turbine VGT or engine operations. A new turbocharger-matching or relaxing of the design constraints may help to achieve that.

Following the review of the engine characteristics, a new turbocharger match was identified. A comparison between the two turbocharger maps is shown in Figure 5.12. Match 1 is the baseline turbocharger, Match 2 is a bigger turbocharger. Match 2 has a bigger turbine and new compressor that are used to increase the efficiency and turbo power in the high engine speed region. However, this is suspected of sacrificing the low speed performance (which is planned to be recovered by the EDC's contribution).

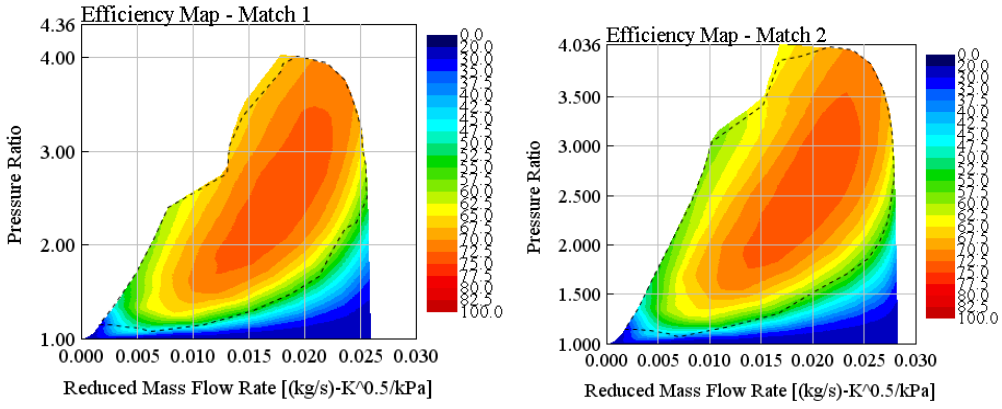

(a) Compressor map- Match 1 (b) Compressor map Match 2

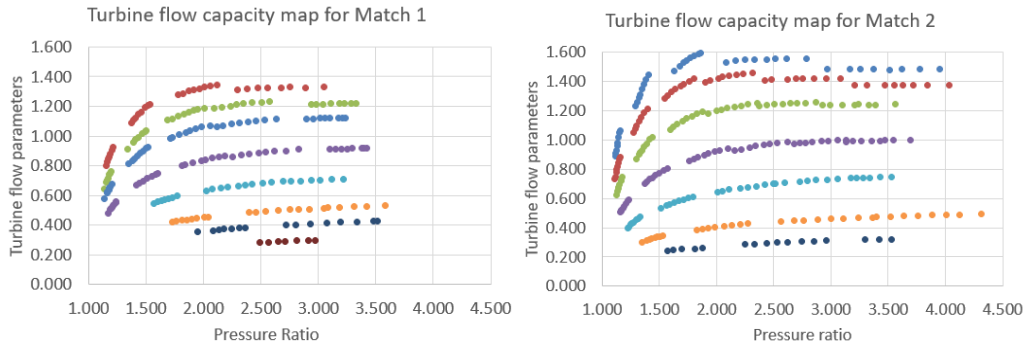

(c) Turbine map- Match 1 (d) Turbine map-Match 2

Figure 5.12 Properties of the two turbocharger maps.

Figure 5.13 shows the brake torque and power of the two different matches, under the same boundary conditions. Match 2 (the new matching) has a higher high speed torque and power (136PS) but a lower low speed output. After adjusting the engine, all of the constraints were broken through under this situation (Figure 5.14).

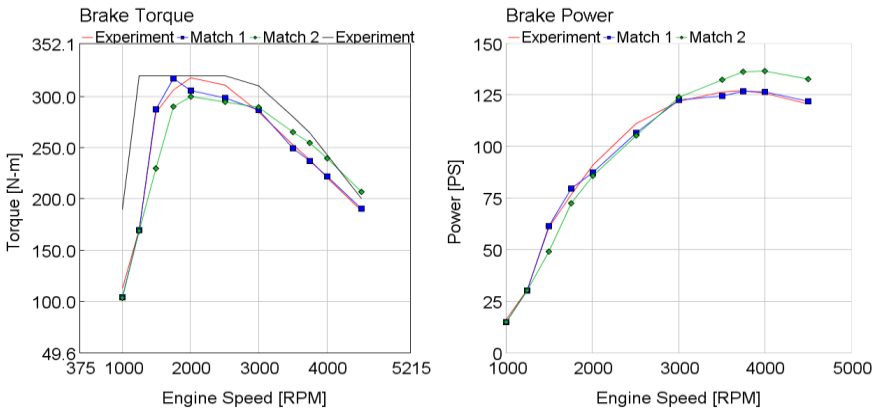

Figure 5.13 Engine brake torque and power for the two matches

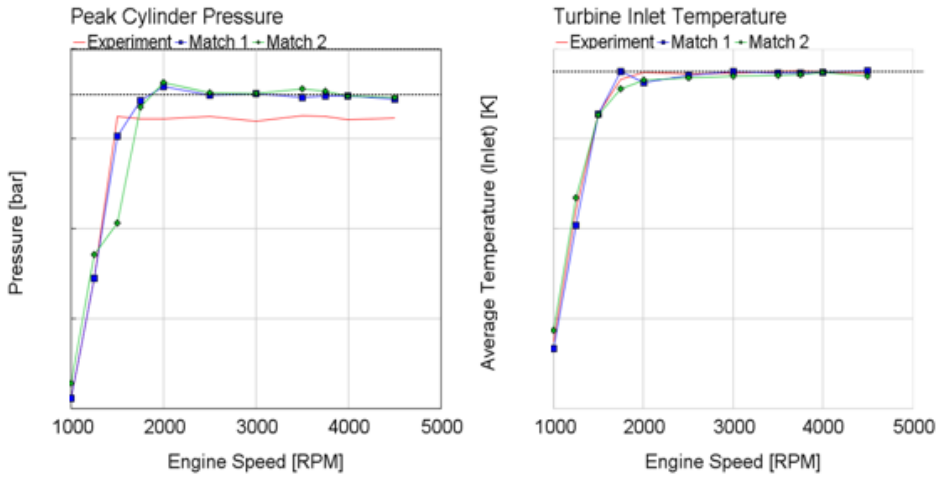

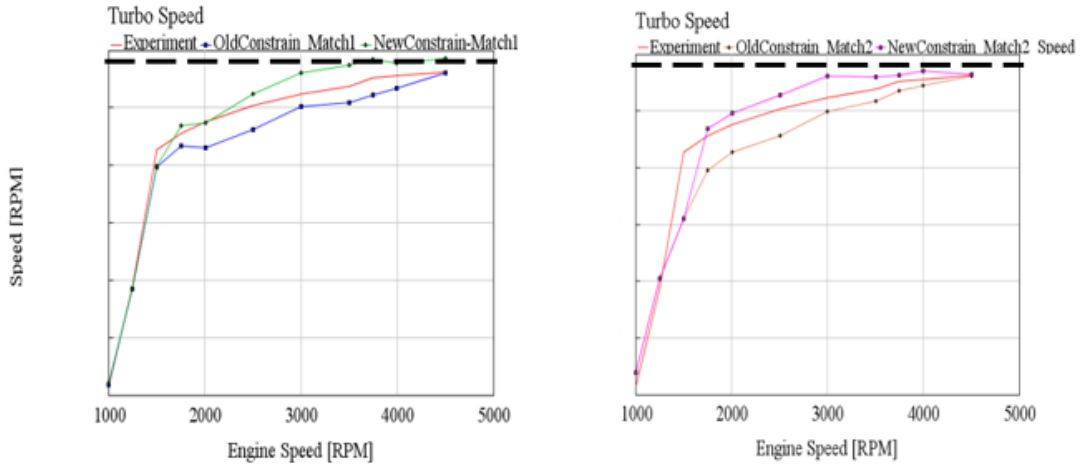

Figure 5.14 Design constraints were broken through for the two matches.

In order to achieve the 140PS output, it was considered extending the engine design constraints. By extending each constraint to 5 to 10% more, new optimisations are raised for target output.

With the new boundary conditions, the simulation results for both match 1 and match 2 are given below. For both match 1 and match 2, the brake torque can achieve an even higher level than the target. One thing that should be noticed that in this condition is that the turbocharger speed is in the limit range, but did not consider the design margin.

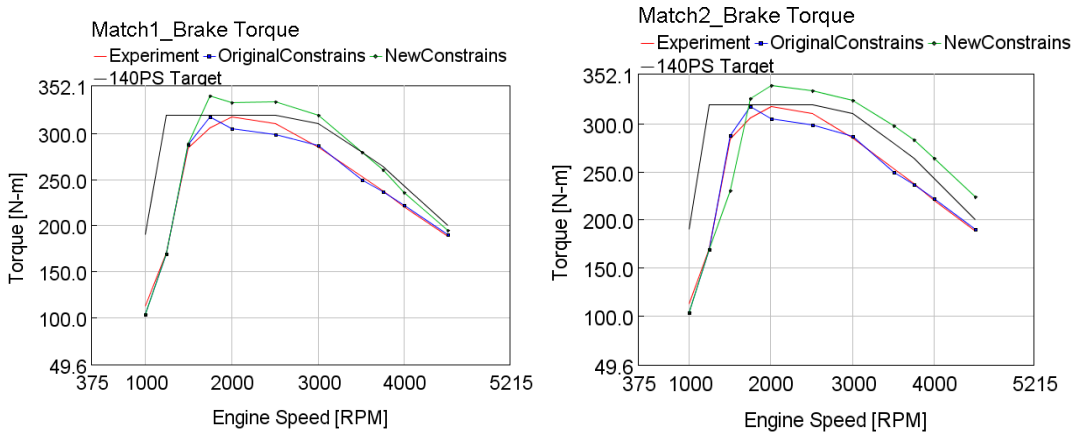

Figure 5.15 Brake torque for match 1 and match 2 under the new constraints.

After considering the turbo speed design margin, it was found that match 1 can deliver 139.6PS power at 3500RPM and 139PS at 3750RPM. Match 2's peak power dropped from 151PS to 141PS from 3500RPM to 4000RPM, but it can still meet the power target. The peak torque is 340Nm at 2000RPM.

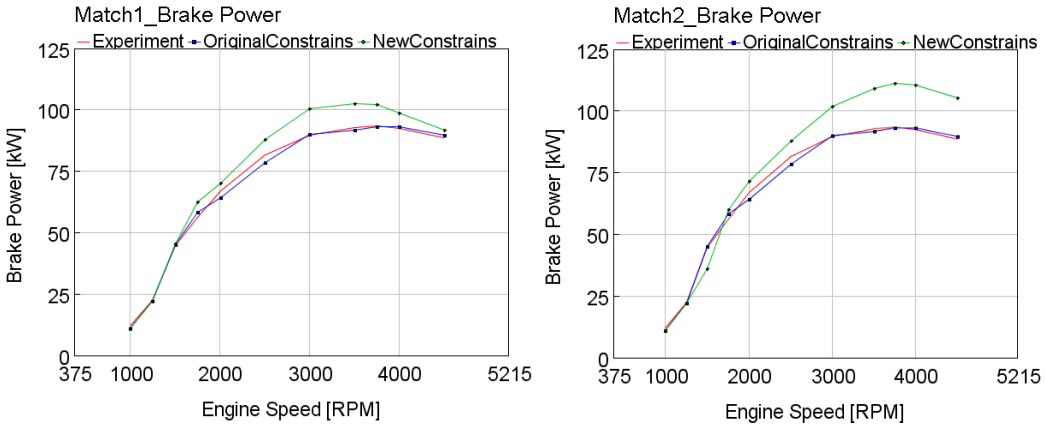

Figure 5.16 System peak power after considering the turbocharger speed design margin

It can be concluded that, if we consider the turbocharger speed limit design margin as 7%, both Match 1 and Match 2 can achieve the 140PS output. If the design margin is increased to 10%, Match 1 may be unable to deliver 140PS any longer.

Match 2 is able to provide a higher peak power, but this is compromised by a lower low speed maximum torque which will increase the power requirements of the EDC. Figure 5.17 shows the engine brake torque output for the two matches, compared with the experiment data. An EDC is needed from 1000 to 1500 RPM, for a higher low speed torque. Match 1 has a higher torque output than Match 2 at 1500RPM, but a lower torque from engine speed 2000RPM.

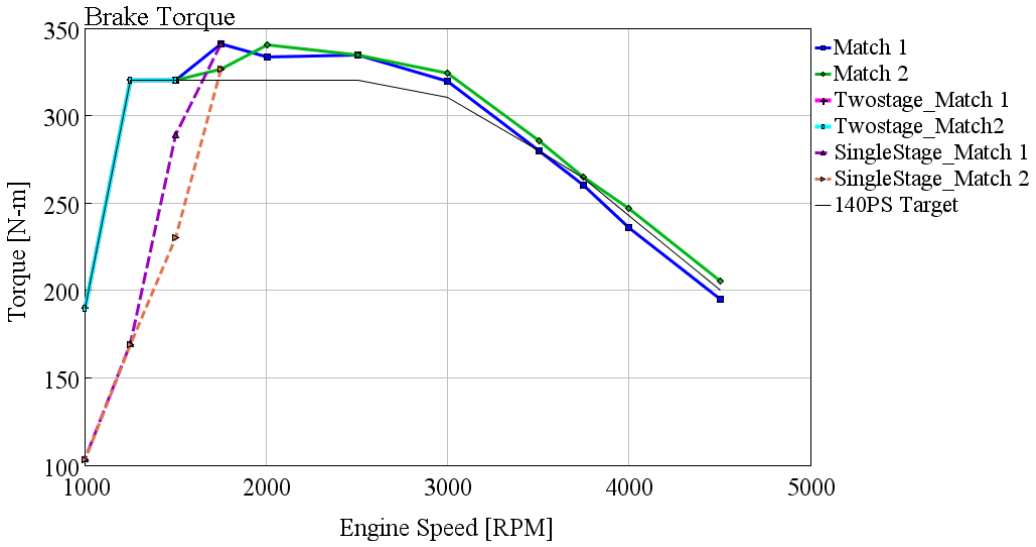

Figure 5.17 Brake Torque for the two matches

For two-stage matching, the compressor surging problem and EDC power limit need to be considered. Figure 5.18 shows the compressor operating points for both Match 1 and Match 2. It can be seen that, in the low speed area, Match 1 and 2 compressors almost surged. There are 2 points (2000RPM to 2500RPM) that already surged for Match 1, due to the compressor mapping differences between the experiment and the simulation. Figure 5.19 shows the system output in the two-stage situation when EDC is involved from 1000 to 1500 RPM for the target torque. Both Match 1 and Match 2 can reach the target, but the EDC operating condition is different. Figure 5.19 shows the EDC power needed and the EDC operating points, while Match 2 needs about 100 to 200 W more power in each case.

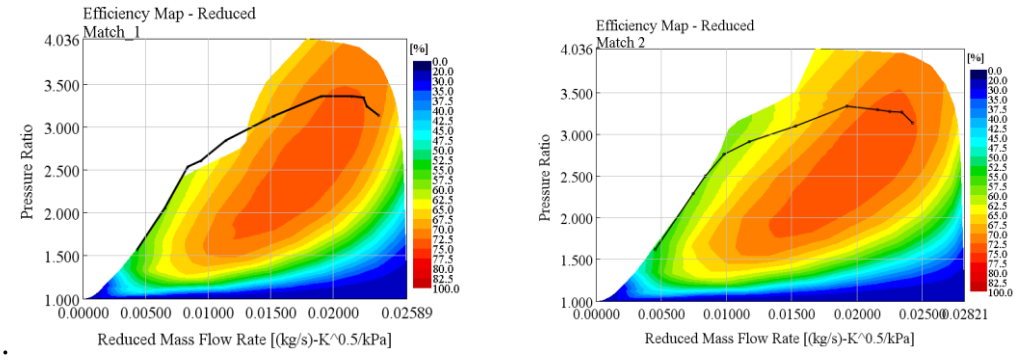

(a) Match 1 (b) Match 2

Figure 5.18 Compressor operating points for Match 1 and Match 2 in two-stages.

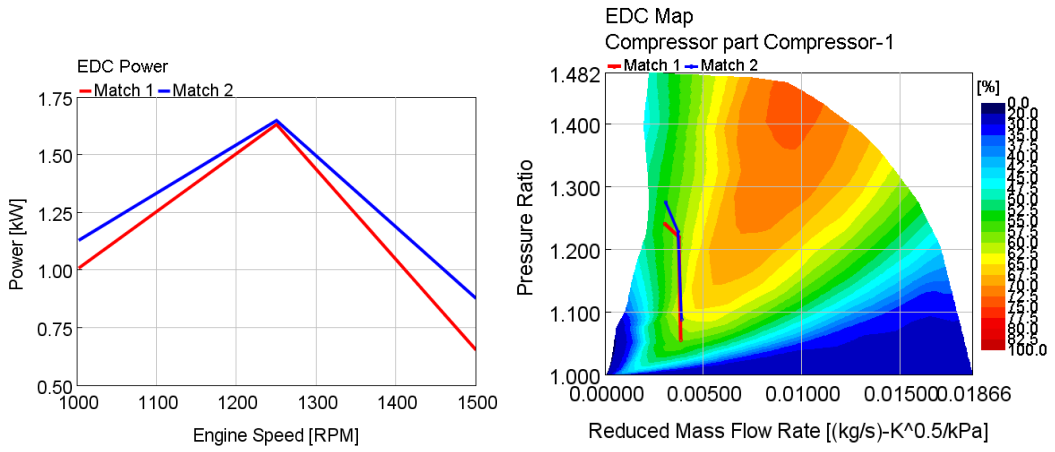

(a) EDC Power (b) EDC operating points

Figure 5.19 EDC operating conditions for the two matches.

Based on the results above, it is hard to deliver target peak torque and power within the engine and air path design limit. However, in order further to optimize the system's performance, a genetic algorithm is used to control the system more efficiently. The factors controlled and constraints considered shown in Table 5.3.

Factors can be adjusted	**Constraints considered**
VGT position	Peak cylinder pressure
Start of the Combustion Angle	Turbine inlet temperature
EDC Power	Compressor Surging
	Turbo speed
	EDC speed limit.

Table 5.3 Simulation factors that need to be considered.

Changing the factors above will affect each other. Moreover, if the EDC is driven by an engine crankshaft instead of a battery, it will become independent, and the controlling logic will become more complicated. Here, the minimum and maximum values of the VGT, SOC and EDC power are set in the GA (Genetic Algorithm) controller, under the constraints of the five measurements outlined above. The engine system is required to achieve the maximum torque possible at a particular engine speed. The Genetic Algorithm Optimizer in GT-Power helps users to find the local best points under specific assumptions, learns itself and conducts the optimisation automatically. The evolution of the optimisation is shown in Figure 5.20.

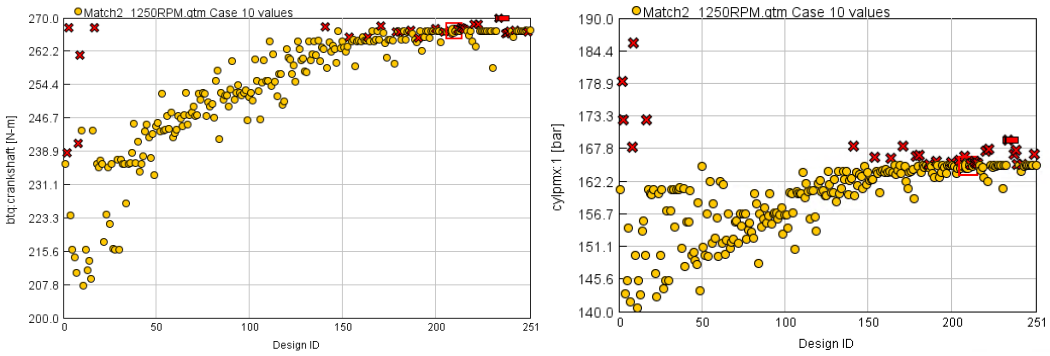

(a) Brake torque converging trade-off (b) Peak cylinder pressure constrain converging trade-off

Figure 5.20 GA results output for engine brake torque and PCP.

This research is applied to Match 2, as it has a bigger turbocharger, which sacrifices much low speed performance, so the GA method can help to investigate its maximum low speed performance. Based on the results, it can be seen that Match 2 can deliver, at most, a 266 Nm torque under certain limits and designs at 1250RPM, which is still lower than the 320Nm requirement, but this method shows that it offers advantages in terms of complicated system optimisation.

Based on the matching investigations above, Match 1 is still the most appropriate match for this case, and it is unnecessary to enlarge the turbocharger size any further in order to achieve a higher peak power but sacrifice the low speed performance.

The research in this part shows that after introducing more components and controllers, the optimization of system performance become far more complicated. Comparing with typical two-stage turbocharger system, EDC makes the matching process more flexible, GA method is a good way to find the best local solution under the given constrains. There is no restrict standard in boosting control for this two-stage EDC system, the critical factors that need to be considered are:

- Boosting distribution between the turbocharger and EDC.
- Exhaust pipe limits.
- Electric system power limit and electric capacity.

5.2.1.2 Air path experimental demonstration for proposed matching

The two-stage EDC system engine's performance was studied in the previous section. The EDC and turbocharger can help the engine to increase its low speed torque, by pumping more air into the engine cylinder. The boosting ability of this air path can be verified on the test rig, with a similar boundary condition to the turbocharger and EDC. Three low-speed full load points were selected from Figure 5.17 with Match 1, and the information is shown in Table 5.4.

Engine Speed (RPM)	Compressor PR	EDC PR	Turbine PR	Comp Corrected MFR (kg/s)	Turbine MFR(kg/s)
1000	1.48	1.02	1.62	0.0492	0.0516
1250	2.26	1.2	2.26	0.0428	0.0448
1500	2.55	1.25	2.45	0.0240	0.0252

Table 5.4 Experiment boundary conditions for the 3 low speed points.

As the compressor inlet air temperature is not the same in the simulation and experiment, the compressor corrected mass flow rate is used to evaluate the model.

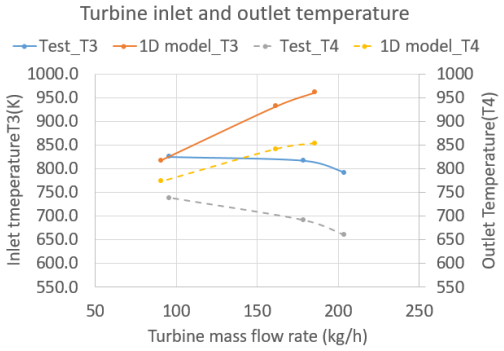

(c)

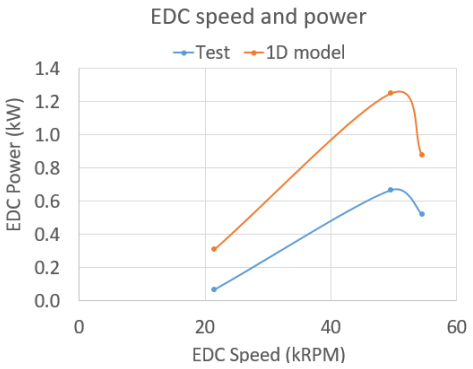

(d)

Figure 5.21 (a) and (b) shows the matching of the operating points, for the EDC, compressor and turbine. Most of the results matched well, however, but there are some differences regarding turbo speed matching and exhaust flow matching, possibly due to the engine difference between the test rig and the simulation.

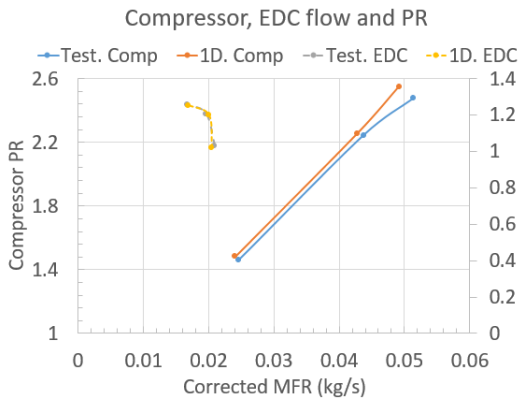

(a)

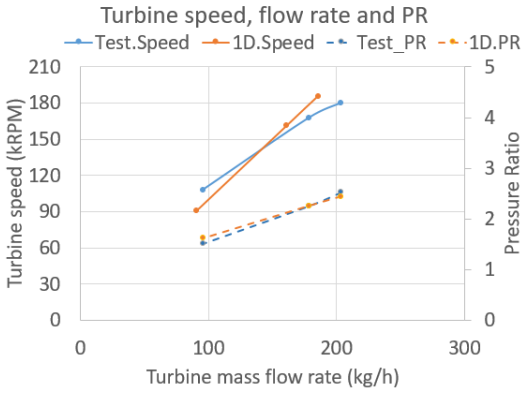

(b)

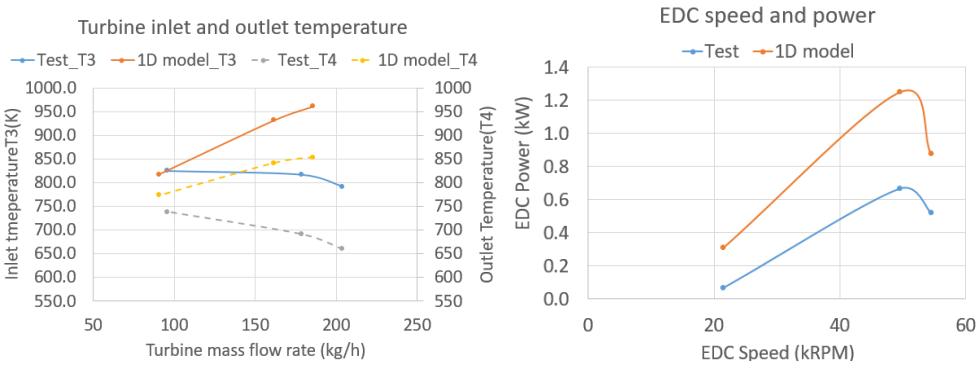

(c) (d)

Figure 5.21 EDC and turbocharger operating points matching between the simulation and the experiment. (a) Compressor flow and pressure ratio. (b) Turbine flow, pressure ratio and speed. (c) Turbine inlet and outlet temperature. (d) EDC speed and power.

Figure 5.21 (c) shows the matching of turbine inlet and outlet temperature, the turbine temperature was not matched as because the intercooler and engine are different between the simulation and the experiment. However, the trade-off between test and simulation is the same for both T3 and T4. Figure 5.21(d) shows the EDC power matching, in experiment, this value is calculated based on the EDC map and operating points without considering E-motor efficiency, in simulation there was an assumption of the electric system heat loss, which made the difference here.

In this part, a demonstrating test was carried out for the two-stage EDC system, it also verified the engine model air path, by matching the compressor and turbine mass flow, pressure ratio and speed. This experiment shows that the engine gas stand test rig can be used to demonstrating the air path performance of a real engine system (or model).

5.2.2 Two-stage VGT and EDC transient performance

This section discusses the sensitivity of the VGT position and EDC power in the step load transient process. The transient simulation methodologies were introduced in Chapter 4.

The transient simulations are all performed ignoring the electrical load of the alternator on the engine crankshaft. Firstly, the baseline transient model's performance will be presented in this section, followed by a series of three results, covering:

- The sensitivity to the EDC power strategy
- The sensitivity to the VGT control strategy
- The sensitivities of the Air fuel ratio

For the transient simulation, the engine heat release model, combustion rate, and heat transfer model have been changed to the transient mode. The transient operating point is from the 2000RPM 5bar part to the 2000RPM full load condition. It is important to note that the model has not been completely updated for transient capability.

During the transient. A number of control actuators are available to influence the transient response of the engine:

- EDC power level (kW used and duration of activation)
- EDC bypass valve
- Turbocharger VGT (position and duration in the over-closed position)

Figure 20 shows one of the controlling transient profile of each components, and how these variables may vary during the transient load step (transient process starts at 1.0s). These will be explored later.

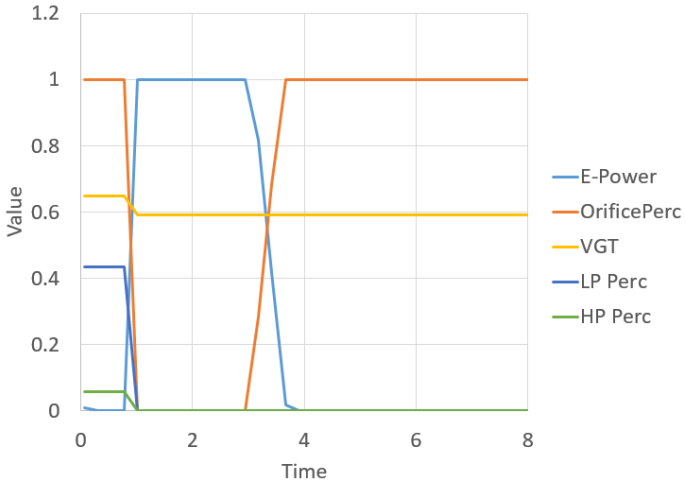

Figure 5.22 One of the transient variables' operating situation.

5.2.2.1 Engine transient response vs EDC power

Figure 5.23(a) and (b) show the first transient setting case, in order to see how different EDC power levels affect the engine torque response during a 2000 rpm fixed load step. Three power settings, of 1, 2 and 3kW, are compared and are found to reduce the 5-90% load response time by 0.95s, 1.42s and 1.56s, respectively.

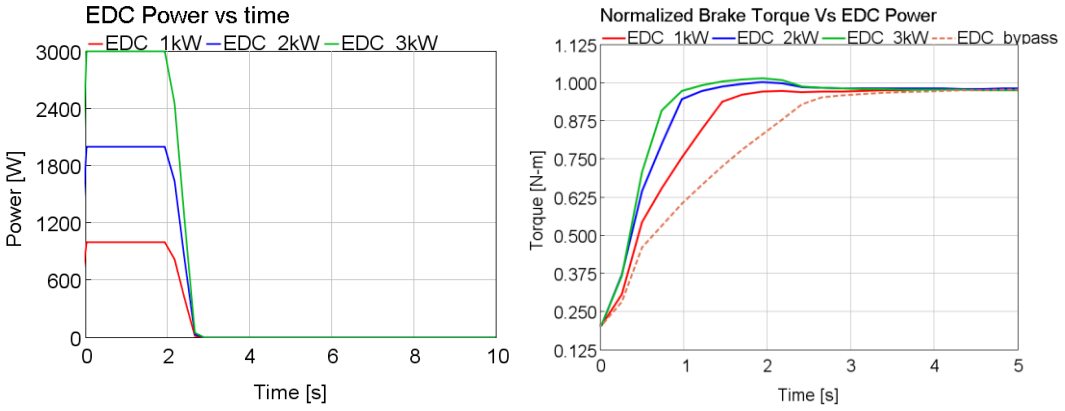

(a) (b)

Figure 5.23(a). EDC power input during transient; (b). Normalized Engine Brake torque with different EDC power.

Figure 5.24(a) and (b) show the effect of EDC on time. It can be seen that, above 3s, there will be minimal additional benefit from the extended use of the EDC.

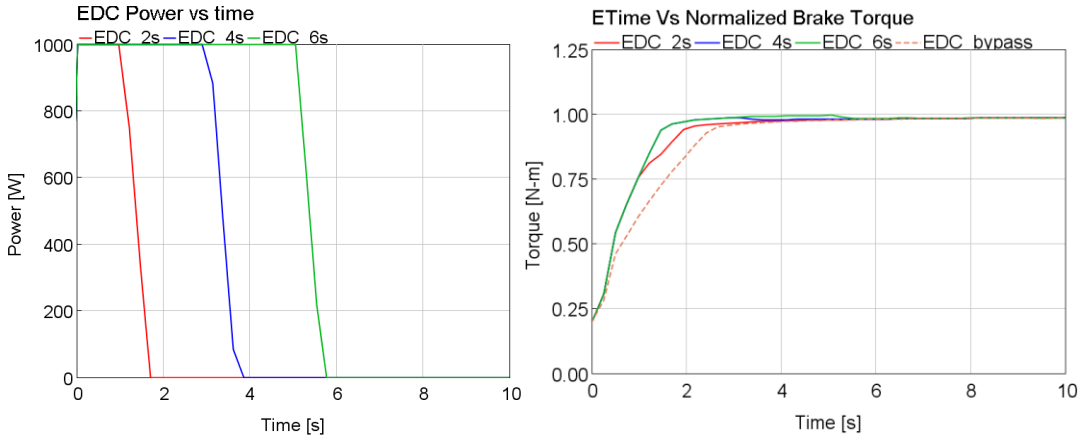

(a) (b)

Figure 5.24. (a). EDC Power vs time; (b). Normalised engine torque transient response.

Figure 5.25 shows the response time for achieving a 95% engine target load under different EDC power settings (power value and continuing time). The x axis represents the total amount of electrical energy used by the EDC which will increase with the EDC power level and/or EDC on time. However, diminishing returns can be seen. Typically, at a 2000rpm full load, the EDC is inactive; however, here it is shown how it can improve the transient response. The inclusion of the EDC reduces the time to 95% of the target torque from 2.3s to around 0.75s, though 7kJ extra electricity was consumed. If the EDC power is the same but works for a different length of time, most of the benefits occur through activating the EDC over the first 0.5-1s of the transient.

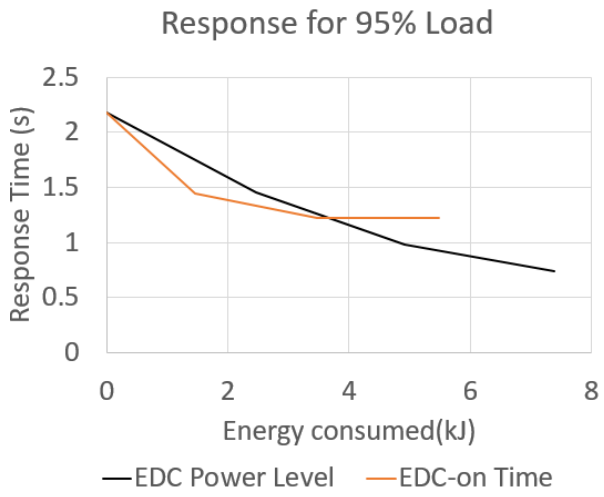

Figure 5.25. Response time for different EDC power and power continuing time

5.2.2.2 VGT Rack position control

The VGT can also be used to improve the transient performance by "over-closing" the guide vanes to spool up the turbocharger faster. However, this will increase the engine back-pressure, which will, in turn, reduce the torque response. Figure 5.26 shows the VGT rack position over time and its consequent engine torque response. When the rack position is 0.3 and 0.2, the torque response has been increased by 0.12s and 0.3s, respectively. However, when it is further reduced to 0.1, the torque response improvement is only 0.2s, compared to the baseline.

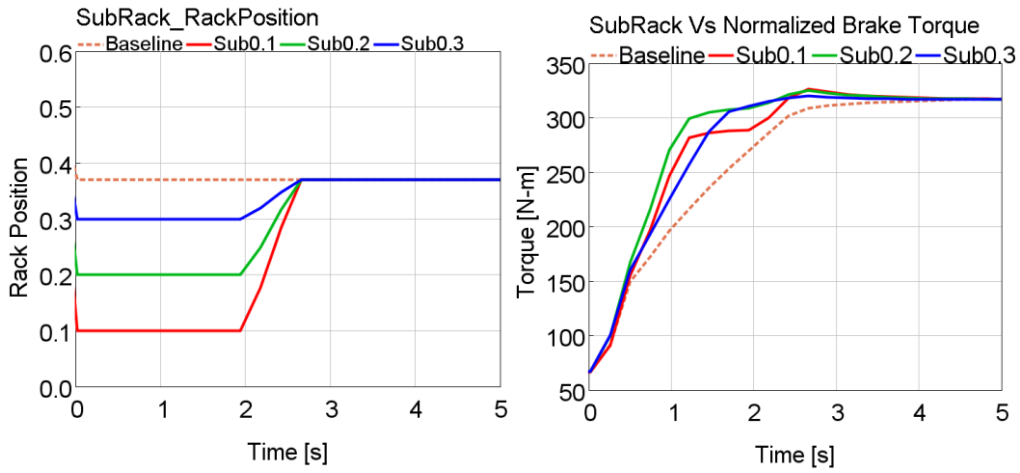

(a) (b)

Figure 5.26. (a). VGT Rack position. (b). Engine brake torque.

The duration of VGT "over-closing" is also of interest. Figure 5.27 shows the result if VGT is held in a lower rack position for a different time range (0.3s, 0.6s, and 0.9s). Holding the VGT guide vane in a lower position for a longer time can improve the transient by up to 0.25s.

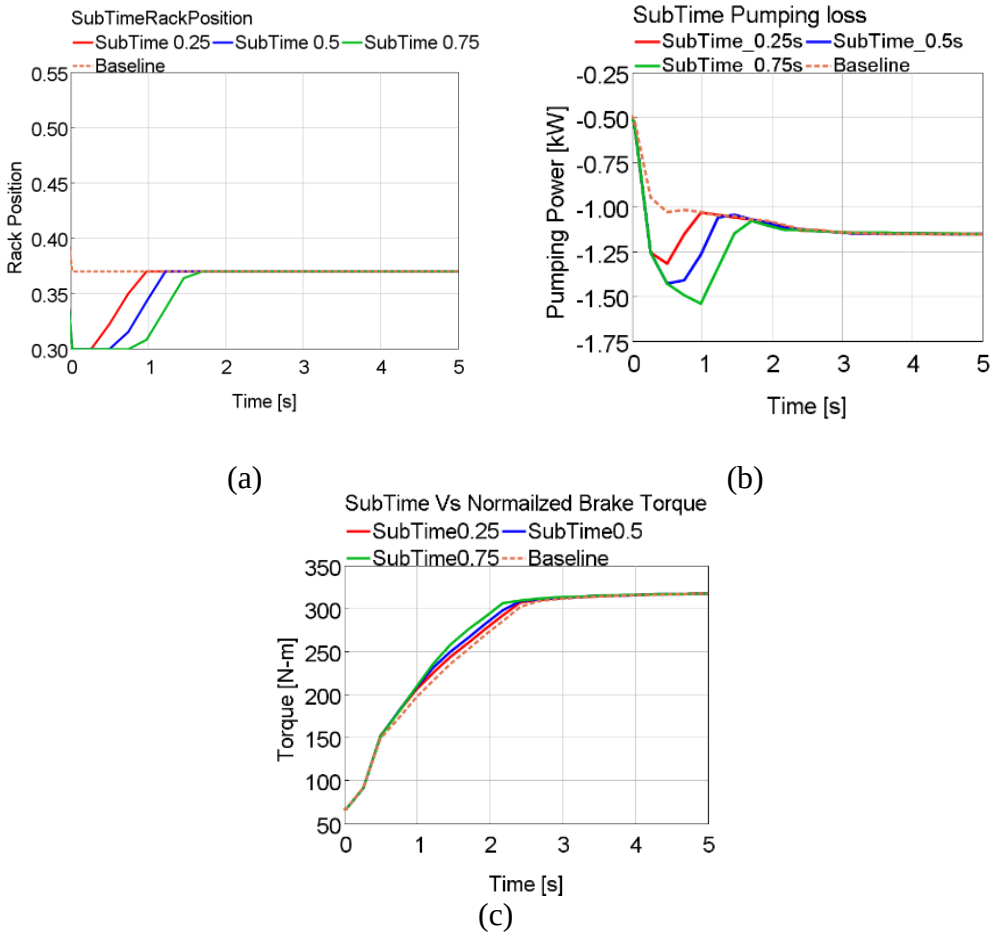

(a) (b)

(c)

Figure 5.27 (a). VGT Rack position; (b).Engine pumping loss. (c) Engine brake torque,

Figure 5.28 summarises the relationship between energy consumption and engine transient time for all the cases above. Hold the VGT into a lower position can increase the transient speed, and the pumping loss increased was less than 0.6 kJ, this case depends on what the VGT position was held, if the subrack position is much lower, faster transient response and more pumping loss was supposed to be produced, over closing the VGT can help reduce transient time to about 1.45s. However, what cannot be ignored is that over-closing the VGT too much will reduce the engine peak torque. When the rack position is lower than 0.2, the transient time will be increased because the backpressure is too high.

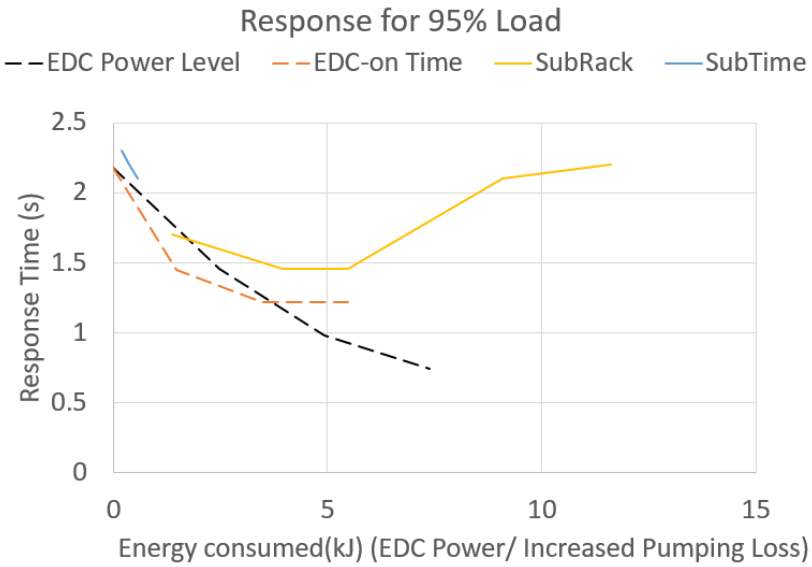

Figure 5.28. Energy Consumption against response time for different cases

Based on all of these results above, the transient response can be increased by either the assistance of EDC or by over-closing the VGT. In Figure 5.28, when the transient response time was reduced from 2.25s to 1s, the extra electricity consumed by the EDC was about 5kJ. When it comes to over-closing the VGT, the increased pumping loss is also close to 5kJ. However, what cannot be ignored is that over-closing the VGT will reduce the engine peak torque. When the rack position is lower than 0.2, the transient time will be increased because the backpressure is too high.

5.2.2.3 Air fuel ratio effects on transient performance

The air to fuel ratio (AFR) is one of the main factors to consider when dealing with diesel engine soot emissions. These emissions are more likely to occur during a rapid load transient where the fuelling is limited by an AFR limiter. Therefore, for a given change in engine torque, the sooner the engine can move away from this limit, the easier it will be to reduce the soot emissions. By using the EDC to vary the airflow during the transient, an increase in airflow can be achieved without applying backpressure to the engine. This, in turn, will increase the AFR which makes it possible to control the emissions at source in the cylinder. This approach was analysed in the simulation environment.

For the simulation setting, the transient process happened at time 0s, with an engine speed of 1250RPM, from 5bar BMEP to full Load condition. Figure 5.29 shows the relationship between the engine brake torque transient time and engine AFR ratio. In this case, the VGT rack position is fixed to remain the same, but the engine fuel rate and EDC-driven power are different for the same target torque in each case. As the AFR limit rises, less fuel will be required in this case, but more electric power will be needed for boosting. The transient response speed is similar, which was affected by both the AFR limit and the EDC power. These results show that, by using the EDC to provide an additional airflow, the same engine torque response can be achieved with reduced air to fuel ratios. Figure 5.28(d) shows that an increase in the AFR of 1 requires approximately a 0.4kW increase in EDC power.

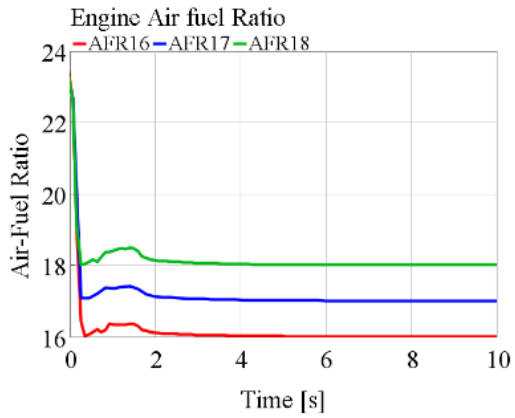

(a)

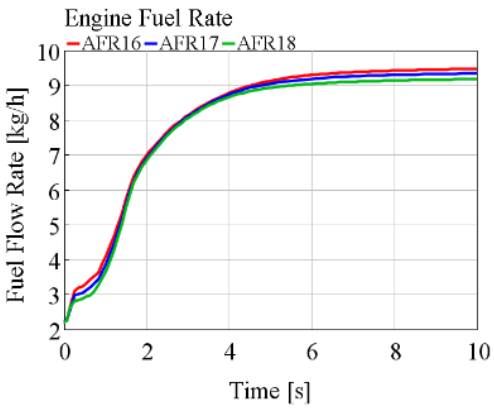

(b)

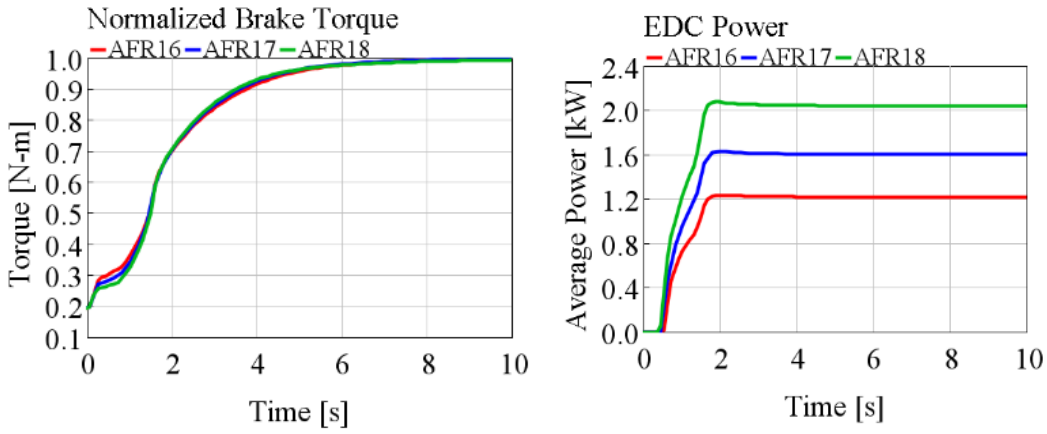

(c) (d)

Figure 5.29 (a) Engine Air fuel ratio. (b) Engine fuel rate. (c) Engine brake torque transient response. (d) EDC Power.

The simulation results in this part showed that by increasing the air flow by EDC (without increasing engine backpressure), the air-fuel ratio could be increased and allow a more lean combustion, this can help the system save more fuel but deliver the same torque.

5.2.3 Study of intercooler and HP-EGR position in two-stage air path

In both Chapter 3 and Chapter 4, the possibility of different components arrangements for this air path system was introduced. In this section, the effects of the intercooler location and HP EGR locations (in Chapter 3) on the engine system will be discussed which, at an initial stage, offers potential ideas for this area in the future.

As shown in Figure 5.30, the intercooler can be either upstream or downstream of the EDC, and this will affect the temperature at the engine inlet air path (T1 to T5 shown in Figure 5.30). The simulation will be operated in the engine full load curve. EDC will only be involved in low speed cases and bypassed in other cases. The two EGRs will be closed as they are not needed under the full load condition.

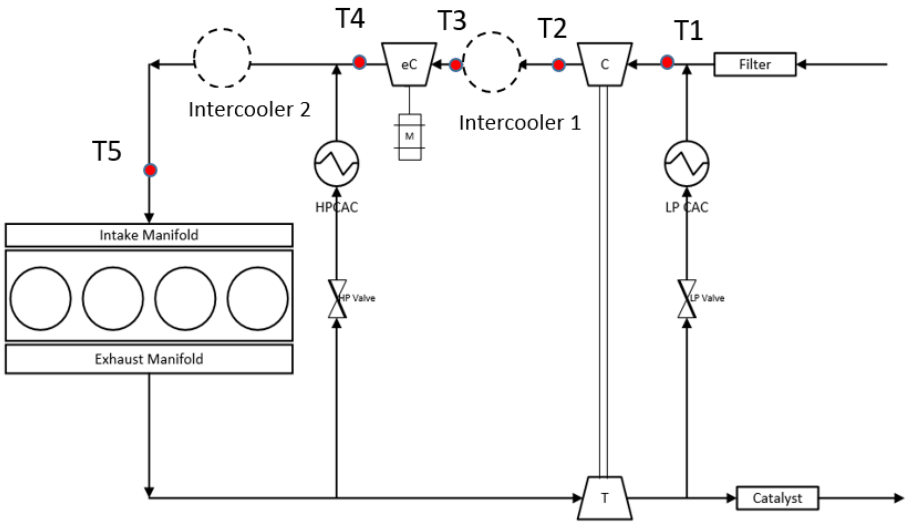

Figure 5.30 Intercooler location swapping.

The engine torque and mass flow rate is matched well for the two cases, as shown in Figure 5.31. EDC is involved from 1000 RPM to 1500 RPM, then bypassed.

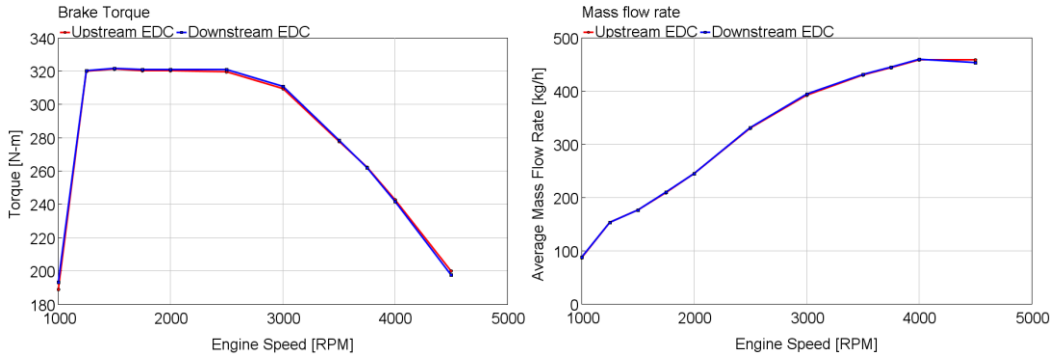

(a) (b)

Figure 5.31 (a) Engine torque; (b) Engine inlet mass flow rate.

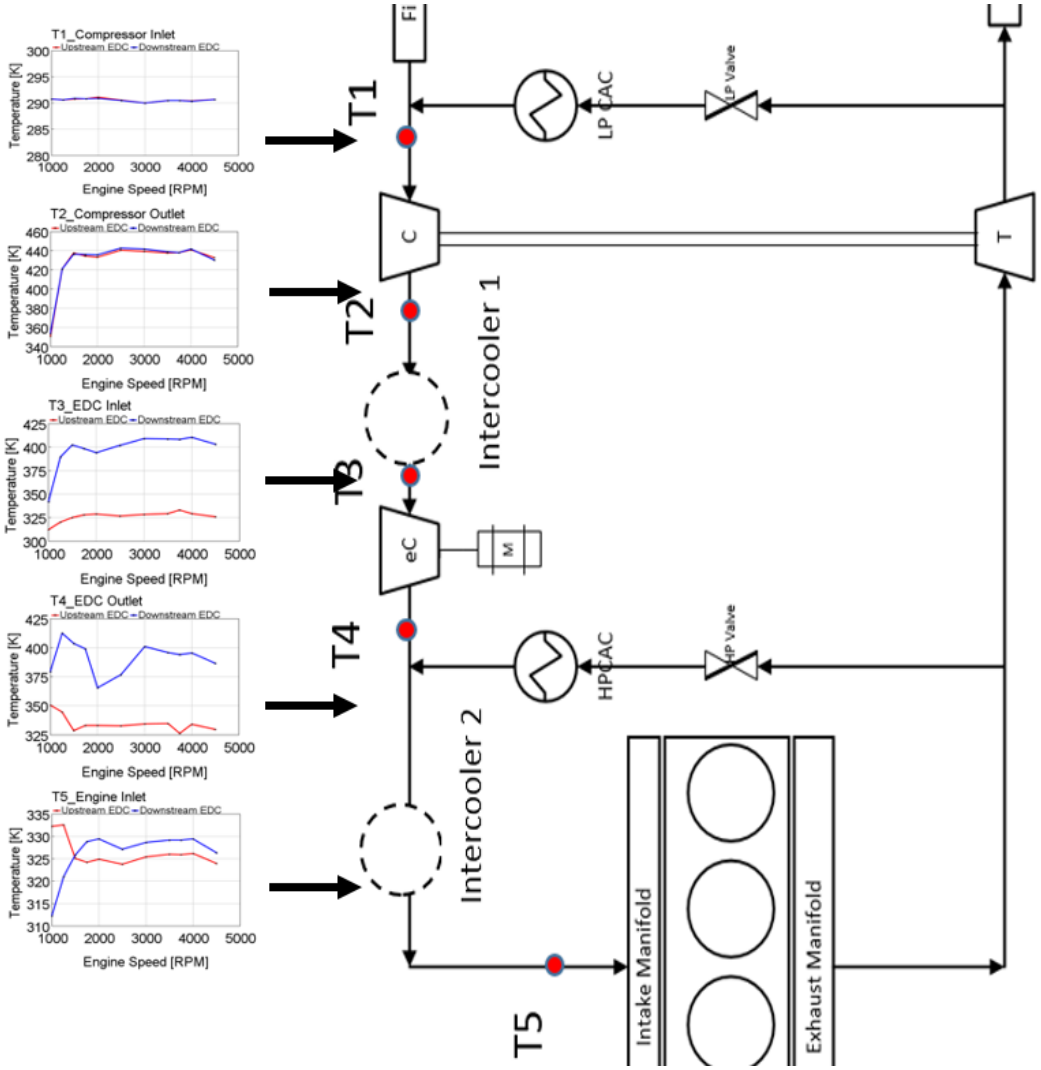

Figure 5.32 Temperature results for each measuring point.

It can be seen from Figure 5.32 that the intercooler location only affects the EDC operations and engine inlet temperatures. If the intercooler lies upstream of the EDC, this will result in a lower EDC inlet temperature (T3), lower EDC outlet temperature (T4), and lower engine inlet temperature (T5) in single stage situations (but higher ones in two-stage situations). Low temperature combustion is currently a trend in modern engines, as it can increase the engine's fuel efficiency and reduce the NOx and soot emissions (using HCCI, EGR), which may help to lower the combustion temperature. However, in low speed cases, the temperature is higher if the EDC is used (as boosted air by the EDC was not cooled down). In most of the driving cycles, the vehicle is more likely to be operated in low speed cases which means that, in those regions, the engine will suffer a penalty in terms of inlet air gas temperature. Figure 5.33 shows the operating points on the compressor and EDC map for the two cases.

For the compressor, it has little influence. The Downstream EDC case has slightly higher pressure, related to the higher T2 shown in Figure 5.32 because, the closer the intercooler is created, the higher the flow resistance; EDC, in this case, has a lower pressure ratio and higher reduced mass flow rate due to the temperature differences.

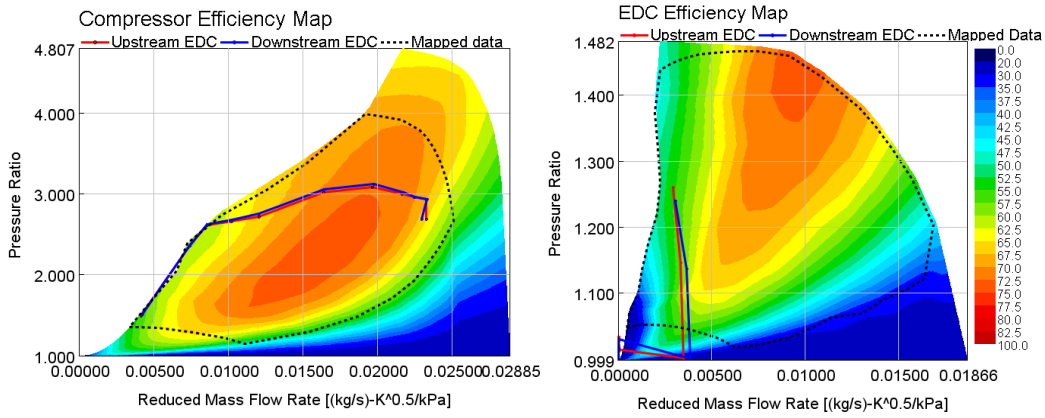

(a) (b)

Figure 5.33 Engine operating points on (a) A compressor map, and (b) an EDC map

As the intercooler model in this system is set to be an oversized cooler, so transient performance in this part is not analysed.

The HP EGR outlet port position can also be adjusted, as mentioned in Chapter 3. It is more interesting to see how the layouts affect the system's transient performance. In the steady state condition, the EDC and intercooler will only affect its mass flow rate. The HP EGR has the following route design (already introduced in Chapter 3), the HP EGR route, Mid EGR route 1 (EGR pre-intercooler), and Mid EGR route 2 (EGR post-intercooler), as shown in Figure 5.1.

In the simulation, all three routes were discussed. The engine was operated from a 2000RPM 5bar 20% load to a 2000RPM full load. The EDC is bypassed, given the assistance of EDC and closed VGT more to compare with experiment results. The operating conditions are shown below:

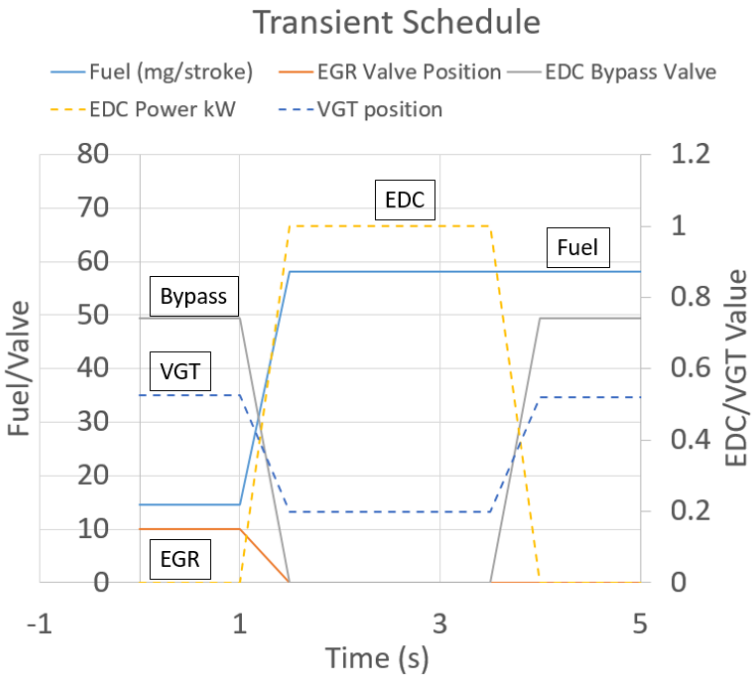

Figure 5.34 Transient schedule

EDC and VGT will be operated under certain conditions (higher speed or a lower VGT position). An example of the engine mass flow rate and HP EGR flow is shown in Figure 5.35(a) and (b). The EDC contribution does not affect the EGR flow, but the VGT could because, as it increased the HP EGR inlet pressure, a higher exhaust flow was pumped into the EGR path. The engine flow is increased by either the EDC or VGT. Figure 5.35(c) and (d) shows the O2 fraction in the EGR path and EDC outlet. The HP EGR O2 rate is increased faster, and the EDC outlet O2 rate undergoes little change. This result is unreliable as, in the 1D model, the EGR and air composition were not modelled and validated by a very accurate method, but simply based on a typical model so, for the simulation, our later comparisons will mainly focus on the mass flow.

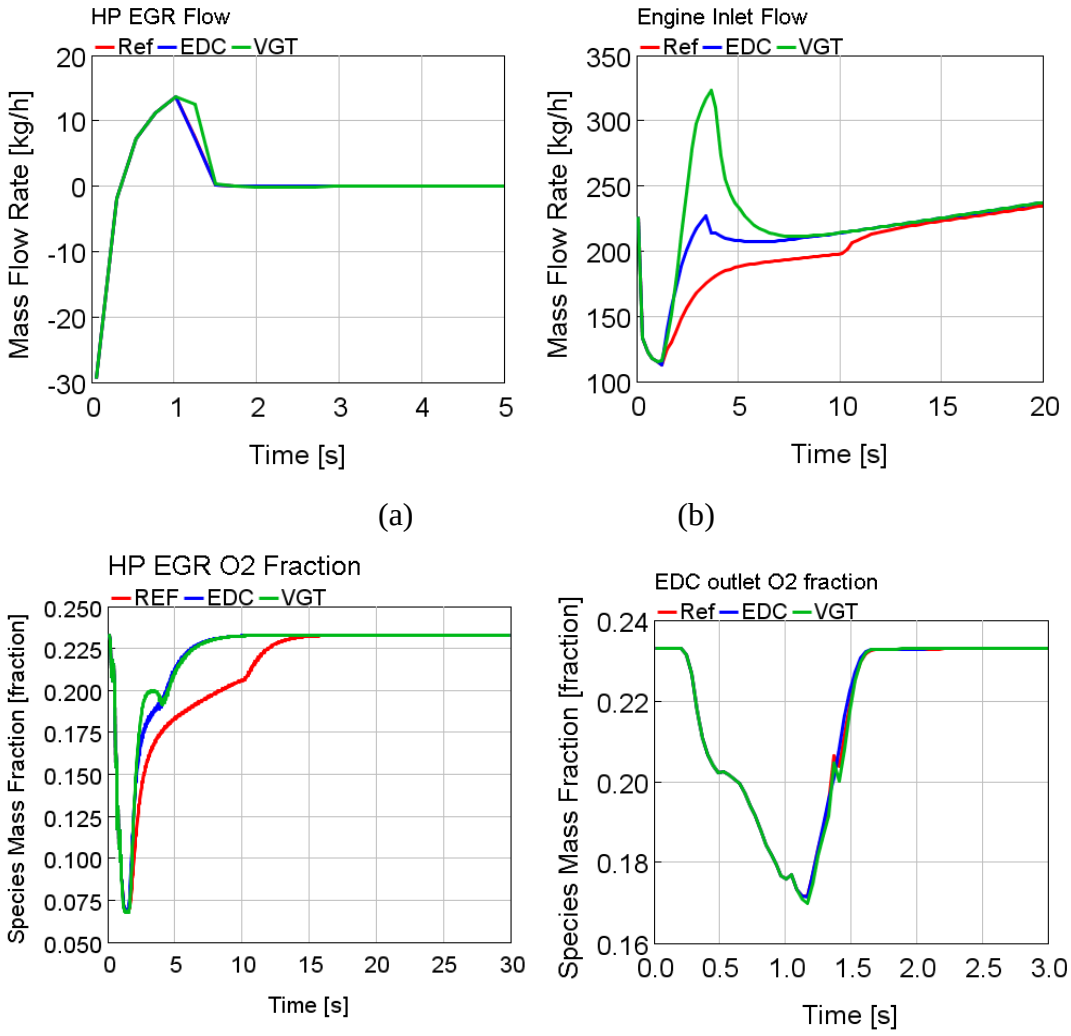

Figure 5.35(a) HP EGR flow. (b) Engine inlet flow (c) O2 Fraction at the HPEGR (d) O2 Fraction at the EDC outlet

Figure 5.36 shows the HP EGR mass flow and engine inlet flow for the three air path designs. Clearly, HP EGR route has the lowest engine flow but highest EGR flow under the same boundary condition, because in this case, the EGR outlet is downstream of the EDC, and so not boosted by the EDC. The model in this section cannot perfectly predict the EGR performance, as the EGR model, coolers, valves were not validated, so it can be regarded simply as a reference. The experiment requires further investigation.

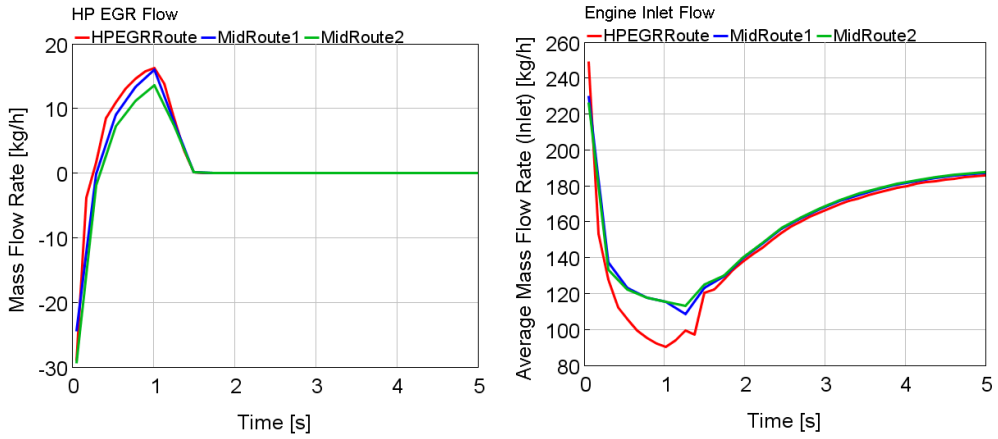

Figure 5.36 Mass flow rate (a) HPEGR (b) Engine inlet

The experiment was designed by following the same method as used in section 1.2. In that section, the HP EGR transient performance has already been introduced, which is in Mid route 1. A similar test was performed for Mid route 2. The mass flow transient comparison between these two cases is shown in Figure 5.37. The compressor flow was unaffected by the routing, but the EGR flow is much lower in Mid route 1. However, these data are unreliable, as the oscillations that occurred during the transient may have been due to the temperature pulsation around the HP EGR Vcone.

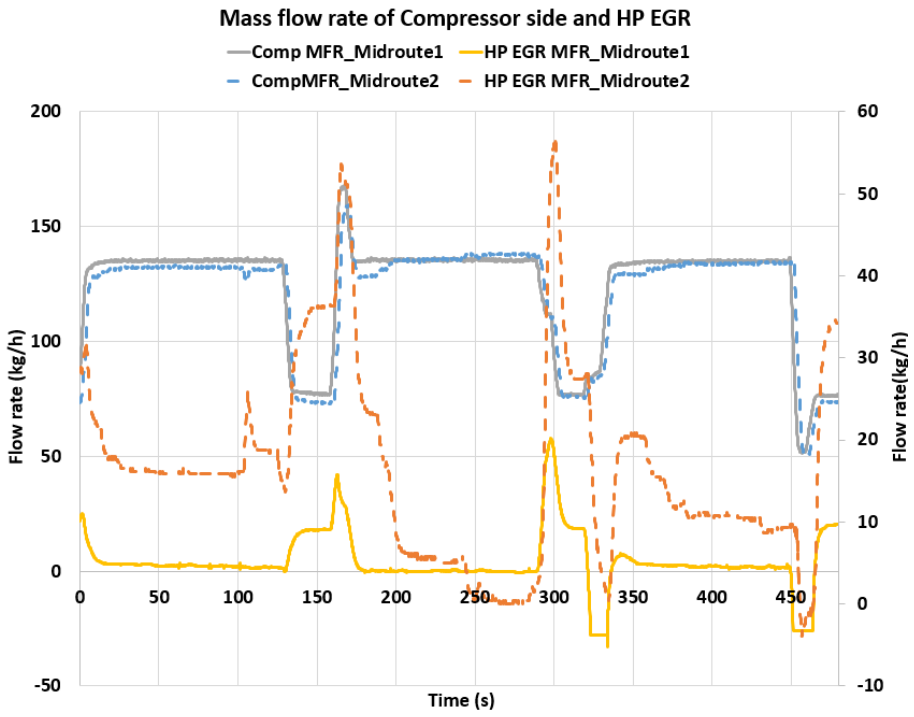

Figure 5.37 Compressor and EGR mass flow rate between Midroute1 and Midroute2.

The EGR mixing situation is shown in Figure 5.38. Mid route 2 has a slower response, possibly because the intercooler shows resistance to the flow, which slows down the mixing process.

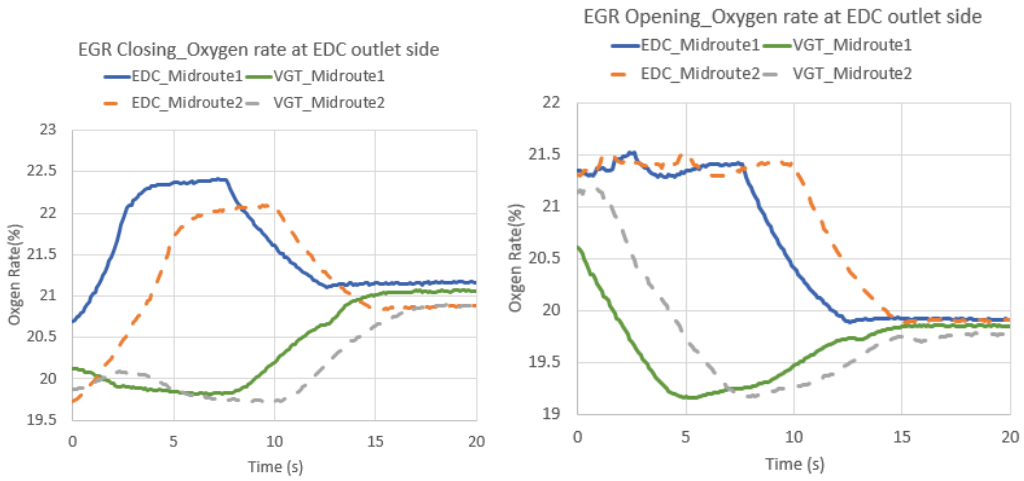

Figure 5.38 (a) EGR mixing in the closing transient process. (b) EGR mixing in the opening transient process.

5.3 Summary

The studies on the two-stage system with EDC were discussed in this chapter, including the air path tests on the engine gas stand, and its related research in the field of diesel engine modelling.

Section 1 mainly discussed the steady state and transient performance of this air path, based on the experiment design introduced in Chapter 3. The sensitivity of the VGT rack position and EDC speed were compared, and it was found that both closing the VGT and increasing the EDC speed can help to raise the boost pressure. However, a lower VGT position will lead to a higher engine backpressure, so the engine pumping loss is increased. A higher EDC speed will consume extra electrical power, which was limited by the system's electric system design. Validated tests have been applied on both the LP and HP EGR, and both the VGT and EDC can affect the EGR flows in the steady state situation. Besides, a transient study between EDC, VGT and HP EGR was also considered, as EDC and VGT can affect the HP EGR mixing during the transient process. A series of back to back comparison experiments were designed. The results showed that high speed EDC and lower positioned VGT could help to increase the EGR transient flow and mixing speed (according to the O2 rate changes). In the

meantime, if the VGT is opened too fast in this process, there will be a backflow involved from the compressor to the turbine side.

Section 2 presents a study on the similar two-stage EDC air paths for a 1.6L diesel engine, as further research on this system based on the experiment outlined in section 1. The aim of this study is to understand the design and control trade-offs which must be managed in such an electrified boosting system. The same two-stage boosting system, including an EDC and a VGT is used. The air path also includes low and high pressure EGR loops. The work was performed using a combination of 1D modelling and experiments conducted on a novel transient air path test facility. Firstly, the matching between the boosting system and engine was investigated and optimised. Considering the hard design limit, related two-stage validating tests were performed on the test rig for the same air path; the two-stage engine system performance was validated by the external engine stand test results, in the full load steady state condition. For the transient study, driving the EDC at higher speed, closing the VGT more than the target position during transient and operating the AFR at a lower limit can increase the time required to reach the target torque. The response time was reduced by 0.1s to around 2s, but all of these controlling methodologies will decrease the engine's efficiency.

The intercooler and HP EGR location was discussed next, in both the simulation and experiment phases. The intercooler position mainly affects the engine and EDC inlet temperature. The EDC had a lower pressure ratio but higher reduced mass flow if the intercooler was downstream of the EDC, mainly because the inlet air temperature of the EDC does not cool down. The EGR location depends on whether the EGR flow is boosted or not by the EDC, and whether the EGR outlet is located upstream of the EDC so that, when the EDC is working, the mixing process and EGR flow will be higher. This has been demonstrated in both the simulation and experiment. The research in this part is still a very initial attempt, and further investigation should be designed to obtain more accurate measurements and ideas, focusing on how they affect engine combustion.

Chapter 6 – Modelling of decoupled electric turbocharger system

This chapter will focus on the modelling and simulation works for the decoupled electric turbocharger (DET) system.

This study will make use of the simulation method from the previous research. The DET research was based on the 2.0L turbocharged petrol engine model. The original turbocharger was decoupled and connected with two electric motors separately. The steady-state performance of DET was discussed based on the turbocharger scaling method in Chapter 4, focusing on the energy balance between e-compressor and e-turbine, also considering system efficiency with the assumption of the electric system property.

After that, the DET system was applied to the same single stage engine model, investigating the transient performance of WLTC cycle and 0 to 60mph acceleration process, in order to find out its benefit in both energy-saving and transient performance side. This study is based on the previous work from other colleagues, the whole model was not designed by the author independently, so this chapter will only focus on the work that finished by the author himself, the controlling design for EDC and E-turbine in drive cycles.

This chapter is a case study based on the results explained in Chapter 5, in order to find out the potential of power generating ability for DET system.

Work in this chapter has been published in: Liu, Y., Burke, R.D., Akehurst, S. and Zhang, Q., 2017, October. Numerical Investigation Into the Performance and Efficiency Trade-Off for a Mechanically Decoupled Electric Boosting System. In ASME 2017 Internal Combustion Engine Division Fall Technical Conference. American Society of Mechanical Engineers Digital Collection.

6.1 DET system characteristics and power generating ability

In this section, a series of results will be plotted and explained, including DET performance, the ability of power generation in real driving cycles and electric system efficiency, gear ratio sensitivities. The effect of turbine size on power generation is carefully illustrated. The smaller turbine has a better transient response in low speed region but delivers bigger backpressure, which will increase the engine fuel consumption and pumping loss. The bigger turbine has low efficiency at low speed and low load region, and this will lead to a fact that when the engine is running in this region, the power generated from turbine cannot drive the compressor to get enough boost pressure. With a suitable turbine, both transient response and total SFC of engine can be optimised.

Both full load and part load conditions will be discussed, the engine simplified torque map was shown in Figure 4.16. In all cases, the engine BMEP was adjusted to be the same to allow for a direct comparison between different turbine sizes. The turbine waste-gate is fully closed, which ensures that the exhaust energy is used by the turbine completely.

Figure 6.1 shows the effect of turbine size on engine backpressure. For the same engine BMEP, smaller turbine needs to rotate faster to allow enough mass flow rate pass through. In this case, turbine speed is fixed so that higher backpressure is produced; this will make increase engine pumping losses. With higher pumping loss, but the same BMEP, more fuel needs to be injected into the engine. This, in turn, will lead to a higher exhaust temperature, which could have a benefit on turbine power that can be recuperated into electricity.

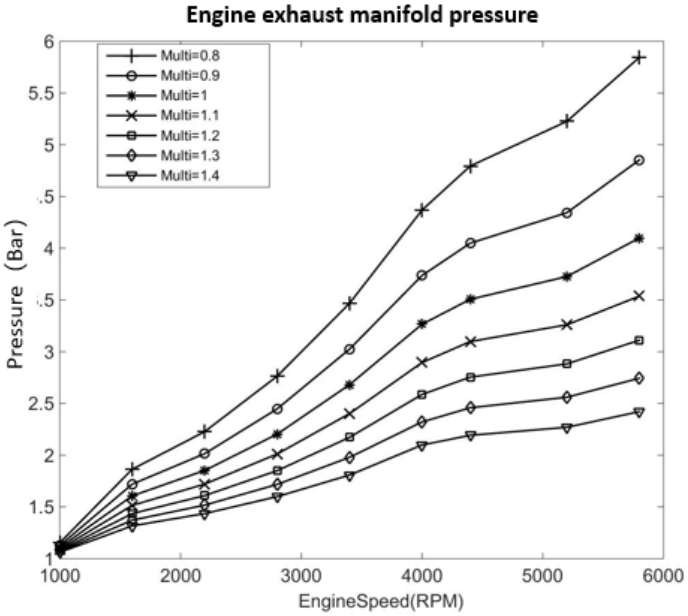

Figure 6.1 Engine exhaust manifold pressure at full load with the changing of turbine mass flow multiplier.

Figure 6.2 shows the power needed in the compressor side. Smaller turbines increase the engine backpressure, which will increase pumping losses. Due to the matching between turbocharger and engine, the power needed for the compressor is increased if a smaller turbine is used, the reason is that the requirement of boost pressure in this condition is increased.

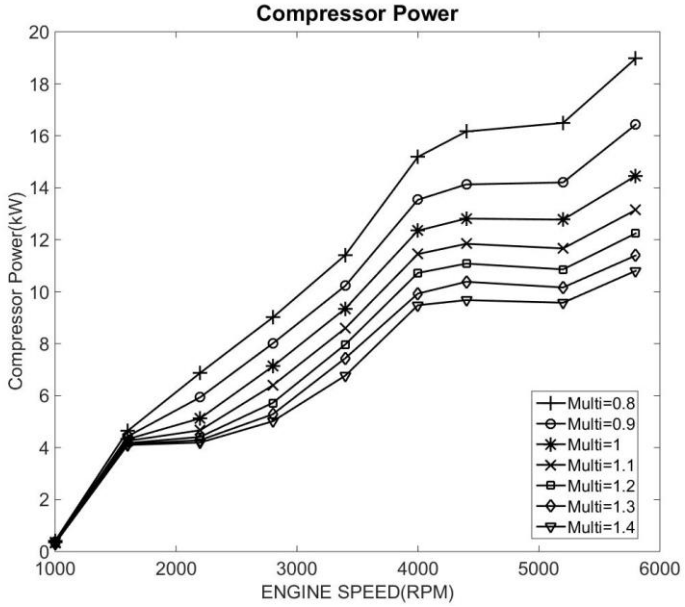

Figure 6.2 Compressor Power with adjusting of turbine mass flow multiplier

Figure 6.3 shows the turbine power generated comparing with compressor power needed (only the max compressor power is shown with dash line) in both full load and

40% load condition. Smaller turbine can generate much more power in the same condition. In full load but low speed conditions, turbine power is not enough to drive the compressor, and extra external power would be needed. In 40% load and low speed conditions, the compressor is not needed and can be bypassed; all turbine energy can be stored.

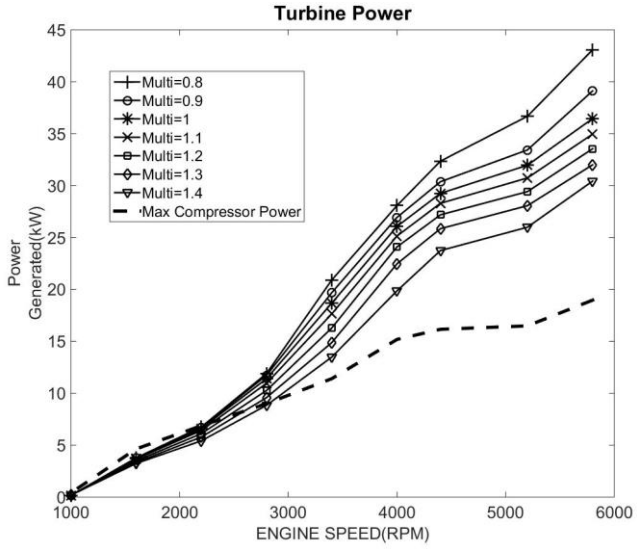

(a)

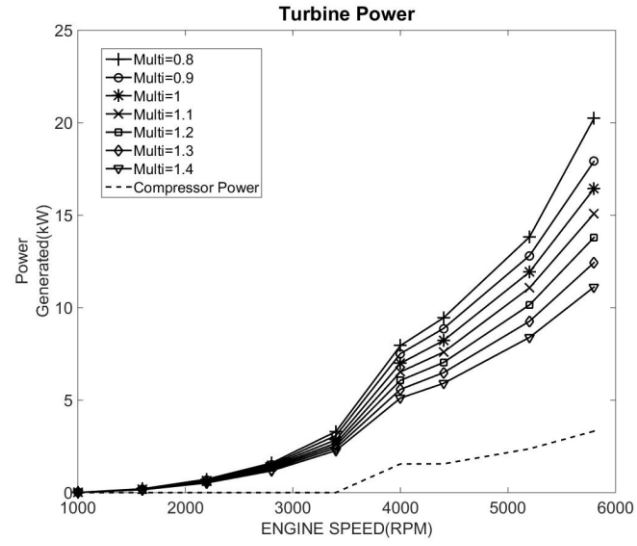

(b)

Figure 6.3 Turbine and compressor power in (a) 100% and (b) 40% Load

From the results above, the following observations can be made for the performance of decoupled electric turbocharger:

1. Smaller turbines can generate more power in the same engine operating point but will produce higher backpressure and cost more fuel.
2. As the turbine becomes smaller, engine pumping loss is increased, which will reduce the engine brake power. To counter this and maintain the same level of BMEP, higher boost pressure is required, which increases the compressor power.
3. In high load but low speed condition, energy generated from the turbine is not enough to drive the compressor for target boost pressure, external power input is needed.

Those results shown above considered no energy losses between the turbine and compressor. The use of an electric motor and generator introduce losses into the system. Some assumptions about efficiency have been made, which was indicated in the methodology part. With all the data from simulated steady-state conditions, an electrical energy usage map can be produced for all turbine sizes. Figure 6.4 (a) shows the system efficiency of baseline engine with traditional turbocharger, Figure 6.4 (b) shows the efficiency difference between DET system and traditional system, in high load but low speed region, baseline engine has a better efficiency with approximately 0.7% higher, however, in the rest region on the map, DET system has better fuel efficiency, especially in high speed but low load region, more than 1.5% efficiency benefit is achieved. In all, it can be seen that DET system has a potential to improve the fuel economy and system efficiency because it can generate more energy from the exhaust and take it for other uses comparing with traditional turbocharger in most operating points on engine map.

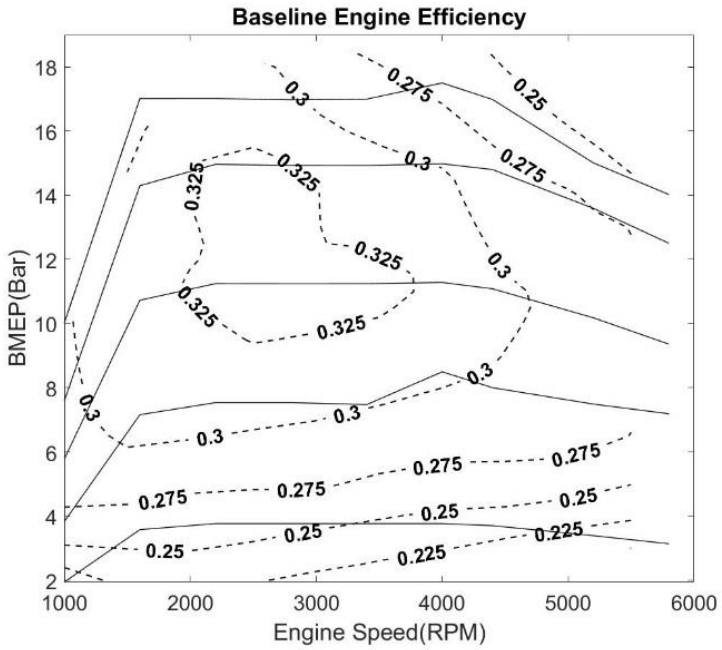

(a)

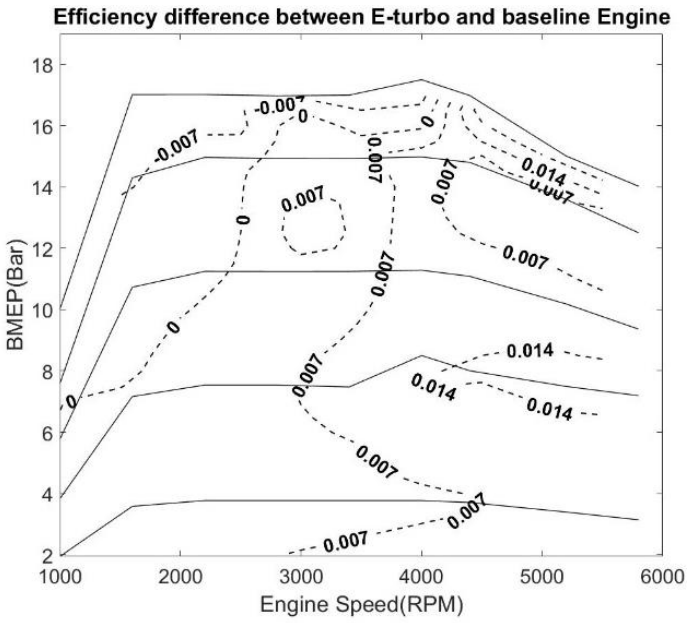

(b)

Figure 6.4 (a) Baseline Engine Efficiency. (b) Efficiency difference between DET and Baseline Engine

An example with scaling factor 1 is shown in Figure 6.5 (a). In this map, the left top side is the region that power generated in DET system is negative, which means extra power input is needed to drive the system. In the most extreme condition of low speed torque, the power requires is almost 2kW. The right top side is the area that the system can generate more than 5kW, which could be stored for later use or used for other

electrical loads. Figure 6.5(b) shows the power generated map for MFM=0.8 and Figure 6.5(c) shows the differences in how much power can be generated between turbines with 1 MFM and 0.7 MFM. It can be found that as turbines become larger, they can generate more power than smaller turbines in the same engine operating point when the engine works in high load condition. In high load condition, engine needs the compressor to deliver more air; meanwhile, more exhaust energy is produced, a bigger turbine can generate more energy under a high efficiency circumstance. However, smaller turbines will suffer a high speed and high backpressure but generated less power. In low load condition, exhaust energy is not enough to allow bigger turbine works in high efficiency region, less power eight in this region, inversely, smaller turbines can get more energy and works in higher efficiency at those operating points. These characteristics will impact the vehicle fuel economy in different driving cycles and how should the engine be matched with the DET.

In this thesis, the limitations of electric motor and generator have not been considered, however, from Figure 6.5(a) and Figure 6.5(b), the power that compressor needed can be up to 15kW, in order to supply enough boost in high speed and load region, which is a challenge for current electric devices.

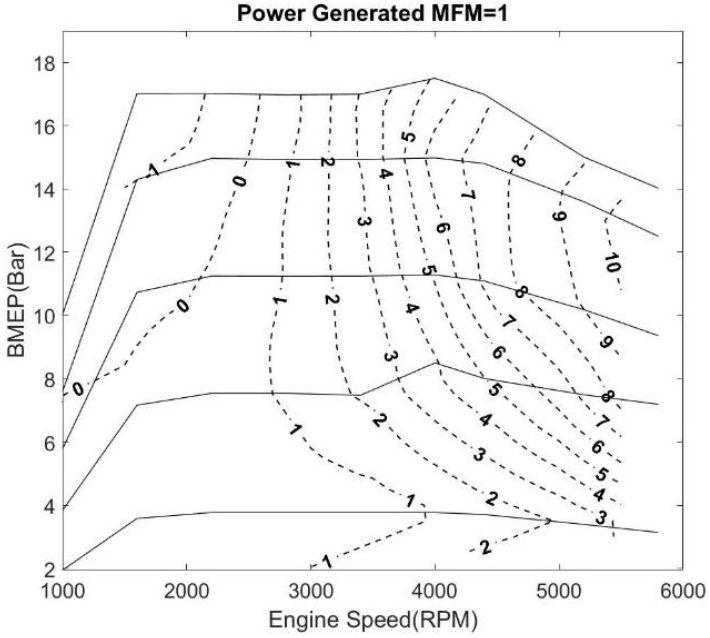

(a)

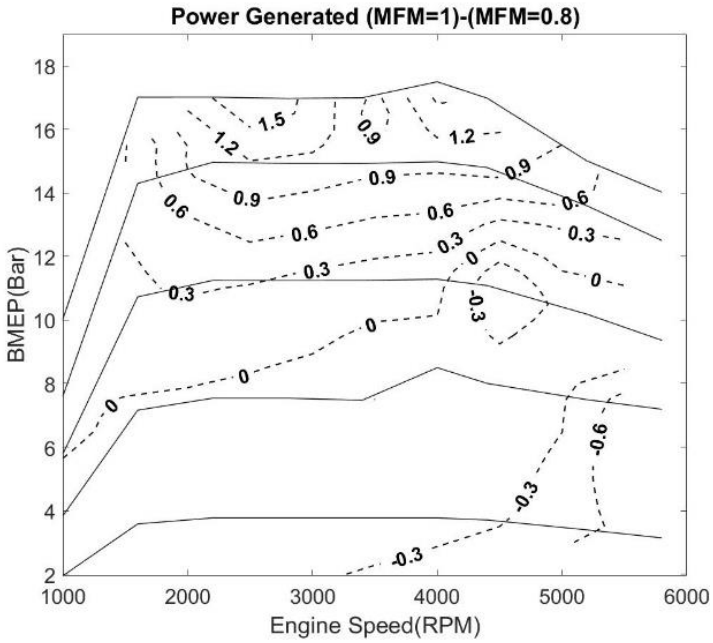

(b)

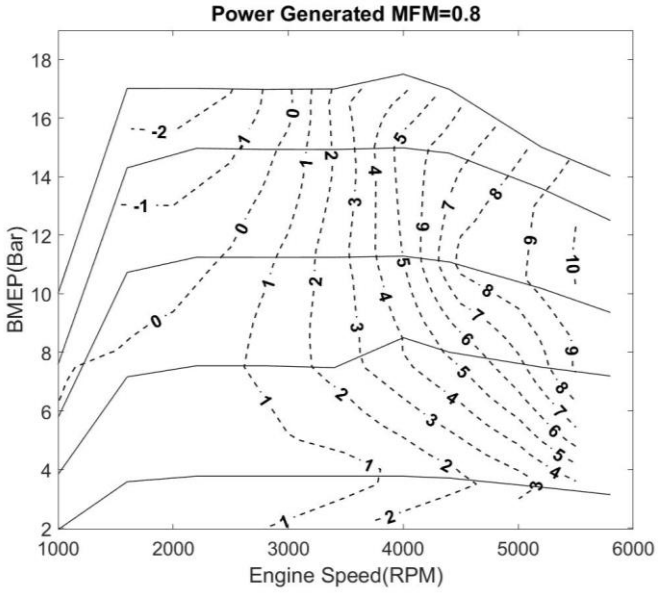

(c)

Figure 6.5 Electric Turbocharger Power map (a) MFM=1; (b) Power difference contour map; (c) MFM=0.8.

6.2 Power Generating ability in real driving cycles

The simulated driving cycles have been introduced in Chapter 4; different drive cycle will have different engine load, speed requirements (Figure 6.6). Those cycle maps can be used to interrogate the efficiency maps such as that illustrated in Figure 6.5.

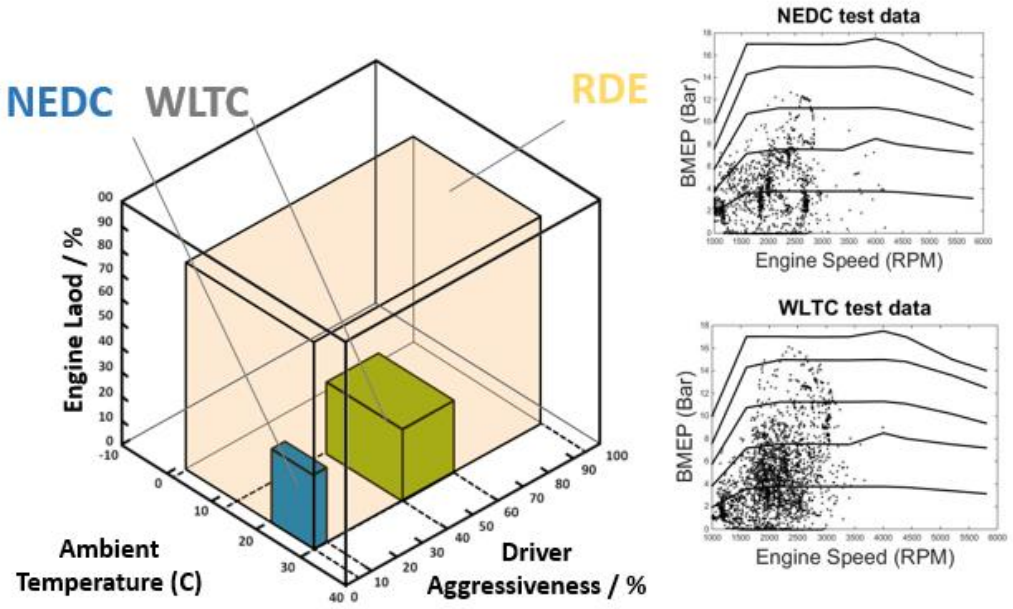

Figure 6.6 Different driving scenarios situation(adapted from (Burke et al., 2019)).

Thirteen different driving cycle tests have been discussed including NEDC, WLTC standard driving cycles and eight real road driving tests with different routes. The measurement comparing here is the average power generated in the system for the whole driving period. Figure 6.7 shows the power generation condition in different driving cycles, and the result shows that decoupled electric turbocharger can generate up to 0.38kW average power in the whole on-road cycle No.6 when MFM=1. In NEDC and WLTC cycle, the e-turbo system can always generate energy and store it into the battery (0.21kW and 0.23kW average power respectively). However, in cycle No.1, the energy consumption of the compressor exceeds that of the turbine due to significant running in the low speed/high torque region (this results in an average negative power of -0.04kW).

For most of the duty cycles, the net power is positive. The power generated increases by increasing the turbine mass flow multiplier at the beginning but then decreases; the

reason is that a smaller turbine can have better power generating ability comparing with the bigger one. However, if the turbine size is too small, it will lead to unacceptable backpressure and limit the exhaust mass flow rate which will make it harder to generate enough power. Also, if the turbine is too big, it will have low efficiency in low engine speed conditions, the energy generated in this condition will be much less. NEDC cycle is particular here, the power decreases as the turbine size increases. The reason is that in NEDC cycle, most operating points lay in the low speed/medium load region and only several points are in of region. A smaller turbine will suit this situation better. From Table 4.3, all the on-road cycles are tested by three different drivers with different average speed. Figure 6.7 shows that the driving behaviour of different drivers and average driving speed will significantly affect how well the e-turbo benefits the full system efficiency. Cycles No.1 and No.2 are tested by Driver A who prefers driving in low engine speed with small vehicle gear ratio: from figure 8a, this means less energy is generated. Drivers who prefer driving in higher engine speed with a higher gear ratio can make e-turbo generate more power during driving time. In cycles No.5 to 7 which were tested by driver C has different average speed, higher vehicle average speed lead to a higher power generating results.

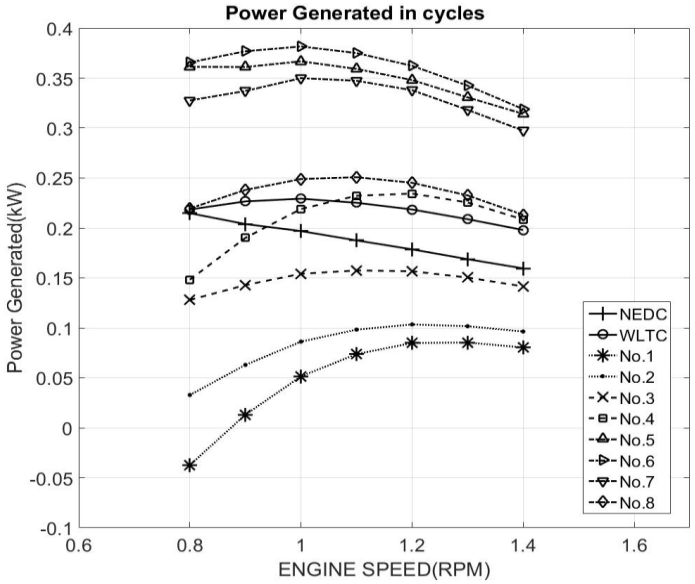

Figure 6.7 Power generated per km over various drive cycles for different size turbines.

For most of the duty cycles, the net power is positive. The power generated increases by increasing the turbine mass flow multiplier at the beginning but then will decrease if turbine is too big, the reason is that smaller turbine can have better power generating

ability comparing with bigger turbine, however, if its size is too small, it will lead to an unacceptable backpressure and limit the exhaust mass flow rate which will make it harder to generate enough power. Also, if the turbine is too big, it will have low efficiency in low speed condition, the energy generated in this condition will be much less. NEDC cycle is special here, the power decreases as the turbine size increases. The reason is that in NEDC cycle, most operating points lay in the low speed medium load region and only several points are in high speed region, a smaller turbine can suit with this situation better. From table 3.3, all the on-road cycles are tested by three different drivers with different average speed. Figure 4.8 shows that the driving behaviour of different drivers and average driving speed will significantly affect how well the e-turbo benefits the full system efficiency. Cycles No.1 and No.2 are tested by Driver A who prefers driving in low engine speed with small vehicle gear ratio: from figure 8a, this means less energy is generated. Drivers who prefer driving in higher engine speed with a higher gear ratio can make e-turbo generate more power during driving time. In cycles No.5 to 7 which were tested by driver C has different average speed, higher vehicle average speed lead to a higher power generating results, because engine needs to burn more fuel in higher to allow a vehicle with higher speed, exhaust energy increased which makes turbine generates more power.

6.3 Electric efficiency and gear ratio sensitivity in steady state condition

The results in Figure 6.7 are presented based on standard assumptions of electrical efficiency. The simulations were repeated with a range of electrical efficiencies for the WLTC and NEDC.

Turbine power generated in WLTC and NEDC is shown in Figure 6.8. For WLTC and NEDC cycle, every 3% efficiency drop in each electric device will lead to about 0.02kw power losses. Bigger turbine has smaller losses, about 0.01kW for WLTC and 0.02kW for NEDC when MFM is 1.4. Because in WLTC cycle, the engine mainly operates in medium speed and load region, which helps the turbine to generate more power. A small increase in turbine size can get a higher power output.

In contrast, in the NEDC cycle, the engine operates mainly in the low speed region. Table 6.1 shows the system efficiency with different electric efficiency in NEDC and WLTC. System with larger turbine will have a higher total efficiency and cost less fuel; smaller turbine can help to generate more energy however cost more fuel which leads to a lower total efficiency (even lower than baseline engine efficiency). For different size of the turbine, the result shows that the bigger turbine has a better benefit to engine fuel economy and energy saving. However, the bigger turbine will have a bad performance in a low speed region. Comparing with baseline engine fuel consumption and efficiency, when MFM is less than 1.1, the fuel consumption of e-turbo system more than baseline engine, when electric system efficiency (except battery efficiency which is 80% here) is lower than 72%, the vehicle suffered in lower total efficiency in WLTC.

	Scaling Factor / Data Tag	**0.8**	**1**	**1.4**	**Base Engine**
NEDC	T72C90 (%)	26.25	26.49	26.70	26.22
	T58C72 (%)	26.23	26.35	26.59	
	Fuel Amount(kg)	14	13.84	13.69	13.75
WLTC	T72C90 (%)	28.13	28.45	28.66	28.20
	T58C72 (%)	27.85	28.20	28.47	
	Fuel (kg)	2.19	2.17	2.15	2.16

Table 6.1 System Efficiency under different electric efficiency

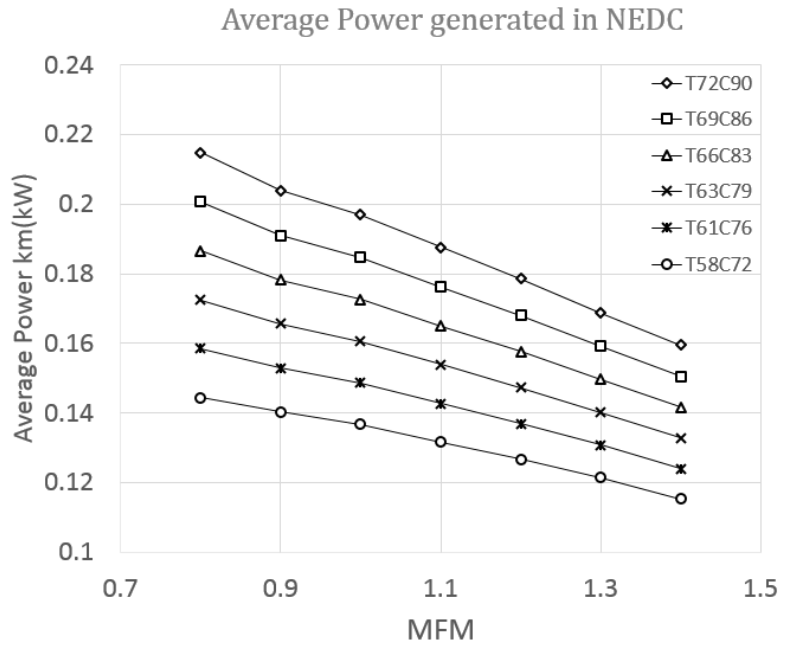

(a)

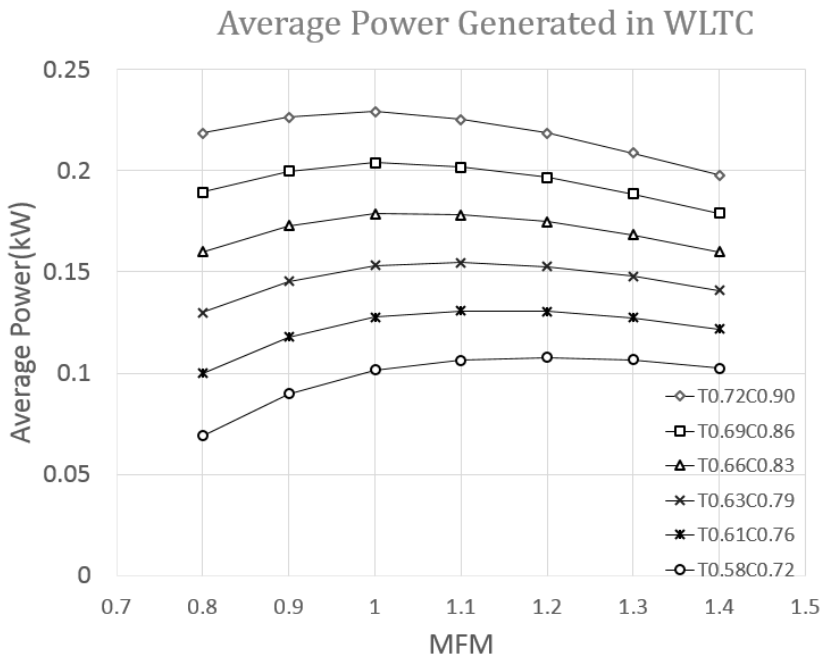

(b)

Figure 6.8 Electric energy harvesting per KM for different size turbines over (a) NEDC and (b) WLTC

The results presented in this paper strongly depend on the engine operating point and are therefore sensitive to vehicle gear ratio. The variation in gear ratio was achieved using a gear ratio factor k_{gear} which adjusted the engine torque and speed. For a target wheel speed, the engine speed will be faster by the increasing of gear ratio factor.

The gear ratio factor can also be interpreted as an engine speed multiplier such that:

$$k_{speed} = \frac{1}{k_{gear}} \quad (1)$$

Figure 4.10 shows the value of electric power that the turbine can generate in NEDC and WLTC with different engine speed multiplier. The increasing of SPM helps to generate more power, which means lower vehicle gear ratio which made the engine operates at a higher speed when the vehicle is running, will make the turbine generate more power. However, the vehicle gear ratio will affect its fuel consumption, peak speed and accelerating ability. Table 6.2 shows the system efficiency of NEDC and WLTC under different engine speed multiplier. In Figure 6.9 a) and b), E-turbo engine with higher gear ratio can achieve a better total efficiency comparing with base engine system, besides, as gear ratio deceased, engine speed decreased. If the gear ratio becomes smaller, more energy can be generated in E-turbo system; however, more fuel is burned, and system efficiency is decreased, when gear ratio is 1.3 times bigger, 3kg and 0.56kg more fuel is burned in NEDC and WLTC respectively, system efficiency is also reduced by 3% and 4% for standard size turbine. In this model, energy losses; the assumed to be the same; however, when gear ratio is smaller, the engine speed is reduced, which can further help reducing engine friction losses and pumping losses.

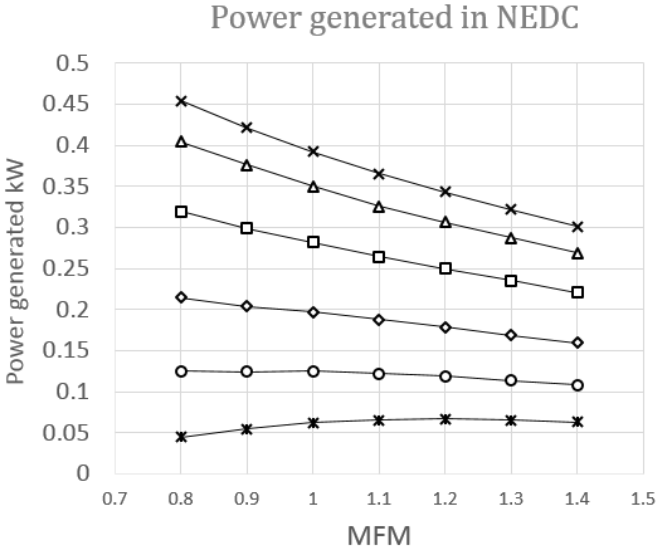

(a)

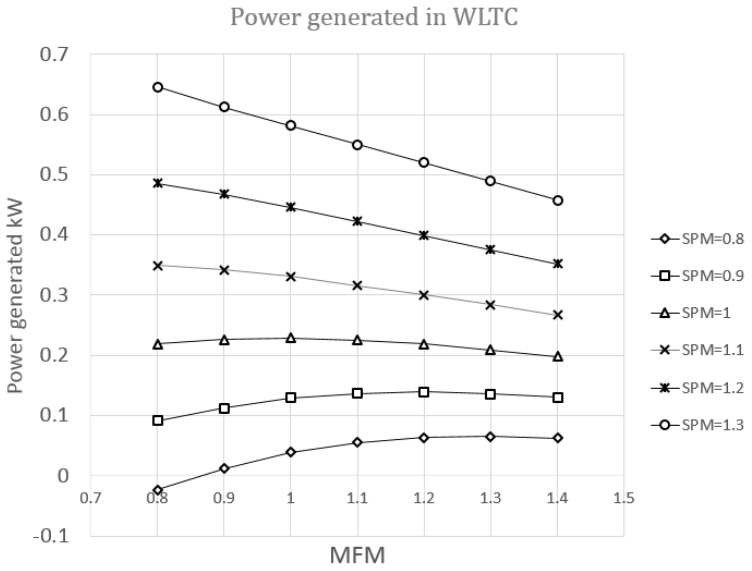

(b)

Figure 6.9 Gear ratio sensitivity (a) NEDC (b) WLTC

	Scaling Factor / Data Tag	0.8	1	1.4
	0.8	27.59%	27.72%	27.83%
NEDC	Fuel Amount	12.11	12.05	12
	1.3	23.69%	24.19%	24.67%
	Fuel Amount	15.34	15.03	14.73
WLTC	0.8	28.94%	29.06%	29.12%
	Fuel Amount	1.934	1.928	1.924
	1.3	25.12%	25.68%	26.21%
	Fuel Amount	2.536	2.482	2.43

Table 6.2 System Efficiency with different engine speed multiplier

6.4 Controlling design for DET in a two-stage situation

The drive cycle study result shows that DET can help to increase the engine's total efficiency and fuel economy. Engines with a smaller turbine will need more fuel but generate more power than engines with a bigger turbine. When the electric system efficiency (including battery, inverter, and power loss in transmission) is lower than 72%, the total efficiency can fall below the baseline engine. From the results above, adding another turbocharger may help to reduce the load of the electric system in this situation. As mentioned above, the two-stage system can make more use of the exhaust

energy, saving electricity and improving the transient response. A DET that is coupled with an upstream-located turbocharger is a very interesting topic, as there may be the potential to obtain extra energy from the exhaust without losing transient performance.

As the engine system has an inlet throttle valve, waste-gate and E-turbine bypass valve, it is possible to optimise the system further by controlling the logic between those valves and DET, to increase the transient and fuel economy further. The configuration of the whole model is shown in Figure 6.10. In order to manage the different controlling jobs efficiently, a Simulink controlling model is coupled with the 1D GT-Power engine model (which is the same as in the previous study). It can adjust the EDC speed by controlling the EDC motor power, adjust the turbine generator torque and control the waste-gate valve, E-turbine bypass valve and throttle valve position.

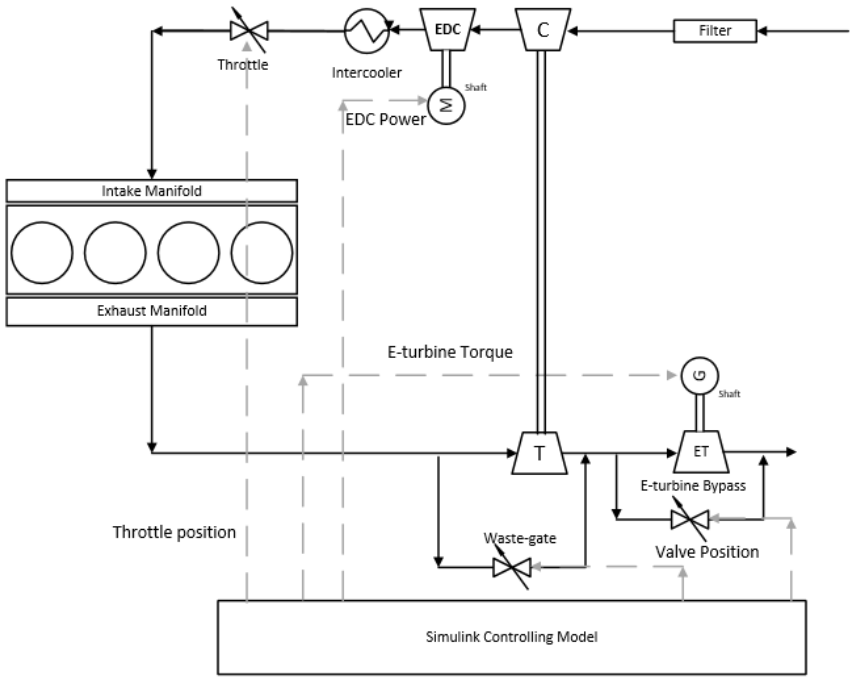

Figure 6.10 Configuration of the DET transient controlling model

The structure of the Simulink model is shown in Figure 6.11. By dealing with the feedforward tables and the PID controllers inside, the system can achieve the target engine torque, BMEP and e-turbine torque (which is set by the user using a certain logic). The Output Judgement here is the controlling method for this system, which tells the system when the EDC and E-turbine should be set at a low load or bypassed.

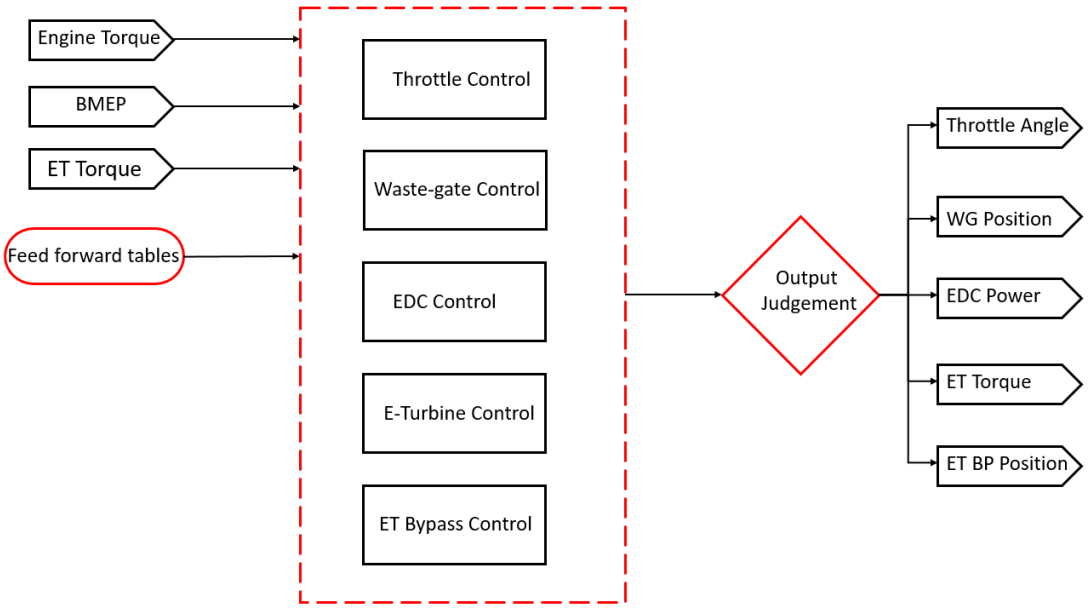

Figure 6.11 Simulink controlling model structure

The model torque and BMEP map were mapped previously by a colleague, and this lies outside the scope of this thesis. In general, the EDC is bypassed in high speed and high load situations and will be fully accelerated in low speed regions during transient. This will lead to a problem: the EDC can actually help to increase the boosting speed, which the turbocharger can do but with a longer response time (the so-called turbo-lag). Some overlap exists between the EDC boosting and turbocharger boosting area on the engine map, which will lead to energy wastage on the EDC side. Re-designing the controlling logic may help the system to achieve higher efficiency without losing transient performance.

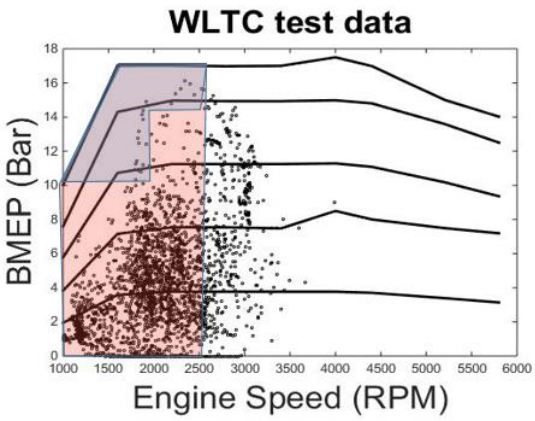

Figure 6.12 The EDC operating region

Figure 6.12 shows an example of how the EDC operates on an engine map. The red area shows the general region where the EDC will be introduced to help to increase the boost and transient speed; the blue area is actually the area where the EDC always needs to be for higher low speed output. The controlling optimisation steps for the EDC and related components are shown below:

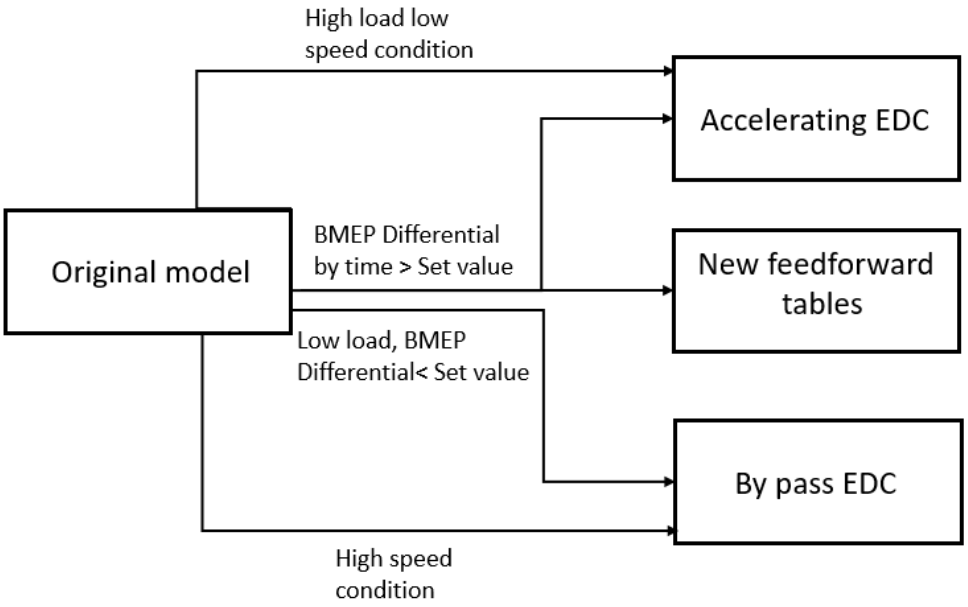

Figure 6.13 Optimised controlling logic for the EDC and other components

The EDC will be used in the low speed high load region (the blue area shown in Figure 6.12), to increase the low speed peak output; it will also be used at a low speed low load when the turbocharger response is too slow, as the EDC can cover this 'transient lack' through acceleration. However, unlike with the general controlling method, when the difference between the actual BMEP and the target BMEP shrinks and the BMEP differential by time becomes lower, the turbocharger can boost the system without much lag, The EDC then will be bypassed and decelerated. In this way, the electricity cost for the EDC will be reduced. Also, when the controllers are running in this mode, the feedforward tables for those controllers (shown in Figure 6.11) need to be adjusted based on the step load transient simulations (which are not explained repeatedly, since the step load transient performance of the EDC was explained in the previous chapter), to help the system to respond faster. Figure 6.14 shows the response of two different controlling models for the WLTC cycle. There is some over-controlling during the period from 1500 to 1800s, due to the fact that the set value of the PID gains is slightly

higher for the EDC. This can be regarded as noise, as the EDC always has an upper limit power which will slow down its peak transient speed.

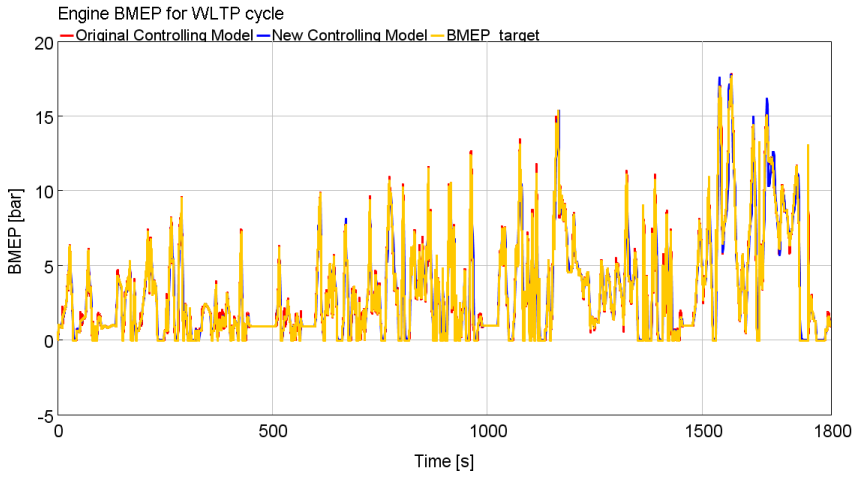

Figure 6.14 BMEP results for the WLTC cycle under different controlling models

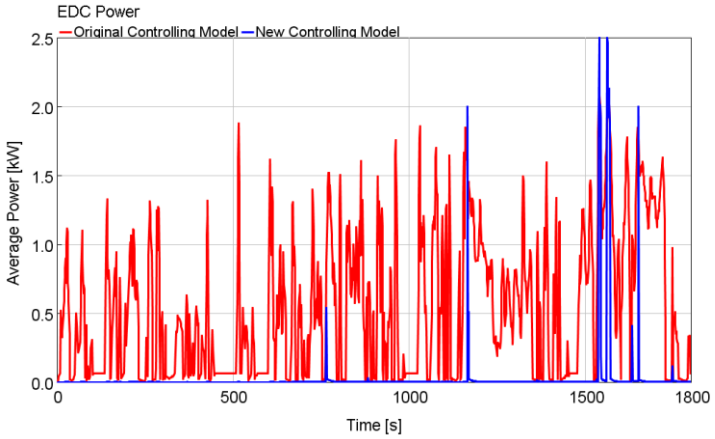

(a)

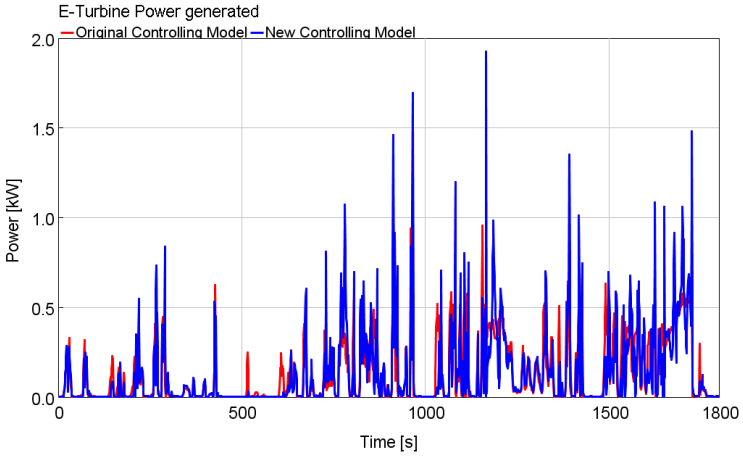

(b)

Figure 6.15 (a) EDC power consumed. (b) E-Turbine power generated.

Figure 6.15 shows the EDC power and E-Turbine power. It can be seen that, compared with the original model, the EDC is no longer used most of the time, and is involved for the period from 1500 to 1800s, in which the BMEP target is quite high and the transient needed quite fast. The E-Turbine power generated also changes, due to the feedforward table changing the throttle and bypass valve. Figure 6.16 shows the accumulated energy from DET for both the original controlling model and the new controlling model. It can be seen that the E-Turbine energy generated remains similar (changing from 237 kJ to 244 kJ), while the EDC energy consumed changes considerably (dropping from 954.37 kJ to 47.22 kJ). It should be noted that the power transmitting losses were not considered here in the electric systems.

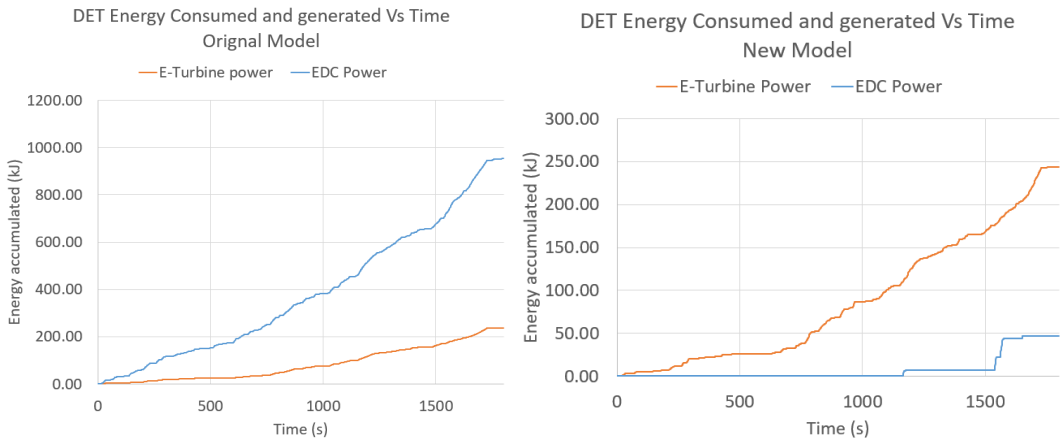

(a) (b)

Figure 6.16 DET energy consumed and generated by the EDC and E-Turbine (a) Original Model (b) New Model

The final drive ratio's (the whole ratio of the vehicle's) effects on this two-stage DET system has also been investigated. By adding a simplified vehicle driveline model to the Simulink part, we simulate the gear ratio switching process for the 0-100 km/h process, so that the transient response and DET power change can be observed.

A multiplier factor has been applied on both the engine speed and BMEP:

$$R_{actual} = R_{original} * (1 + FDR)$$

$$BMEP_{actual} = \frac{BMEP_{original}}{1 + FDR}$$

The FDR value is the final drive ratio multiplier, changed from -7.5% to 7.5%.

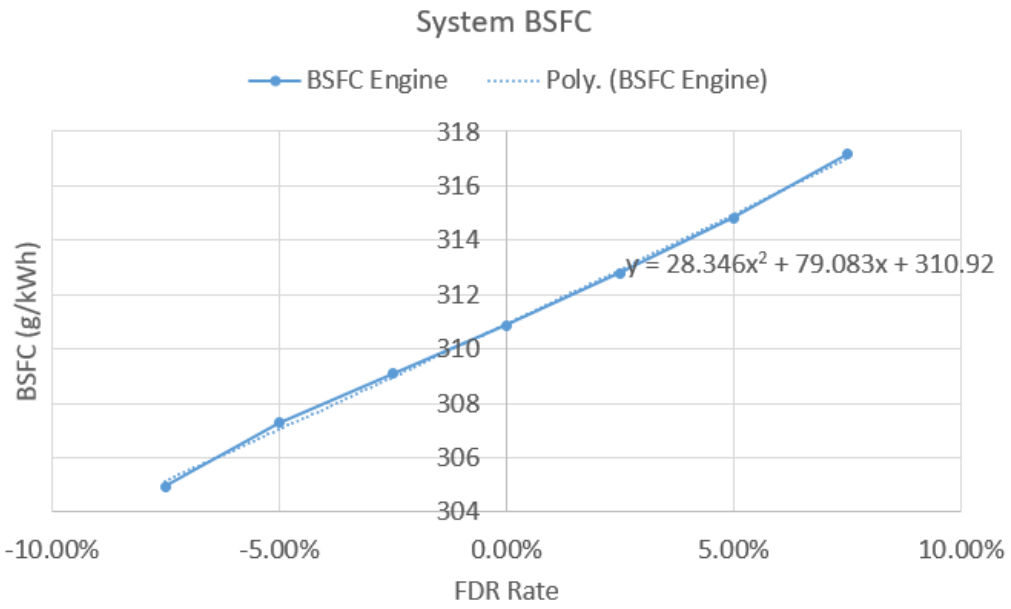

(a)

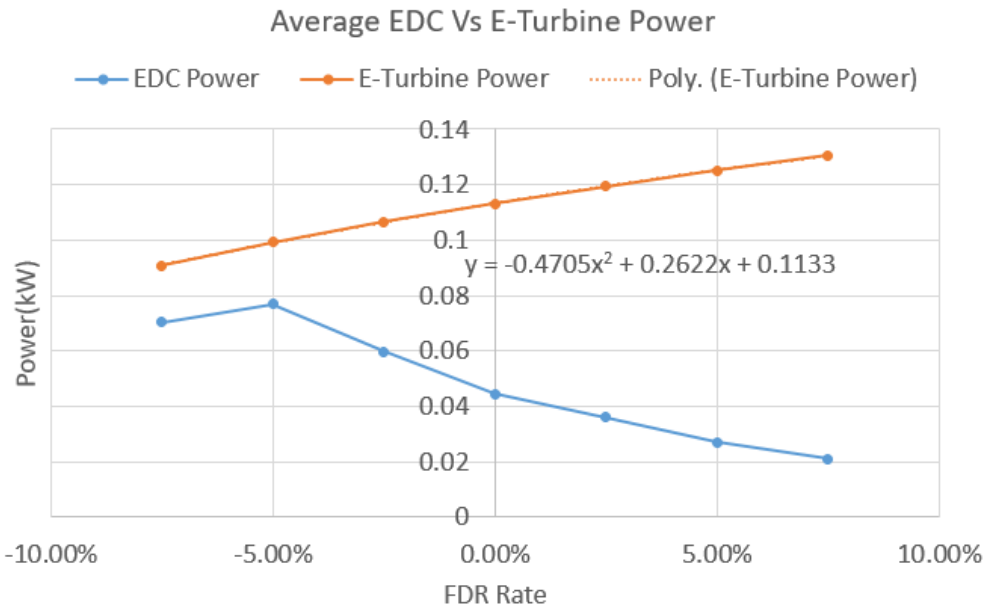

(a)

Figure 6.17 (a) System BSFC (b) DET average power

Figure 6.17 shows the engine's BSFC and DET average power change by FDR rate. Clearly, as the FDR increases, the DET system can generate more power (more power on the E-Turbine side and less power on the EDC side); however, the system's BSFC also increases, so there is a compromise in this phase. If the energy from the DET is added to the whole system's energy consumption (fuel energy + DET energy), the equivalent BSFC for the whole system can be calculated (the result is shown in Figure

6.18). The energy from the DET side is calculated without considering the electrical system's efficiency, which reduces the reliability of this result, but the trade-off is still interesting since, as the FDR increases, the whole system becomes less efficient.

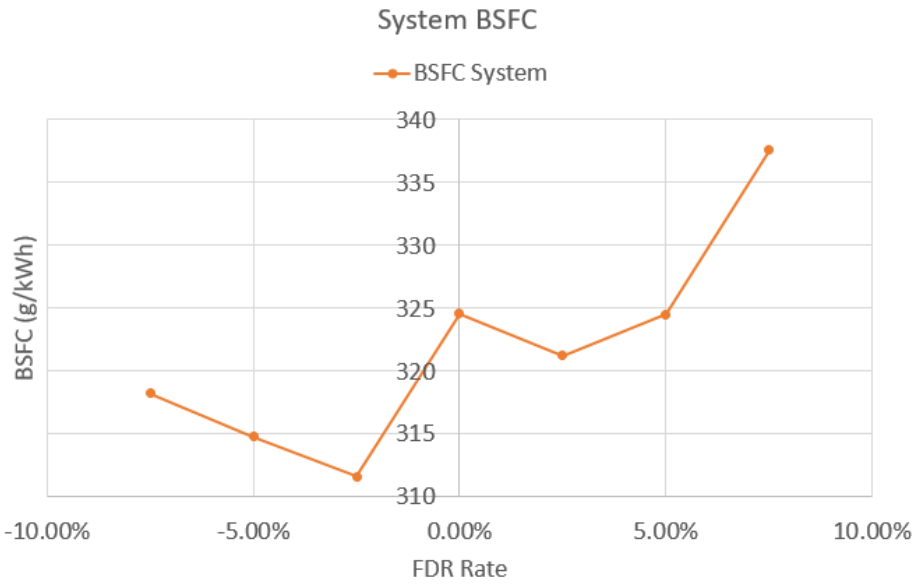

Figure 6.18 System equivalent BSFC

The 0-100km/h transient acceleration results are plotted in Figure 6.19 (a), the gear ratio changing situation is shown in Figure 6.19 (b). The vehicle starts accelerating at 3s, reaching 100 km/h at 7.38s to 8.26s.

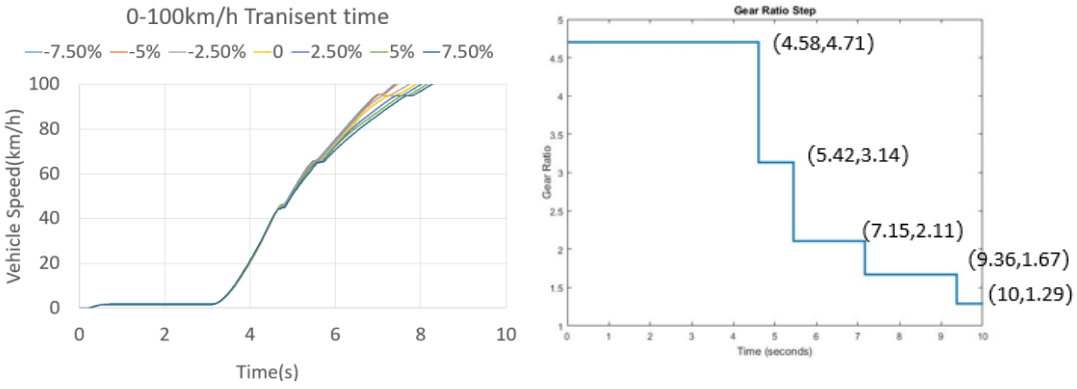

Figure 6.19 (a) 0-100km/h acceleration results (b) Gear ratio situation

6.5 Summary

The previous study in the last chapter demonstrated how an electrically-driven compressor (EDC) could help to increase the system's transient performance and low speed output. The 1D simulations carried out in this chapter focused on the

performance of the DET engine system in both the single-stage and two-stage situation, which is an EDC with an extra electric turbine, harvesting the energy in the exhaust.

The study considered both steady state behaviour and transient drive cycle performance based on this gasoline engine model using GT-Power. In steady state simulations, the influence of the transient operating process is simplified into quantities of steady state duration, which helps to evaluate the E-turbo performance under various driving scenarios. The turbine diameter varied from 58mm to 78mm (representing 50-150% of the baseline turbine size), and the electric turbocharger achieved a maximum of 1.5% improvement in system efficiency. A series of mean value engine models were created for different sized turbines to predict the BMEP, turbine power generation and overall system efficiency – these were then used to evaluate performance over different duty cycles. The mechanically-decoupled electric turbocharger can generate up to 0.38kW average power in an RDE simulation which can significantly increase the engine fuel economy. In the NEDC and WLTC cycles, the e-turbo system can always generate energy and store it in a battery (0.21kW and 0.23kW average power over the whole cycle, respectively). In several real road driving tests, the energy consumption of the compressor exceeds that of the turbine due to significant running in the low speed/high torque region (0.04kW in a specific on-road cycle simulation).

In a transient study, the DET was mounted together with a single turbocharger. The feedforward control of the system has been optimised to produce better transient performance. The controlling logic for the EDC and E-turbine has been redesigned, and a remarkable electricity benefit has been achieved. For the whole WLTC cycle, the E-turbine energy generated changed from 237 kJ to 244 kJ; the EDC energy consumed underwent a big difference, dropping from 954.37 kJ to 47.22 kJ. This model has been applied to the 0-100 km/h acceleration process, in order to investigate the effects of different final drive ratios on the system's efficiency on the BSFC side. It can be observed that, by increasing final drive ratio, 01-100km/h accelerating speed and the electricity generated by the DET system will increase; however, the engine's BSFC became worse.

Chapter 7 – Inner-insulated turbocharger turbine research

Inner-insulated turbocharger is one of the latest techniques applied on turbochargers, trying to achieve 'T4 enhancement' (Get exhaust gas warm and keep it warm). This chapter studied the insulated turbocharger performance in both simulation and experiment side, comparing it with the standard turbocharger that has the same internal turbine wheel design.

The structure of insulated turbocharger will be briefly introduced, coming with the 3D and 1D modelling for this device. The turbocharger is designed by BorgWarner, which are not the work of this thesis. The author will use 1D modelling method to embed the heat transfer effects into the 1D turbocharger model, simulate the steady state and transient thermal effects of the insulated turbine. This model is mainly for validating the 3D modelling results from BorgWarner, and the further experiment results in the second section.

The insulated turbocharger will be tested on the engine gas stand test rig introduced in Chapter 3. The same tests will also be done for standard turbocharger, for achieving back to back comparison. The two turbochargers will be compared under steady state, transient condition, including thermal shock, engine warm-up, and cold and warm start WLTC cycle.

Work in this chapter has been published in: Burke, R., Liu, Y., Vijayakumar, R., Werner, J. and Dalby, J., 2019. Inner-Insulated Turbocharger Technology to Reduce Emissions and Fuel Consumption from Modern Engines (No. 2019-24-0184). SAE Technical Paper.

7.1 Validation of the inner-insulated turbocharger.

This section (Burke et al., 2019) (External resources) is not the original output of this thesis but has to be here to be the fundamental resources for the research in this thesis.The design and the model of the inner insulated turbocharger has been introduced in Chapter 4 section 3. The standard turbocharger and insulated turbocharger has been mapped on a steady state gas stand test rig.

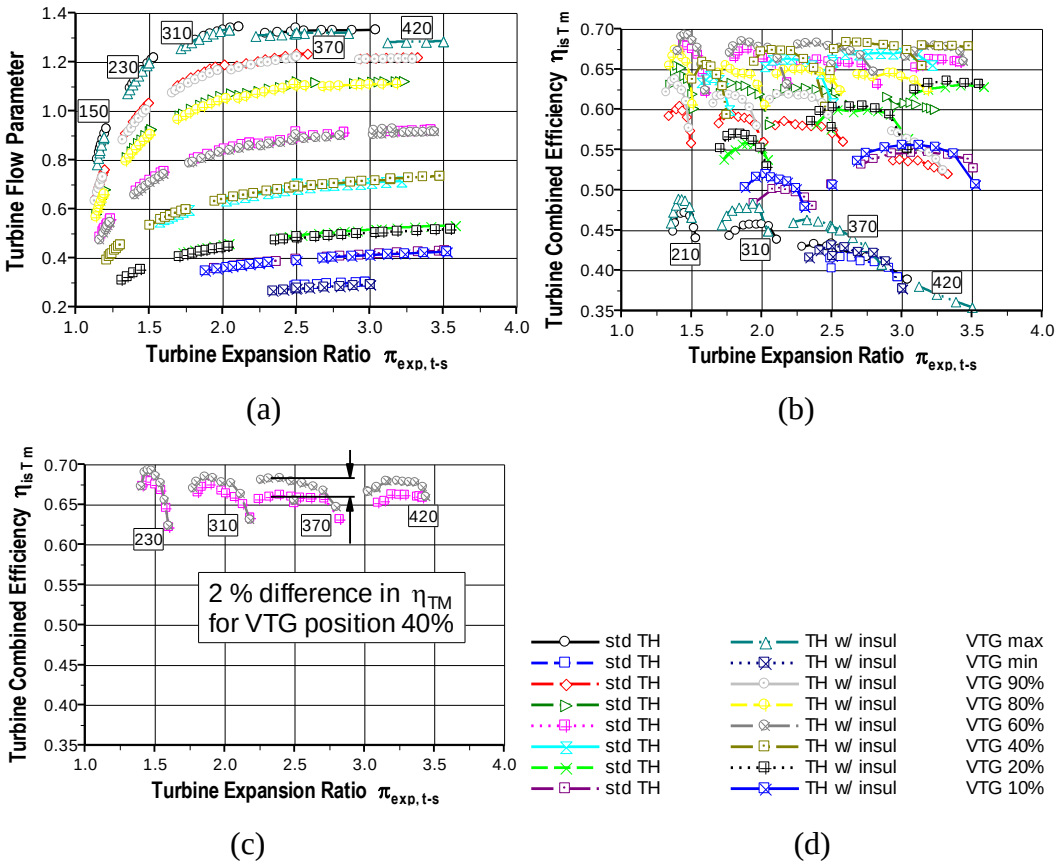

Figure 7.1 Turbine mapping results for two turbochargers (a) Turbine flow capacity map, (b) Efficiency map, (c) Efficiency for 40% position. (d) Plot legends layout.

Figure 7.1(a) shows the turbine flow characteristics over the turbine expansion ratio and mass flow parameter under different VGT position. The numbers in the diagrams indicate the circumferential speed in m/s for the turbine wheel for a maximally opened VTG and are the same for the other curves below in the diagram. Figure 7.1(b) shows the calculated turbine efficiencies for both turbochargers, again compared for the same speeds and VTG positions. For lower speeds such as 210 m/s, the values for the isentropic turbine efficiency is too high due to an over-estimation of the compressor

power based on heat fluxes. When analysing these results more in detail for VTG position where the vanes are opened 40%, there is a small improvement in the combined turbine efficiency of ~ 2% for the inner-insulation visible, this is shown in Figure 7.1(c).

The turbine efficiency is the combined value for isentropic and mechanical efficiency. Since for this measurement, a different bearing housing was applied (two different turbocharger samples) the difference could be explained by mechanical differences between both turbocharger compared here. On the other hand, the inner-insulated turbine housing has a surface with different roughness values that may have influenced the isentropic efficiency. The measurements would need to be repeated again with additional samples to prove this benefit and confirm that this benefit lays not within the confidence interval for hot gas stand measurements. For the purpose of study, it can be confirmed that there is negligible difference in aerodynamic performance between the two turbochargers.

Figure 7.2 reveals the assumptions used for the CAE models. The heat loss of the flow is in equilibrium with the energy stored in the housing structure, together with the heat flow to ambient. The uni-directional coupling used here neglects the temperature decrease of the flow due to the heat loss along its flow path and their impact onto the mechanical power of the turbine. Thus the heat loss of the system will be slightly higher predicted than in reality. Nevertheless, the accumulated heat loss represents the T4 temperature reduction compared to the adiabatic predicted T4 temperatures which are determined by adiabatic CFD simulations. The T4 enhancement potential of the inner-insulated T/H design is carried out relatively by comparing its heat loss to the heat loss of the reference T/H what is expressed in Figure 7.2(b). The difference in heat loss is a direct measure of the T4 enhancement carried out for this particular 3D computer aided design (CAD) design concept.

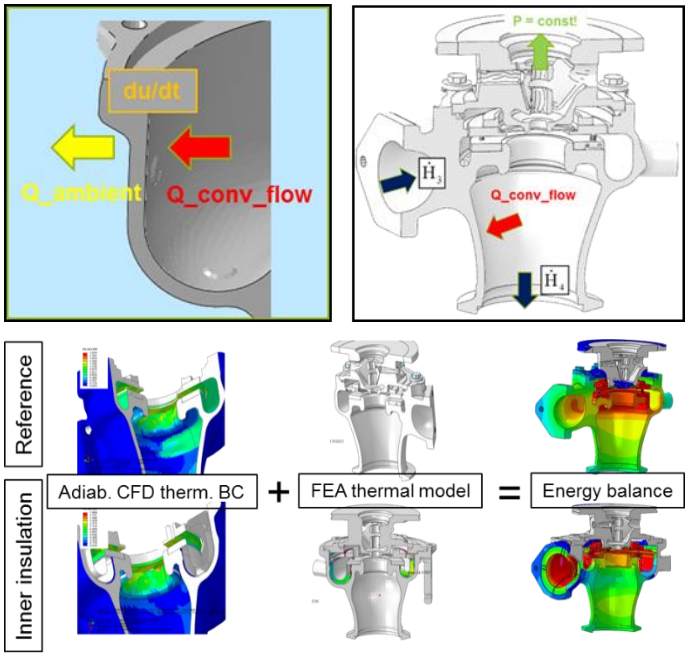

Figure 7.2 Heat balance approach

The overall objective of this work is to quantify the benefits of the inner-insulated turbocharger within the 1.6L diesel engine system with 48V mild hybrid boosting system, incorporating an electrically heated catalyst system. The system benefits will be quantified through an optimization exercise based on both systems-level simulation of the powertrain and related experiments. This is achieved by comparing the performance of powertrain using the standard turbocharger compared to the inner-insulated prototype. To capture the performance of the inner-insulated turbocharger, a 1D lumped capacitance model of the turbocharger is created which stimulates the reduced heat losses compared to a conventional turbocharger. The modelling methodology is shown in Figure 7.3.

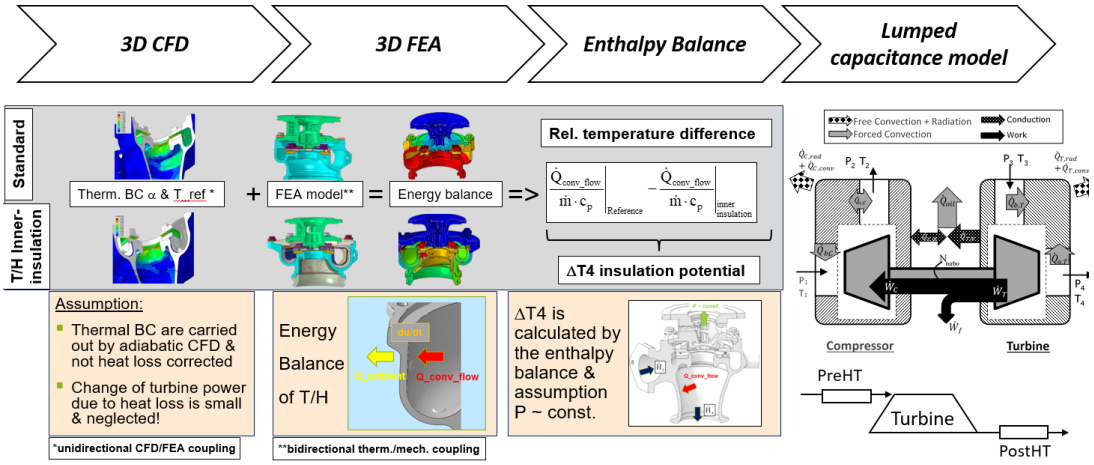

Figure 7.3 CAE method for the research

7.2 Insulated turbocharger modelling and experiment design

To make the comparison more precise, the insulated turbocharger and non-insulated turbocharger will use the same turbine wheel with shaft and compressor, the only change is the turbine housing, which will be installed or uninstalled on the turbine wheel depends on the experiment requirement.

7.2.1 Steady state tests

For steady state verification tests, the methodology is shown below:

1. Ignore the engine operating state, as the test is performed on the engine-gas stand rig, so the engine is regarded as a flow source to the turbine.
2. The insulated turbo is firstly tested, by operating the turbine VGT position, compressor backpressure valve, engine speed, engine throttle and boost rig pressure/temperature, to cover the general flow and torque region for the 1.6L diesel engine with this turbo (including matching the turbo speed, turbine pressure ratio, turbine mass flow rate, and turbine inlet temperature). (2 series of low BMEP tests and 1 High BMEP Test)

3. A back-to-back comparison is conducted using the same compressor wheel/brating housing with only the turbine housing being switched (rather than the complete turbocharger)
4. All of the turbine boundary conditions are matched: turbine speed, turbine VGT, turbine inlet temp, and turbine pressure ratio and turbine mass flow rate

The parameter that is evaluated is the turbine outlet temperature, to ensure that the turbine is operated under the same conditions for the tests of both the insulated and non-insulated turbochargers.

7.2.2 Transient test

In this part, three different groups of transient tests will be done in order to see how insulated turbocharger performs in different transient process.

Firstly, engine warm up process will be performed on the test rig, the engine stays in ambient environment, will start warm up at 1500 RPM, 100 Nm torque, the whole warm up process last 1000s, a back to back comparison will be done between the insulated and non-insulated turbine with the same tests, by swapping the turbine housing.

Secondly, the WLTC cycle will be tested on the rig, under the same start points and controlling method for both two turbos. VGT position in this process is not changed. As the test rig at compressor side is a gas stand, so the design of this test is trying to maintain the boundary conditions for the turbine (Speed, Torque, T3/P3, P4, mass flow), but ignore the working situation of compressor. The same cycle will also be performed on the heat transfer model introduced in the last section.

Thirdly, a simplified RDE (Real road emission) cycles will also be introduced. This test is to help verifying the 3D CAE results generated by the co-operators. Figure 7.4 shows the example of real driving cycles, the period from downhill to uphill has been taken as a targeting cycle (later half shown on the figure). Based on its exhaust temperature and related mass flow rated, it has been simplified to a stage transient cycle which only has 3 step changes and 3 operating points, shown in Figure 7.5.

During the test, the engine will be operated to maintain the turbine boundary conditions the same as the simplified cycle.

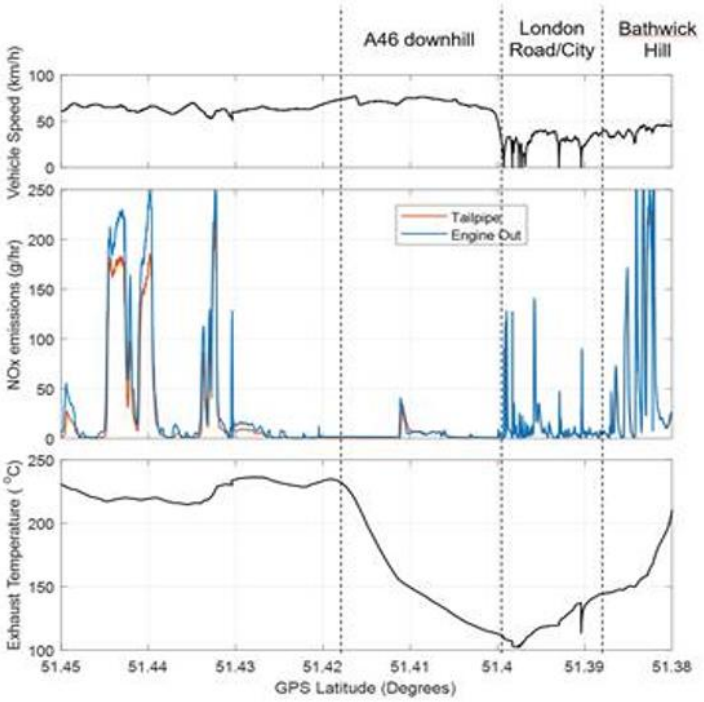

Figure 7.4 Example of real driving scenario

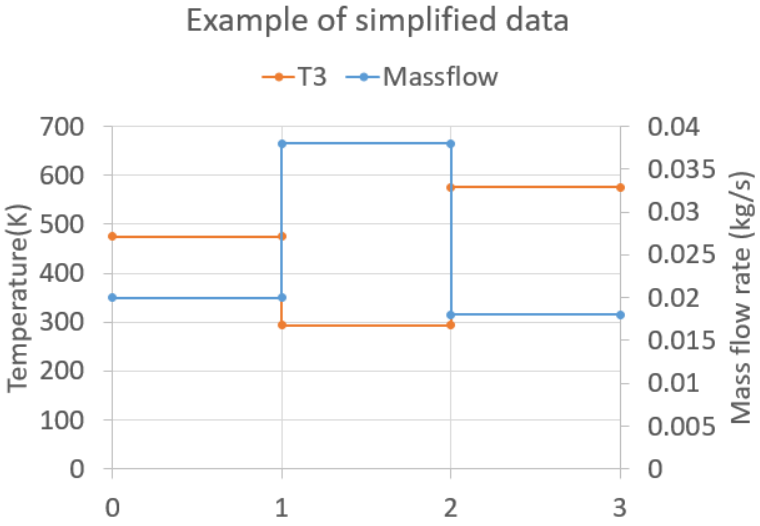

Figure 7.5 Simplified cycle

Transient experiment research for insulated turbocharger is still at very initial state in this area, and this thesis cannot cover every critical research topic for this special devices. However, those simulations and experiment designed above can help people get a straightforward concept of how will insulated turbocharger performs in modern

engine system. At last of this section, a flow chart can be given for the insulated turbocharger research, shown below:

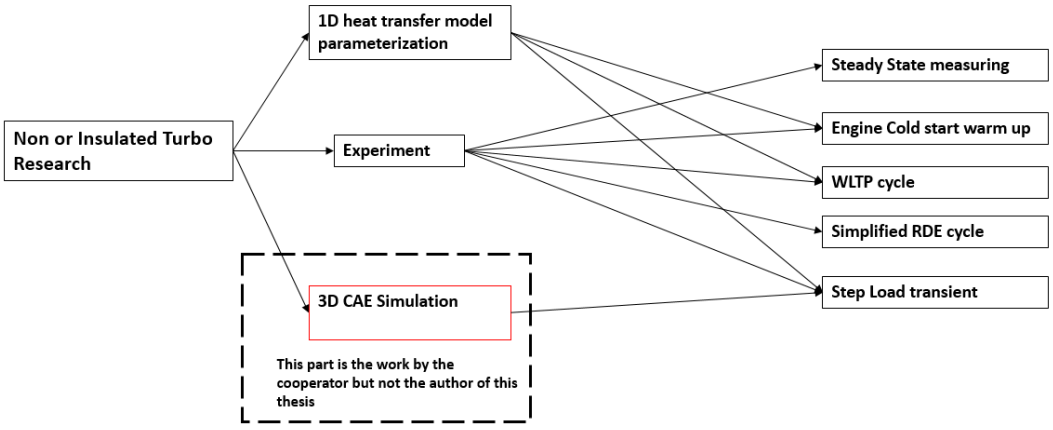

Figure 7.6 Research method flowchart

7.3 Steady-state experimental validation of the insulated turbine

The insulated turbocharger is expected to have reduced heat loss at the same operating points on the turbine map compared with the non-insulated turbo. For similar tested points, this would result in a higher turbine outlet temperature (T4). The testing methodology was introduced based on the engine test rig introduced in Chapter 3.

The test results are shown in Figure 7.7. The boundary condition for the insulated turbine and non-insulated turbines is perfectly matched. Points 1~6 and 7~ 12 aim to simulate the low BMEP condition air path, while points 13~ 17 aim to simulate the high BMEP air path. The T4 result is shown in *Figure* 7.8. A 5-14K T4 benefit is achieved based on the engine flow and load.

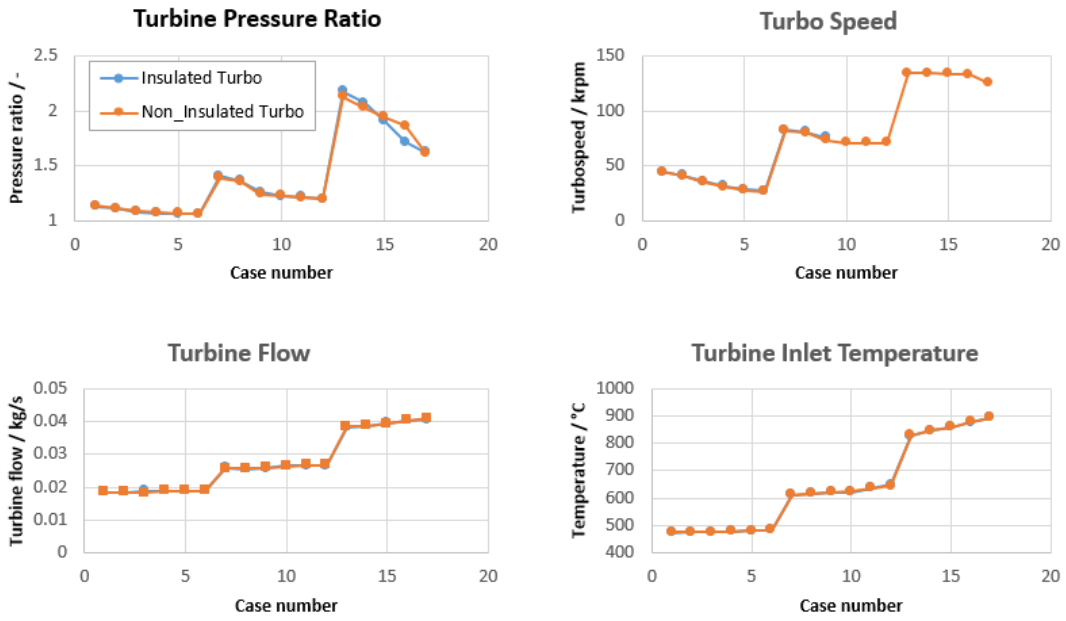

Figure 7.7 Turbine operating points for the steady state tests.

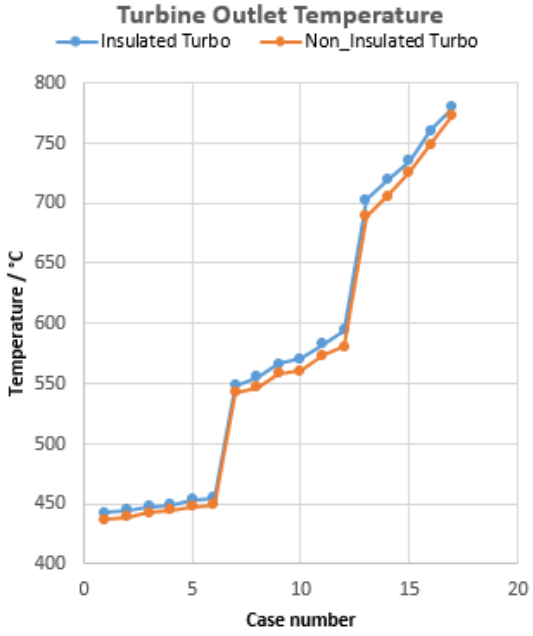

Figure *7.8 Turbine outlet temperature for the two* turbochargers

7.4 Transient study on the insulated turbine

As introduced in Section 1, the transient performance of the insulated turbine is the most important and exciting topic to study in this part, where different transient processes are investigated to demonstrate further the benefits of the insulated turbocharger turbine.

7.4.1 Cold start process study

An engine cold start experiment was conducted on the air path test rig described in Chapter 3. The turbine inlet and outlet temperatures were altered to verify the turbine heat transfer model. The ambient temperature is 298K. The engine was started at 1300rpm, and produced the exhaust conditions of 1.25bar turbine inlet pressure and 300K turbine inlet temperature, then increased to 400K (after stabilising). The thermal transient plot presented in Figure 7.9 shows that 1000s is required for the turbine and exhaust pipe to warm up in this situation.

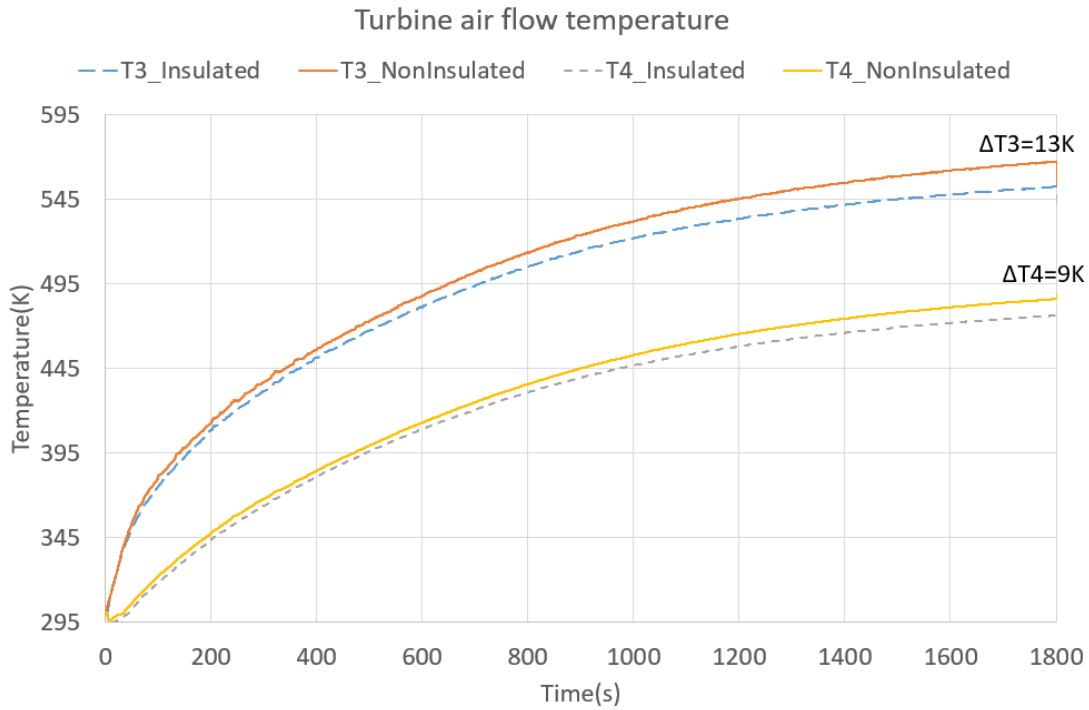

Figure 7.9: Turbine T3 and T4 experiment test results.

It can be seen that the T3 is unmatched for two turbochargers (Figure 7.9), due to the difficulty in controlling the engine exhaust, but the ΔT4 is still smaller than the ΔT3, due to either the benefit of insulation or the difference between the exhaust and ambient temperature. Turning to the simulation, as there is no engine in the turbine-only model (Figure 4.23), several boundary conditions are considered the same, including the turbine speed, turbine pressure ratio, turbine VGT position and exhaust mass flow rate. The data are shown in Table 7.1:

Turbine speed	**Pressure Ratio**	**Turbine VGT position**	**Mass flow rate**
28.2 kRPM	1.25	15% (0.8 in Sim after calib)	0.026 kg/s

Table 7.1 Turbine boundary conditions for standard turbocharger model validation

The turbine inlet and outlet temperature for both the experiment and simulation results are shown in Figure 7.10. The total transient speed and trend are similar, but the change rate is not identical; based on this result, it can be used to predict the thermal performance of the turbine.

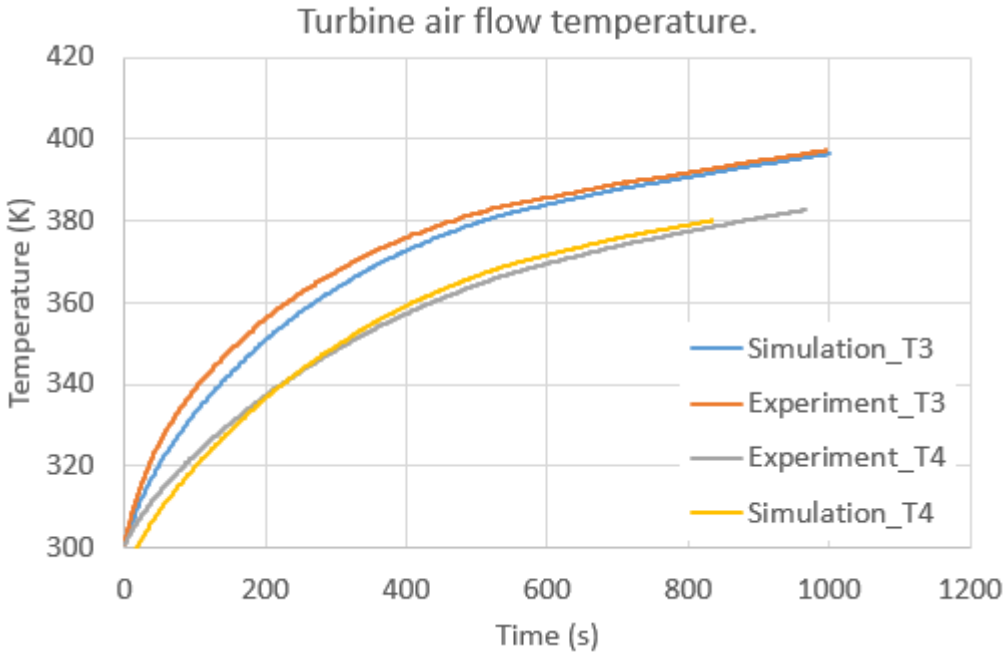

Figure 7.10: Simulated T3 and T4 results under the same boundary conditions.

Following the validation of the baseline turbine heat transfer model, the insulated turbocharger model was used to study further its benefit in the engine cold start situation, compared with the T4 results. Figure 7.11 shows the T3 and T4 temperatures

with the non-insulated turbocharger and the insulated turbocharger. It can be observed that the insulated turbocharger can help to increase the warm-up process: at 1000s, the insulated turbocharger's outlet temperature is 5 degrees higher than that of the non-insulated one.

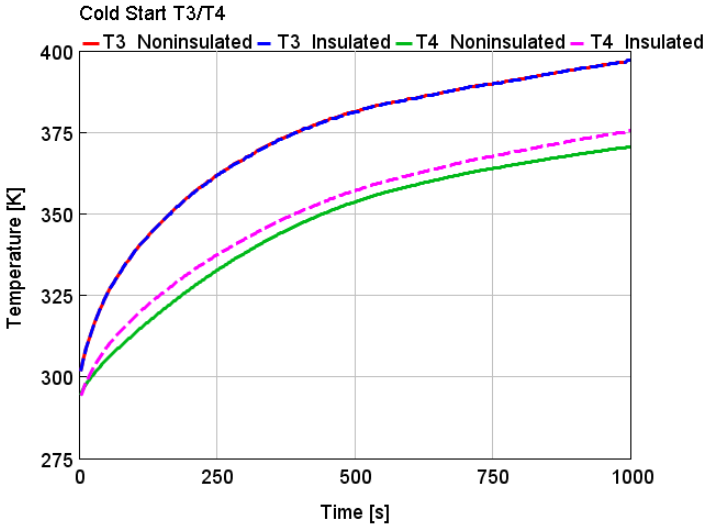

Figure 7.11 T3/T4 simulation results for two turbochargers.

7.4.2 Step load (Thermal Shock) investigation

A step load study is the main method used to obtain the transient thermal performance of the insulated turbocharger. A 3D simulation, 1D calibrated simulation and related experiments are compared. The 3D simulation dataset is regarded as the primary setting for the 1D simulation and experiment boundary conditions.

The 3D simulation was used to simulate a thermal-shock cycle for standard T/H fatigue analysis, as shown in Figure 7.12:

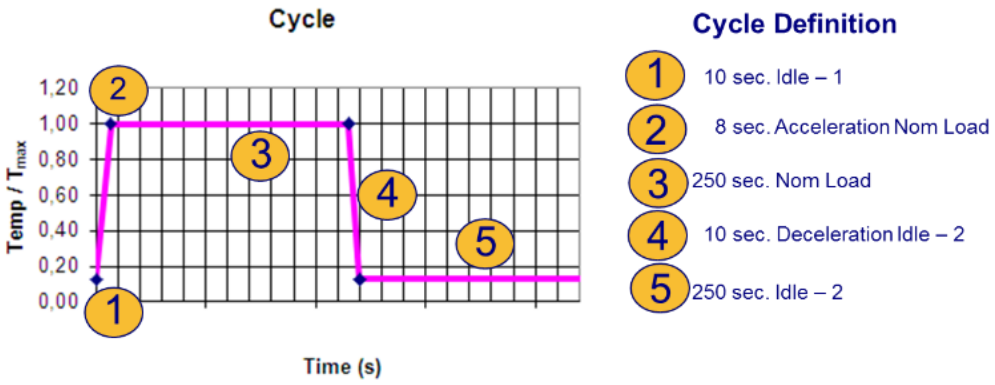

Figure 7.12 Defined transient load cycle

Figure 7.13 reveals the simulated heat fluxes of the hot gas into the volutes over this duty cycle. The inner-insulated turbocharger has reduced the heat flux by 50-70% compared to the standard turbocharger.

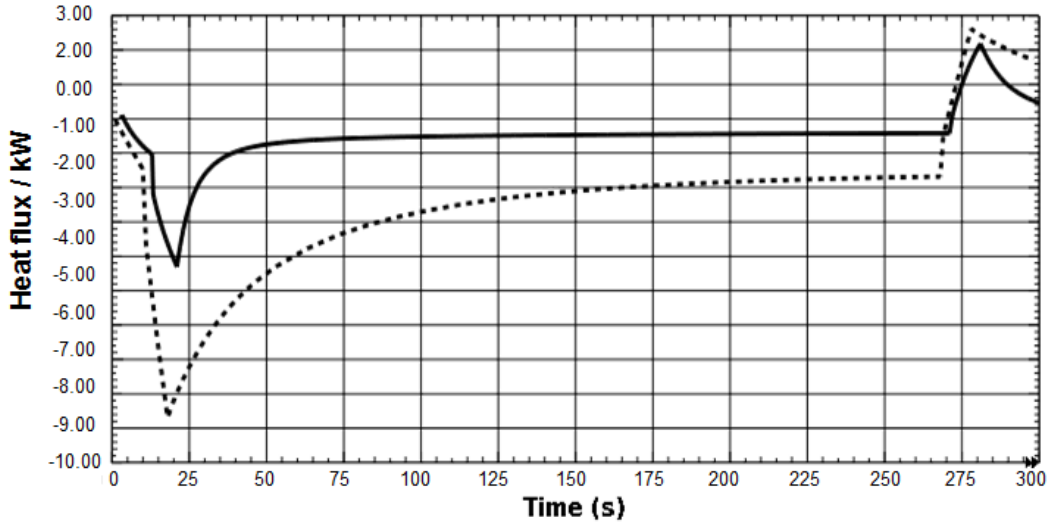

Figure 7.13 Heat fluxes into the volute over the cycle

Figure 7.14 shows the heat fluxes to the ambient, which is only 30% with the inner-insulated turbocharger.

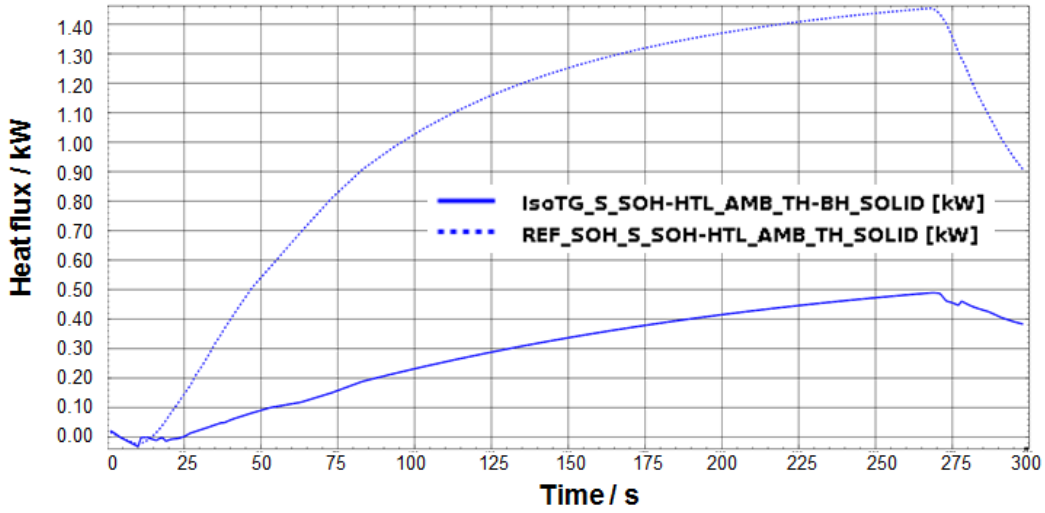

Figure 7.14 Heat flux to the ambient

A similar step load 1D simulation t that shown in Figure 7.12 was undertaking to compare the standard and insulated turbocharger heat fluxes. This 1D model result is shown in Figure 7.15, which has a high correlation with the 3D results. As there is no engine template in the HT model, the gas inlet temperature and pressure (which should be the engine outlet temperature and pressure) are set to be a step profile. Unlike the

3D simulation, every single component is not individually analysed but only the heat loss for the whole system is evaluated.

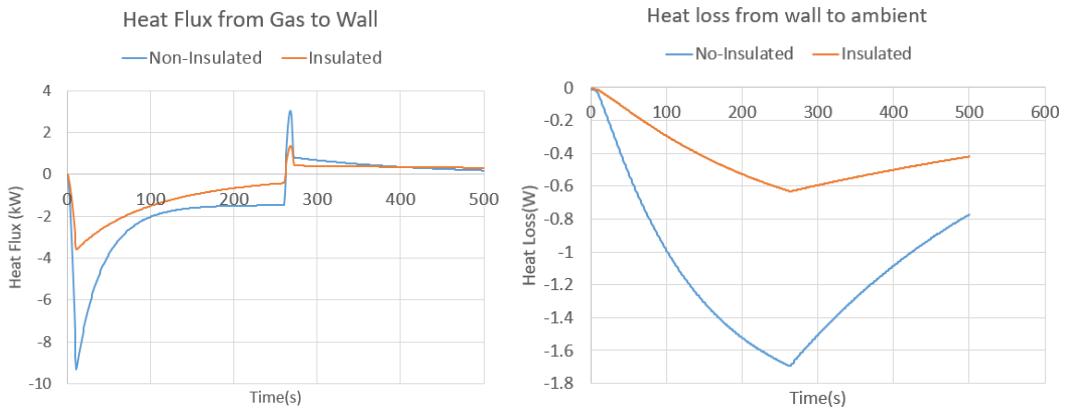

(a) (b)

Figure 7.15 (a) Heat flux from the exhaust gas to the turbine housing wall. (b) Heat loss from the turbine housing to the ambient.

Figure 7.15 shows the heat flux from the gas to the turbine housing and from the turbine housing to the ambient, respectively. The heat flux from the gas to the turbine housing can be well-simulated, but the heat loss from the wall to the ambient is imprecise in this case, as there exists an air gap between the two metal layers in the insulated turbocharger, so adding a heat transfer multiplier based on a non-insulated turbocharger cannot perfectly simulate the second convection between the air gap and the two walls. However, as this model can predict the heat flux coming into and out of the gas well, it can be used to evaluate T4. Further differences can be observed in Figure 7.16, which shows the T4 temperature of the gas and turbine housing.

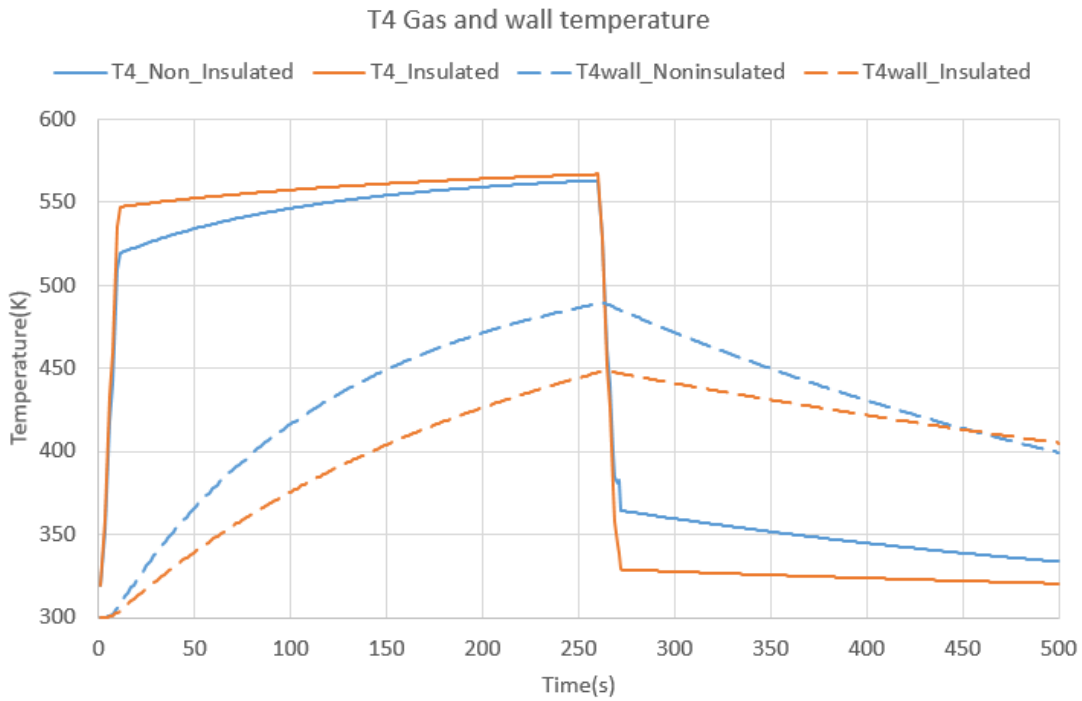

Figure 7.16 T4 temperature results for the two turbochargers.

Insulating the turbocharger can reduce heat loss and increase the turbine inlet and outlet temperature rapidly. This benefit will reduce as time passes but can also help to maintain the turbine flow temperature when the exhaust gas is at a low temperature.

7.4.3 WLTC cycle investigation

It is also interesting to investigate the insulated turbocharger's benefit in a simulated WLTC cycle. Figure 7.17 shows the T3 and T4 temperatures plus the related wall temperature for the two turbochargers. It can be seen that, for the majority of the time, the insulated turbine has a higher T3 and T4 temperature than the normal one; however, in the end, the non-insulated turbine has a higher T3 and T4, because the non-insulated turbo has a higher Twall temperature so, if the gas temperature drops too low, which is far lower than the wall temperature, there will be heat input into the gas. This will increase the T3 and T4, as shown in Figure 7.17, where the last plot portrays the heat input rate to the fluid.

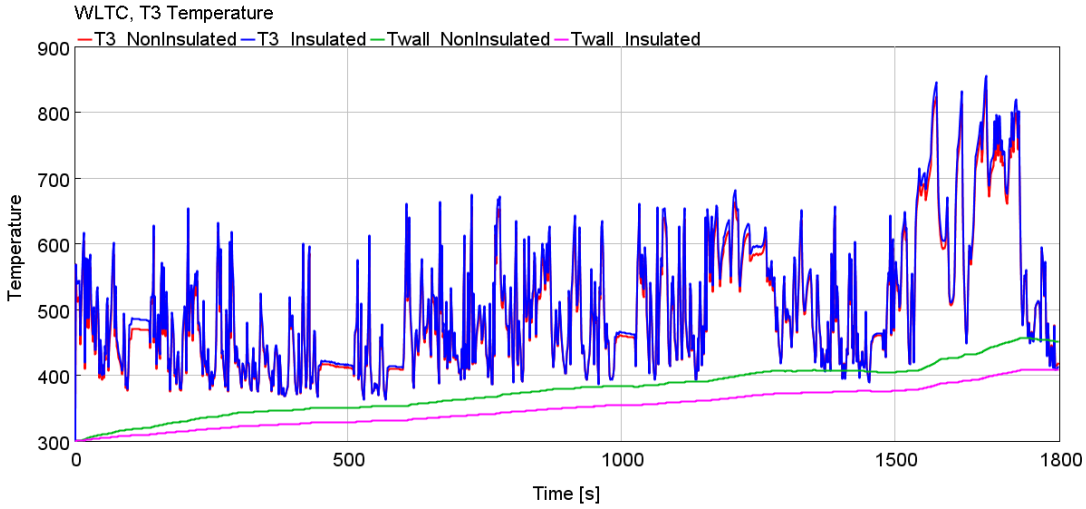

(a) T3 temperature results for the WLTC cycle.

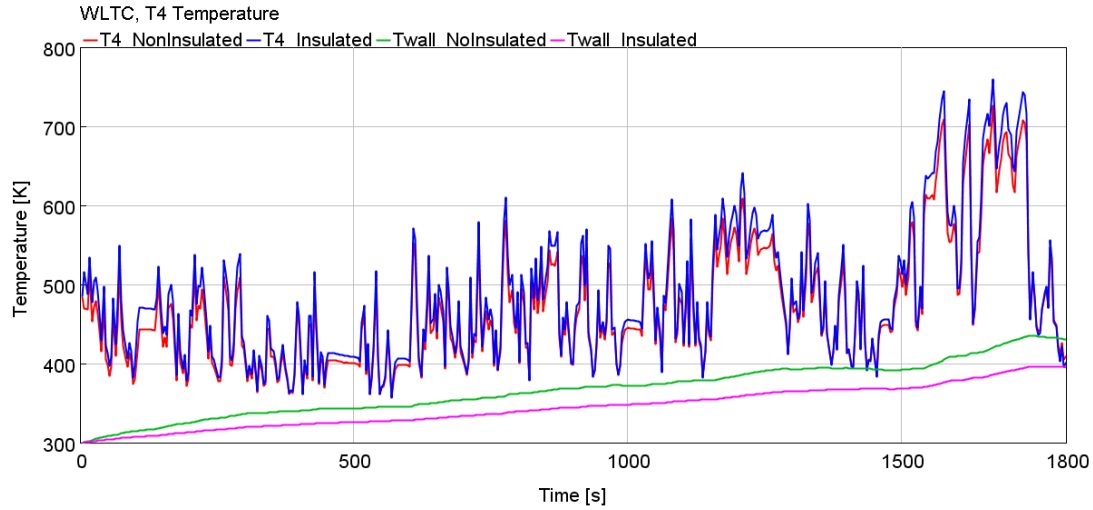

(b) T4 temperature results for the WLTC cycle.

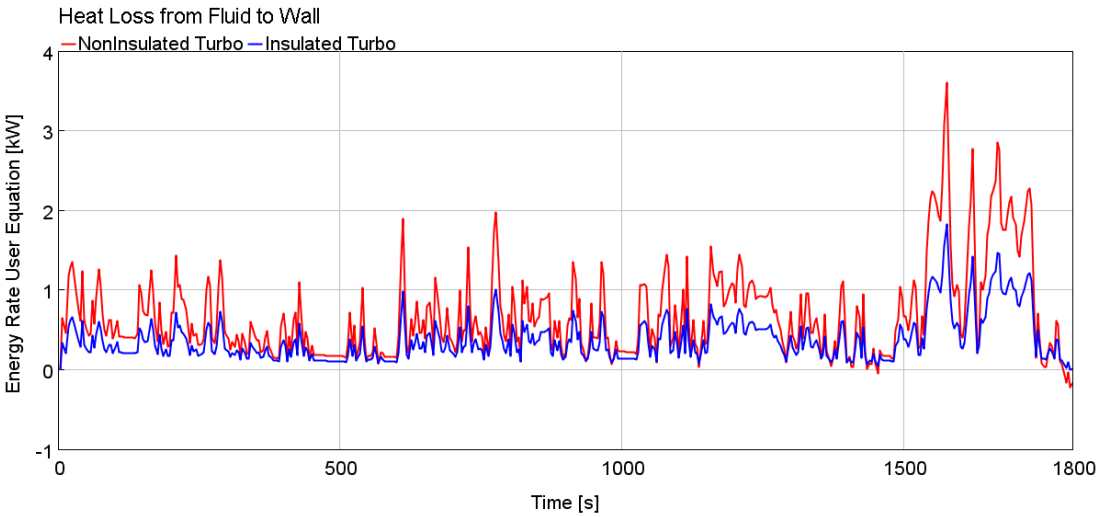

(c) Heat input rate from the fluid to the wall

Figure 7.17 T3 and T4 temperature results for the WLTC cycle.

Table 7.2 shows the temperature differences between the non-insulated and insulated turbocharger in WLTC T3 and T4. The average T4 temperature has been increased by 13.5K for the insulated case. Figure 7.18 shows the cumulative energy loss from the fluid to the turbine housing wall. It can be seen that 44% of the heat flux has been reduced, which is 527 kJ in the WLTC cycle.

	NonInsu_EndPoint	NonInsu_Avg	Insu_EndPoint	Insu_Avg
T3 (K)	417.0	498.7	411.8	506.2
T4 (K)	410.2	470.2	401.9	483.7
Increasing T in Avg	T3: 7.5K		T4: 13.5K	

Table 7.2 WLTC temperature differences

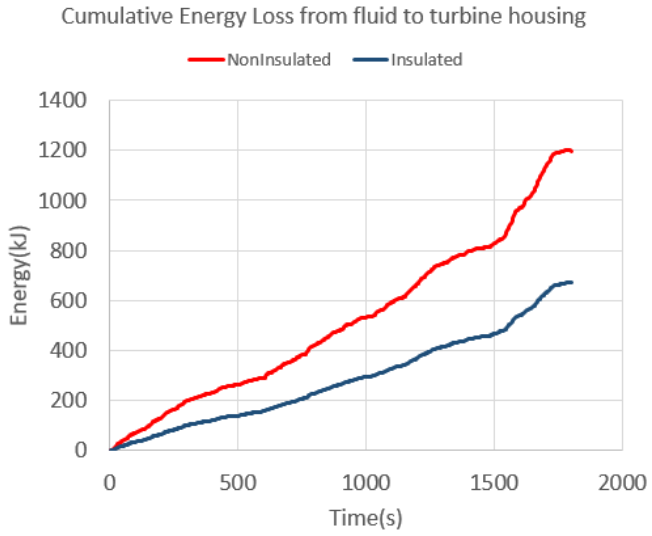

Figure 7.18 Cumulative energy loss from fluid to turbine housing.

In the experiment, firstly, the cold WLTC cycle is performed on the test rig, and the VGT position kept the same for the whole cycle. The T3/T4 temperature results are revealed in Figure 7.19. Almost no benefit was observed in T4, and about a 0.8kRPM average turbo speed benefit is achieved, possibly because the insulated turbocharger has a tiny benefit in the low temperature but high flow region, but still has a 'warming' effect as the turbine extracts more energy during this process.

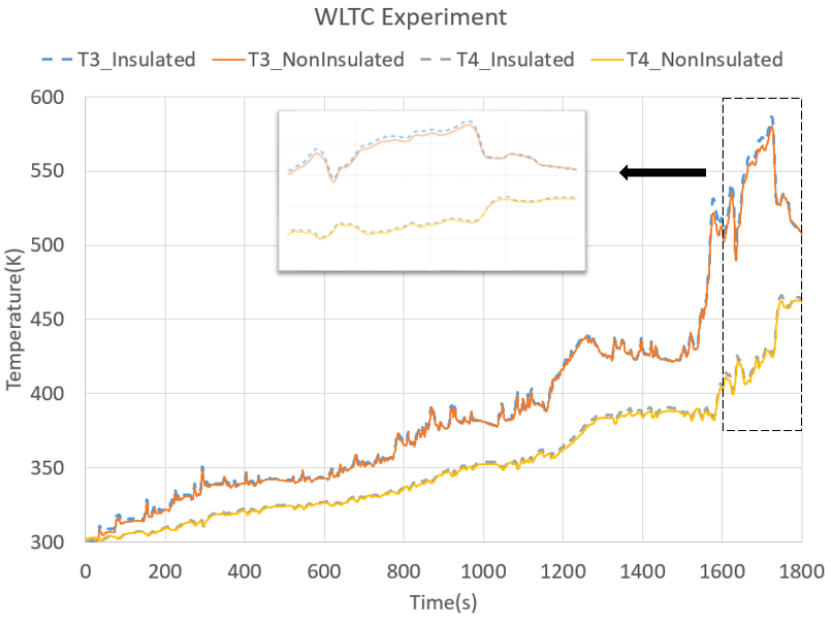

Figure 7.19 Experiment results of the WLTC turbine T3/T4 temperature

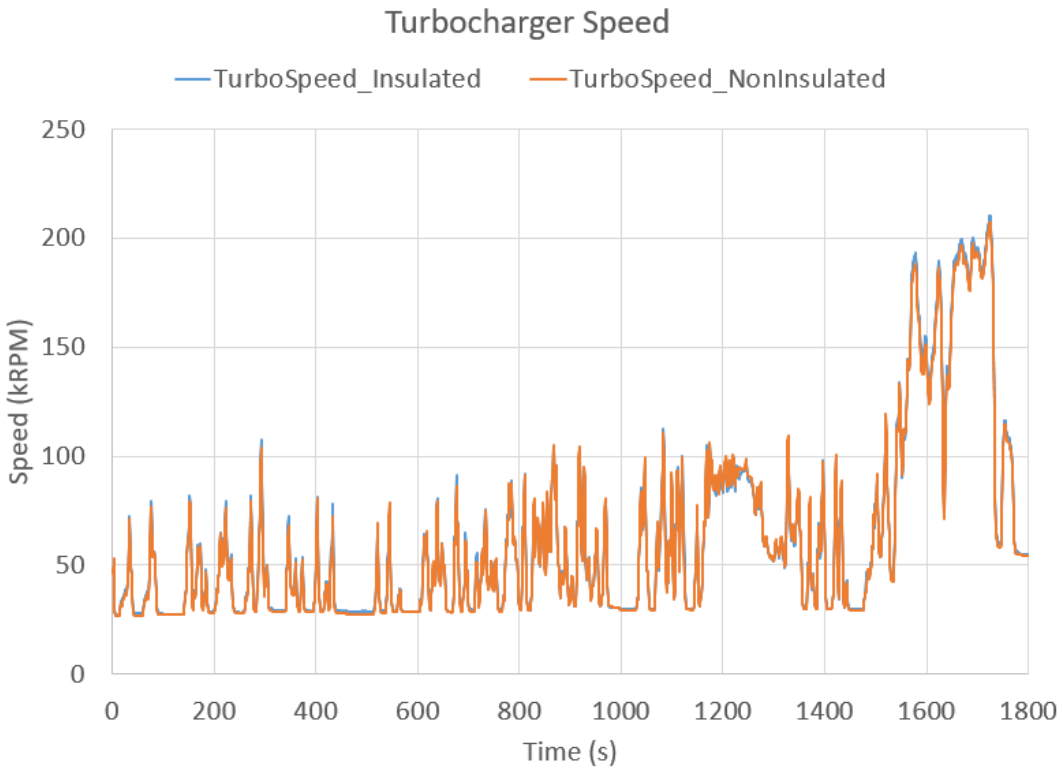

Figure 7.20 Turbo Speed in the WLTC cycle for the two turbochargers

	NonInsu_EndPoint	NonInsu_Avg	Insu_EndPoint	Insu_Avg
T3 (K)	507.7	391.2	506.8	393.0
T4 (K)	461.9	352.1	463.8	353.6
TurboSp (kRPM)	54.2	61.1	54.9	61.9
Increasing for each factor	T3: 1.8K T4: 1.5K, Turbo Speed: 0.8 kRPM.			

Table 7.3 A Comparison of the WLTC Experiment Results.

7.4.4 Further research on the insulated turbocharger

The studies outlined in the previous sections show that the insulated turbine has a thermal benefit in the steady state condition, but the transient experiment results failed to demonstrate the same effect, as the T4 or turbo speed benefit is either small or negative. The reason for this may be:

1. Although the design of the turbine wheel and the inner volute are the same, however, due to manufacturing errors, the roughness of the inner surface may be different.
2. Most of the transient experiments above were started from a low temperature, so the whole turbine is not warmed up, especially for the inner insulation, as it changes the thermal inertia of T/H.

3. The test rig has a settling tank on the downstream of the turbine, which was used to reduce the pulsating effects of the exhaust flow; however, its huge volume significantly increased the system's thermal inertia, which makes it difficult for researchers to control the system's thermal boundary conditions.

4. As it was difficult to maintain the same turbo speed throughout the testing, the heat that the two turbines generated may be different due to the design.

Further, an experiment is needed to try to deal with the issues mentioned above.

1. In order to reduce the manufacturing errors, the same turbine wheel and connected compressor is used for the following tests, and the outer T/H and insulation will be swapped manually if needed.

2. The settling tank is bypassed in order to eliminate its thermal effect on the exhaust.

3. As the turbo speed is hard to control in a transient study, the VGT is fixed to be the same, and the turbo speed is considered another value to evaluate the thermal performance of the insulated turbocharger.

4. The whole engine's system is warmed up for a long time, in an attempt to reduce the system's thermal inertia effects on the turbine housing.

A step load process is designed based on a tested RDE cycle, including three stages:
1. Motorway driving stage: low engine speed, medium engine torque.
2. Downhill driving stage: medium engine speed, low engine torque.
3. Uphill driving stage: low engine speed, high engine torque.

The example of the test design is shown in Figure 7.4 and Figure 7.5.

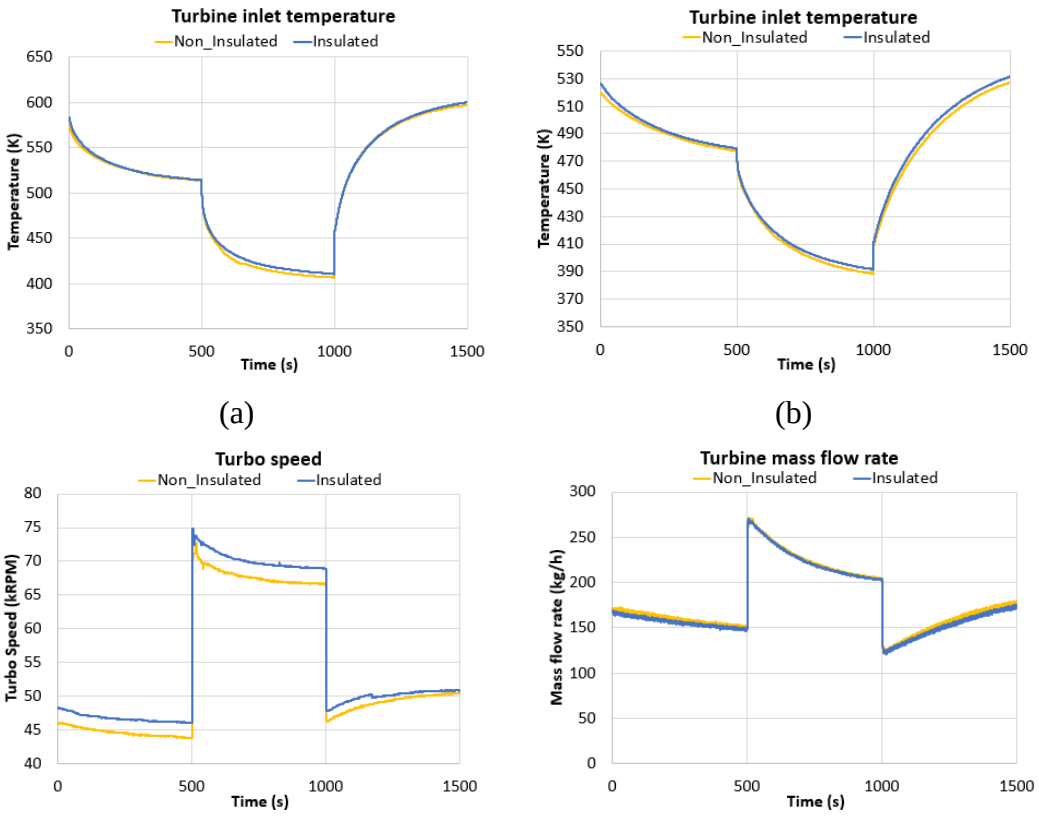

Figure 7.21 Turbine-related experiment results

Figure 7.21 shows the results of the test. The T3 and T4's results are shown in (a) and (b), where it can be seen that the T3 is the same for both turbochargers in the first stage, but the non-insulated turbocharger has a lower T3 and T4 in the second and third stages. Even though they are under the same engine speed and load, the T4 is 527.1 and 531.6, respectively, and there is a 4K T4 benefit for the insulated turbocharger. Figure 7.21 (c) and (d) shows the turbine speed and mass flow rate. There are 2 kRPM constant speed benefits for the insulated turbo under the same VGT position, and the mass flow is briefly the same (the errors lie in the acceptable range).

The results in this section show that, after adjusting the test, there is a small thermal benefit for the insulated turbocharger under a transient situation. More benefit can be observed with regard to turbo speed, as the inner flow of the turbine is warmer for the insulated turbine, and thus it should achieve better efficiency and extract more energy from the exhaust flow.

7.5 Summary and potential improvements

In this section, a thermally inner-insulated turbocharger is proposed to increase the T4 (to lower the catalyst light-off time), which does not require any control modification and can be implemented easily. As the aerodynamic performance of the insulated and standard (non-insulated) turbochargers is almost identical, any change in the T4 is entirely due to the inner-insulation. The objective of this work was to quantify the benefits of the inner-insulated turbocharger.

Steady state tests for the two turbochargers demonstrated that the insulation could increase the T4 for the turbocharger turbine under different engine speed and load conditions.

For the engine warming up, step load and WLTC transient study, external 3D modelling results were used to parameterise a simple 1D lumped capacitance model which was capable of predicting similar aerodynamic behaviour of the two turbines. When compared with the experimental results, the model was shown to over-estimate

the benefits of the inner-insulation, and only a small benefit can be observed in the experiment, possibly due to the inaccurate model, cooling test condition or manufacturing errors.

The re-designed test demonstrated that the insulated turbocharger could obtain a T4 enhancement based on a warmed up engine, and a 2kRPM turbo speed benefit was achieved at the same time due to the increased turbine inner gas temperature.

This section explained the steady and transient performance of the insulated turbocharger; however, more thermal tests should be planned in the future to investigate its benefit further. The best way would be to constrain the turbo speed by adjusting the VGT position during the transient process, with the same engine boundary condition. A more obvious T4 benefit should be observed in this period, and a hot start WLTC or RDE can be performed as demonstrations.

Chapter 8 – The 3D optimisation of the T-Piece junction in the two-stage air path

In this chapter, the 3D topology optimisation of a specific T-Piece duct in the two-stage turbocharged engine inlet air path has been investigated. By applying Computational Fluid Dynamics (CFD) to the individual component, the inflow of turbocharger can be potentially optimized and improve the turbocharger efficiency.

The baseline model is supplied by the manufacturer, which is a CAD model for a gasoline engine inlet air path. The design target is the T-Piece (T-PIECE) junction between electrically driven compressor (EDC, Upstream), and turbocharger (Downstream). The boundary conditions were taken from the 1D system with the same air path layout. In this chapter, a combined optimization methodology with ANSYS Fluent and Tosca Fluid is presented, modified the shape of T-Piece junction for reducing its pressure drop and curling flow.

The strategy has 4 stages. Firstly, the original full air path was simplified based on a series of initial simulations, and the only exists parts are the pipework directly connected to the T-PIECE with bending, in order to reduce the time cost on simulation. Secondly, Tosca Fluid was used for the initial T-PIECE geometry optimization, under the given design space; this is mainly for reducing the backflow and recirculating area. Then, the add-on app in ANSYS Fluent called Adjoint solver had been used for further optimizing the generated T-PIECE geometry (typically a further 20-50 iterations). Finally, the updated air path connected with a 3D compressor model, further studying its benefit on compressor efficiency and power.

8.1 Baseline model simulation.

The details of the baseline 3D model and research methodology has been introduced in Chapter 3 and Chapter 4. The simulation and optimisation are focused on a T-Piece junction in a two-stage turbocharged engine inlet air path.

This section presents the CFD setup, mesh convergence study and simulation results for the baseline fluid model shown in Figure 3.34. The configuration of the CFD solver is the same for the parametric, non-parametric and Adjoint Solver optimisations. ANSYS Fluent is used for all simulations and the configuration of the solver is detailed in Table 8.1

Parameter	Value
Analysis Type	Steady
Time steps	Conservative Auto
Inlet type	Mass flow
Outlet type	static Pressure
Inlet Temp	298K static
Turbulence Model	k-ω SST
Wall	No-slip, adiabatic
Converge Criteria	RME 5e-6
Advance Scheme	High Resolution

Table 8.1 CFD setup for the simulations

The mesh size used is different for the parametric and non-parametric optimisation and therefore two mesh independence studies were conducted. As the parametric approach consists of a Design of Experiments approach to create a surrogate model on which optimisation is performed, a finer mesh can be used as the number of CFD calculations is known in advance. For the non-parametric optimisation, the 3D calculation is the cost function of the optimisation and therefore a coarser mesh with fewer cells is required. In the context of this paper, the mesh independence studies are not intended to find the minimum number of cells required for simulation, but rather ensure that the number of cells that have been chosen are suitable to deliver stable results.

For the parametric optimisation, only the T-piece is simulated. The mesh convergence study results are shown in Table 8.2: 2,056,883 cells have been used in the simulation.

When comparing this to mesh sizes ranging from 400k to 4.4M, the mass flow in the EDC and bypass legs, and the compressor efficiency only vary by a maximum of +/- 0.3%.

Table 8.2 Mesh convergence study of T-piece junction for the baseline model.

Number of Cells	Norm. EDC Mass Flow Rate	Norm. Bypass Mass Flow Rate	Norm. Comp Efficiency
474,902	-0.3%	+0.2%	+0.2%
538,550	-1.0%	+0.6%	+0.1%
666,869	-0.2%	+0.1%	+0.0%
2,056,883	***1***	***1***	***1***
2,818,081	+0.2%	-0.1%	+0.0%
3,454,607	-0.4%	+0.2%	+0.0%
4,442,091	-0.1%	+0.0%	+0.2%

The CFD results for the baseline fluid model is displayed in Figure 8.1. Based on the boundary condition illustrated, the fluid velocity streamline can be simulated. The average inlet speed of bypassport and EDC is 21.5 and 21 m/s, the average outlet speed of turboport is 49.8 m/s. It can be noticed that there are increasingly kinetic energy losses in the two bending areas one is at TP, another is at the 90 deg pipe of turbo inlet. There is a potential to increase the flow energy and reduce its pressure drop by optimizing the TP.

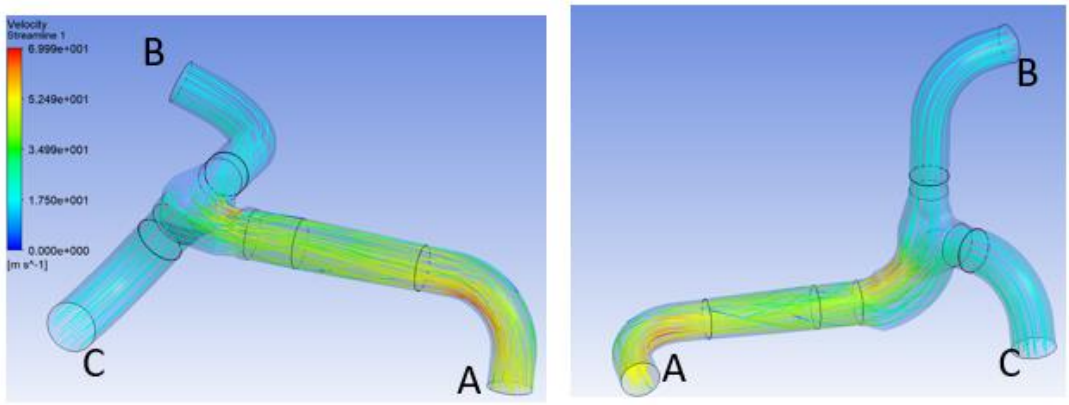

Figure 8.1 Fluid velocity streamlines.

In order to describe the flow velocity at the turboport, the curling and velocity in the normal and tangential situation is used to explain it. Figure 8.2 (a) and (b) shows the velocity at turboport area in tangential and normal direction, the max speed of tangential velocity is 12.35 m/s, for the normal direction it is 52.8m/s. The vortex factor *Velocity.curling* in ANSYS is used to evaluate how the flow performs when this

value is lower; then there are less curling flow and flow kinetic energy can be used more efficiently. The *Velocity.curling* factor at the bypass inlet port of TP is regarded as a reference value, which 4137.19 s-1, this is a mass flow averaged value. From Figure 8.2(c), it can be found that in most area, the curling value is around 2500 s-1, which is good, but when it comes to the margin of the fluid, the curling value is close to 35000 s-1, this is because of the inflation effects of pipe and the design of that 90 deg bend pipe, the average curling factor value is 7868 s-1.

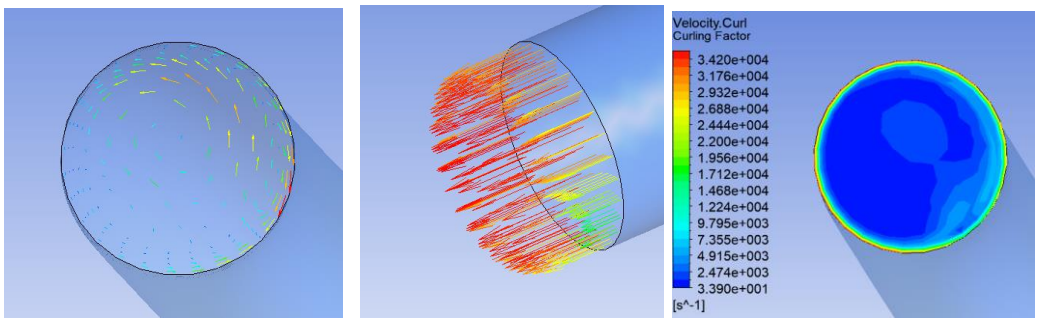

(a) (b) (c)

Figure 8.2 (a) Tangential velocity vector at Port A (b) Normal velocity vector at Port A (c) Flow curing factor at Port A

Curling Factors	Tangential Velocity	Normal Velocity	Velocity curling	Reference Velocity curling at inlet
Turbo Port A	12.35m/s	52.8 m/s	7868 s-1	4137.19 s-1

Table 8.3 Cross-section curling results.

Pressure drop is the main factor need to be discussed. In this thesis, factor mass flow average pressure is used to compare with others, it will help to simplify the calculation. For this baseline model, the boundary condition at Port A is -5300 Pa, the pressure drop between Port C and Port A is 1741.83 Pa, between Port B and Port A is 1866.52 Pa. The value is not that big, less than 0.02 bar pressure drop here means the supposed optimized value will also be much lower, empirically, it won't have many effects on compressor efficiency, that's why the curling factor is also an important metric.

Based on the simulation above, the compressor model introduced in Chapter 3 was mated with the T-Piece air path, in order to see how the system performs with involving of the compressor. The compressor wheel radius is 25.5 mm, has 7 blade

sets. The fluid velocity streamlines are shown in Figure 8.4. The turbo compressor is operated at 80,000 RPM. Comparing with the case without compressor, there is 0.005 kg/s flow difference in the two air tracks. The pressures at compressor inlet and outlet are 94.29 kPa and 132.93 kPa with a pressure ratio of 1.41. As there are two inlet flow types in this model (from port B and port C), ANSYS cannot generate the efficiency based on its single inlet compressor efficiency algorithm. Therefore, the compressor efficiency is calculated based on Newton's law. In this case, the compressor efficiency is 76.96 % (not including the turbine and shaft).

Port name	**Mass flow (kg/s)**	**Pressure (kPa)**
Port A	0.0941	132.93
Port B	0.0347	97
Port C	0.0594	97

Table 8.4 Simulation results for baseline air path.

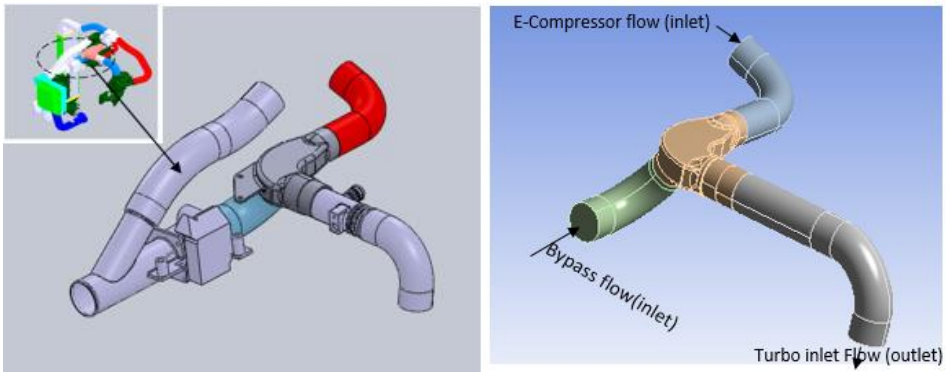

(a) (b)

Figure 8.3 (a) Engine system CAD model and components, (b) Simplified air path flow domain for simulation and optimisation.

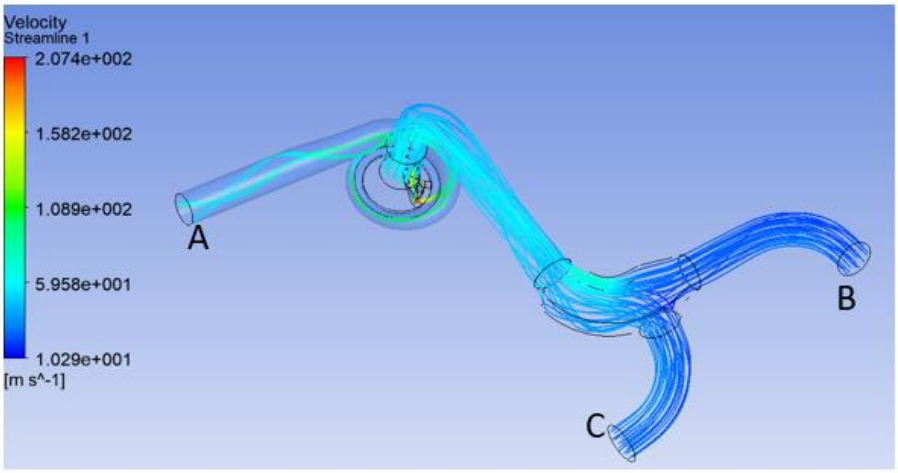

Figure 8.4 Fluid velocity streamlines

8.2 Parametric Optimization.

Parameterization is a common method in geometry optimization. As the original T-Piece was not a parameterized design, it was simplified and parameterized as a group of pipes. The parametrization method has been introduced in Chapter 4, however, due to the limit of the design space for the whole air path system, only some of the parameters were considered, the parameters and the examples of parameterized T-PIECE junction are shown in Figure 8.5.

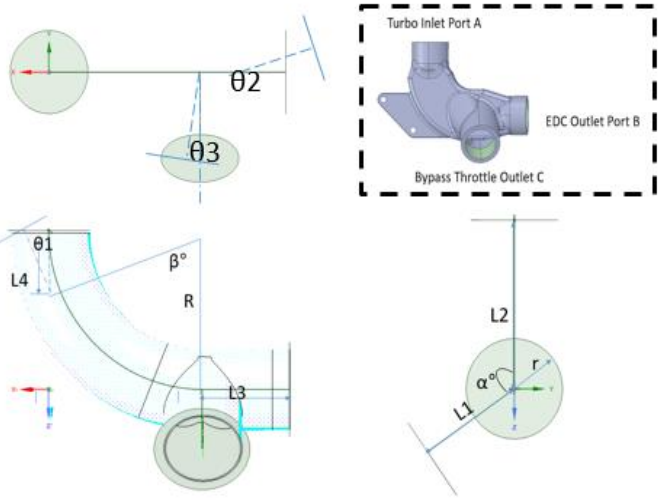

L1	Dist from C to pipe axle
L2	Dist from A to Intr plane
L3	Dist from B to Intr plane
L4	Dist from A to Arc track Starting Point
α	Angle between L1 and L2
β	Angle of Arc track
r	Pipe port inner radius
θ1	A angle betw Axle and Z Axle
θ2	B angle betw Axle and X Axle
θ3	C angle betw Axle and X Axle

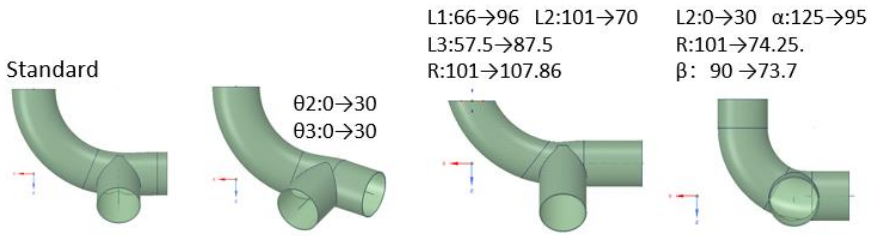

Figure 8.5 Examples of T-Piece junction Parameterization

The whole baseline air path model after parameterizing is shown in Figure 8.6. The pressure drop between Bypassport and Turboport is 2232Pa, between EDCport and Turboport, is 2126 Pa, which is generated by ANSYS Fluent.

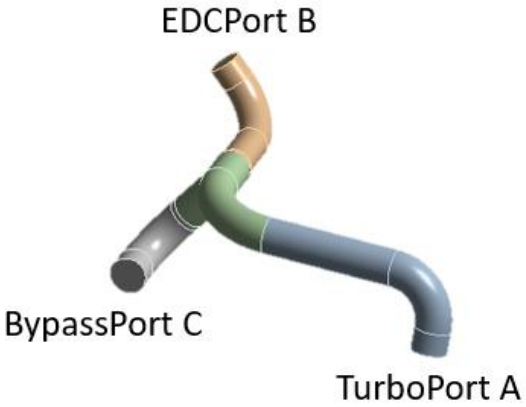

Figure 8.6 Air path with parameterized T-PIECE

Based on the parameterisations shown in Figure 8.5, the different geometry designs have been calculated with ANSYS Fluent. Figure 8.7 shows the pressure distribution within the cross-section of the turbocharger compressor port in dependency of the different T-piece geometry.

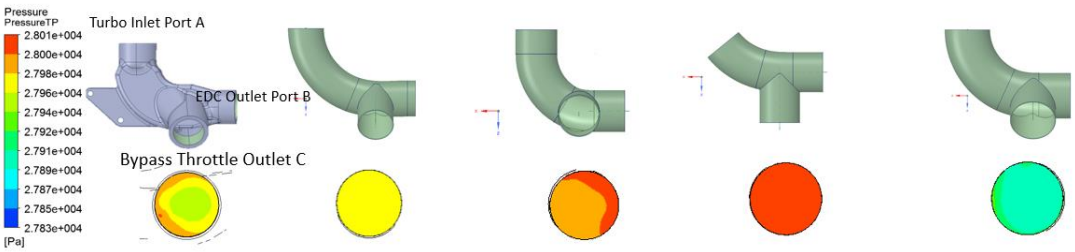

Figure 8.7 Turboport pressure contour related to different geometry parameters.

From Table 8.5, it can be seen that the parameters L2 and θ1 are the most important parameters that affect the pressure drop. However, these two parameters will significantly change the locations of the adjacent pipes, which will make the air path interfere with other components (non-feasible design).

Factor name	**Factor description**	**Degree of correlation Pressure Drop (C to A)**
L2	Distance from A to Intr plane	-0.84
θ1	A angle between Axle and Z Axle	0.52
θ2	B angle between Axle and X Axle	0.39
θ3	C angle between Axle and X Axle	-0.25

Table 8.5 The degree of correlation: between parameters and the pressure drop from port C to port A.

The parameterization method demonstrates that the T-Piece geometry design has the potential to reduce the flow pressure drop and that the flow domain geometry will greatly affect the flow properties and velocity vectors. However, this kind of design is just an initial step. It will change the whole engine air path design that will increase the costs and design complexity.

8.3 Non-parametric topology optimization

Based on the model in Figure 8.8, the Tosca model was generated by software Tosca Fluid, which is an optimization tool working together with ANSYS Fluent. The final geometry calculated by Tosca Fluid depends on the boundary conditions and the defined design space. In this thesis, all different Tosca Fluid simulations are based on the same boundary conditions. A series of design spaces were investigated. The design space difference plays a significant role in T-Piece result shapes. Tosca Fluid calculates the flow velocity vectors based on the boundary conditions for each design space. If the size of the design space is beyond the reality or the connection regions at inlet and outlet is abrupt, unexpected results will be generated. Examples are shown in Figure 8.9.

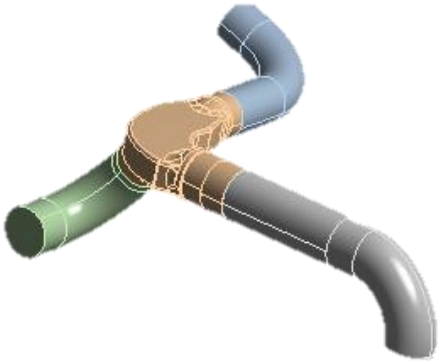

Figure 8.8 Simplified air path flow domain for simulation and optimization

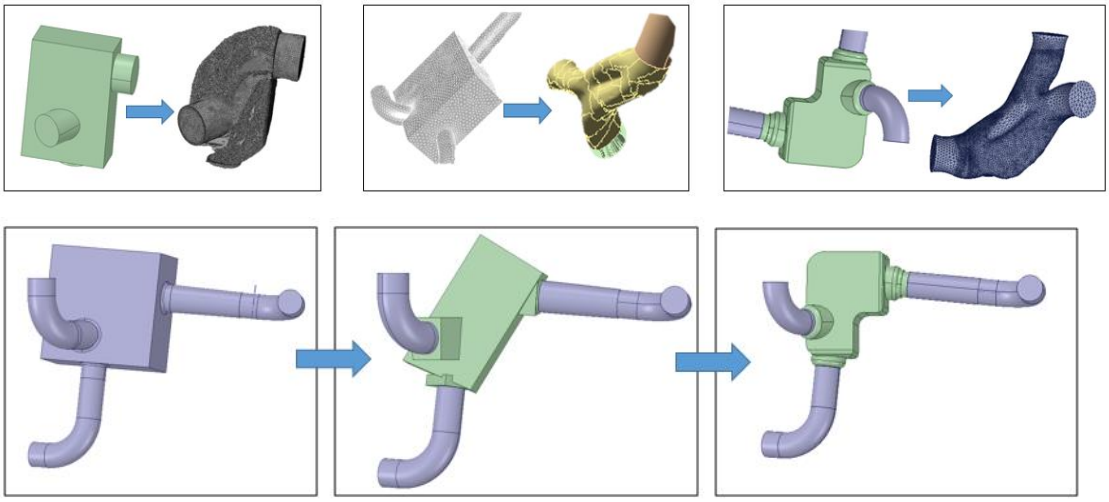

Figure 8.9 The effects of designed space on final optimized results

In Tosca Fluid, the final shape generated depends on many different initial parameters set in advance. The most important parameter is the cut-off value; this means how much of the fluid volume will be cut off based on the optimization result. A higher cut-off value will make the final geometry volume smaller. Figure 8.10 shows the T-Piece shape under different cut-off values ranging from 0.5 to 0.56. The T-Piece with a cut-off value of 0.53 has been selected for the further CFD simulations.

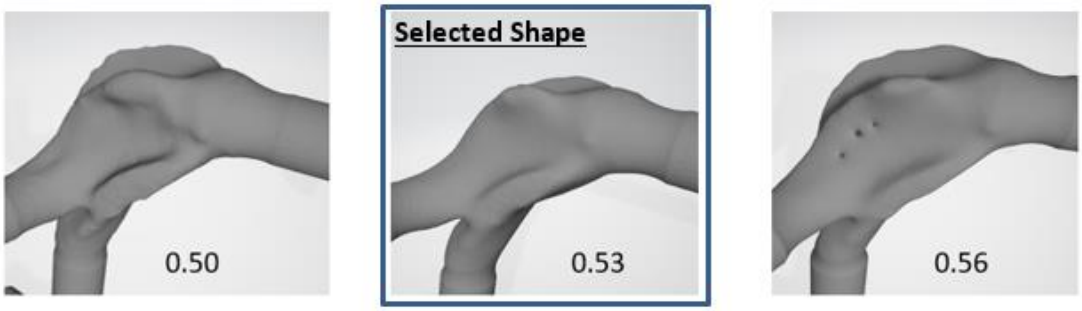

Figure 8.10 T-Piece generated with different cut-off values

For the non-parametric optimization using Tosca Fluid, the CFD boundary condition setup is the same as the setting in baseline model shown in Table 8.1. The mesh size is considerably smaller. Firstly, a lower number of cells is used, and secondly the simulation space comprises both the T-piece and the compressor. It should be noted that in the simulations, the exact number of cells also changes because the geometry changes at each iteration. The mesh convergence study is conducted for the final iteration in the optimization and the result is shown in Table 8.6. The simulation uses 996,183 cells. When comparing this to mesh sizes ranging from 500k to 2.3M, the mass flow in the EDC and bypass legs, and the compressor efficiency only vary by a maximum of +/-0.4%.

Table 8.6 Mesh convergence study of T-piece junction for non-parametric model.

Number of Cells	Norm. EDC Mass Flow Rate	Norm. Bypass Mass Flow Rate	Norm. Comp Efficiency
495,503	-0.3%	+0.3%	-0.1%
548,494	+0.1%	-0.1%	0.0%
668,317	+0.3%	-0.2%	+0.1%
996,183	***1***	***1***	***1***
1,400,509	-0.2%	+0.2%	-0.5%
1,757,780	-0.1%	+0.1%	-0.7%
2,329,651	-0.4%	+0.4%	-0.9%

Figure 8.11 below shows the velocity streamline of the Tosca T-Piece air path and the velocity curling factor of Turboport. The flow speed at Port B and C is 21, and 27.6 m/s, at A, is 47.7 m/s. The curling factor contour plot at Turboport and the pressure drop results is in figure 20. Its mass flow average value in this area is 7165 s-1, which is 700 s-1 lower than the baseline model result. For pressure drop result, Comparing with baseline model, they have been improved 0.3 kPa in both B to A and C to A side.

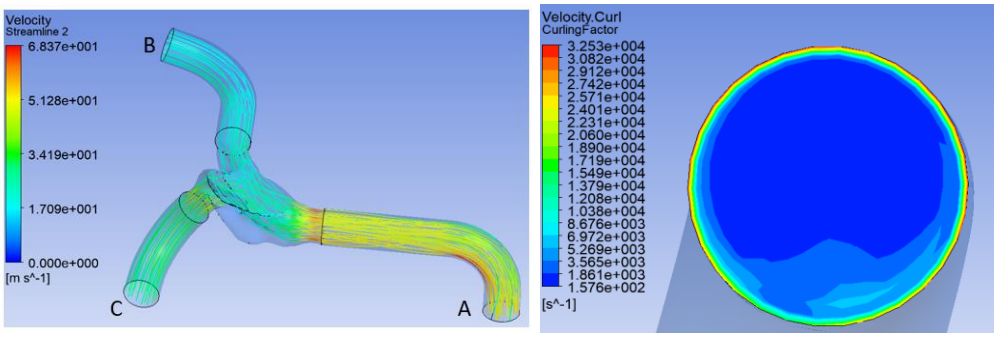

(a) (b)

Figure 8.11 (a) Velocity streamline for Tosca T-Piece air path. (b) Velocity curling factor of Turboport

	PD B to A(Pa)	PD C to A(Pa)	Velocity curling (s-1)
Baseline Model	1866.52	1741.83	7868
Tosca Model	1532.61	1489.42	7165s

Table 8.7 Pressure drop results of the model.

The same compressor is mated with the Tosca optimized T-Piece air path, under the same boundary conditions as previously used. The mass flow rates of port B and C are 0.0461 and 0.0481 kg/s; there is a 0.002 kg/s flow difference in the two air tracks. The pressure at compressor inlet and outlet is 95.52 kPa and 136.3 kPa; pressure ratio is 1.43. Compressor efficiency is 77.76 %, which corresponds to a 1 % increase compared to the baseline.

	Baseline		**Tosca Optimised**	
Port Name	**Mass flow (kg/s)**	**Pressure (kPa)**	**Mass flow (kg/s)**	**Pressure (kPa)**
Port A	0.0941	132.93	0.0942	136.3
Port B	0.0347	97	0.0461	97
Port C	0.0594	97	0.0481	97

Table 8.8 Simulation results comparison for the baseline model and optimized model

Based on the two groups of simulations, it can be observed that the T-Piece shape will not only impact the airflow pressure drop and flow swirl situation but will also impact

the flow distribution in two path (bypass and EDC pass). After connecting with the compressor, even the inlet pressure boundary condition is the same, but the air mass flow results of both inlet ports are different.

Figure 8.12 shows the Tosca optimised results in terms of streamlines and flow velocities. Compared to the baseline model (see Figure 8.4), the topology optimised design shows reduced flow velocities, especially in front of the outlet of the T-piece junction. Main reasons are a larger radius as well as a reduced main-jet velocity by a larger cross-section in front of the outlet. The flow may better follow a radius at lower local flow speeds.

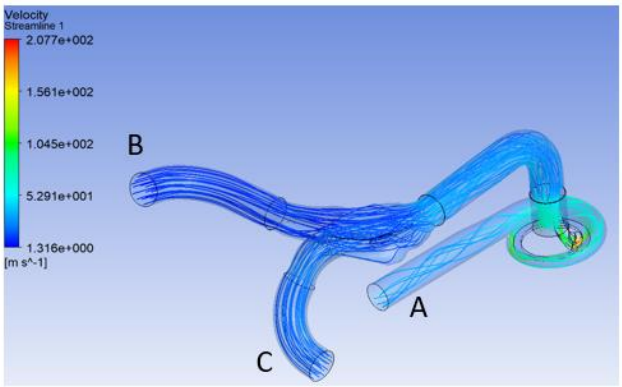

Figure 8.12 Velocity streamlines with Tosca TP air path and compressor.

In order to make it more clear, how the T-Piece shape affects the compressor efficiency, a series of simulations were designed to progressively change the compressor speed from 50 kRPM to 14 kRPM. In all cases, the EDC port and bypass port inlet pressures were maintained at 96 kPa, and the total mass flow rate was 0.09415 kg/s (as for the previous simulation).

The relationship between turbo RPM and compressor efficiency is shown in Figure 8.13(a). The Tosca model has higher efficiency in low speed region, with a 2 % improvement achieved at 60 kRPM. The improved efficiency will help the compressor to deliver a higher boost under the same inlet pressure and total mass flow from the bypass port and EDC port. The compressor outlet pressure is shown in Figure 8.13(b).

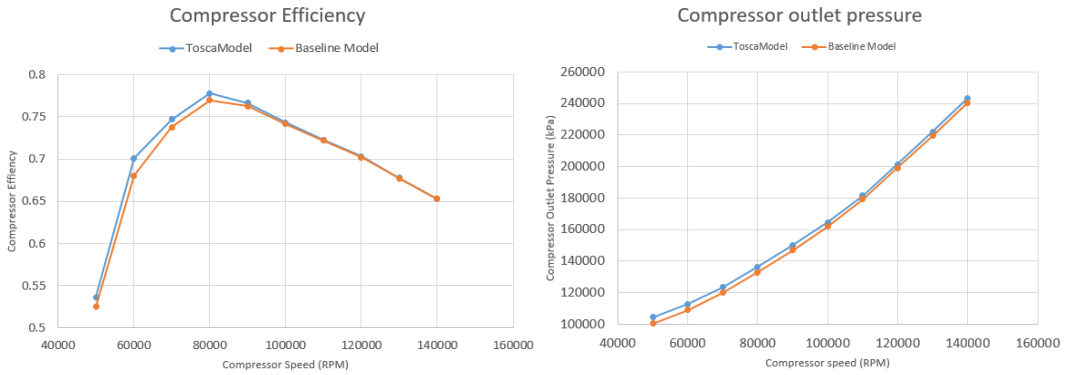

(a) (b)

Figure 8.13 (a) Compressor efficiency (b) Compressor outlet pressure

8.4 Further reflection on T-Piece geometry

Another optimization method to improve the T-Piece geometry has been investigated based on the Tosca Fluid and the following Adjoint Solver optimization. In this section, the results are only focused on the air path. The compressor model has not been considered.

The Adjoint Solver is an add-on app in ANSYS Fluent. It can help to optimize the outer fluid surface geometry to optimize the set observation. In this simulation, the Adjoint Solver was used as the post-processing tool helping to optimize the Tosca T-Piece and to reduce the pressure drop. The final optimized meshing differs only slightly from the original surface produced by the non-parametric optimization using Tosca Fluid. Figure 8.14 shows the final optimized meshing comparing with the original surface. There was a transformation that is hard to visualize.

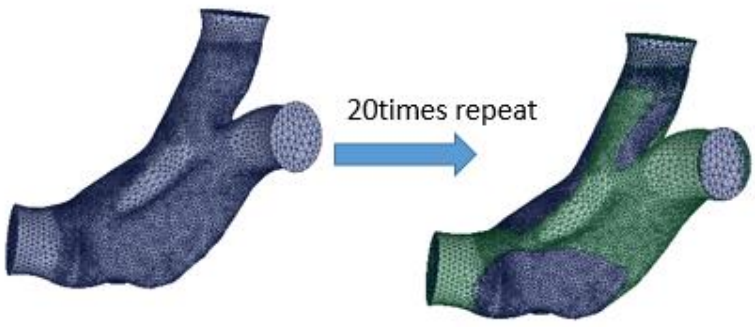

Figure 8.14 Adjoint solver application on T-PIECE

There are two optimization targets: the pressure drop from the bypass port to the turbocharger compressor inlet, and the pressure drop from EDC port to the turbocharger compressor inlet. A specific value was used to evaluate how the optimization works. In the 20 iterations, the trade-off of this value is shown in Figure 8.15. The pressure drop changed from 1637 Pa to 1517 Pa and 1674 Pa to1672 Pa; i.e. up to 100 Pa benefit. In this application, the additional benefit from this method does not appear to justify the additional effort required.

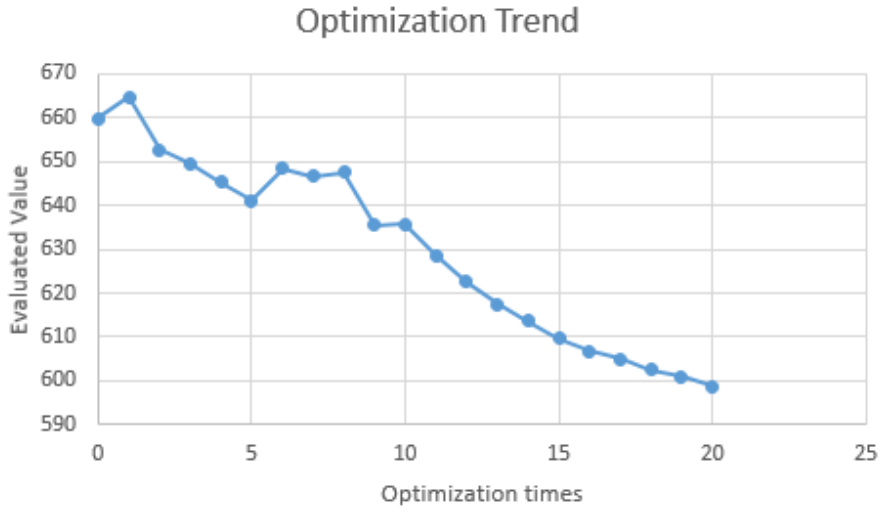

Figure 8.15 Trade-off for pressure drop evaluated value.

8.5 Summary and potential improvements

This chapter described the investigations of optimizing a two-stage turbocharged engine inlet air path. Different methods have been used for the optimization of the design of a T-Piece junction in the intake side. The focus was on a non-parametric topology optimisation approach considering both the pressure drop and the efficiency of the turbocharger compressor downstream of the junction. Tosca Fluid and ANSYS Workbench are the two major software tools for T-Piece topology optimization and CFD simulation. The T-Piece junction between the electrically driven compressor (EDC) and the turbocharger compressor has been optimised for lower pressure drop and reduced swirl compared to the baseline design. The pressure drop was reduced by

0.3 kPa (15 %) and the turbocharger compressor efficiency increased by up to 2 % (compressor efficiency rise from 68 % to 70 %). Further optimisation using the ANSYS Fluent adjoint solver has also been investigated – however, these results did not offer a substantial improvement in performance over the non-parametric approach for this application.

The study in this section is still in component level, two operating points were simulated. Taking a further step, this model can be embedded into the full 1D engine system model, to replace the 1D T-piece junctions in two stage turbocharger system. However, there are some difficulties that needs to be emphasised:

1. The current 3D model just simulated two points which is not enough to demonstrate its reliability in system simulation, much more operating points should be simulated first to cover different situations.
2. The 3D simulation is a time and money cost work, especially for the non-parameterization geometry. The model should be simplified, the timeline and cost should be carefully considered.
3. This model did not consider the thermal effects between the flow and the pipe wall, if an extreme accurate result is required, a heat transfer model is needed to be added, which further increases the complexity of the model.

The downside for the 1D and 3D co-simulation is that, as the changing of 1D simulation settings, the boundary condition of the 3D model will be changed, which means the 3D model needs to be adjusted and checked for converge on the solutions, this is hard to be managed. Due to the time and hardware limits in current simulation, and also the 1D-3D co-simulation is out of the scope of this thesis, there is no verification study of the T-Piece models in 1D system environment. However, if the compressor efficiency benefit of the T-piece is considered in the two-stage electric boosting system, a reduction of the electricity consumption is supposed to be observed, higher compressor efficiency offers the turbine VGT a chance to open more, this will reduced the engine pumping loss and increase the engine efficiency. The only cost for the optimisation above in real life may only be a replacement of the T-piece junction, which is worth.

Chapter 9 –Conclusion

This chapter summarised the main findings for this thesis. The findings will be introduced by the section order and against the objectives outlined in Chapter 1.

A reflection will be given for the findings above, to formulate an overall methodology for two-stage mild hybrid system matching and optimization.

Since there are still targets missed due to the unforeseen difficulties, the weakness of this thesis will be followed by.

At last, the suggestions and recommendations of the future work will be put to the end of this section.

9.1 Findings of the thesis

Before summarizing the output of this thesis, it needs to be emphasized that this thesis studied the electric boosting airpath in both system and component level, this is uncommon comparing with other similar thesis/publications (only focus on system level or component level). Based on the results explained from Chapter 4 to Chapter 8, the electric boosting system performance can be improved by optimizing the controlling between different components (VGT, E-Motor, EGR, Waste-gate, turbocharger size), the benefits are observed in factors like system efficiency, fuel or electricity consumption, transient response. The components only study focus more on the property of themselves, in this thesis, the benefit of the insulated turbine is to 'keep the exhaust warm', and get T4 enhancement, this is not obvious for people to understand that how it help improve the vehicle performance in real life. In this way, the insulated turbine is modelled into a 1D simplified version, and added into the whole engine system, to evaluate its real benefit in fuel consumption and emission reduction. The component study clearly explained how the insulation creates higher T4 (by analysing the heat fluxes inside the structure), the system study demonstrated how this help to improve the whole airpath performance. The 3D study in Chapter 8 is also similar to this. Component study helps clarify how the T-Piece geometry reduce the pressure drop, recirculate flow and increase the flow uniformity, when this component is attached with a compressor, an efficiency benefit is observed due to the optimization of the flow. The T-Piece can surely be applied on the electric boosting system, the optimized flow is supposed to help the whole engine system increased its efficiency and transient response.

Coming to the summary of the findings of this thesis, it investigated the potential and design of mild hybrid boosting system with different layouts. The research background of hybrid boosting technologies, the challenges in air path design and engine downsizing was briefly discussed in Chapter 1, followed by the aim and objectives of this thesis.

Review of electric boost system and air path design to downsized engine

In chapter 2, a comprehensive literature review was carried out for turbocharger technologies and mild hybrid system status. Boosting technologies in engine systems were introduced, variable geometry turbine and electric boosting technology are more important for modern turbocharger vehicle since they can help to increase the engine transient performance and reduce the vehicle emission. The challenges of multi-stage boosting system design were focused on. The issues of surging, sizing, transient performance and efficiency trade-off for complicated turbocharger system have been analysed, with the examples of how they been solved by the related technologies. Electric assisted boost system has been demonstrated to be an advanced design for downsizing the engine without sacrifice the transient performance. It can also help to reduce the vehicle emission by combining with mild hybrid air-path design (electric aftertreatment system). The difficulties for emission reduction during this process was given at the end, discussed the interactions of the air path design.

Test Facilities and Modelling Method

Chapter 3 described the test facilities and experimental setup for the thesis research. A two-stage engine-gas stand test facilities have been constructed. This rig is able to undertake steady and transient study for two-stage electric boost system, the air path configuration is flexible, as the routing can be adjusted based on research requirements. A series demonstrating test was conducted in order to show how the rig works under different test design. Furthermore, the 1D and 3D simulation tools were introduced in this chapter, briefly illustrated how the model works parallel with test results, and how they contributed to discovering the potential and advantages of hybrid boost system and insulated turbocharger technology.

Modelling Methodologies

Chapter 4 focused on the methodologies used in the modelling side, including 1D modelling and 3D modelling. Two different electric boost system models were explained: two-stage electrically driven compressor system and decoupled electric turbocharger system. The heat transfer modelling method for insulated turbocharger

study was followed by, mainly described how to use 1D modelling method capturing with turbine heat transfer effects in different cases. In the end, the 3D optimization for T-piece junction at the engine inlet side was discussed; the baseline model and settings are given there.

Study on the two-stage electrically driven compressor system

Chapter 5 studied the two-stage system with EDC in both experiment and simulation. Steady state and transient experiments are accomplished for investigating the sensitivity of VGT and EDC control. In the experiment, it was found that both closing the VGT and increasing the EDC speed can help to raise the boost pressure. However, a lower VGT position will lead to a higher engine backpressure, so the engine pumping loss is increased. A higher EDC speed will consume extra electrical power, which was limited by the system's electric system design. These two devices can also affect the EGR mixing, high speed EDC and lower positioned VGT could help to increase the EGR transient flow and mixing speed (according to the O2 rate changes). The similar two-stage air path with the same turbocharger and EDC has been applied on a 1.6L diesel engine. Firstly, the matching between the boosting system and engine was investigated and optimised, and the results have been validated by the external engine testing results. In the transient process, operating the EDC, VGT and AFR properly can reduce the response time, by 0.1s to 2s; however, these methods will reduce the system efficiency. The intercooler and HP EGR has also been discussed under different air path route design. EDC operation will be affected by the hot flow from EGR if it was located downstream of the HP EGR, intercooler mainly affects either engine inlet temperature or EDC inlet temperature.

Modelling of decoupled electric turbocharger system

Chapter 5 demonstrated how the EDC increase system transient performance and low speed torque. This chapter focused on the performance of the DET engine system in both the single-stage and two-stage situation. The study considered both steady state behaviour and transient drive cycle performance based on this gasoline engine model using GT-Power. In steady state simulations, the influence of the transient operating process is simplified into quantities of steady state duration, which helps to evaluate

the E-turbo performance under various driving scenarios. The DET can generate 0.2 to 0.38 kW average power in different cycles, however, the total electric efficiency has to be bigger than 72%. In a transient study, the DET was mounted together with a single turbocharger. The feedforward control of the system has been optimised to produce better transient performance. The electricity consumption and transient response has been improved.

Comparing with the system studied in Chapter 5, this system is more complicated as it has an extra electric turbine, the controlling of the turbocharger changed from VGT control into waste-gate control, their effect on engine performance in system level is somehow similar. Their advantages and disadvantages are below:

1. With proper control design, the decoupled turbocharger system has a potential to be more efficient than the system with turbocharger and EDC, the electric turbine in LP stage generated the heat energy in the exhaust. If the electric system efficiency is higher than a certain threshold (72% in this thesis), the decoupled electric turbocharger will become viable. If the efficiency is low, then the system needs extra energy (more electricity or fuel) to achieve the same output.
2. The decoupled electric system is more expensive as it needs an extra motor-generator and a turbine. And the decoupled design is easy for packaging on real engine system.
3. The two systems in Chapter 5 and 6 still has two control mechanisms each, the system in Chapter 5 is an EDC with turbine VGT. Chapter 6 is an EDC+E-turbine (with wastegate). The decoupled system has more flexibility since the turbocharger turbine and E-turbine can be bypassed by the waste-gate, it will better help balance the engine intake flow and exhaust energy harvesting (comparing with VGT.)
4. In a more extreme case, the E-Turbine in the decoupled system will allow the user to discharge the exhaust and reduce the pumping losses (or even help engine to pump in air), although the design of turbine geometry is not efficient in region that pressure ratio is less than 1. This is an extra point that is interesting to research further.

The research in this chapter only has simulation study, there is no experiment verification for the results. Further research should be considered in real test.

Case study: Inner-insulated turbocharger research

In this Chapter, a thermally insulated turbocharger is proposed to increase the aftertreatment system inlet temperature. The steady state tests showed that the insulation could increase the T4 for the turbocharger turbine under different engine speed and load conditions. In the transient study, tiny (1.5K) temperature benefit can be observed in the experiment, which is different from simulation due to the inaccuracy of the model. In engine warm up tests, the T4 enhancement was also low, but a 2 kRPM turbo speed benefit was achieved at this process due to the increased turbine inner gas temperature. This section explained the thermal performance of the insulated turbocharger, more thermal tests should be planned in the future with the constrain of turbo operating points, a more apparent T4 benefit should be observed.

Case study: Optimization for T-PIECE-junction in the two-stage air path

This Chapter described the investigations of optimising a two-stage turbocharged engine inlet air path. Different methods have been used for the optimisation of the design of a T-piece junction in the intake side. The focus was on a non-parametric topology optimisation approach considering both the pressure drop and the efficiency of the turbocharger compressor downstream of the junction. Tosca Fluid and ANSYS Workbench are the two major software tools for the T-piece topology optimisation and CFD simulation. The T-piece junction between the electrically driven compressor (EDC) and the turbocharger compressor has been optimised for lower pressure drop and reduced swirl compared to the baseline design. The pressure drop was reduced by 0.3 kPa (15 %) and the turbocharger compressor efficiency increased by up to 2 % (compressor efficiency rise from 68 % to 70 %). Further optimisation using the ANSYS Fluent adjoint solver has also been investigated – however, these results did not offer a substantial improvement in performance over the non-parametric approach for this application.

9.2 Formalisation method of hybrid two-stage boosting system

This thesis studied the optimization of a two-stage hybrid boosting system, investigated the relationship between different components, for example, EDC, VGT, EGRs. Based on the certain findings in previous chapters, for the specifically given engine, a formulized hybrid two-stage boost system matching method can be summarized here, follows the steps below:

1. Find the quantity of airflow required by the engine, this will be the function of engine swept volume, speed, pressure and density. Select the suited size turbine, based on the turbine expansion ratio, and corrected mass flow rate and efficiency. Since the turbine is VGT type in this project, the coverage of turbine operating region on engine map also need to be considered at the same time, try to make the major area stay in the highest efficiency region.

2. With pressure ratio and corrected mass flow rate requirement, based on the turbine speed range calculated from turbine side, the right size compressor will be picked for achieving the target boost pressure with the highest efficiency, real selection procedure in this process will involve numerical interpolations of maps.

Steps 1 and 2 are generally taken by turbocharger manufacturers, after getting different combinations of compressor and turbine selections, the simulation of turbocharger and engine matching could be accomplished.

3. Simulating the turbocharger performance and its impact on engine system, selected the best combination of turbine and compressor, which should generally consider the factors below:

- Target torque in certain speed: to see if turbocharger can satisfy the boost to achieve target torque under a certain amount of mass flow.

- Turbine and compressor efficiency: look at the pulse operation state on compressor map and the typical operation region on a compressor map, let the engine load spline lies as close to the highest efficiency region as it can.
- Engine in-cylinder pressure and engine backpressure: there should be an in-cylinder pressure limit, if the engine is highly boosted, the in-cylinder pressure will be exceeded, which means the turbine is too small, a bigger turbine should be used for releasing some of the backpressure but achieve the same power on the compressor side.
- Turbine inlet and outlet temperature requirement: turbine inlet temperature is generally limited by the design of engine outlet manifold, the outlet temperature is usually required by the aftertreatment system, so a suitable size of the turbine should be picked to satisfy both these two parameters.

4. After determining the best turbine and compressor combination with engine system, verified its performance, further steps could be taken for EDC selection based on transient and low speed torque requirement, follows the key points below:

- Determine the operating region that EDC needs to be involved, either for achieving higher torque in low engine speed region or increase the transient performance. Calculate the mass flow rate limit of those operating points, select the suitable EDC that is small enough but can fully cover those mass flow range with the highest efficiency as possible as it can.
- Determine the limit of EDC operating condition, which should consider mass flow limit, surge limit, over-speeding limit, acceleration limit and over-heat limit.
- Notice: If E-turbine is also considered in the design, a proper size turbine should also be selected based on the operating region, considering the flow capacity, temperature and turbine efficiency; besides, packaging is an important issue.

5. With certain EDC and turbocharger which mounted on the given engine, then the matching between EDC and VGT turbocharger could be down in this step, mainly focus on the Boost duty allocation between turbo-compressor and EDC, there is a

compromise, during the design, the engineer can either consider let turbo-compressor work as much as it can (close to surge) to reduce the power consumption of EDC or reducing the load of turbo-compressor but rotate the EDC faster, this is actually a compromise between engine fuel consumption and battery electricity consumption (it has already been discussed in detail in D1.02). After that, the EDC controlling methodology should be designed for transient improvements. In low flow region (typically in the two-stage application, EDC are always small and operated in low flow region), this is to achieve a better transient response with lower electricity consumption.

6. After matching the turbocharger and EDC with the engine, rest of the attached components could be considered and optimized in the air-path, in THOMSON project, the following factors are considered before briefly, all of these studies are trying to increase the flow uniformity and reduce the pressure drop, gas heat loss.

- Turbocharger, EDC and intercooler position consideration: The arrangement of these three components will affect the engine inlet air temperature, operating points position on EDC and compressor map, this problem is complicated and still need to be further investigated. (The Turbocharger---Intercooler—EDC layout is used here at the beginning based on previous research experience.)
- High pressure EGR outlet position: since the EGR gas will affect the inlet flow temperature, the EDC will impact the mixing speed of EGR gas and fresh air, it needs to be considered if EDC should be put before or after EGR, in this project, EDC stays after HP-EGR outlet port since it is supposed to increase the transient mixing speed of the two gases.
- Size of intercooler: the intercooler in two-stage system will affect EDC inlet(outlet) temperature and mixed gas from EGR, so a suitable size of intercooler will increase the cooling efficiency of the system, also slightly higher inlet gas temperature will increase the engine combustion efficiency a little.
- Insulated turbocharger consideration on turbine outlet temperature optimization: this is a specific application in this project, the insulated turbocharger can exactly increase the T4 under the same operating condition, however, based on previous experiment data, if turbocharger is managed to achieve the same pressure ratio, the operation of turbocharger will be tiny

different for the insulated and non-insulated one, this will have a significant influence on heat extracting on turbine side.

- Air path T-Piece (Y-connection): this is actually a case study on the optimization of engine inlet airflow since two-stage boost system is involved, many 90-degree bended T-Piece is involved to bypass EDC, this will lead to the recirculating flow, pressure drop and reduce the flow uniformity, here the optimization of T-Piece is done to improve flow condition.

The six steps above are the primary matching and optimization process, and the key points are shown in the flow chart below:

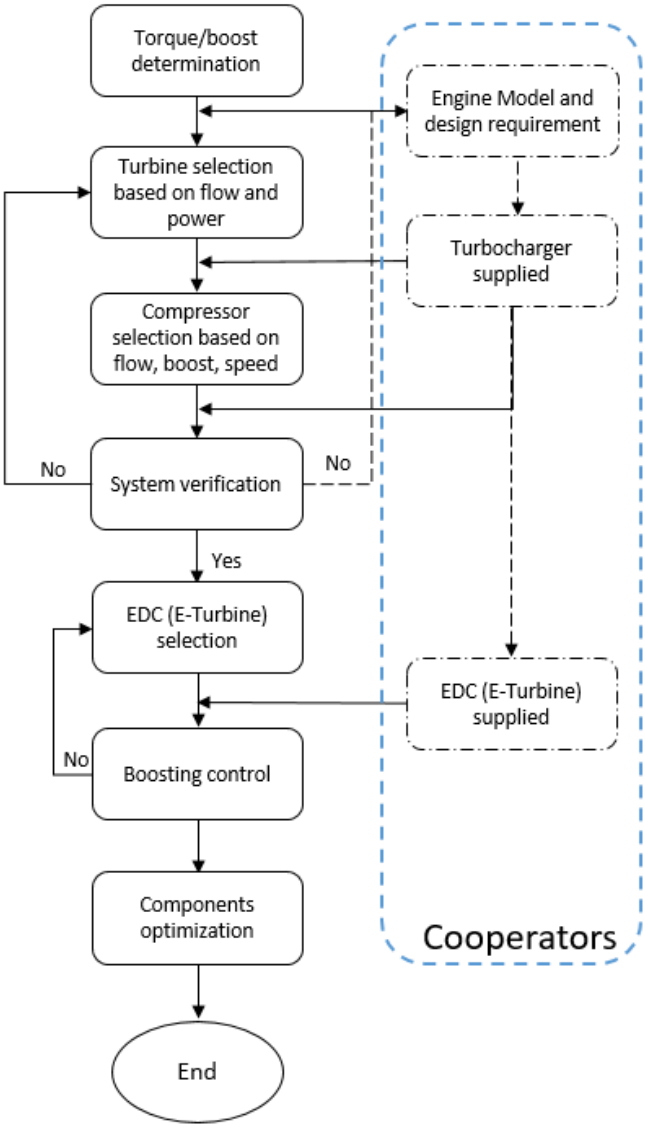

Figure 9.1 Matching process flowchart.

9.3 Limitations of the research presented in this thesis

Compared to other researches on the two-stage or electric turbocharger research, this thesis focuses more on system performance, with simulations and experiments. However, due to the inexperience in experiment design and transient control, some transient results can not directly demonstrate the supposed objectives. Engine performance cannot be regarded as a factor to evaluate the air path performance, because the test rig is not fully engine stand, the compressor air path is fully separated from the system.

In simulation parts, different models have been used for a different research topic, and there are some intersections however more differences. Most of the simulation results in this thesis are qualified to explain the benefit or weakness of electric boosting devices, however the numbers generated from the models cannot be regarded as 'real', as they were not validated by the experiments, due to the limitation of test rig design.

For thermal tests, due to the difficulties of controlling the turbine inlet temperature, and the thermal inertial effects of different components. It is unable to perfectly achieve the back to back comparison between insulated and standard turbocharger, especially in transient scenarios. T3 is hard to be matched, and the heat stored in the system cannot be ensured to be the same. Also, the results show that under the same boundary condition, insulated turbocharger gets higher efficiency but the outlet flow temperature is still not as high as simulation. It is hard to describe the internal thermal changes inside the insulation in the current stage, as 1D modelling method has its own limitation, geometry differences were ignored, which thus plays a very significant role in this research.

3D T-Piece optimization is the last research of this thesis, this is just an initial step for the whole design, as the optimized geometry haven't been further simplified for manufacturing, and there is no related experiment research to validate the model.

9.4 Future work

This thesis mainly focuses on the boosting system optimization, attached with two case studies of the air path components, insulated turbine and T-Piece. The air path has been tested and validated on the EGS rig.

The hybrid boosting system could be further investigated on engine stand test rig. The simulation results in Chapter 5 and Chapter 6 already demonstrated that EDC and E-turbine could increase the engine boost pressure and harvest energy from exhaust without the increasing of pumping loss; there also engine transient torque benefit. It is necessary to put the air path onto the engine stand rig to validate those simulation results. During these processes, if possible, mass flow meter, thermocouples and Lambda CAN with reaction higher frequency can be used, these will help increase the transient measurements accuracy.

In the thermal research for the insulated turbocharger, the heat transfer between the turbine, bearing housing and compressor could be considered further. Although the model is a one-dimensional design which is not enough to describe the turbocharger thermal performance in detail, Chapter 7 shows it still helps to improve the simulation accuracy for the aftertreatment system. In the experiment side, more thermocouples could be attached to the turbine housing. With more thermal nodes on it, by applying the turbine housing temperature into simulation, the calibration of heat transfer coefficients will be improved. At last, more tests could be done on an engine stand for the insulated turbocharger; in Chapter 7, it can be seen that the insulation can improve turbine efficiency under the same boundary condition; however just tiny T4 enhancement was achieved. The VGT controller can be re-designed to maintain the turbo speed in the tests so that it can be ensured turbocharger was operated on the same points, T4 benefit is supposed to be more significant.

For the T-Piece optimization part, only two cases were studied in this thesis, which represents the high flow and low flow case, respectively. It is valuable to run more cases for transient situation or single stage situation (when EDC is bypassed).

Reference

SAE Power Test Code Standards C, 1995. SUPERCHARGER TESTING STANDARD. SAE International.

Aeristech, 2016. *Full electric Turbocharger* [Online]. Available from: http://www.aeristech.co.uk/full-electric-turbocharger-technology/ [Accessed 10/10 2019].

Amann, M., Alger, T. & Mehta, D., 2011. The effect of EGR on low-speed pre-ignition in boosted SI engines. *SAE International Journal of Engines,* 4(1), pp. 235-245.

Arnold, S., 2009. Single sequential turbocharger: a new boosting concept for ultra-low emission diesel engines. *SAE International Journal of Engines,* 1(1), pp. 232-239.

Arsie, I., Cricchio, A., Pianese, C., De Cesare, M. & Nesci, W., 2014. *A comprehensive powertrain model to evaluate the benefits of electric turbo compound (ETC) in reducing CO2 emissions from small diesel passenger cars.* (0148-7191). SAE Technical Paper.

Assanis, D., Ekchian, J., Frank, R. & Heywood, J., 1985. A computer simulation of the turbocharged turbo compounded diesel engine system: A description of the thermodynamic and heat transfer models.

Attard, W., 2007. *Small engine performance limits-turbocharging, combustion or design.* SAE Technical Paper Series.

Atzler, F., Wegerer, M., Mehne, F., Rohrer, S., Rathgeber, C. & Fischer, S., 2015. *Fuel Consumption and Emissions Effects in Passenger Car Diesel Engines through the Use of a Belt Starter Generator.* (0148-7191). SAE Technical Paper.

Avola, C., Copeland, C., Burke, R. & Brace, C., *Numerical investigation of two-stage turbocharging systems performance*. In: ASME 2016 Internal Combustion Engine Division Fall Technical Conference, 2016. American Society of Mechanical Engineers Digital Collection.

Avola, C., Copeland, C., Duda, T., Burke, R., Akehurst, S. & Brace, C., 2015. *Review of Turbocharger Mapping and 1D Modelling Inaccuracies with Specific Focus on Two-Stag Systems.* (0148-7191). SAE Technical Paper.

Baar, R., Biet, C., Boxberger, V., Mai, H. & Zimmermann, R., 2014. New evaluation of turbocharger components based on turbine outlet temperature measurements in adiabatic conditions. *ISROMAC-15, Honolulu, HI, Feb*, pp. 24-28.

Backlund, O., Keen, P., Rydquist, J., Giselmo, K. & Sundin, L., 1991. *Volvo's MEP and PCP Engines: Combining Environmental Benefit with High Performance.* (0148-7191). SAE Technical Paper.

Bahadori, A., 2014. Chapter 5 - Gas Compressors. *Natural Gas Processing*, 1st Edition. Gulf Professional Publishing. pp. 223-273.

Baines, N., Wygant, K.D. & Dris, A., 2010. The analysis of heat transfer in automotive turbochargers. *Journal of Engineering for Gas Turbines and Power,* 132(4), p. 042301.

Baines, N.C., 2005. *Fundamentals of turbocharging.* Concepts NREC White River Junction, Vermont.

Balis, C., Middlemass, C. & Shahed, S., 2003. *Design & development of e-turbo for SUV and light truck applications. (No. CONF-200308-109). Garrett Engine Boosting Systems (US).*

Bell, C., Zimmerle, D., Bradley, T., Olsen, D. & Young, P., 2016. Scalable turbocharger performance maps for dynamic state-based engine models. *International Journal of Engine Research,* 17(7), pp. 705-712.

Benson, R.S. & Svetnicka, F., 1974. Two-stage turbocharging of diesel engines: a matching procedure and an experimental investigation. *SAE Transactions*, pp. 2749-2766.

Bhinder, F., 1984. *Supercharging compressors-problems and potential of the various alternatives.* (0148-7191). SAE Technical Paper.

Bielaczyc, P., Woodburn, J. & Szczotka, A., 2016. *Exhaust emissions of gaseous and solid pollutants measured over the NEDC, FTP-75 and WLTC chassis dynamometer driving cycles.* (0148-7191). SAE Technical Paper.

Bohn, D., Heuer, T. & Kusterer, K., 2005. Conjugate flow and heat transfer investigation of a turbo charger. *J. Eng. Gas Turbines Power,* 127(3), pp. 663-669.

BorgWarner, 2017. *Design and Function of a Turbocharger-Turbine\BorgWarner Turbo Systems.* [Online]. Available from: http://www.turbos.bwauto.com/products/turbochargerTurbine.aspx [Accessed 15/10 2019].

BorgWarnerTurboSytems, 2018. *BorgWarner Turbo Sytems compressor maps* [Online]. Available from: https://www.quora.com/What-is-the-power-loss-for-diesel-engine-at-altitude [Accessed 09/12 2019].

BOSCH, 2019. *48V battery-Compact energy storage for low-voltage hybrid system* [Online]. Available from: https://www.bosch-mobility-solutions.com/en/products-and-services/passenger-cars-and-light-commercial-vehicles/powertrain-systems/electric-drive/48v-battery/ [Accessed 10/23 2019].

Breitbach, H., Metz, D., Weiske, S. & Spinner, G., 2015. Application and Design of the Electrically Driven Compressor from BorgWarner. *MTZ worldwide,* 76(10), pp. 16-21.

Buckingham, E., 1914. On physically similar systems; illustrations of the use of dimensional equations. *Physical review*, 4(4), p. 345.

Burke, R., Copeland, C., Duda, T. & Rayes-Belmote, M., 2016. Lumped capacitance and three-dimensional computational fluid dynamics conjugate heat transfer modeling of an automotive turbocharger. *Journal of Engineering for Gas Turbines and Power,* 138(9), p. 092602.

Burke, R., Liu, Y., Vijayakumar, R., Werner, J. & Dalby, J., 2019. *Inner-Insulated Turbocharger Technology to Reduce Emissions and Fuel Consumption from Modern Engines.* (0148-7191). SAE Technical Paper.

Burke, R., Vagg, C., Chalet, D. & Chesse, P., 2015. Heat transfer in turbocharger turbines under steady, pulsating and transient conditions. *International Journal of Heat and Fluid Flow*, 52, pp. 185-197. SAE Technical Paper.

Burke, R.D., 2016. A Numerical Study of the Benefits of Electrically Assisted Boosting Systems. *Journal of Engineering for Gas Turbines and Power,* 138(9).

CASCOUSA, 2019. *Dynamic Displacement Compressors* [Online]. Available from: https://cascousa.com/compressed-air-101/types-of-compressors/dynamic-displacement-compressors/ [Accessed 09/12 2019]. SAE Technical Paper.

Casey, M., 1985. The effects of Reynolds number on the efficiency of centrifugal compressor stages. *Journal of Engineering for Gas Turbines and Power,* 107(2), pp. 541-548.

Chen, S.K. & Flynn, P.F., 1965. *Development of a single cylinder compression ignition research engine.* (0148-7191). SAE Technical Paper.

Conley, B., Sadeghi, F., Griffith, R.C. & McCormack, J.W., 2019. Experimental Investigation of the Dynamic Loads in a Ball Bearing Turbocharger. *Journal of Tribology*, 141(11).

Cormerais, M., Chesse, P. & Hetet, J.-F., 2009. Turbocharger heat transfer modeling under steady and transient conditions. *International Journal of Thermodynamics,* 12(4), pp. 193-202.

Cummins, 2019. *How a Turbocharger Works* [Online]. Available from: https://www.cummins.com/components/turbo-technologies/turbochargers/how-a-turbocharger-works [Accessed 30/09 2019].

Dalby, J., Fiquet, F., Ward, A., Stoffels, H., Burke, R., Zaldua-Moreno, N., Neveling, M., Liu, Y. & Pace, L., 2019. *Hybrid Powertrain Technology Assessment through an Integrated Simulation Approach.* (0148-7191). SAE Technical Paper.

DBS, 2017. *DBS Electric Supercharger (eSC) for Engine Downsizing* [Online]. Available from: https://www.smmt.co.uk/2017/06/dbs-electric-supercharger-esc-engine-downsizing/ [Accessed].

De Bellis, V., Bozza, F., Teodosio, L. & Valentino, G., 2017. Experimental and numerical study of the water injection to improve the fuel economy of a small size turbocharged SI engine. *SAE International Journal of Engines,* 10(2), pp. 550-561.

De Cesare, M., Cavina, N. & Brugnoni, E., 2019. *Conceptual Design and Analytic Assessment of 48V Electric Hybrid Powertrain Architectures for Passenger Cars.* (0148-7191). SAE Technical Paper.

Dimitriou, P., Burke, R., Zhang, Q., Copeland, C. & Stoffels, H., 2017. Electric turbocharging for energy regeneration and increased efficiency at real driving conditions. *Applied Sciences,* 7(4), p. 350.

Divekar, P.S., Ayalew, B. & Prucka, R., 2010. *Coordinated electric supercharging and turbo-generation for a diesel engine.* (0148-7191). SAE Technical Paper.

Drury, W., Patel, C., Atkins, A. & Wearing, A., 2019. High Power Density, 48V Electrified Drivetrain Technology for Future Hybrid and Electric Vehicles. *SAE International Journal of Advances and Current Practices in Mobility,* 1(2019-26-0034).

Duda, T., 2017. Turbocharger performance and surge definition on a steady flow turbocharger test stand.

Dufour, G., Carbonneau, X., Cazalbou, J.-B. & Chassaing, P., Practical use of similarity and scaling laws for centrifugal compressor design. In: ASME Turbo Expo 2006: Power for Land, Sea, and Air, 2006. American Society of Mechanical Engineers Digital Collection, pp. 1131-1140.

Eiser, A., Fitzen, M., Heiduk, T., Mendle, J., Zahlmann, S. & Bäumel, F., 2009. 3.0 l TFSI. *MTZ worldwide,* 70(9), pp. 10-18.

Ekberg, K. & Eriksson, L., 2017. Improving fuel economy and acceleration by electric turbocharger control for heavy duty long haulage. *IFAC-PapersOnLine,* 50(1), pp. 11052-11057.

EnggCyclopedia, 2019. *Compressors* [Online]. Available from: https://www.enggcyclopedia.com/2011/05/compressors/ [Accessed 09/12 2019].

Ernst, B., Kammeyer, J. & Seume, J.R., Improved map scaling methods for small turbocharger compressors. In: ASME 2011 Turbo Expo: Turbine Technical Conference and Exposition, 2011. American Society of Mechanical Engineers Digital Collection, pp. 733-744.

Evans, D. & Ward, A., 2005. *Minimising turbocharger whoosh noise for diesel powertrains.* (0148-7191). SAE Technical Paper.

Franco, V. & Mock, P., 2015. The European real-driving emissions regulation. *The International Council on Clean Transportation*.

Fraser, N., Blaxill, H., Lumsden, G. & Bassett, M., 2009. Challenges for increased efficiency through gasoline engine downsizing. *SAE International Journal of Engines*, 2(1), pp. 991-1008.

Fricke, F., Bhardwaj, O.P., Holderbaum, B., Scofield, T., Grußmann, E. & Kollmeier, M., 2016. *Investigation of Insulated Exhaust Manifolds and Turbine Housings in Modern Diesel Engines for Emissions and Fuel Consumption Reduction.* (0148-7191). SAE Technical Paper.

Galindo, J., Navarro, R., García-Cuevas, L.M., Tarí, D., Tartoussi, H. & Guilain, S., 2019. A zonal approach for estimating pressure ratio at compressor extreme off-design conditions. *International Journal of Engine Research,* 20(4), pp. 393-404.

Galindo, J., Serrano, J., Climent, H. & Varnier, O., 2010. Impact of two-stage turbocharging architectures on pumping losses of automotive engines based on an analytical model. *Energy Conversion and Management,* 51(10), pp. 1958-1969.

Golloch, R. & Merker, G.P., 2005. Downsizing bei verbrennungsmotoren. *MTZ-Motortechnische Zeitschrift,* 66(2), pp. 126-131.

Gurney, D., 2001. *The design of turbocharged engines using 1D simulation.* (0148-7191). SAE Technical Paper.

Hamedi, M., Doustdar, O., Tsolakis, A. & Hartland, J., 2019. Thermal energy storage system for efficient diesel exhaust aftertreatment at low temperatures. *Applied energy,* 235, pp. 874-887.

Hasegawa, R. & Yanagihara, H., 2003. HCCI combustion in DI diesel engine. *SAE transactions*, pp. 1070-1077.

Hawley, J., Wallace, F., Cox, A., Horrocks, R. & Bird, G., 1999. Variable geometry turbocharging for lower emissions and improved torque characteristics. *Proceedings of the Institution of Mechanical Engineers, Part D: Journal of Automobile Engineering*, 213(2), pp. 145-159.

Heywood, J., 1988. *Internal Combustion Engine Fundamentals.* McGraw-Hill Education.

HONDA, 2019. *VTEC TURBO-The New Era Turbo Engine* [Online]. Available from: https://global.honda/innovation/technology/automobile/Vtec-turbo-picturebook.html [Accessed 09/12 2019].

Hopf, A., Bartsch, G., Krämer, F. & Weber, C., 2017. *CFD topology and shape optimization for port development of integrated exhaust manifolds.* (0148-7191). SAE Technical Paper.

Hopmann, U. & Algrain, M.C., 2003. *Diesel engine electric turbo compound technology.* (0148-7191). SAE Technical Paper.

Hu, B., 2016. *Application of divided exhaust period and variable drive supercharging concept for a downsized gasoline engine.* University of Bath UK.

Hu, B., Tang, H., Akehurst, S., De Freitas, A., Burtt, D. & Shawe, J., 2015. *Modelling the Performance of the Torotrak V-Charge Variable Drive Supercharger System on a 1.0 L GTDI-Preliminary Simulation Results.* (0148-7191). SAE Technical Paper.

Hudson, C., Gao, X. & Stone, R., 2001. Knock measurement for fuel evaluation in spark ignition engines. *Fuel,* 80(3), pp. 395-407.

Hyvönen, J., Haraldsson, G. & Johansson, B., 2003. Supercharging HCCI to extend the operating range in a multi-cylinder VCR-HCCI engine. *SAE transactions*, pp. 2456-2468.

Ibaraki, S., Yamashita, Y., Sumida, K., Ogita, H. & Jinnai, Y., 2006. Development of the 'hybrid turbo,'an electrically assisted turbocharger. *Mitsubishi Heavy Ind. Tech. Rev,* 43(3), pp. 1-5.

Incropera, F. & DeWitt, D., 1985. Introduction to heat transfer.

Jääskeläinen, H., 2016. *Variable Geometry Turbochargers* [Online]. DieselNet.com. Available from: https://www.dieselnet.com/tech/air_turbo_vgt.php [Accessed 01/10 2019].

Japikse, D. & Baines, N., 1994. *Introduction to turbomachinery.*

Johansson, S., Nilsson, P.H., Ohlsson, R. & Rosén, B.-G., 2011. Experimental friction evaluation of cylinder liner/piston ring contact. *Wear,* 271(3-4), pp. 625-633.

Johnson, T. & Joshi, A., 2018. Review of vehicle engine efficiency and emissions. *SAE International Journal of Engines,* 11(2018-01-0329), pp. 1307-1330.

Karamanis, N. & Martinez-Botas, R., 2002. Mixed-flow turbines for automotive turbochargers: steady and unsteady performance. *International Journal of Engine Research,* 3(3), pp. 127-138.

Katrašnik, T., Trenc, F., Medica, V. & Markič, S., 2005. An analysis of turbocharged diesel engine dynamic response improvement by electric assisting systems. *Journal of engineering for gas turbines and power,* 127(4), pp. 918-926.

Kawamoto, A., Takahashi, Y., Koiken, T. & Nakamura, F., 2001. *Variable geometry system turbocharger for passenger car Diesel engine.* (0148-7191). SAE Technical Paper.

Keller, R., Scharrer, J. & Pelletti, J., 1996. *Alternative performance turbocharger bearing design.* (0148-7191). SAE Technical Paper.

Kern, M., Horn, W., Hiller, S.-J. & Staudacher, S., 2011. Effects of tip injection on the performance of a multi-stage high-pressure compressor. *CEAS Aeronautical Journal,* 2(1-4), pp. 99-110.

King, J., Heaney, M., Saward, J., Fraser, A., Criddle, M., Cheng, T., Morris, G. & Bloore, P., Hyboost: An intelligently electrified optimised downsized gasoline engine concept. In: Proceedings of the FISITA 2012 World Automotive Congress, 2013. Springer, pp. 483-496.

Kirchner, T. & Eigenberger, G., 1996. Optimization of the cold-start behaviour of automotive catalysts using an electrically heated pre-catalyst. *Chemical Engineering Science,* 51(10), pp. 2409-2418.

Kleeberg, H., Tomazic, D., Lang, O. & Habermann, K., 2006. *Future potential and development methods for high output turbocharged direct injected gasoline engines.* (0148-7191). SAE Technical Paper.

Knoll, M., Kühn, M. & Boettcher, J., 2018. Verbessertes Thermomanagement durch neue Isolationssysteme. *MTZ-Motortechnische Zeitschrift,* 79(2), pp. 52-57.

Kopeliovich, D., 2017. *Ecological Aspects Of Engine Bearings* [Online]. SubsTech. Available from: http://www.substech.com/dokuwiki/doku.php?id=ecological_aspects_of_engine_bearings [Accessed 23/07 2019].

Korin, E., Reshef, R., Tshernichovesky, D. & Sher, E., 1999. Reducing cold-start emission from internal combustion engines by means of a catalytic converter embedded in a phase-change material. *Proceedings of the institution of mechanical engineers, Part D: Journal of Automobile Engineering,* 213(6), pp. 575-583.

Kresse, T. & Rubbert, S., 2011. Loading device for internal-combustion engine has turbine shaft and compressor shaft of electrical machine which are propelled as driving motor or generator operated electrical machine over machine shaft. *DE Patent 102010011027 A,* 1.

Kunde, O., Hansen, J., Zenner, T., Kapus, P., Obst, C., Queenan, B. & Bjornesson, H., The new 2.0 SCTi EcoBoost gasoline engine from Ford. In: 19th Aachen Colloquium, 2010.

Kurzke, J. & Riegler, C., A new compressor map scaling procedure for preliminary conceptional design of gas turbines. In: ASME Turbo Expo 2000: Power for Land, Sea, and Air, 2000. American Society of Mechanical Engineers Digital Collection.

Lake, T., Stokes, J., Murphy, R., Osborne, R. & Schamel, A., 2004. *Turbocharging concepts for downsized DI gasoline engines.* (0148-7191). SAE Technical Paper.

Lecointe, B. & Monnier, G., 2003. *Downsizing a gasoline engine using turbocharging with direct injection.* (0148-7191). SAE Technical Paper.

Lee, B., 2009. Dual-Stage Boosting Systems: Modeling of Configurations, Matching and Boost Control Options.

Lee, B., Filipi, Z., Assanis, D. & Jung, D., 2009a. Simulation-based assessment of various dual-stage boosting systems in terms of performance and fuel economy improvements. *SAE International Journal of Engines,* 2(1), pp. 1335-1346.

Lee, B., Jung, D., Assanis, D. & Filipi, Z., Dual-stage turbocharger matching and boost control options. In: ASME 2008 internal combustion engine division spring technical conference, 2009b. American Society of Mechanical Engineers Digital Collection, pp. 267-277.

Lee, W., Schubert, E., Li, Y., Li, S., Bobba, D. & Sarlioglu, B., Electrification of turbocharger and supercharger for downsized internal combustion engines and hybrid electric vehicles-benefits and challenges. In: 2016 IEEE Transportation Electrification Conference and Expo (ITEC), 2016a. IEEE, pp. 1-6.

Lee, W., Schubert, E., Li, Y., Li, S., Bobba, D. & Sarlioglu, B., 2016b. Overview of electric turbocharger and supercharger for downsized internal combustion engines. *IEEE Transactions on Transportation Electrification,* 3(1), pp. 36-47.

Lefebvre, A. & Guilain, S., Study of different boosting technologies and their effect on the transient response of a very downsized Diesel engine. In: SIA Diesel Powertrain Congress, Conference Proceedings, 2012.

Leufvén, O., 2010. *Compressor modeling for control of automotive two stage turbochargers.* Linköping University Electronic Press.

Lim, M.-S., Kim, J.-M., Hwang, Y.-S. & Hong, J.-P., 2016. Design of an ultra-high-speed permanent-magnet motor for an electric turbocharger considering speed response characteristics. *IEEE/ASME Transactions on Mechatronics,* 22(2), pp. 774-784.

Liu, Y., Burke, R.D., Akehurst, S. and Zhang, Q., 2017, October. Numerical Investigation Into the Performance and Efficiency Trade-Off for a Mechanically Decoupled Electric Boosting System. In ASME 2017 Internal Combustion Engine Division Fall Technical Conference. American Society of Mechanical Engineers Digital Collection.

Liu, Y., Vijayakumar, R. and Burke, R., 2018, November. Analysis of the opportunities and trade-offs for an 48v electrified air path. In ASME 2018 Internal Combustion Engine Division Fall Technical Conference. American Society of Mechanical Engineers Digital Collection.

Lüddecke, B., Filsinger, D. & Ehrhard, J., 2012. On mixed flow turbines for automotive turbocharger applications. *International Journal of rotating machinery,* 2012.

Luján, J.M., Bermúdez, V., Piqueras, P. & García-Afonso, Ó., 2015. Experimental assessment of pre-turbo aftertreatment configurations in a single stage turbocharged diesel engine. Part 1: Steady-state operation. *Energy,* 80, pp. 599-613.

Luján, J.M., Serrano, J.R., Piqueras, P. & Diesel, B., 2019. Turbine and exhaust ports thermal insulation impact on the engine efficiency and aftertreatment inlet temperature. *Applied energy,* 240, pp. 409-423.

Lumsden, G., OudeNijeweme, D., Fraser, N. & Blaxill, H., 2009. Development of a turbocharged direct injection downsizing demonstrator engine. *SAE International Journal of Engines,* 2(1), pp. 1420-1432.

Luttermann, C. & Mährle, W., 2007. *BMW High Precision Fuel Injectionin Conjunction with Twin-Turbo Technology: a Combination for Maximum Dynamic and High Fuel Efficiency.* (0148-7191). SAE Technical Paper.

Marelli, S., Gandolfi, S. & Capobianco, M., 2017. *Heat transfer effect on performance map of a turbocharger turbine for automotive application.* (0148-7191). SAE Technical Paper.

Marelli, S., Marmorato, G., Capobianco, M. & Boulanger, J.-M., 2016. *Towards the Direct Evaluation of Turbine Isentropic Efficiency in Turbocharger Testing.* (0148-7191). SAE Technical Paper.

Marelli, S., Usai, V., Capobianco, M., Montenegro, G., Della Torre, A. & Onorati, A., 2019. *Direct Evaluation of Turbine Isentropic Efficiency in Turbochargers: CFD Assisted Design of an Innovative Measuring Technique.* (0148-7191). SAE Technical Paper.

Matsura, Y., Nakazawa, N., Kobayashi, Y., Ogita, H. & Kawatani, T., 1992. *Effects of various methods for improving vehicle startability and transient response of turbocharged diesel trucks.* (0148-7191). SAE Technical Paper.

Misté, G.A. & Benini, E., Performance of a turboshaft engine for helicopter applications operating at variable shaft speed. In: ASME 2012 Gas Turbine India Conference, 2012. American Society of Mechanical Engineers, pp. 701-715.

Miyashita, K., Kurasawa, M., Matsuoka, H., Ikeya, N. & Nakamura, F., 1987. Development of high efficiency ball-bearing turbocharger. *SAE transactions,* pp. 466-473.

Mizythras, P., Boulougouris, E. & Theotokatos, G., A methodology for single turbocharger-marine engine matching. In: 2nd International Conference on Modelling and Optimisation of Ship Energy Systems, 2019. University of Strathclyde, pp. 241-247.

Mock, P., Kühlwein, J., Tietge, U., Franco, V., Bandivadekar, A. & German, J., 2014. The WLTP: How a new test procedure for cars will affect fuel consumption values in the EU. *International Council on Clean Transportation,* 9, pp. 35-47.

Müller, M., Hendricks, E. & Sorenson, S.C., 1998. *Mean value modelling of turbocharged spark ignition engines.* (0148-7191). SAE Technical Paper.

Navrátil, J., 2006. 2-stage turbocharger matching for a light-duty diesel engine. *Technical Report, Engine Simulation, Ricardo Consulting Engineers Ltd, Prague, Czech Republic*.

Nelson, S., Filipi, Z. & Assanis, D., 2003. The use of neural nets for matching fixed or variable geometry compressors with diesel engines. *Journal of Engineering for Gas Turbines and Power,* 125(2), pp. 572-579.

Olmeda, P., Dolz, V., Arnau, F. & Reyes-Belmonte, M.A., 2013. Determination of heat flows inside turbochargers by means of a one dimensional lumped model. *Mathematical and computer modelling,* 57(7-8), pp. 1847-1852.

Osada, H., Aoyagi, Y. & Shimada, K., 2012. Diesel Combustion Improvement Using High Boost, Wide Range and High Rate EGR in a Single Cylinder Engine (Third Report). *Transactions of Society of Automotive Engineers of Japan,* 43(4).

Ostrowski, G., Neely, G.D., Chadwell, C.J., Mehta, D. & Wetzel, P., 2012. *Downspeeding and supercharging a diesel passenger car for increased fuel economy.* (0148-7191). SAE Technical Paper.

Pallotti, P., Torella, E., New, J., Criddle, M. & Brown, J., 2003. *Application of an electric boosting system to a small, four-cylinder SI engine.* (0148-7191). SAE Technical Paper.

Panting, J., Pullen, K. & Martinez-Botas, R., 2001. Turbocharger motor-generator for improvement of transient performance in an internal combustion engine. *Proceedings of the Institution of Mechanical Engineers, Part D: Journal of Automobile Engineering,* 215(3), pp. 369-383.

Pavlovic, J., Ciuffo, B., Fontaras, G., Valverde, V. & Marotta, A., 2018. How much difference in type-approval CO2 emissions from passenger cars in Europe can be expected from changing to the new test procedure (NEDC vs. WLTP)? *Transportation Research Part A: Policy and Practice,* 111, pp. 136-147.

Payri, F., Olmeda, P., Arnau, F.J., Dombrovsky, A. & Smith, L., 2014. External heat losses in small turbochargers: Model and experiments. *Energy,* 71, pp. 534-546.

Pesiridis, A., Salim, S. & Martinez-Botas, R., Turbocharger matching methodology for improved exhaust energy recovery. In: Proc. of the 10th Int. Conf. on Turbocharging and Turbochargers, 2012. pp. 203-218.

Plianos, A. & Stobart, R., 2008. *Modeling and control of diesel engines equipped with a two-stage turbo-system.* (0148-7191). SAE Technical Paper.

Ramanathan, K., West, D.H. & Balakotaiah, V., 2004. Optimal design of catalytic converters for minimizing cold-start emissions. *Catalysis today,* 98(3), pp. 357-373.

Reifarth, S., 2010. EGR-systems for diesel engines (Doctoral dissertation).

Rick, A. & Sisk, B., 2015. *A simulation based analysis of 12V and 48V microhybrid systems across vehicle segments and drive cycles.* (0148-7191).

Romagnoli, A., Manivannan, A., Rajoo, S., Chiong, M., Feneley, A., Pesiridis, A. & Martinez-Botas, R., 2017. A review of heat transfer in turbochargers. *Renewable and Sustainable Energy Reviews,* 79, pp. 1442-1460.

Romagnoli, A. & Martinez-Botas, R., Heat transfer on a turbocharger under constant load points. In: ASME Turbo Expo 2009: Power for Land, Sea, and Air, 2009. American Society of Mechanical Engineers, pp. 163-174.

Romagnoli, A. & Martinez-Botas, R., 2012. Heat transfer analysis in a turbocharger turbine: An experimental and computational evaluation. *Applied Thermal Engineering,* 38, pp. 58-77.

Rose, A., 2013. *Application of a Continuously Variable Transmission to Engine Boosting and Exhaust Energy Recovery Systems.* University of Bath.

Rose, A.T., Akehurst, S. & Brace, C., 2011. Modelling the performance of a continuously variable supercharger drive system. *Proceedings of the Institution of Mechanical Engineers, Part D: Journal of Automobile Engineering,* 225(10), pp. 1399-1414.

Ryder, O., The design and testing of an electrically assisted turbocharger for heavy duty diesel engines. In: I Mech E Turbocharger Conference (2006.5), 2006.

San Andres, L., Rivadeneira, J.C., Gjika, K., Groves, C. & LaRue, G., 2006. Rotordynamics of Small Turbochargers Supported on Floating Ring Bearings—Highlights in Bearing Analysis and Experimental Validation. *Journal of Tribology,* 129(2), pp. 391-397.

Saulnier, S. & Guilain, S., 2004. *Computational Study of Diesel Engine Downsizing Using Two-StageTurbocharging.* (0148-7191). SAE Technical Paper.

Schumann, F., Sarikoc, F., Buri, S., Kubach, H. & Spicher, U., 2013. Potential of spray-guided gasoline direct injection for reduction of fuel consumption and simultaneous compliance with stricter emissions regulations. *International Journal of Engine Research,* 14(1), pp. 80-91.

Serrano, J., Guardiola, C., Dolz, V., Tiseira, A. & Cervello, C., 2007. *Experimental study of the turbine inlet gas temperature influence on turbocharger performance.* (0148-7191). SAE Technical Paper.

Serrano, J., Olmeda, P., Arnau, F., Reyes-Belmonte, M. & Lefebvre, A., 2013. Importance of heat transfer phenomena in small turbochargers for passenger car applications. *SAE International Journal of Engines,* 6(2), pp. 716-728.

Serrano, J., Tiseira, A., Usaquen, T.R. & Mijotte, G., 2017. *Fast 2-D heat transfer model for computing internal temperatures in automotive turbochargers.* (0148-7191). SAE Technical Paper.

Serrano, J.R., Guardiola, C., Piqueras, P. & Angiolini, E., 2014. *Analysis of the aftertreatment sizing for pre-turbo DPF and DOC exhaust line configurations.* (0148-7191). SAE Technical Paper.

Serrano, J.R., Olmeda, P., Arnau, F.J., Reyes-Belmonte, M.A. & Tartoussi, H., 2015. A study on the internal convection in small turbochargers. Proposal of heat transfer convective coefficients. *Applied Thermal Engineering,* 89, pp. 587-599.

Shaaban, S., 2004. Experimental investigation and extended simulation of turbocharger non-adiabatic performance. Thesis. Hannover: Universität.

Shahed, S.M., 2006. *An analysis of assisted turbocharging with light hybrid powertrain.* (0148-7191). SAE Technical Paper.

Sirakov, B. & Casey, M., 2013. Evaluation of heat transfer effects on turbocharger performance. *Journal of Turbomachinery,* 135(2), p. 021011.

Sjöberg, M. & Dec, J.E., 2005. An investigation into lowest acceptable combustion temperatures for hydrocarbon fuels in HCCI engines. *Proceedings of the Combustion Institute,* 30(2), pp. 2719-2726.

Stoffels, H., Dunstheimer, J. & Hofmann, C., 2017. *Potential of Electric Energy Recuperation by Means of the Turbocharger on a Downsized Gasoline Engine.* (0148-7191).

Stoffels, H. & Schroeer, M., 2003. NVH aspects of a downsized turbocharged gasoline powertrain with direct injection. *SAE transactions*, pp. 2101-2109.

Stone, C., 1988. The efficiency of Roots compressors and compressors with fixed internal compression. *Proceedings of the Institution of Mechanical Engineers, Part A: Power and Process Engineering,* 202(3), pp. 199-205.

Stone, R., 1999. Introduction to internal combustion engines.

Tancrez, M., Galindo, J., Guardiola, C., Fajardo, P. & Varnier, O., 2011. Turbine adapted maps for turbocharger engine matching. *Experimental thermal and fluid science,* 35(1), pp. 146-153.

Tang, H., 2016. *Application of variable geometry turbine on gasoline engines and the optimisation of transient behaviours.* Thesis. University of Bath.

Tavčar, G., Bizjan, F. & Katrašnik, T., 2011. Methods for improving transient response of diesel engines–influences of different electrically assisted turbocharging topologies. *Proceedings of the Institution of Mechanical Engineers, Part D: Journal of Automobile Engineering,* 225(9), pp. 1167-1185.

Teng, C. & Homco, S., 2009. Investigation of compressor whoosh noise in automotive turbochargers. *SAE International Journal of Passenger Cars-Mechanical Systems,* 2(2009-01-2053), pp. 1345-1351.

Terdich, N., 2014. Impact of electrically assisted turbocharging on the transient response of an off-highway diesel engine.

Terdich, N., Martinez-Botas, R.F., Romagnoli, A. & Pesiridis, A., 2014. Mild hybridization via electrification of the air system: electrically assisted and variable geometry turbocharging impact on an off-road diesel engine. *Journal of Engineering for Gas Turbines and Power,* 136(3), p. 031703.

Thirouard, M., Mendez, S., Pacaud, P., Chmielarczyk, V., Ambrazas, D., Garsi, C., Lavoisier, F. & Barbeau, B., 2009. *Potential to improve specific power using very high injection pressure in HSDI diesel engines.* (0148-7191). SAE Technical Paper.

Thomas, A.M., Samuel, J. & Ramesh, A., Mean-Line Modelling of a Variable Geometry Turbocharger (VGT) and Prediction of the Engine-Turbocharger Coupled Performance. In: ASME 2017 Gas Turbine India Conference, 2018. American Society of Mechanical Engineers Digital Collection.

Timmann, M. & Renz, M., 48V at Mercedes-Benz–options for further applications. In: 14. Internationales Stuttgarter Symposium, 2014. Springer, pp. 645-663.

Turkcan, A., Altinkurt, M.D., Coskun, G. & Canakci, M., 2018. Numerical and experimental investigations of the effects of the second injection timing and alcohol-gasoline fuel blends on combustion and emissions of an HCCI-DI engine. *Fuel,* 219, pp. 50-61.

Turner, J., Pearson, R. & Kenchington, S., 2005. Concepts for improved fuel economy from gasoline engines. *International Journal of Engine Research,* 6(2), pp. 137-157.

Turner, J., Popplewell, A., Marshall, D., Johnson, T., Barker, L., King, J., Martin, J., Lewis, A., Akehurst, S. & Brace, C., 2015. SuperGen on ultraboost: variable-speed centrifugal supercharging as an enabling technology for extreme engine downsizing. *SAE International Journal of Engines,* 8(4), pp. 1602-1615.

Turner, J., Popplewell, A., Patel, R., Johnson, T., Darnton, N., Richardson, S., Bredda, S., Tudor, R., Bithell, C. & Jackson, R., 2014. Ultra boost for economy: extending the limits of extreme engine downsizing. *SAE International Journal of Engines,* 7(1), pp. 387-417.

Uthoff, L.H. & Yakimow, J.W., 1987. *Supercharger versus turbocharger in vehicle applications.* (0148-7191). SAE Technical Paper.

VanDyne, E., Brinks, B.T., Riley, M.B. & Brown, J.W., 2013. Super-turbocharger having a high speed traction drive and a continuously variable transmission. Google Patents.

Wakisaka, Y., Hotta, Y., Inayoshi, M., Nakakita, K., Sakata, I. & Takano, T., 2009. Emissions reduction potential of extremely high boost and high EGR rate for an HSDI diesel engine and the reduction mechanisms of exhaust emissions. *SAE International Journal of Fuels and Lubricants,* 1(1), pp. 611-623.

Wallace, F. & Cox, A., The Ultimate performance potential of compounded diesel engines for heavy vehicles. In: IMECHE CONFERENCE TRANSACTIONS, 1998. MECHANICAL ENGINEERING PUBLICATIONS, pp. 253-270.

Wallace, F., Tarabad, M. & Howard, D., 1983. The Differential Compound Engine—A New Integrated Engine Transmission System Concept for Heavy Vehicles. *Proceedings of the Institution of Mechanical Engineers, Part A: Power and Process Engineering*, 197(3), pp. 209-218.

Wan, M., 2016. *Turbocharging* [Online]. Autozine Technical School. Available from: http://www.autozine.org/technical_school/engine/Forced_Induction_3.html [Accessed 01/10 2019].

Watel, E., Pagot, A., Pacaud, P. & Schmitt, J.-C., 2010. *Matching and evaluating methods for Euro 6 and efficient two-stage turbocharging diesel engine.* (0148-7191). SAE Technical Paper.

Watson, N. & Janota, M., 1982. *Turbocharging the internal combustion engine.* Macmillan International Higher Education.

Wearing, A.D., Haybittle, J., Bao, R., Baxter, J.W., Rouaud, C. & Taskin, O., Development of High Power 48V Powertrain Components for Mild Hybrid Light Duty Vehicle Applications. In: 2018 IEEE Energy Conversion Congress and Exposition (ECCE), 2018. IEEE, pp. 3893-3900.

Wetzel, P., 2013. *Downspeeding a light duty diesel passenger car with a combined supercharger and turbocharger boosting system to improve vehicle drive cycle fuel economy.* (0148-7191). SAE Technical Paper.

Wijetunge, R., Criddle, M., Dixon, J. & Morris, G., 2004. Comparative Performance of Boosting Systems for a High Output, Small Capacity Diesel Engine. *STA paper F2004F195*.

Wu, B., Han, Z., Yu, X., Zhang, S., Nie, X. & Su, W., 2019. A method for matching two-stage turbocharger system and its influence on engine performance. *Journal of Engineering for Gas Turbines and Power*, 141(5), p. 054502.

Xiao, B., Hellstrom, E., Kelly, T., Stolzenfeld, T., Bell, D., Jankovic, M., Buckland, J. & Rollinger, J., Dynamic Pressure Ratio Allocation for Electric Supercharger and Turbocharger Coordination. In: 2018 Annual American Control Conference (ACC), 2018. IEEE, pp. 2455-2460.

Xin, Q., 2011. *Diesel engine system design.* Elsevier.

Yanbin, L., Weilin, Z., Yangjun, Z., Shuyong, Z., Junyue, Z. & Xuemin, H., 2015. A Matching Method for Two-Stage Turbocharging System. *Journal of Engineering for Gas Turbines and Power*, 137(2), p. 022604.

Yang, B., Fang, X., Zhang, L., Zhuang, F., Bi, M., Chen, C., Li, G. & Wang, X., 2019a. Applicability of empirical models of isentropic efficiency and mass flow rate of dynamic compressors to jet engines. *Progress in Aerospace Sciences*.

Yang, M., Hu, C., Bai, Y., Deng, K., Gu, Y., Qian, Y. & Liu, B., 2019b. Matching method of electric turbo compound for two-stroke low-speed marine diesel engine. *Applied Thermal Engineering*, 158, p. 113752.

Zeng, T., Upadhyay, D., Sun, H. & Zhu, G.G., Physics-based turbine power models for a Variable Geometry Turbocharger. In: 2016 American Control Conference (ACC), 2016. IEEE, pp. 5099-5104.

Zhang, K., 2010. Air charge system emulation for diesel engine. Thesis. University of Bath.

Zhang, Q., 2015. *Experimental and analytical investigation into the two stage turbocharging systems for diesel engines.* Thesis. University of Bath.

Zhao, D., Stobart, R. & Mason, B., Optimising the energy efficiency and transient response of diesel engines through an electric turbocharger. In: 2019 American Control Conference (ACC), 2019. IEEE, pp. 298-303.

Zhen, X., Wang, Y., Xu, S., Zhu, Y., Tao, C., Xu, T. & Song, M., 2012. The engine knock analysis–An overview. *Applied Energy*, 92, pp. 628-636.